NASA Conference Publication 2363

Remote Sensing of Snow and Evapotranspiration

Thomas Schmugge, *Editor*
NASA Goddard Space Flight Center
Greenbelt, Maryland

Proceedings of the Second U.S./Japan Snow and Evapotranspiration Workshop held in Honolulu, Hawaii, U.S.A. November 15–19, 1983

National Aeronautics and Space Administration

Scientific and Technical Information Branch

1985

CONTENTS

FOREWORD

The second US/Japan Workshop on Remote Sensing of Snow and Evapotranspiration was held in Honolulu, Hawaii, USA from November 15 to 19, 1983. Five scientists from each country participated in the workshop. The workshop was held at the Resource Systems Institute of the East-West Center which is located on the Manoa campus of the University of Hawaii. The cordial hospitality and logistical support provided by the institute was greatly appreciated.

These workshops were part of a cooperative research project between National Aeronautics and Space Administration on the American side and the National Institute of Resources of the Science and Technology Agency on the Japanese side to study the use of remote sensing technology to determine snowpack properties and evapotranspiration fluxes. This project was conducted on the basis of an agreement from the Joint Committee of US/Japan Cooperation in Research and Development in Science and Technology concluded in May, 1980. This workshop represents the final formal activity of this project.

After several smaller meetings in the US and data exchanges between investigators the first formal workshop under this project was held in Tokyo during March, 1982. This meeting laid the basis for increased exchanges during the following year particularly in the area of snow research. This cooperation culminated in the second workshop held at the East-West Center. In these workshops the most recent results of research on the remote sensing of snow properties and evapotranspiration were exchanged through the presentation of papers and informal discussion. This report is a summary of that workshop and includes the written versions of the presented papers. While this workshop and report conclude the formal cooperation within the project both sides agreed that informal exchanges of data and models by the individual scientists should be continued in the future.

U.S./JAPANESE JOINT RESEARCH PROJECT

SUMMARY REPORT OF DISCUSSIONS

East-West Center
University of Hawaii
Honolulu, Hawaii

A joint meeting on research on the use of remote sensing of snow and evaportranspiration was held November 15-19, 1983, at the East-West Center on the campus of the University of Hawaii in Honolulu with a field trip to an irrigation-water management site of the Oahu Sugar Company.

A number of interesting papers were presented by researchers from both countries. The results indicate that significant progress has been made in all the areas of snowmelt modeling, snowpack properties and evapotranspiration research. A summary of the accomplishments of the project follows. Specific research results are documented in the papers of the reporters. These meetings and the exchanges of papers have made the scientists in each country aware of the research going on in the other country and has stimulated the research of each group and helped them to overcome problems. Therefore, it is recommended that the direct collaboration between the individual groups be continued.

SNOW RESEARCH

Snowmelt Modeling

In the snowmelt runoff portion of this project snowmelt runoff models from both the U.S. and Japan were employed for simulation of discharge on basins in both countries. The U.S. model (Rango-Martinec) was tested by the U.S. participants on the Kings River basin in California for four years and on the Okutadami River basin in Japan for 1 year. The Japanese model was not available to the U.S. participants for testing, however, a user manual is in preparation. The Japanese participants tested both the Japanese model and the Rango-Martinec model on the Okutadami River basin for 3 years. The simulation results as presented in the respective papers are very comparable when the goodness-of-fit statistics are evaluated. On the average, the results for the Kings and Okutadami basins are nearly the same although they are widely diverse basins. In the only year when the U.S. and Japanese participants both tested the Rango-Martinec model (1979), the goodness-of-fit parameters are very similar. Finally, the Rango-Martinec model and the Japanese model produce similar simulations for the same years on the Okutadami basin. Remotely sensed snowcover extent data are critical for both models. The Rango-Martinec model requires a minimum of 2-3 snowcover scenes during the snowmelt season. The Japanese model can be used effectively when even fewer satellite snowcover observations are available so that it can be applied in severe cloud-cover situations. Depending on availability of data, either model could be used for simulations of snowmelt-runoff. The Rango-Martinec model has been widely tested, and its performance on Okutadami indicates that it can operate successfully in a basin with a wet, deep snowpack. The Japanese model, however, has only been tested (successfully) on the Okutadami basin and needs additional testing on other basins with different snow conditions.

Another aspect of the snowmelt-modeling was an attempt by the Japanese participants to estimate the maximum seasonal snow water equivalent for a basin by using a grid-based snowmelt accounting method. The Okutadami basin was superimposed with a grid and the maximum snow water equivalent was estimated by combining date of snow disappearance from Landsat, degree-day totals (melt), and precipitation data. The distribution of maximum snow water equivalent can be used to generate a snowcover map that can be checked with NOAA-AVHRR data.

This cooperative project between Japan and the U.S. has permitted a valuable international exchange resulting in great progress toward employing remote sensing data in snowmelt-runoff modeling. The research thus far has established the means for efficiently using satellite snowcover data in runoff models. The research has also developed techniques for operating such runoff models in situations where very few snow cover observations are possible. Continued operation should result in operational techniques for snowmelt-runoff forecasting using remote sensing.

Microwave Snowpack Properties

The Japanese participants presented a paper entitled "Studies on Physical Properties of Snow Based on Multichannel Microwave Sensor Data". The data were obtained using the breadboard model of MSR (Microwave Scanning Radiometer) to be installed in MOS-1 (Marine Observation Satellite-1), Japan's first earth observation satellite. The U.S. participants presented a paper entitled "Microwave Radiometer Observations of Snowpack Properties and Comparison of U.S.—Japanese Results". Both papers described the results and analysis of field experiment data taken by microwave radiometers over snowpacks. The microwave responses from the Hokkaido site gave similar results as those reported by previous U.S. field experiments. However, due to deeper snow depth in the Hokkaido site, a different algorithm is required to interpret the microwave data. The joint U.S.-Japan project provided us the opportunities to share knowledge gained from studying different snowpacks. Analysis of these data will extend our understanding of microwave responses for deep snowpacks.

The SMMR measurements over the Japanese test site (Hokkaido) and the U.S. test sites (North Dakota) were analyzed for snow water equivalent determinations. The Japanese scientists presented a paper entitled "Analysis of Nimbus SMMR data" and the U.S. investigators also discussed the Nimbus SMMR data analysis in their paper listed above. Results from five sets of Nimbus-7 SMMR data were reported. The results from the North Dakota site match well with the existing radiative transfer model. However, the results from the Hokkaido site are more diverse due to varying surface cover conditions. Different snow water equivalent retrieval algorithms are required due to different vegetation cover and mountain topography.

Future field experiments (1983-1984 in Vermont, and 1984 in Japan) and an aircraft experiment (1985 in Japan) are planned. These observations will further improve our understanding of microwave signatures of snow. The future satellite data from the Japanese MOS-1 will help fill data gaps between the Nimbus-7 SMMR and any future spaceborne microwave system for snowpack study, as well as, serve as an atmospheric parameter study.

RECOMMENDATIONS FOR FUTURE SNOW RESEARCH

Snowmelt Modeling

— The Japanese Model, originally developed for operation in areas where cloud cover restricts satellite observations, should be tested on a wide variety of basins. After appropriate modifications, a user manual should be written and published.

- A forecasting algorithm should be developed for the Rango-Martinec model so that it can be used for operational water management. Additionally, improved precipitation and evapotranspiration algorithms should be substituted into the model to improve performance during the non-snowmelt season.
- Techniques should be developed for obtaining reliable snowcover extent data for model application. One improvement would entail use of digital NOAA 1 km data which are available daily. For reliable, all weather data acquisition, the long-term solution would involve development of a multichannel radar instrument for snow mapping.
- Continued cooperation between the U.S. and Japanese investigators is recommended in order to ultimately develop an operational, remote sensing-based snowmelt-runoff forecasting system. This involves both data acquisition with appropriate sensors and a widely applicable snowmelt-runoff forecasting model.

Microwave Snowpack Properties

Due to frequent cloud cover over snow sites in Japan, microwave techniques are the way to provide snow cover area and snow water equivalent information for snowmelt runoff models. Snow properties are very important not only because of their relations with snowmelt runoff generation, but also because of their direct relationship to the global energy balance/hydrological cycle study. Future exchange of knowledge between scientists from two countries are essential to further the understanding of snow properties. Satellite data are very useful in studying the snowpack properties.

- It is strongly recommended that: 1) studies of snowpack properties using microwave technology be continued, and 2) investigations into the atmospheric (water vapor and cloud) influence on the microwave response from a snowpack be included in the continuing exchange program.
- Continuing exchange of the satellite data between U.S. and Japan for future snow studies is required.

EVAPOTRANSPIRATION RESEARCH

Results

Since the first meeting of the U.S./Japanese working group, the scientists of both countries have continued their studies on the use of remote sensing for evapotranspiration studies. In the U.S. these efforts have included expanding the model studies to account for vegetation cover and the performance of sensitivity studies to understand the effects of differing sampling intervals for the meteorological data used in the ET estimation models. The vegetation model was tested with a small data set from the Tsukuba test site.

An aircraft research mission was performed in May and June, 1983, over U.S. test sites in eastern Maryland and Delaware. The aircraft carried both thermal and microwave radiometers for

the remote sensing of surface temperature and surface soil moisture. The remote sensing observations will be compared with ground measurements of each parameter to check calibrations and then used in the models to estimate ET. Analysis of these data will continue for the next year or two to evaluate the use of remote sensing inputs.

Since the first meeting, Japanese scientists have examined the calibration of a Priestley-Taylor type of equation using remotely sensed thermal infrared data. These data were taken during an aircraft flight experiment January 1983 in the Tsukuba area. Evapotranspiration was calculated for a wide variety of surfaces. Differences with vegetation type were not large because of the moist conditions and low solar insolation in winter. It is hoped to repeat the flight experiment in summertime conditions when greater differences are expected. Ground-based remotely sensed data have been analyzed to study the variation of the Priestley-Taylor model parameter α with time of day and season. Some of the variations were found to be due to seasonal advection changes and some to moisture stress and insolation differences.

The Japanese scientists presented two papers dealing with their evapotranspiration research: Estimation of Regional Evapotranspiration using Remotely Sensed Land Surface Temperature—Part I—Measurement of Evapotranspiration at the Environmental Research Center, University of Tsukuba and Determination of Priestley-Taylor Parameter, and Part II—Application of Equilibrium Evapotranspiration Model to Estimate Evapotranspiration by Remote Sensing Technique. The U.S. scientists presented a paper on "The Estimation of Daily Evapotranspiration Using Remotely Sensed Surface Temperature and Soil Moisture" and a paper entitled "Microwave Remote Sensing of Soil Moisture" which covered the recent advances on this problem. There was considerable discussion of the data from the Tsukuba test site and the U.S. scientists expressed a desire to use some of these data for calibration studies with their models.

Conclusions

Material exchanged during the cooperative agreement has demonstrated that remotely sensed data are of use in estimating evapotranspiration, either through the use of a Priestley-Taylor type of expression and land cover data or through the use of an energy/moisture balance approach. In both cases, the estimation of the model parameters needs further study, particularly for tall or structured vegetation. The relationship between the radiometric temperature and the temperature in a vegetation canopy also needs to be studied further. In addition, methods need to be developed for using soil moisture data available through microwave techniques. Some of the questions concerning the modelling of vegetation can probably be answered by looking at time series of data where different conditions exist during the observation period. The field site of the Environment Research Center at the University of Tsukuba, Japan, may provide suitable data, and a data set from 1982 of hourly data from a meteorological tower, together with concurrent lysimeter, soil moisture and temperature data, will be provided to the U.S. coinvestigators to assist in their continuing research.

U.S./JAPAN SNOW PROPERTIES AND EVAPOTRANSPIRATION PROJECT INVESTIGATORS MEETING AND WORKSHOP

Dates: November 15-19, 1983

Location: Room 3005, John A. Burns Hall
East-West Center
University of Hawaii
Honolulu, Hawaii

PROGRAM

November 15:

9:00 - 10:00	Opening Remarks (I)
10:00 - 12:00	Snowmelt Runoff Modeling (II)
12:00 - 1:00	Lunch
1:00 - 4:00	Snowpack Properties (II)
4:00 - 6:00	Reception

November 16:

9:00 - 12:00	Snowpack Properties (II)
12:00 - 1:00	Lunch
1:00 - 3:00	Evapotranspiration and Soil Moisture (III)
3:00 - 4:00	Workshop Assignments and Discussion of Workshop Objectives

November 17:

9:00 - 12:00	Workshop Groups Meet
12:00 - 1:00	Lunch
1:00 - 2:00	General Session
2:00 - 4:00	Workshop Groups Meet
7:30 - 10:00	Dinner

November 18:

9:00 - 10:00	General Session
10:00 - 12:00	Completion of Draft Report
12:00 - 1:00	Lunch
1:00 - 4:00	Field Trip

November 19:

9:00 - 11:00	Completion of Draft Report
11:00 - 12:00	General Session

LIST OF PARTICIPANTS

Dr. Albert Rango	Chief Hydrology Laboratory USDA/Agricultural Research Service Beltsville, MD 20705
Dr. Kenji Ishihara	President Environmental Research and Technology Institute 39, Ichigayahonmura-cho Shinjuku-ku, Tokyo, Japan 162
Dr. Thomas Schmugge	Hydrological Sciences Branch/Code 924 NASA/Goddard Space Flight Center Greenbelt, MD 20771
Dr. Kiyoshi Tsuchiya	Professor Institute of Color & Image Technology Faculty of Engineering Chiba University Japan 1-33, Yayoi-cho, Chiba-City, Chiba, Japan 260
Dr. Kaname Takeda	Leader of Research Group National Institute of Resources Science & Technology Agency 2-2 Kasumosaseki Chiyoda-ku, Tokyo, Japan 100
Dr. Hiroaki Ochiai	Professor Navigation Department Toba Merchant Marine College 1-1 Ikegami-cho, Toba-City Mie, Japan 517
Dr. Kazuo Kotoda	Associate Professor Environmental Research Center University of Tsukuba Sakuramura, Ibaraki Japan 305
Dr. Alfred T.C. Chang	Hydrological Sciences Branch/Code 924 NASA/Goddard Space Flight Center Greenbelt, MD 20771
Dr. R.J. Gurney	Faculty Research Associate Department of Civil Engineering University of Maryland College Park, MD 20742
Dr. Howard Hogg	Land Processes Branch/Code EE-8 NASA Headquarters 600 Independence Avenue, S.W. Washington, D.C. 20546

PRESENTATIONS

SESSION I

J. BARDACH	East West Center Program
H. HOGG	NASA Land Remote Sensing in the 1980's
K. TAKEDA	General Report of the Researchers on Snowpack Properties, Snowmelt Runoff and Evapotranspiration in Japan

SESSION II

A. RANGO	Snowmelt Runoff Model Utilizing Remotely Sensed Data
K. ISHIHARA	Snowmelt Runoff Model in Japan
K. ISHIHARA	Application of Martinec Rango Model to River Basin in Japan
H. OCHIAI/K. TAKEDA	Distribution of Snow and Water Equivalent Obtained by Landsat Data and Degree Day Method
A. CHANG	Microwave Radiometer Observations of Snowpack Properties and Comparison of U.S. Japanese Results
K. TSUCHIYA	Studies on Physical Properties of Snow Based on Multichannel Microwave Sensor Data
K. TSUCHIYA	Analysis of Nimbus SMMR Data

SESSION III

K. KOTODA	Estimation of Regional Evapotranspiration using Remotely Sensed Land Surface Temperature
R. GURNEY	Use of Surface Temperature and Surface Soil Moisture Observations for Evapotranspiration Estimates
T. SCHMUGGE	Microwave Remote Sensing of Soil Moisture

PRESENTED PAPERS

H. HOGG	NASA Land Remote Sensing in the 1980's
K. TAKEDA	General Report of the Researchers on Snowpack Properties, Snowmelt Runoff and Evapotranspiration in Japan
A. RANGO	Snowmelt Runoff Model Utilizing Remotely Sensed Data
K. ISHIHARA	Snowmelt Runoff Model in Japan
K. ISHIHARA	Application of Martinec Rango Model to River Basin in Japan
H. OCHIAI/K. TAKEDA	Distribution of Snow and Water Equivalent Obtained by Landsat Data and Degree Day Method
A. CHANG	Microwave Radiometer Observations of Snowpack Properties and Comparison of U.S. Japanese Results
K. TSUCHIYA	Studies on Physical Properties of Snow Based on Multichannel Microwave Sensor Data
K. TSUCHIYA	Analysis of Nimbus SMMR Data
K. KOTODA	Estimation of Regional Evapotranspiration using Remotely Sensed Land Surface Temperature
R. GURNEY	Testing an Energy Balance Model for Estimating Actual Evapotranspiration Using Remotely Sensed Data
T. SCHMUGGE	Microwave Remote Sensing of Soil Moisture

NASA'S LAND REMOTE SENSING PLANS FOR THE 1980's

Howard C. Hogg, Kristine M. Butera, and Mark Settle[1]

INTRODUCTION

My remarks this morning will be restricted to the NASA Land Remote Sensing program. Within this context, I will outline the past program which concentrated on near-term applications and will describe the emerging Land Processes program. The major goal of this new program is the improved understanding of long-term land processes. My comments will be largely programmatic in nature.

BACKGROUND

Satellite multispectral land remote sensing originated with the Landsat series of satellites beginning with the launch of ERTS-1 in 1972, (subsequently renamed Landsat-1) which has provided a continuous source of global data.

Research since the launch of Landsat-1 has been primarily directed to the development of analysis techniques and to the conduct of applications studies designed to address resource information needs. These studies were conducted not only in the United States, but in many other countries, as well, because of an early U.S. policy decision which resulted in the widespread availability of Landsat data. The United States has remained a leader in developing this technology because of a continuing NASA commitment to land remote sensing research and development and the availability of a continuing flow of satellite and now Shuttle-acquired remotely sensed data.

Landsats 1, 2, and 3 provided data in four spectral bands in the visible and near infrared regions of the electromagnetic spectrum with an 80 M IFOV (Instantaneous Field of View). Consequently, the vast majority of the early research was directed to better understanding the information contained in these multispectral data. This research resulted in an understanding of the limitations of the current system and an identification of requirements for more advanced capability. The early work also clearly indicated a need for a better understanding of the physics and mathematics of the remote sensing process itself. For example, the analysis of the early Landsat data indicated that the utility of the data would be greatly expanded if the spatial resolution were improved by a factor of 2 to 3. Concurrent research using aircraft scanner data indicated the potential of other wavelengths, particularly those in the short wave infrared region (1-2.5 μm), for improving the utility of multispectral data in vegetation and geological studies. This led to the design of the Landsat Thematic Mapper (TM) in the middle 1970's. The TM, launched in 1982, has seven spectral bands and a 30 meter IFOV for all but the thermal infrared channel. Also, to support the increased volume of data associated with the TM, a new data processing system was initiated to accommodate a high throughput rate and to produce digital tapes on a timely basis.

In addition to the Landsat series of satellites, two other satellite remote sensing systems have provided the opportunity to analyze spectral data not previously available. The Heat Capacity Mapping Mission (HCMM) Satellite, launched in 1978, acquired broad band thermal infrared data

---

[1] Authors are respectively: Acting Chief Land Processes Branch; Program Manager, Fundamental Remote Sensing Science; and Program Manager, Non-renewable Resources at NASA/Headquarters.

which were analyzed for geological and agricultural applications. The HCMM data expressed the natural land surface by representing diurnal variations in thermal radiation from the ground. This mission proved that thermal infrared data were useful for the identification of certain geologic and vegetative features, as well as other surface materials and soil characteristics.

Seasat, also launched in 1978, initiated research in the utility of active microwave sensors for characterizing surface cover and structure. This mission proved the utility of space based radar for the study of geological features, for improving vegetation classification accuracies, and for mapping soil moisture.

Measurement technology continues to develop with emphasis on sensors of finer spectral resolution using both aircraft and the Space Shuttle as platforms. The results to date suggest that finer spectral resolution in both the reflected and thermal infrared regions would be useful for improving our ability to classify surface lithologies. Finer spectral resolution in the visible and reflected infrared also appears promising for vegetation classification and condition assessments.

GLOBAL RESEARCH

In formulating a new program thrust, NASA Headquarters recently completed a planning & review exercise which identified a series of science issues of global significance. They have been documented in a report entitled, *Land-Related Global Habitability Science Issues*. This document is one of several that have been prepared in this planning activity. To date, these individual science issues documents have not been integrated into an overall program plan. Remote sensing research clearly can make a contribution to the understanding of these global issues and, further may be the only technology that can adequately address them on a global basis. Such an undertaking will require a properly focused multidisciplinary Land Science program.

In general, the ability to extract information about vegetation, geology, and hydrology on a continental or global scale was only achieved early in this decade. This capability was primarily the result of the NASA R&D program in Land Resources but was facilitated by parallel developments in computer and communications technology. For example, in technique development between 1978 and 1980, the amount of preprocessed data used by an analyst to estimate crop proportions was cut 50%. The initial technique required four bands and four date acquisitions, while the later technique required only two bands, the greenness and brightness transformations, with the same number of acquisitions. By 1983, the data volume handled by the analyst was further reduced with the development of a greenness profile that required even fewer acquisitions and yet provided for vegetation discrimination based on the rate of green-up and decay of greenness determined from the profile. The concurrent automation of some previously manual techniques led to an overall CPU-analyst time reduction of over 90%. However, this development did not reduce the amount of data that must be acquired and initially processed (registered, transformed, and combined with ancillary data). The effort to reduce data acquisitions and pre-processing has led to research into large area sampling strategies and analysis of data from low spatial resolution sensors such as the AVHRR flown on the NOAA series of satellites.

The combination of large area sampling techniques and preprocessing methods designed to reduce the dimensionality of multispectral imagery will greatly improve our future ability to extract meaningful physical information from remotely sensed data. We are ultimately heading for a day in the not too distant future when multispectral imagery acquired by various sensors on different Earth orbiting satellites may be used to survey regional variations in phytomass on a routine basis. This

type of capability would provide a whole series of new opportunities to study atmospheric and climatic phenomena and man's impact on the long-term habitability of the Earth.

The scope of our geology program has also been enlarged to address a series of basic scientific problems of potentially global significance. During the past year, NASA sponsored researchers have employed remote sensing techniques to study regional geological conditions in arid regions in fundamentally new and different ways. Radar imagery obtained by the Shuttle Imaging Radar-A (SIR-A) experiment in 1981 has led to the discovery of buried drainage channels in the Eastern Sahara Desert. These features have provided important information about the geological and archaeological history of this important region. In addition, NASA researchers are employing reflectance and microwave techniques to gain new insight into rock weathering processes that operate in arid regions. Continuing studies of chemical weathering processes have recently indicated that various types of fungi play a significant role in altering geological materials in desert regions. Microscopic colonies of these fungi have actually been detected on the surfaces of desert rocks situated in the western United States, Australia, and China. We are currently employing Landsat techniques to study the global pervasiveness of this phenomenon and its long-term effect on the albedo of the Earth.

One of the common areas of interest between our geological and botanical researchers in recent days has been the study of mineral-induced stress effects in natural vegetation. Pioneering research conducted by scientists at the Goddard Space Flight Center has indicated that deciduous trees growing in soils with anomalously large concentrations of metallic elements may possess distinctive reflectance characteristics during the fall season. Researchers at the Jet Propulsion Laboratory have also detected indications of vegetation stress in remotely sensed imagery that have been attributed to the local seepage of natural gas near the Earth's surface. These results tentatively suggest that remote sensing techniques may potentially prove to be powerful tools for detecting and monitoring vegetation stress and its geological causal component on a global basis.

Beyond the satellite research program built around the MSS, TM, and limited L-band radar data, the Space Shuttle era provides a new and unique platform for the testing of advanced measurement instruments and the acquisition of remotely-sensed data. The Shuttle may very well play a role in providing some of the continental or global data sets that are required for land science investigations. In fact, a Shuttle project to provide a digital topographic map of the globe is currently being planned.

THE LAND PROCESSES PROGRAM

The responsibility for the NASA land remote sensing program lies in the Land Processes Branch of the Earth Science and Applications Division. Our primary program objective is to develop remote sensing technology for improving the understanding of long term land processes. A secondary objective is to develop remote sensing techniques useful for meeting the information requirements of different user groups. The program integrates three components:

- Remote Sensing Science—to improve our understanding of the remote sensing process by pursuing the physics and mathematics of remote sensing as a generic science.

- Discipline Science—to support discipline science investigations by developing and using remote sensing tools, and

- Technology Development—to develop and test advanced measurement techniques that appear promising for understanding land processes or for resource applications.

Because the overall thrust of the program is to understand long term land processes, such pursuits as the inventory and monitoring of land cover, the description and modelling of physical systems and processes, and the determination of model parameters that can be remotely sensed are important program initiatives.

The current measurement capabilities represented by MSS, TM, and SIR-A and B, coupled with the present level of remote sensing-understanding and the state of knowledge in the discipline earth sciences, will be the foundation on which NASA will build a new Land Processes Program. The science issues to be systematically addressed in the program include:

Energy Balance—to quantify components of the energy balance between the land cover and hydrologic systems and to model the energy flow within and between these systems.

Hydrologic Cycle—to characterize the hydrology in different biomes and clarify the relationship between plant productivity and available water, and their contribution to the energy balance.

Biogeochemical Cycles—to characterize the elemental cycles (primarily phosphorus, sulphur, carbon, and nitrogen) in the different biomes in terms of fluxes between and within the cycles.

Biological Productivity—to determine factors which control the distribution and dynamics of productivity, to model interactions with the hydrology and geochemical cycles, and to assess the influence on the energy balance.

Rock Cycle—to develop an improved understanding of the temporal and spatial scale of rock transport and model the physical process of rock weathering.

Landscape Development—to determine the response of landscapes to different geological and climatic variations, to determine the balance between soil development and soil erosion.

Geological and Botanical Associations—to understand and model the relationship between plant communities and condition as influenced by crustal geology and environmental conditions.

Land Surface Inventory, Monitoring, and Modeling—to determine the location and rates of change of major surface types using predictive models.

To support the Land Processes Program during the 1980's with improved measurement techniques, we plan a series of Shuttle experiments. To effectively conduct these missions, a continuing and well-funded technology development program must be pursued.

Although applications are no longer the primary driver of the NASA land remote sensing program, it is anticipated that some activity will continue in this area. Present plans call for this program element to include technique development, testing, evaluation, and a feedback mechanism in a

problem solving or applications context. A successful model for this kind of activity involves joint research with a user entity where the user provides a test site and ground truth and NASA provides the remote sensing techniques to be tested. The project results are then jointly evaluated.

NASA has invested significantly in land remote sensing. The launch of the first Landsat satellite in 1972 stimulated a decade of research and development and marked the potential for global data acquisition. However, it has only been since the 1980's that global surveys of the Earth's surface could be realistically considered. This is due, in part, to the maturation of remote sensing as a science, but also to the parallel development of computer technology and satellite communications, as well. Thus, the remote sensing community has arrived at a new threshold of capability and investigative thrust.

NASA has formulated the Land Processes Program to provide what we feel should be the direction for future remote sensing research. Our program will emphasize the use of remote sensing for improving the understanding of long term land processes. The nature of these processes will require a global perspective. Secondarily, the program will address user applications. An interdisciplinary association will form the nucleus of the program, to include the discipline sciences, the more generic remote sensing science, and sensor technology development. With the program objective and working components so defined, we feel NASA has developed a rational focus to direct the future of remote sensing research.

D2

GENERAL REPORT OF THE RESEARCHES OF SNOWPACK PROPERTIES, SNOWMELT RUNOFF AND EVAPOTRANSPIRATION IN JAPAN

Kaname Takeda

National Institute of Resources (NIR)
Science and Technology Agency (STA)

At the First Japan/US Snow and Evaporation Workshop held in Tokyo in March, 1982, eighteen Japanese and US sceientists presented their papers and exchanged valuable information. After 2 days sessions in Tokyo, field trips to Japanese test sites were made and further earnest discussions were made under participation of scientists in respective test sites.

The participants of both countries agreed that the Japan/US cooperative project was useful to both countries and should be continued. A joint summary report of the project status was made in which the next steps were formulated. Since the First Workshop, necessary data have been exchanged, and research and experiments have been conducted in accordance with the agreed framework at the Workshop. A summary of the research activities in Japan is as follows:

DISTRIBUTION OF SNOW AND SNOW WATER EQUIVALENT OBTAINED FROM LANDSAT DATA AND DEGREE DAY METHOD

The method of estimating snow water equivalent using Landsat derived snow line information and degree day method was discussed at the First Workshop. The problem in our country is that the useful and sufficient Landsat snow line data are not always available due to the meteorological condition. In order to solve that problem of data acquisition, we developed a new method of estimating distribution of snow and snow water equivalent by combining secular Landsat data with the degree-day method. This method enables us to estimate the maximum snow water equivalent of that year and distribution of snow at given time in the snow melting season, even if the Landsat data are obtained once in a snow melting season of that year. This method, however, involves some problems to be solved, so that it is necessary to conduct more experiments in order to improve its applicability.

SNOWMELT RUNOFF MODEL AND APPLICATION OF MARTINEC RANGO MODEL TO RIVER BASIN IN JAPAN

At the First Workshop, our party presented the paper of snowmelt runoff model. This model had some problems since it was in the development stage. We took Dr. Rango's advice and continued the research. We have now developed a new method applicable to the basins in Japan. Experimental basin in this method is only Okutadami River, therefore, it is necessary to add more case studies in order to develop its applicability and to prepare a manual for users. The Martinec Rango model presented from US was applied to the river basins in Japan to verify its applicability and compared with the Japanese model.

STUDIES ON PHYSICAL PROPERTIES OF SNOW BASED ON MULTI-CHANNEL MICROWAVE SENSOR DATA AND ANALYSIS OF NIMBUS SMMR DATA

Research and experiment with microwve sensors have been continued in Japan since the First Workshop. Microwave radiometer measurements were made from the tower over dry snow under natural and artificial condition in Hokkaido. The result of analysis of the data indicates existence of certain correlation between brightness temperature and snowpack properties.

Meanwhile, NIMBUS SMMR data sent from the US scientists have been analyzed. The correlation was recognized between brightness temperature and depth of snow in dry snow in inland plain area.

Further research and experiment with microwave sensors will be continued by using a moving rack as well as airborne sensor in 1984 and 1985.

ESTIMATION OF REGIONAL EVAPOTRANSPIRATION USING REMOTELY SENSED LAND SURFACE TEMPERATURE

Research and experiment on calculation of evapotranspiration using airborne remote sensing data and a Priestley-Taylor type of equation have been conducted in Tsukuba area. Evapotranspiration from various surfaces was calculated. The differentiation of evapotranspiration with vegetation type is not remarkable, because the magnitude of evapotranspiration is very little in winter. We have been analyzing the experimental data obtained in October 1983.

D3

SNOWMELT-RUNOFF MODEL UTILIZING REMOTELY-SENSED DATA

A. Rango

Hydrology Laboratory
Agricultural Research Service
Beltsville, Maryland 20705

INTRODUCTION

The Snowmelt-Runoff Model (SRM) has been developed to simulate discharge from mountain basins where snowmelt is an important component of runoff. The flow diagram for SRM is shown in Figure 1 which indicates that the model is of simple structure requiring input of only temperature, precipitation, and snow-covered area. The model has been successfully tested on a wide range of basin sizes and elevations (ΔH) as shown in Figure 2. The data requirements for applying SRM to a basin are shown in Table 1. Typically, the optimum conditions are seldom met and less data must be used. SRM can operate with the minimum conditions shown in Table 1. Only three satellite snow-cover observations were available for the application of SRM to the Okutadami basin in Japan, for example. When no runoff records are available, the recession coefficient can be derived from a size relationship with other known basins. Assistance for applying the model is provided in the user manual (Martinec, et al., 1983).

Results from model simulations are shown in Table 2 for 14 basins in 8 countries. The asterisks in Table 2 indicate basins where the snow-cover data were obtained from satellites. The average absolute percent volume difference for all the basins was 3% and the average R^2 value was 85%.

SRM was recently tested as one of 11 models in the World Meteorological Organization project on Intercomparison of Models of Snowmelt Runoff. On the various basin data sets, SRM typically was one of the top three models in performance. Table 3 presents a summary of strengths and weaknesses of SRM for application to a basin. Presently work is being conducted to develop a forecasting procedure for the model which will incorporate snow water equivalent data. In addition, more rigorous precipitation and evapotranspiration algorithms will be added to the model for operation during the non-snowmelt season.

RESULTS

Kings River Basin Simulations

SRM was tested on the Kings River basin in the Sierra Nevada Mountains of California. This was the largest basin on which SRM has been tested. Figure 3 shows the elevation zones (7) and respective areas that the basin was divided into for application of SRM. The elevation range of 171-4341 m is extremely large. Figure 4 illustrates the determination of the zonal mean hypsometric elevations ($\bar{h}$) using an area-elevation curve and balancing the areas above and below the mean elevation. The $\bar{h}$ value is used as the elevation to which base station temperatures are extrapolated for the calculation of zonal degree-days.

Examples of the satellite-derived snow-cover depletion curves are given in Figures 5 and 6 for 1975 and 1976, respectively. The snow-cover depletion curves for each zone are designated by a

capital letter referring to the appropriate zone in Figure 3. It can be seen that the snow cover leaves the basin much more rapidly in the drought year of 1976 than in the near normal year of 1975. The data for construction of the depletion curves came from both the Landsat and NOAA satellites.

Daily temperature, precipitation, and snow cover were then input to the model for the snowmelt seasons of 1973, 1975, 1976, and 1978. Figures 7, 8, 9, and 10 show the correspondence between measured streamflow and SRM computed streamflow for the years 1973, 1975, 1976, and 1978, respectively. The average absolute percent volume difference (Dv) for the snowmelt season for these years is 5.05% and the average R^2 value (daily flows) is 0.79. Even in the extreme drought year (1976) the performance of SRM is quite good.

Okutadami River Basin Simulation

Using data supplied by the Japanese cooperators, SRM was applied to the Okutadami River basin in central Japan. Okutadami has an elevation range of 782-2346 m and the basin was divided into three elevation zones of about 500 m increments as shown in Figure 11. Figure 12 illustrates the determination of the $\bar{h}$ values for each zone using the area-elevation curve. Only three Landsat observations of snow cover were available for the snowmelt season of 1979. However, these three observations were sufficient for defining the zonal snow-cover depletion curves as shown in Figure 13.

The temperature, precipitation, and snow-cover data for 1979 were then fed to SRM and a discharge simulation for 1979 produced. The hydrograph is shown in Figure 14. The difference in volume is −5.36% and the R^2 value was 0.83. With minimum snow-cover data, the performance of SRM was commendable. There were some possible discrepancies in the runoff data that should be checked with the Japanese cooperators. The performance of SRM shows the advantages of a model not requiring several years of records for calibration before it can be run in the simulation mode.

CONCLUSIONS

SRM was run successfully on two widely separated basins. The simulations on the Kings River basin are significant because of the large basin area (4000 km^2) and the adequate performance in the most extreme drought year of record (1976). The performance of SRM on the Okutadami River basin was important because it was accomplished with minimum snow-cover data available. It is concluded that SRM can be used on these two basins. The remotely-sensed snow-cover information is the critical data input for the model.

REFERENCES

Martinec, J., Rango, A., and Major E., 1983: the snowmelt-runoff model (SRM) user's manual, NASA Reference Publication 1100, Washington, D.C., 118 pp.

Table 1
Data Requirements for Model Application

OPTIMUM CONDITIONS

1. TEMPERATURE AND PRECIPITATION RECORDED IN BASIN AT MEAN ELEVATION
2. MULTIPLE CLIMATOLOGICAL STATIONS
3. SNOW COVER OBSERVED ONCE PER WEEK
4. SEVERAL YEARS OF DAILY RUNOFF RECORDS

MINIMUM CONDITIONS

1. TEMPERATURE AND PRECIPITATION OBSERVED IN BASIN VICINITY
2. ONLY ONE CLIMATOLOGICAL STATION
3. 2-3 SNOW-COVER OBSERVATIONS DURING SNOWMELT SEASON
4. NO RUNOFF RECORDS

Table 2
Basin Characteristics and Snowmelt-Runoff Model Simulation Results

Country and Basin	Size (km^2)	Elevation range (m)	Average goodness-of-fit statistics D_v(%)	NSR^2	n
CZECHOSLOVAKIA					
Modry Dul	2.65	554	+1.7	0.95	2
FRANCE					
Durance*	2170	3319	-2.5	0.89	1
JAPAN					
Okutadami*	422	1564	-5.4	0.83	1
POLAND					
Dunajec*	700	1724	-3.8	0.73	1
SPAIN					
Lago Mar	4.5	770	N/A	N/A	N/A
SWITZERLAND					
Dischma	43.3	1478	+0.2	0.88	6
UNITED STATES					
W-3	8.42	331	+3.3	0.82	6
Dinwoody Cr.*	228	2221	+3.3	0.85	2
Bull Lake Cr.*	484	2395	+4.8	0.82	1
South Fork*	559	1408	-1.5	0.89	7
Conejos*	730	1496	+0.5	0.87	7
Rio Grande*	3419	1783	+4.4	0.86	7
Kings River*	3999	4170	+5.1	0.79	4
WEST GERMANY					
Lainbachtal	18.7	1131	N/A	N/A	N/A

D_v = percent volume difference
NSR^2 = Nash-Sutcliffe R^2 value
N/A = not available

Table 3
SRM Strengths and Weaknesses

STRENGTHS	WEAKNESSES
DAILY INPUT OF ONLY TEMPERATURE, PRECIPITATION, AND SNOW COVER	SNOW-COVER DATA NOT COMMONLY OBSERVED
NO CALIBRATION NECESSARY	SATELLITE SNOW-COVER DATA IS SOMETIMES DIFFICULT TO OBTAIN IN A TIMELY FASHION
CAN BE RUN ON MICROCOMPUTER OR EVEN HAND CALCULATOR IF NECESSARY	SNOW WATER EQUIVALENT DATA NOT YET FORMALLY INCORPORATED IN FORECASTING PROCEDURES
SIMPLE DESIGN WHERE NEW ALGORITHMS COULD EASILY REPLACE EXISTING ONES	DOES NOT HAVE RIGOROUS PRECIPITATION AND EVAPOTRANSPIRATION ALGORITHMS FOR OPERATION DURING THE NON-SNOWMELT PERIOD OF THE YEAR
OPERATES EFFECTIVELY ON BASINS IN THE SIZE RANGE 1.0-4000km^2	
USER MANUAL AVAILABLE FOR EASY APPLICATION TO NEW BASINS	
ELEVATION ZONE OPTION AVAILABLE	

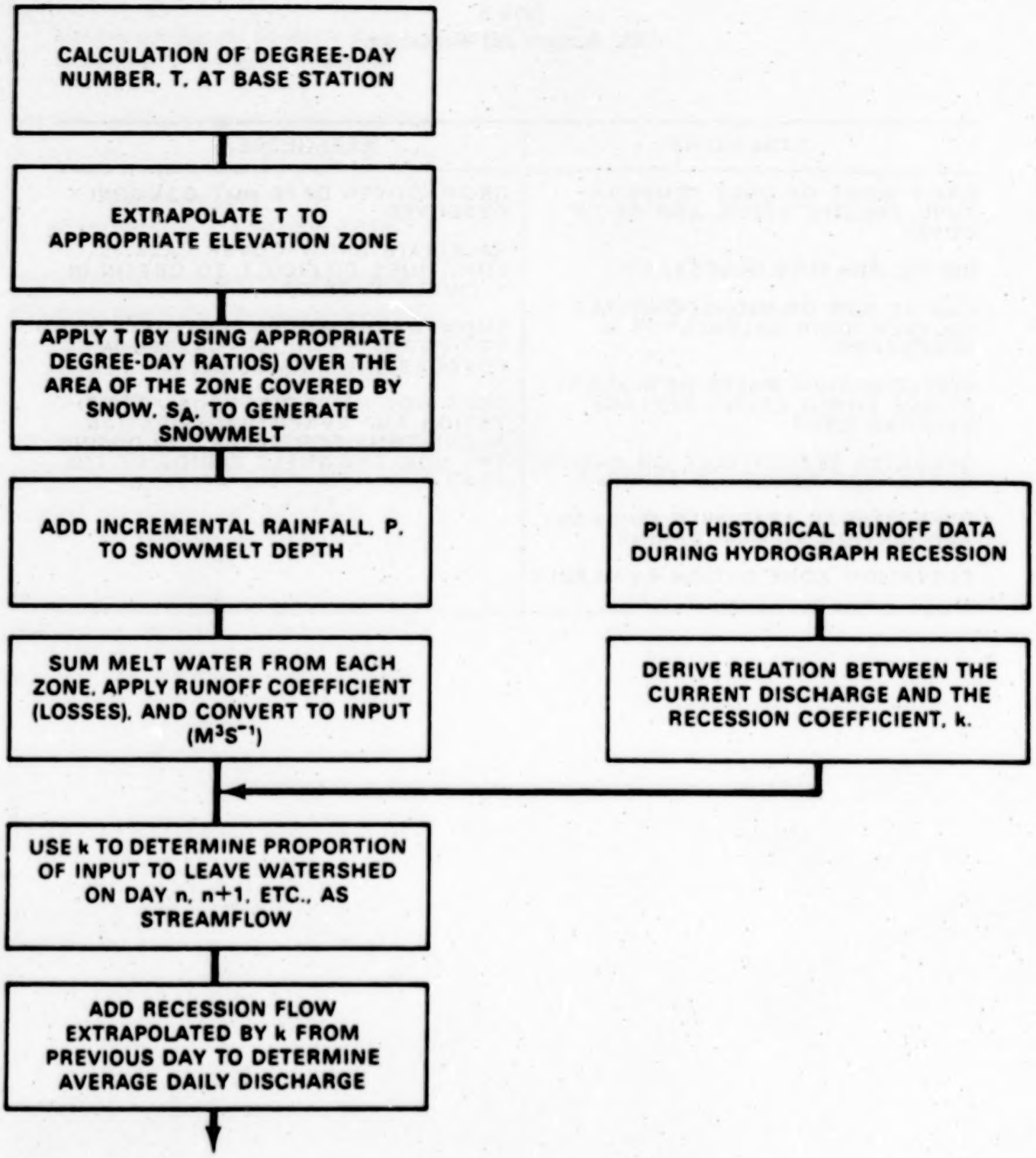

Figure 1. Flow Diagram for Snowmelt Runoff Model

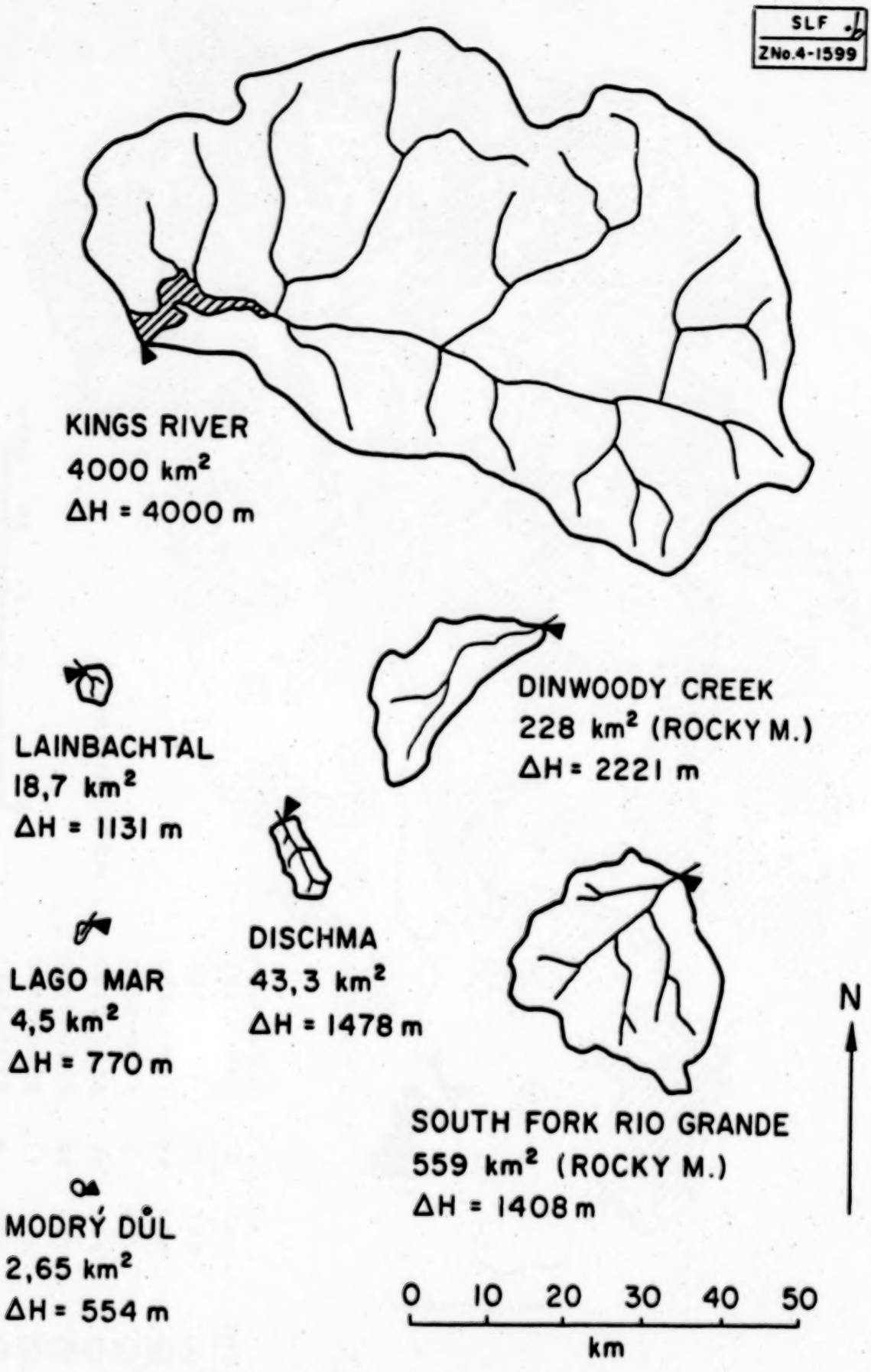

Figure 2. Size and elevation Range of some basins tested using SRM

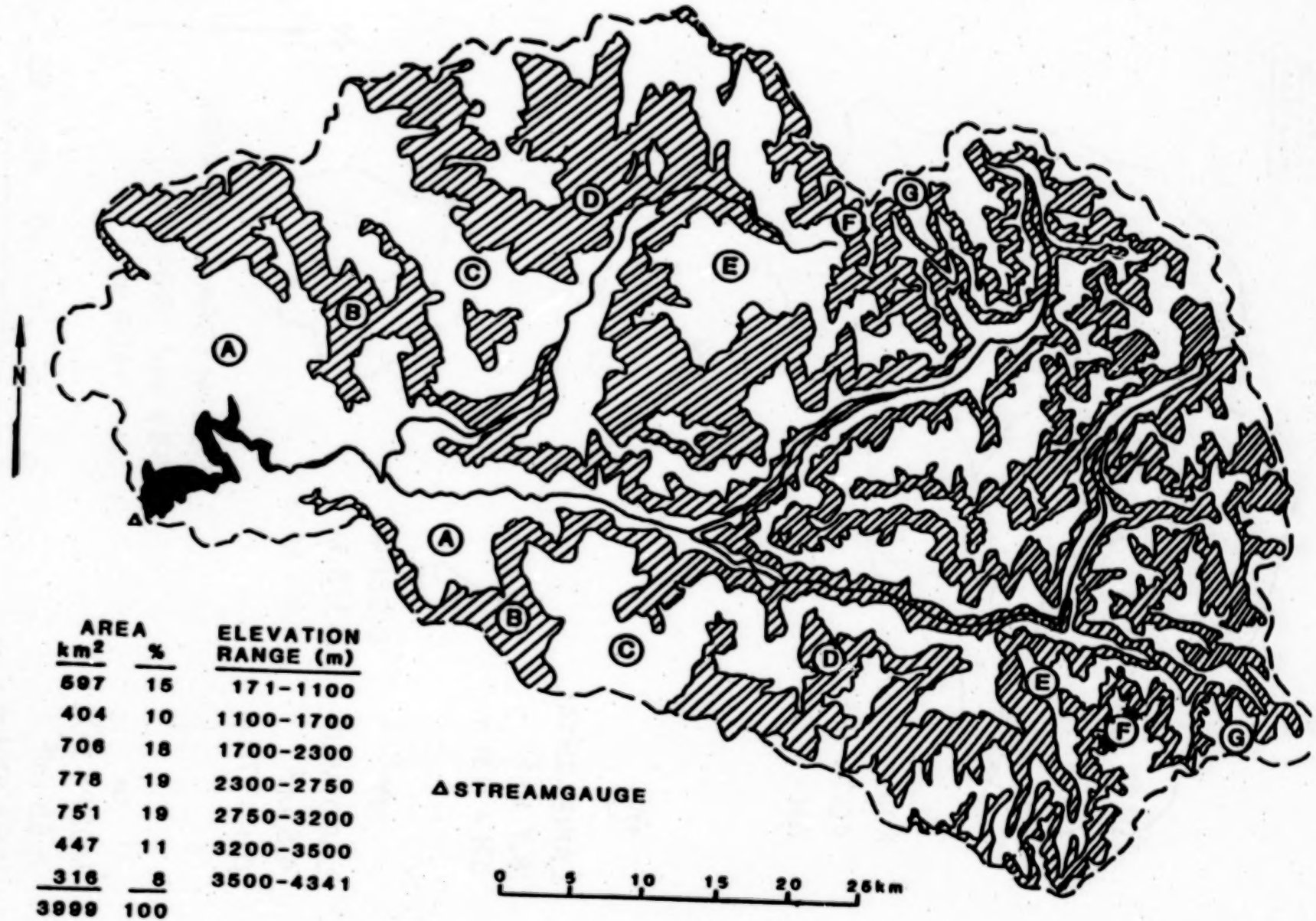

ZONE	AREA km²	AREA %	ELEVATION RANGE (m)
A	597	15	171-1100
B	404	10	1100-1700
C	706	18	1700-2300
D	778	19	2300-2750
E	751	19	2750-3200
F	447	11	3200-3500
G	316	8	3500-4341
	3999	100	

Figure 3. Elevation zones and areas of the Kings River Basin below Pine Flat Dam, California

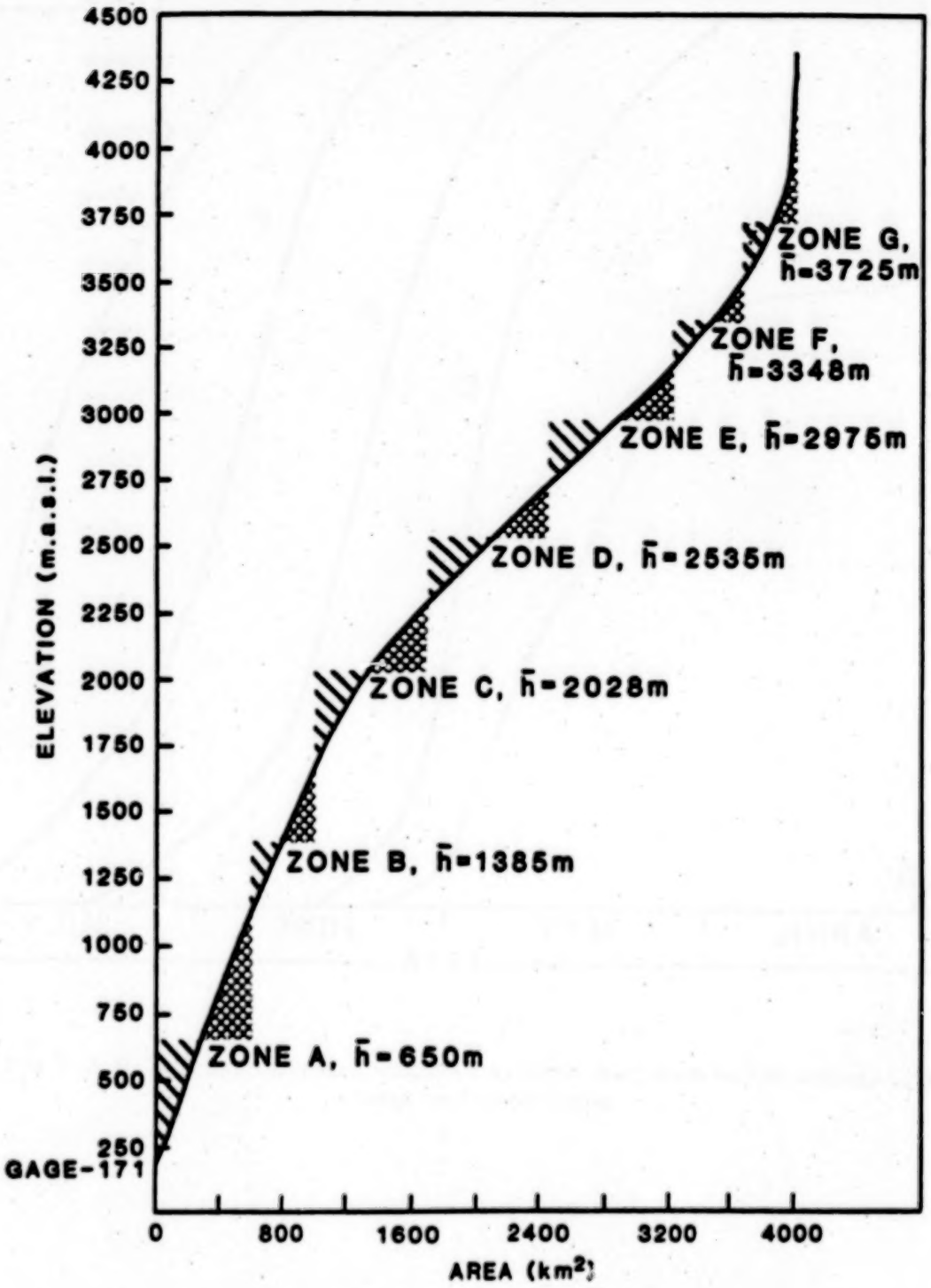

Figure 4. Determination of zonal mean hypsometric elevations ($\bar{h}$) using an area-elevation curve for the Kings River Basin, California

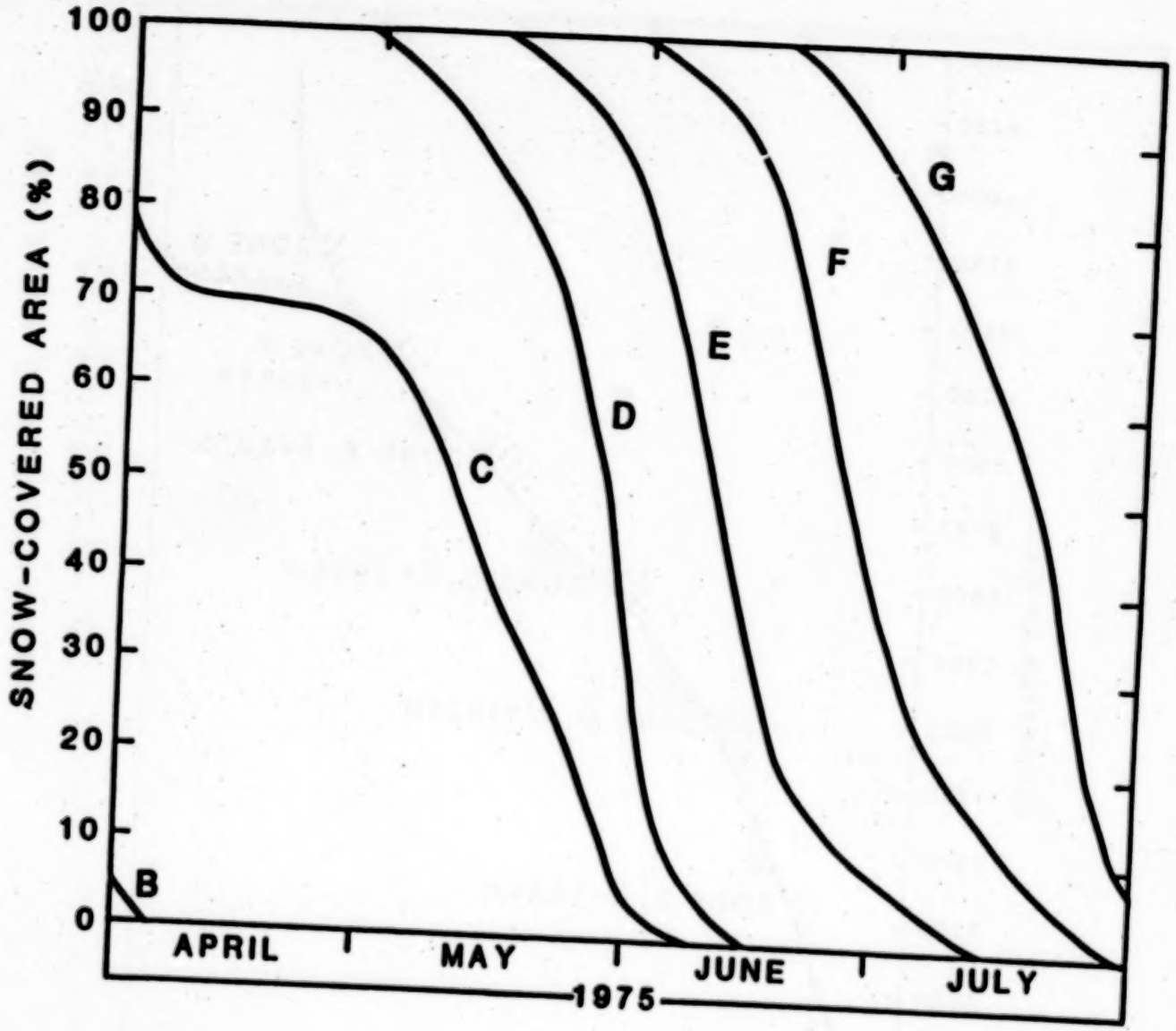

Figure 5. Landsat derived snow-cover depletion curves for elevation zones B, C, D, E, F and G in the Kings River Basin

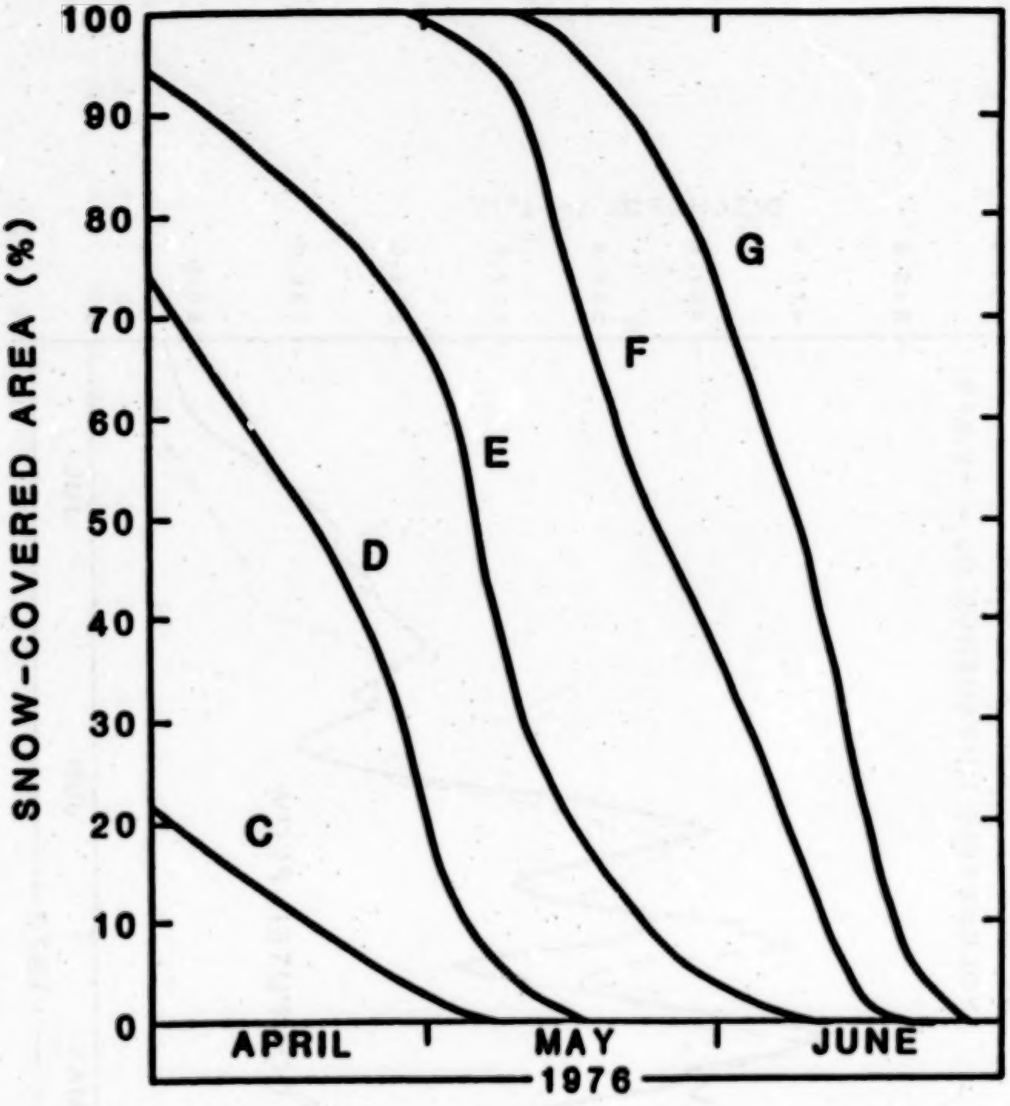

Figure 6. Landsat derived snow-cover depletion curves for elevation zones C, D, E, F and G in the Kings River Basin

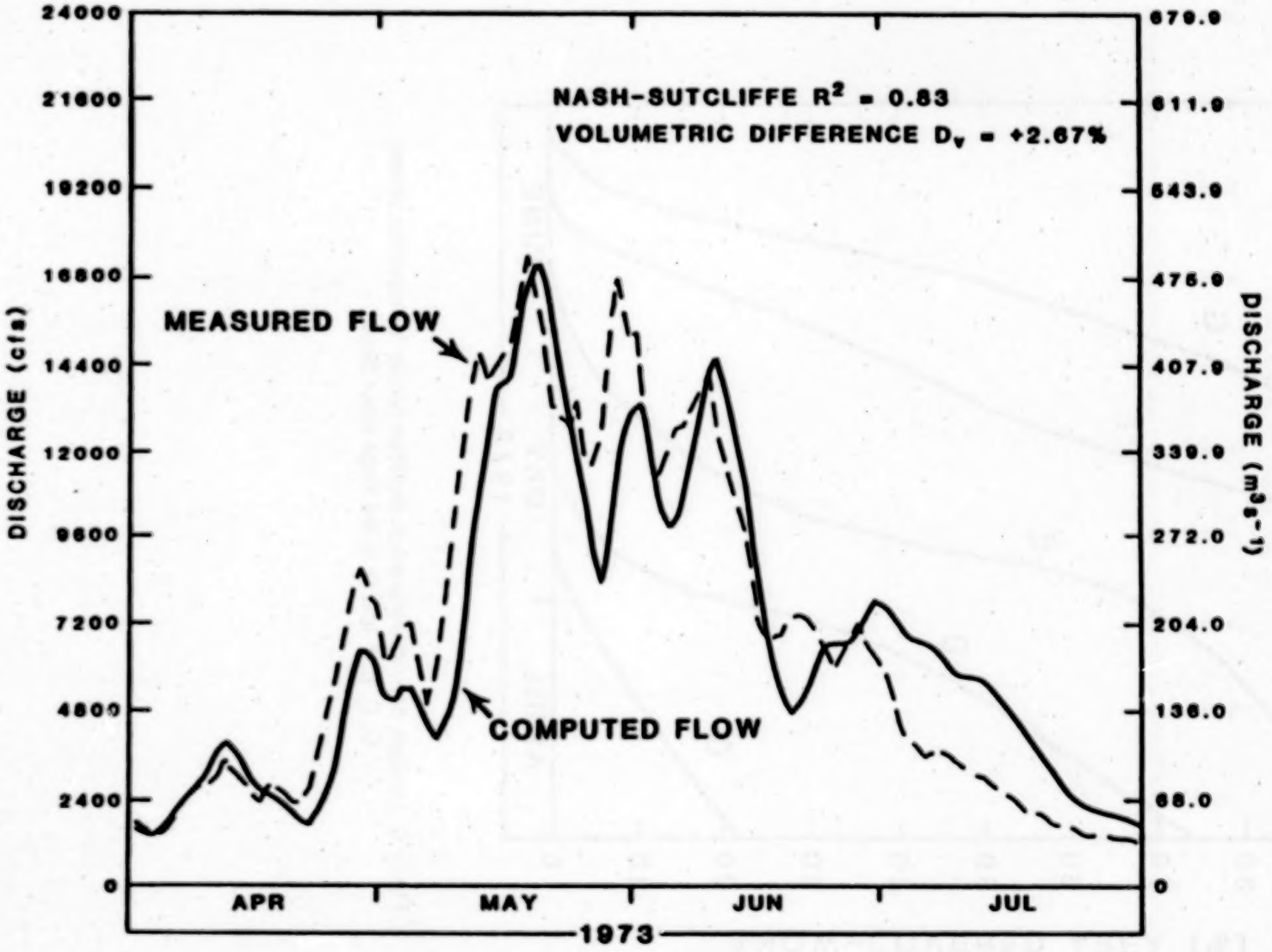

Figure 7. Discharge simulation for the Kings River Basin (3999 km²), California using the snowmelt-runoff model

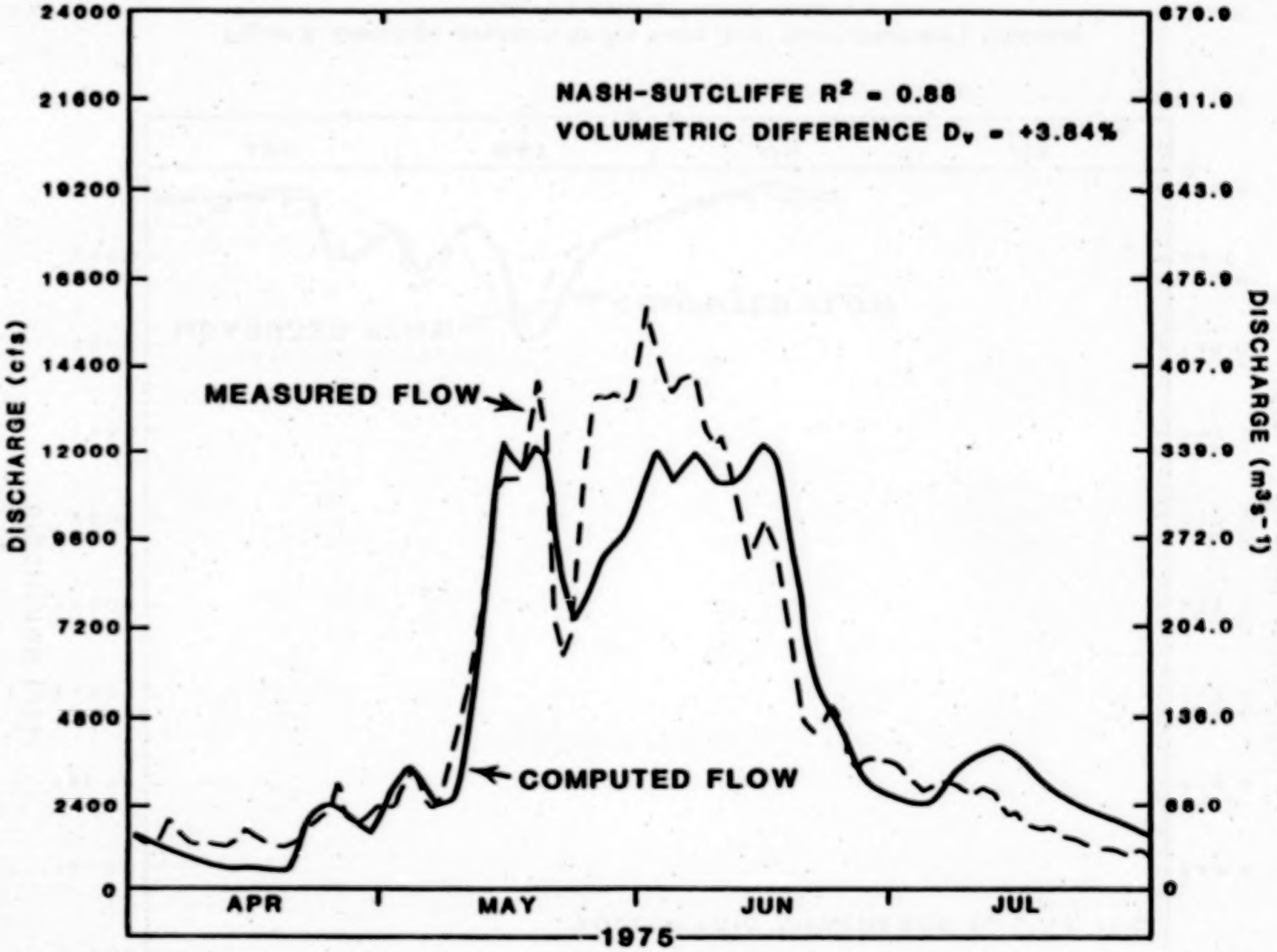

Figure 8. Discharge simulation for the Kings River Basin (3999 km²), California using the snowmelt-runoff model

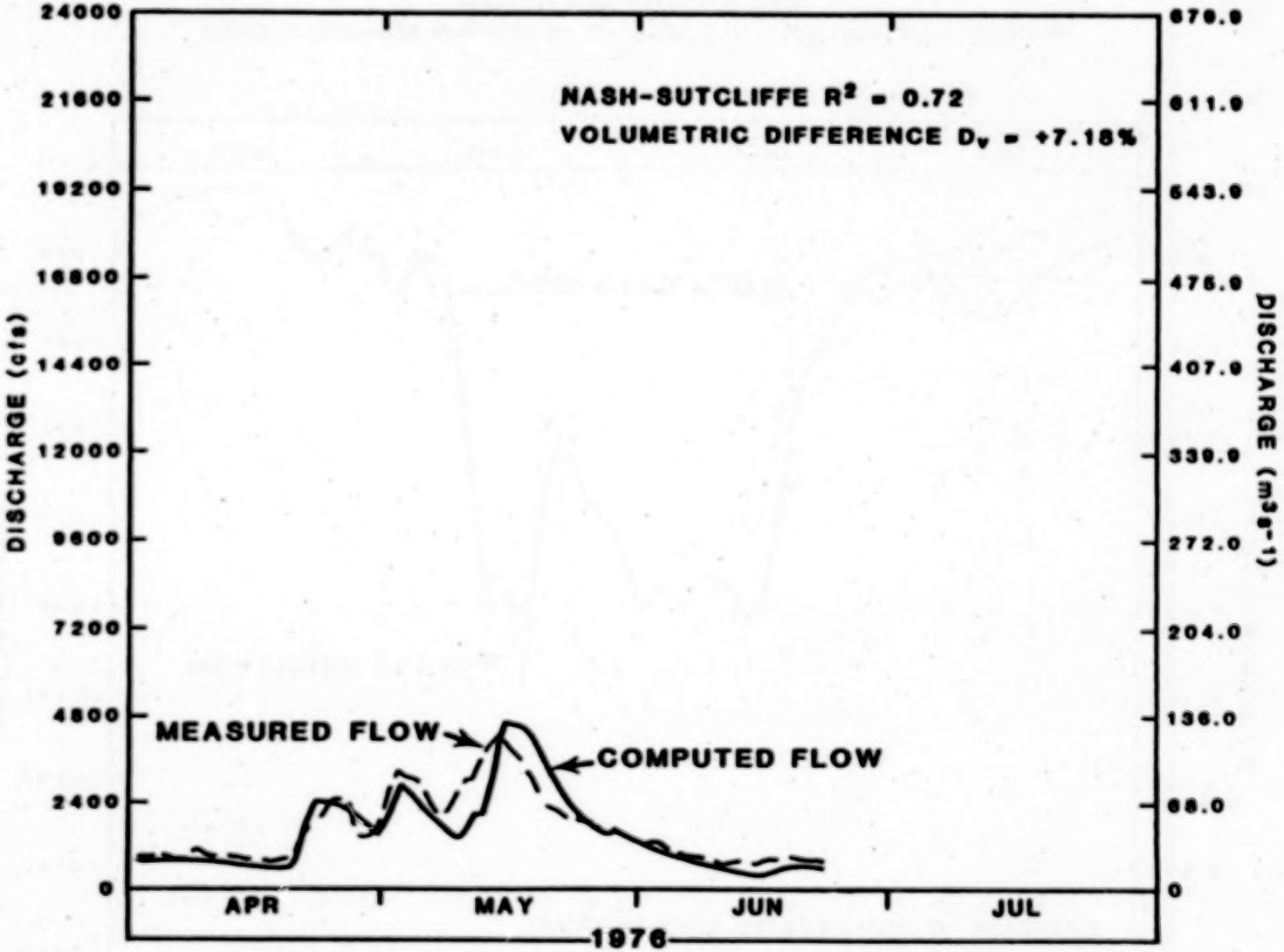

Figure 9. Discharge simulation for the Kings River Basin (3999 km²), California using the snowmelt-runoff model

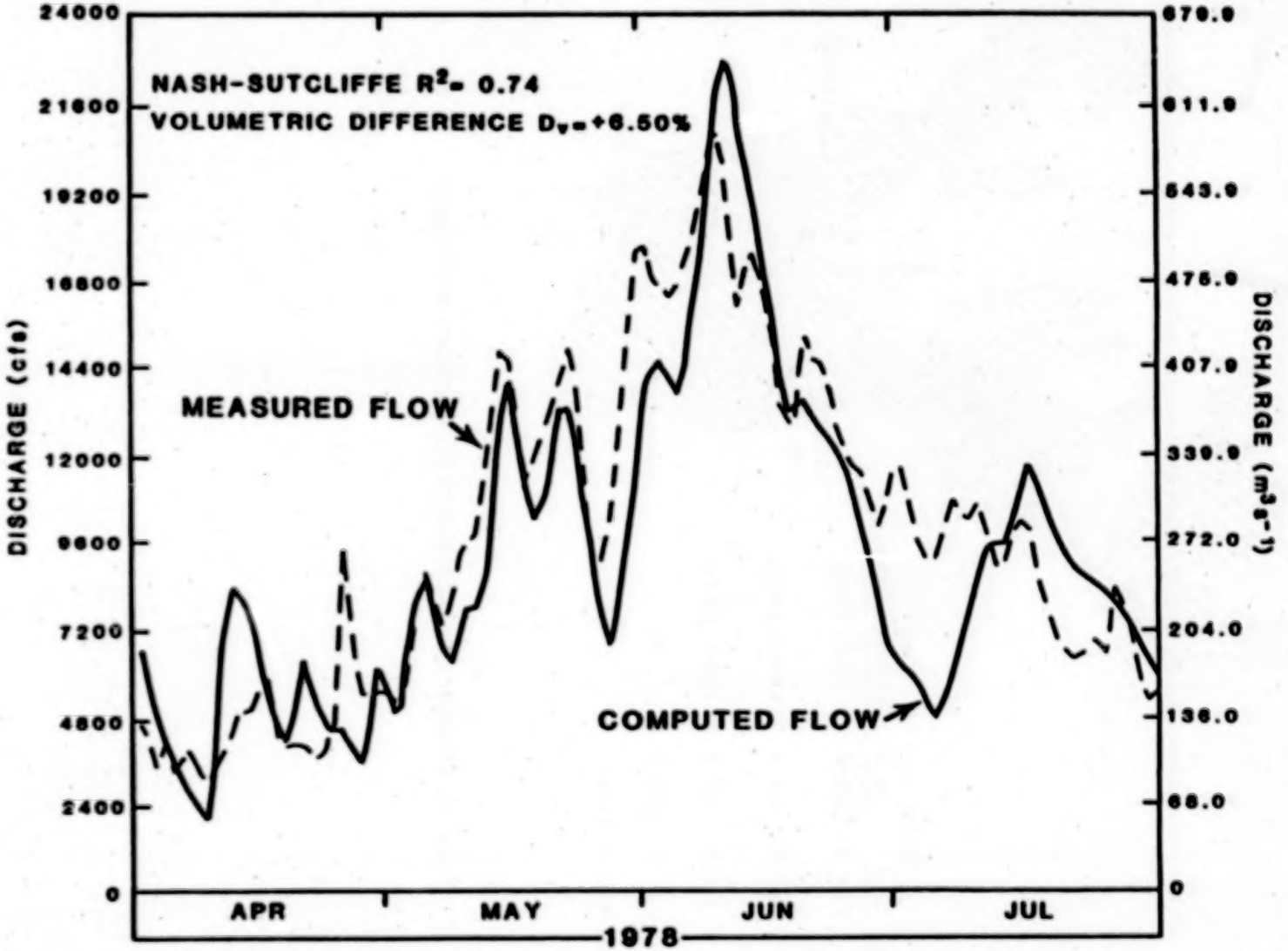

Figure 10. Discharge simulation for the Kings River Basin (3999 km^2), California using the snowmelt-runoff model

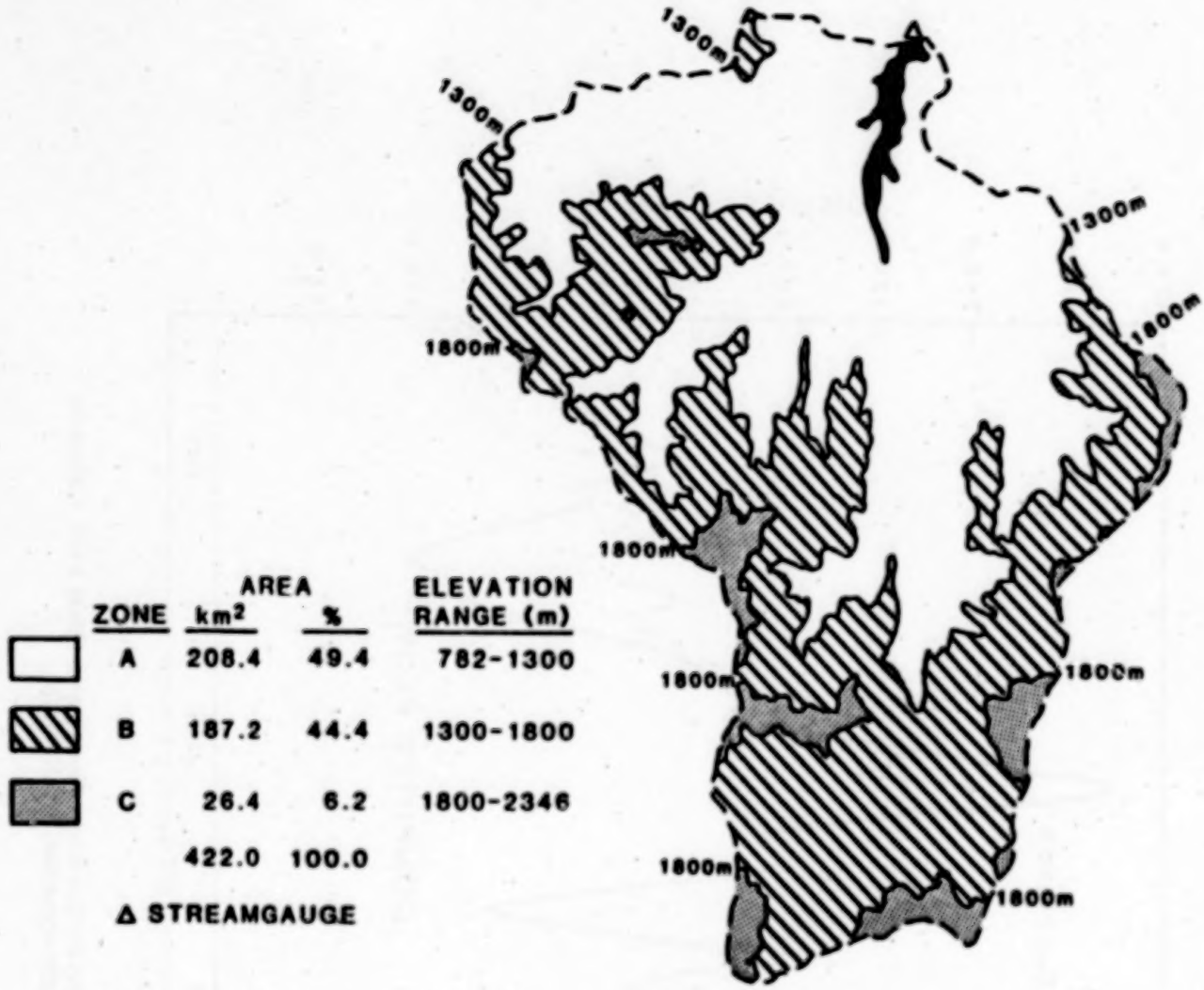

Figure 11. Elevation zones and areas of the Okutadami Basin, Japan

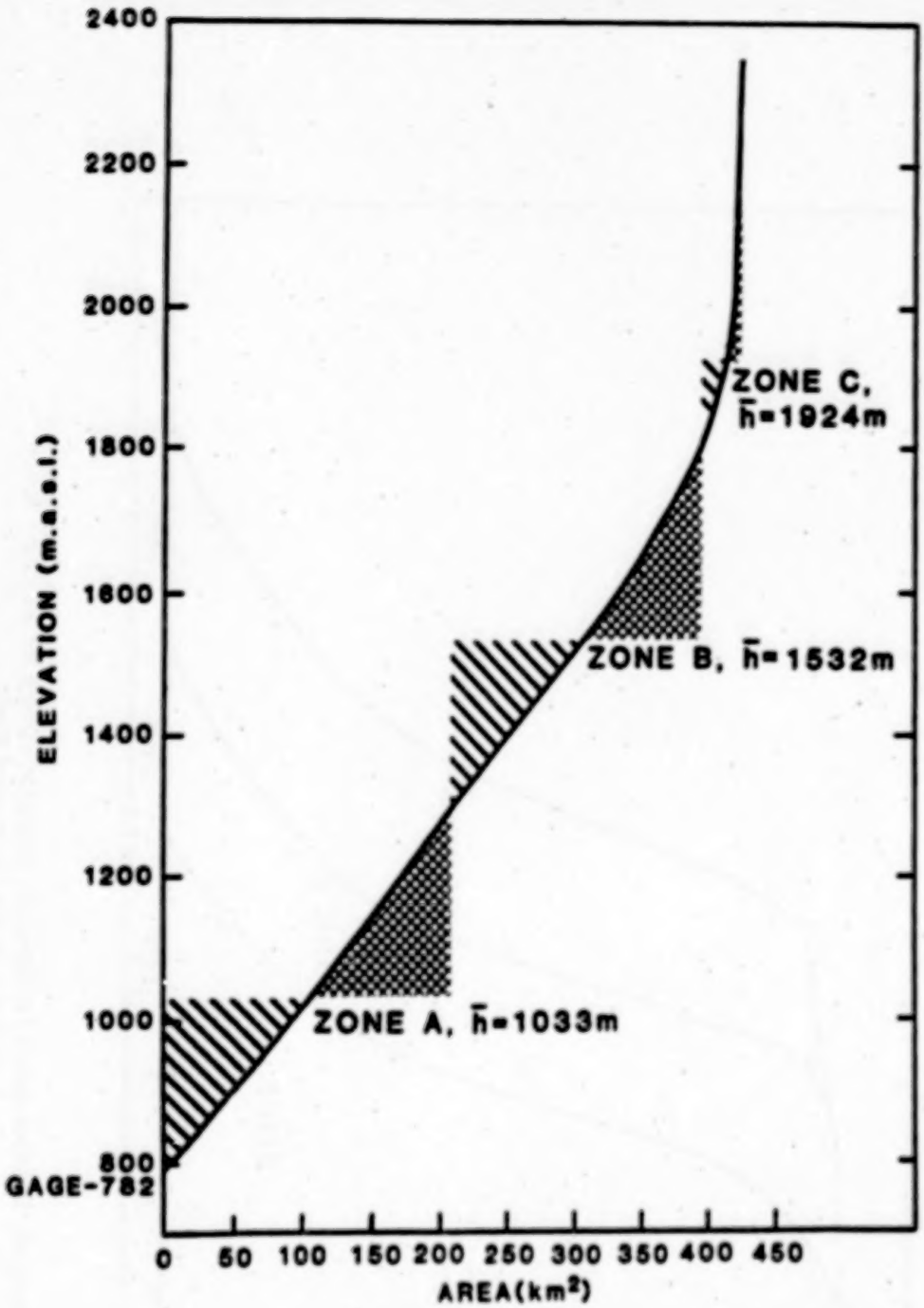

Figure 12. Determination of zonal mean hypsometric elevations ($\bar{h}$) using an area-elevation curve for the Okutadami Basin, Japan

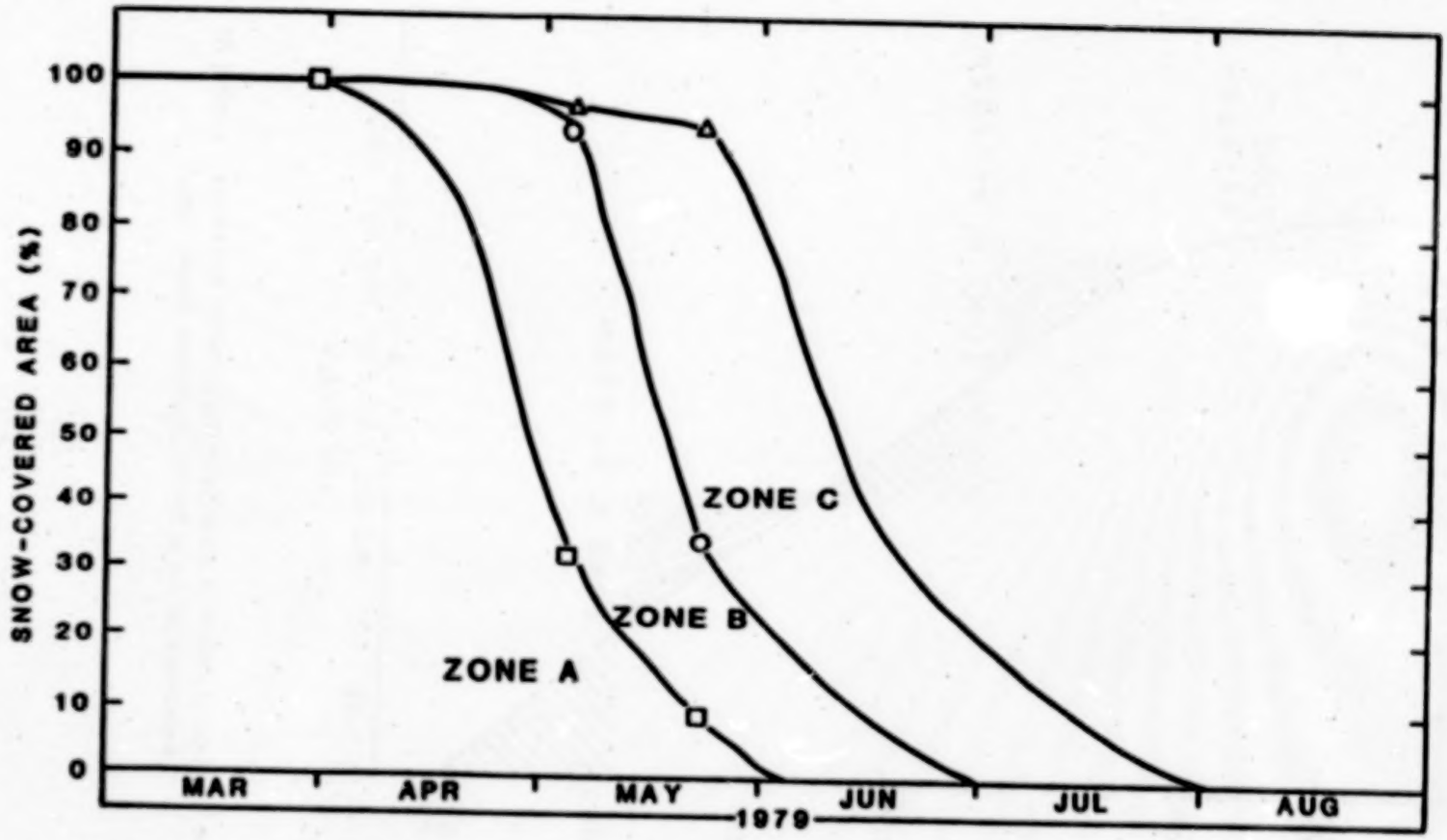

Figure 13. Landsat derived snow-cover depletion curves for elevation zones A, B and C in the Okutadami Basin

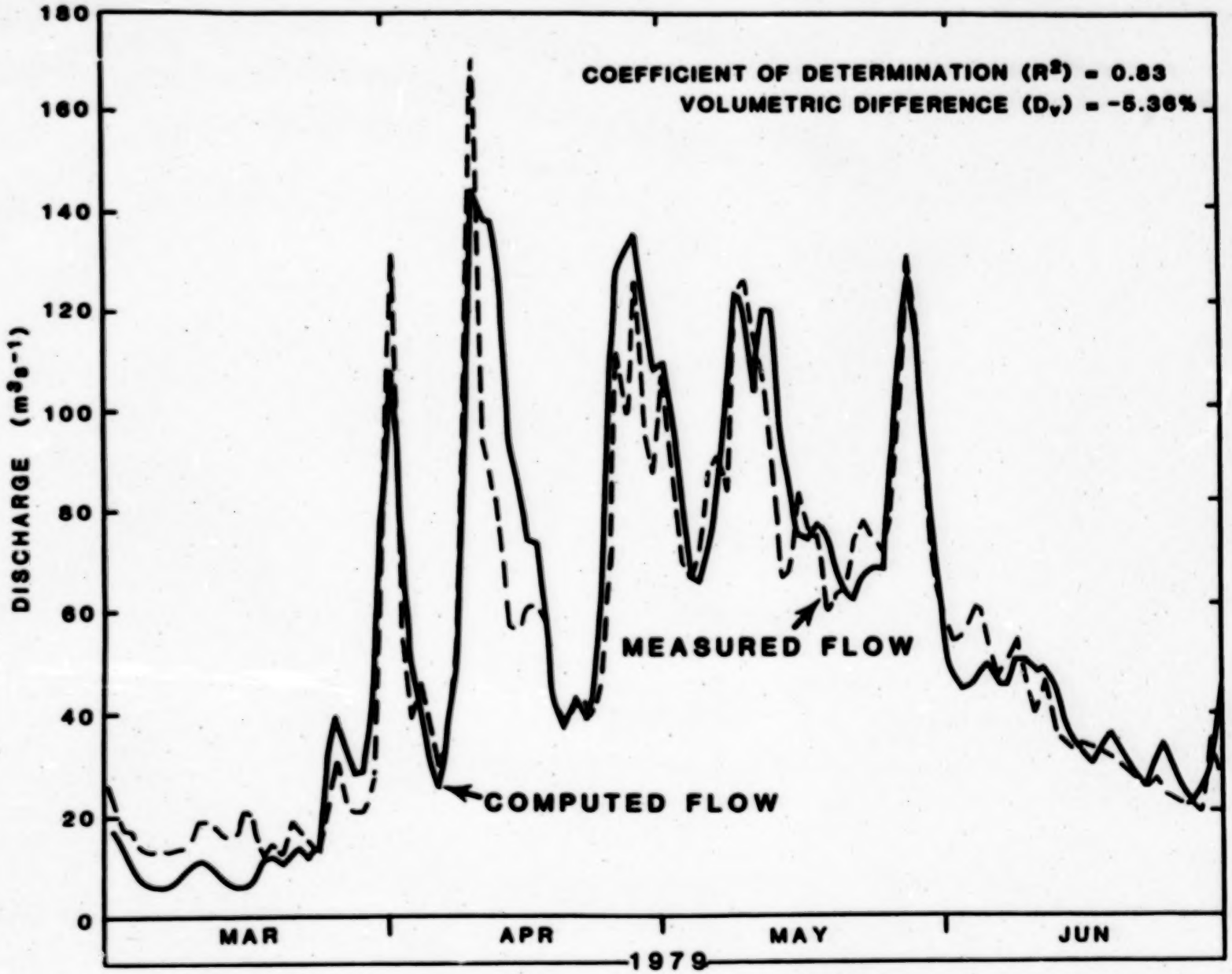

Figure 14. Discharge simulation for the Okutadami Basin (422 km^2), central Japan using the snowmelt-runoff model

N85-23227 D4

SNOWMELT RUNOFF MODEL IN JAPAN

Kenji Ishihara and Yoshiaki Nishimura
Environmental Research & Technology Institute

Kaname Takeda
National Institute of Resources
Science and Technology Agency

INTRODUCTION

Preliminary results [1] of Japanese snowmelt runoff modelling were proposed at First Japan/US Snow and Evapotranspiration Workshop held in Tokyo on March, 1982. Aiming at the daily snowmelt runoff forecasting, the preliminary model was designed through multiple regression analyses based on the hydrological conception. However, it involved several operational defects as follows:

i) containing three input variables of mean air temperature, precipitation and snow cover area at the day of which the inflow ought to be forecast.
ii) insufficient concordance between the hydrological conception and the parameters which resulted from the multiple regression analyses.

In the present study the model was, then, so modified that all the input variables are of the antecedent days. The inflow of the previous day is also taken into account. The new model was developed in use of the 1980 data in the Okutadami River Basin, chosen again as the test basin, and was adapted to the other years for its operative efficiency.

The optimum contribution of the Satellite imagery to the snowmelt runoff forecasting is the extraction of the snow coverage. Japan is, unfortunately, covered with much cloud in snowmelt season. Only in a fortunate season, one can obtain only one or two useful imagery. Unlike US it is, therefore, impossible in Japan to draw the depletion curve of snow coverage based on the imageries. However, a few imageries obtained in the past were effectively utilized for the verification and modification of the depletion curve induced from the snow water equivalent distribution at maximum stage and the accumulated degree-days at one representative point selected in the basin. This point is equipped with data collection facilities and is expected to fully function as DCP.

Together with the depletion curve, the relationship between the basin-wide daily snowmelt amount and the air temperature at the point above were exhibited in form of nomograph for the convenience of the model user.

The Japanese model proposed in the present study is, thus, the practical model of the snow melt runoff forecasting.

TEST BASIN

The Okutadami River basin (area 414 km^2) chosen as the test basin for this analysis is situated in Central Japan shown in Figure 1. The highest and lowest altitudes of the basin are 2346 m and 782 m respectively. The altitude difference is, therefore, 1564 m. This basin is one of the heaviest

snowfall area in Japan; the maximum snow depth recorded in recent 20 years was 598cm at Okutadami Meteorological Observing Station located at the dam site in the basin. The station runs the measurement of snow water equivalent and inflow into the reservoir as well as the general meteorological observation. Located slightly outside the basin is the Hinoemata meteorological observing station of air temperature and precipitation. Two stations above and the representative point (mentioned later), Maruyama, provide all the necessary input data of the model. Those locations are shown in Figure 2.

The snow depth measurements by helicopter at ten to twenty points scattered in the basin are carried out at the maximum stage of snow depth at about the end of every winter season by the Electric Power Development Company. The measurement points by helicopter are shown in Figure 3.

CONCEPT OF SNOWMELT RUNOFF MODEL

Two forms of multiple regression models were considered. First model is as follows;

$$R_n = c + a_1X_{n-1} + a_2X_{n-2} + a_3X_{n-3} + b_1Y_{n-1} + b_2Y_{n-2} + b_3Y_{n-3} \quad (1)$$

$$X_{n-i} = (M_{n-i} + P_{n-i})S'_{n-i} \quad (2)$$

$$Y_{n-i} = P_{n-i}S''_{n-i} \quad (3)$$

where

R_n : daily direct inflow (m^3/sec) into reservoir on the day, n

c : constant

$a_1, a_2, a_3, b_1, b_2, b_3$: partial regression coefficient

M_{n-i} : mean snowmelt amount on the day n−i ($m^3 \cdot sec^{-1} \cdot km^{-2}$)

P_{n-i} : mean rainfall amount on the day n−i ($m^3 \cdot sec^{-1} \cdot km^{-2}$)

S'_{n-i} : area where daily mean air temperature is above 0°C within snow cover area on the day n−i (km^2)

S''_{n-i} : area where daily mean air temperature is above 0°C within non-snow cover area on the day n−i (km^2)

The second model, in which the direct inflow of the previous day, R_{n-1}, is added to the variables of the first model, is as follows;

$$R_n = c + dR_{n-1} + a_1X_{n-1} + a_2X_{n-2} + a_3X_{n-3} + b_1Y_{n-1} + b_2Y_{n-2} + b_3Y_{n-3} \quad (4)$$

where

d : partial regression coefficient

DEPENDENT VARIABLE

Direct Inflow

The dependent variable of the model is the daily direct inflow, R_n, into the reservoir. The base flow which should be subtracted from the daily inflow to obtain the direct inflow, R_n, is expressed by

$$r_t = r_0 (1.0+0.00124t) \quad (5)$$

where

r_t : base flow after t days from the day when first discharge occurs due to snowmelting in the season (m^3/sec)

r_0 : inflow before the snowmelt season starts (m^3/sec)

The equation (5) was empirically determined by the inflow data recorded at the beginning and end of the several snowmelt seasons

INDEPENDENT VARIABLES

Snow Cover Area and Its Related Areas, S_{n-1}, S'_{n-1} and S''_{n-1}

The snow coverage information from Landsat MSS is scarcely obtainable in Japan. Then, the snow line during snowmelt season was considered to appear when snow water equivalent in a mesh (shown in Figure 2) became equal to the snowmelt amount which can be calculated by the degree-day method (mentioned later). In order to extract the snow line, the computation of the snow water equivalent in each mesh at the maximum stage is required. Then, the computation was made by following three methods; the topographic method [3] in use of the extensive snow survey data in 1980, the degree-day method [4] in effective use of two Landsat MSS data fortunately obtained in 1979 and the comparison method [5] in use of the regional snow depth data obtained for several years with helicopter. Next, the date when all the snow deposits disappear was calculated for each mesh, applying the degree-day method. The snow cover area and its related areas, s_{n-1}, s'_{n-1} and s''_{n-1} were then counted for every day during each snowmelt season.

Total Snowmelt Amount, $M_{n-1} \cdot S'_{n-1}$

The degree-day method was adopted for the snowmelt calculation, expressed by

$$M = K\Sigma T \quad (6)$$

where

M : snowmelt amount (g/cm^2)

ΣT : accumulated daily mean air temperature above 0℃ (℃•day)

k : degree-day factor (0.45; average value in preceding studies)

The daily mean air temperature at the Okutadami Meteorological Observing Station was adopted as the standard for the estimation of the air temperature at all meshes assuming the lapse-rate as -0.6 ℃/100 m.

Applying the equation (6), the calculation of the daily snowmelt amount was made for each mesh within the area, S'_{n-i}, during each snowmelt season. By summing up them, the total snowmelt amount in whole basin, $M_{n-i} \cdot S'_{n-i}$ was then obtained.

Total Rainfall Amount, $P_{n-i} \cdot S'_{n-i}$ and $P_{n-i} \cdot S''_{n-i}$

The Okutadami Station is the only one rainfall observation station within the basin running throughout snowmelt season. However, located at the lowest elevation and the northern edge of the basin, it does not give the mean rainfall of the basin. Then, the Hinoemata Station was adopted for this purpose, although it is located at slightly outside the basin. After careful meteorological inspection, it was assumed that the precipitation at Hinoemata is equal to the rainfall amount in each mesh where the daily mean air temperature is above 0℃ both in snow cover and non-snow cover area. The total rainfall amount, $P_{n-i} \cdot S'_{n-i}$ and $P_{n-i} \cdot S''_{n-i}$ were then obtained.

CONSTRUCTION OF SNOWMELT RUNOFF MODEL

Now, all the input data were prepared for the determination of the constant and partial regression coefficients of the equations (4) and (5). The multiple regression analyses were, then, carried out in use of data in 1980. The resultant constructed two models are presented in Table 1.

The comparison between the observed and calculated inflow, exhibited in Figures 4 and 5, shows that the models would stand the practical use the snowmelt runoff forecasting.

NOMOGRAPHS FOR PRACTICAL USE OF MODELS

In course of the model construction, the input variable values were obtained through the complex calculation procedure relating to the mesh. Necessary for the convenience of the practical use of the models is an easy acquisition of the input variable data. Following nomographs were, then, devised.

Nomograph (I) for Basin-Wide Snow Amount at Maximum Stage

The Maruyama shown in Figure 2 was selected among several tens proposed sites in the basin as the best representative site, whose snow water equivalent has a linear correlation with the basin-wide snow amount throughout both snowfall and snowmelt seasons. Based on the six years data is

Figure 6 (nomograph (I)), which exhibits a relationship between the basin-wide snow amount and Maruyama's snow water equivalent at the maximum stage.

The Maruyama is situated at roughly mean altitude of the whole basin and is at present equipped with DCP.

Nomograph (II) for Snow Cover Area

The depletion curve of snow cover area with increasing degree-day at the Maruyama was obtained for four snowmelt seasons, and is exhibited in Figure 7. The curves seem to depend on the snow amount at the maximum stage. Then, the relation was investigated between the snow amount above and the Maruyama's degree-day accumulated up to the first day when the bare ground appears somewhere in the basin, namely, $S_{n-i}/A<1$. A is the basin area. A linear correlation was found as shown in Figure 8. Based on this correlation, the depletion curve was standardized. The resultant curve shown in Figure 9 is the nomograph (II).

Nomograph (III) for Basin-Wide Snowmelt Amount

A clear relation was found between the basin-wide daily snowmelt amount and the daily mean air temperature at the Maruyama through the medium of the ratio (S_{n-i}/A). This relation shown in Figure 10 is the nomograph (III) for $M_{n-i}-S'_{n-i}$.

Nomograph (IV, V) for Basin-Wide Rainfall

In the models, two kinds of basin-wide rainfall amount are taken into account; one in the snow cover area (S_{n-i}) and another in the non-snow cover area ($A-S_{n-i}$).

Regarding the snow cover area, the extraction of the area ($S'_{n-i}n-i$) where the daily mean air temperature is above 0℃ is necessary. For simplicity, the relation was obtained between the total rainfall amount ($P_{n-i}\cdot S'_{n-i}$) and the Hinoemata precipitation (P_{n-i}) through the medium of the product of the Okutadami daily mean air temperature and the ratio (S_{n-i}/A). The relation shown in Figure 11 is the nomograph (IV) for $P_{n-i}\cdot S'_{n-i}$.

As for the non-snow cover area, this area is usually above 0℃ during a snowmelt season, so that $S''_{n-i}n-i \div A - S_{n-i}$. Exhibited in Figure 12 is the nomograph (V) for $P_{n-i}\cdot S''_{n-i}$.

VERIFICATION OF SNOWMELT RUNOFF MODELS

In order to verify the models (Table 1 constructed for the 1980 data, the models were applied to the other two years, 1979 and 1982. All the input values were obtained in use of the nomographs (I)-(V). The results are shown in Figures 13-16. A good agreement can be seen except May 26-28, 1979. A large difference in this period may be caused by heavy rainfall unusually in a snowmelt season which occurred on May 26 and 27. In Japan the rainy season starts at the beginning of June, and often heavy rainfall occurs. The fact above shows that the models should not be applied in case the heavy rainfall happened near the end of snowmelt season when the snow cover area shrinks up to the top of the high mountains.

CONCLUSION

In the present study scarce Landsat MSS data obliged the limited but efficient utilization for the verification of the depletion curve of the snow cover area. In order to construct the models, the complex topographic mesh analyses were carried out. However, the data of final necessity become only the mean air temperature and precipitation for the daily use of the models.

The runoff forecasting procedure is summarized in Figure 17.

REFERENCES

1. Ishihara K., M. Matsuda, Y. Nishimura and K. Takeda (1982): Snowmelt runoff model in Japan. Proc. of First Japan/US Snow and Evapotranspiration Workshop, Mar. 1982, Tokyo, p. 1-24.

2. Martinec, J., A. Rango and E. Major (1983). The Snowmelt-Runoff Model (SRM) User's Manual. NASA Reference Publication 1100, P. 1-110.

3. Ishihara, K. (1956): Estimation of Snow Depth at Ungauged Point Using Regression Analysis of Topographic Effects. Journal of the Japanese Society of Snow and Ice, Vol. 33, No. 3, p. 134-138, (in Japanese).

4. Takeda, K. and Y,. Takahashi (1981): Estimation of Basin-wide Snow Water Equivalent Using Landsat-derived Snow Line and Degree-day Method. Proceedings of the Japan Society of Civil Engineers, No. 311, p. 81-92 (in Japanese).

5. Electric Power Development Company (1980): Data Report of Snow, Weather and Discharge in Okutadami Region (1957-1959). p. 1-424.

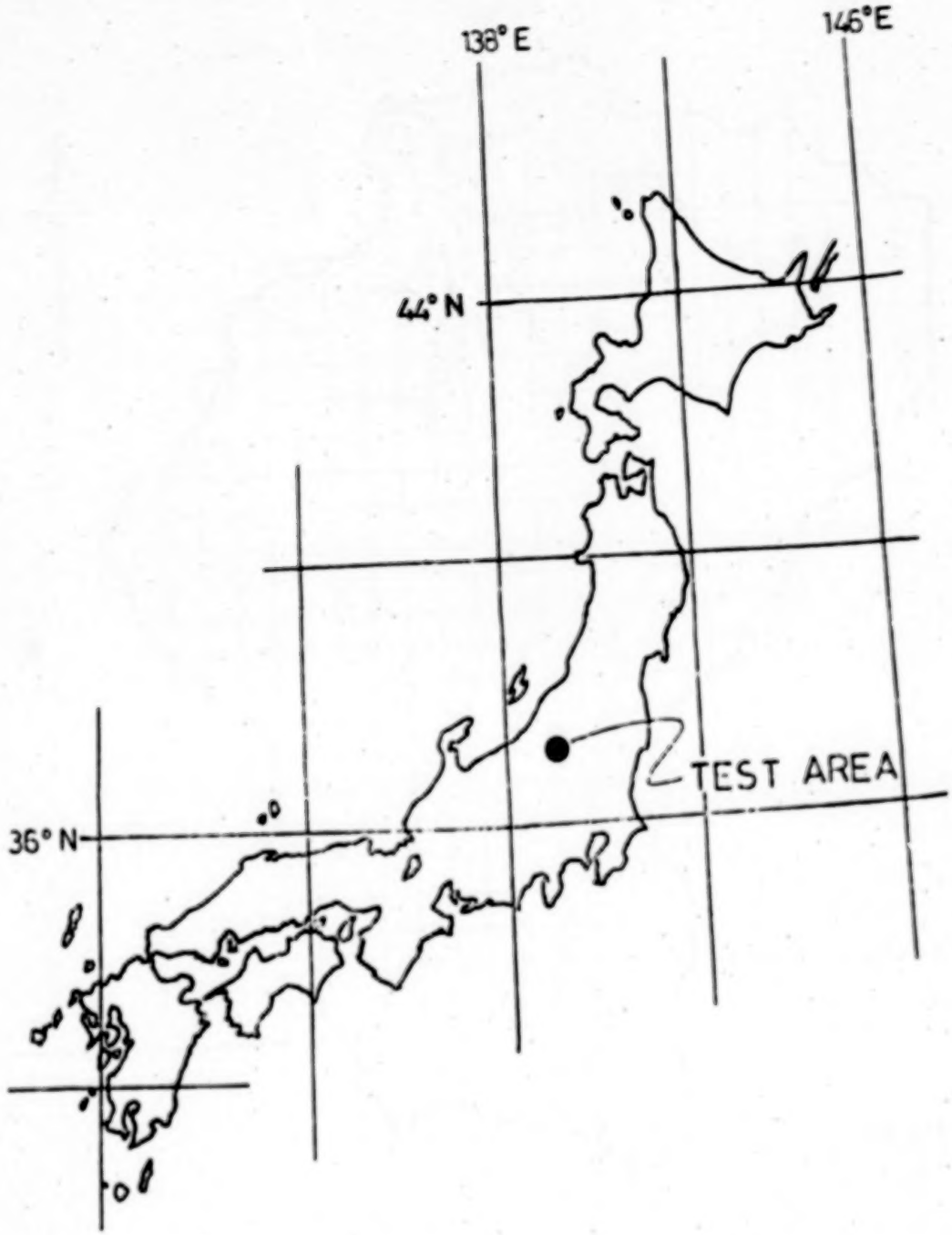

Figure 1. Location of The Test Basin

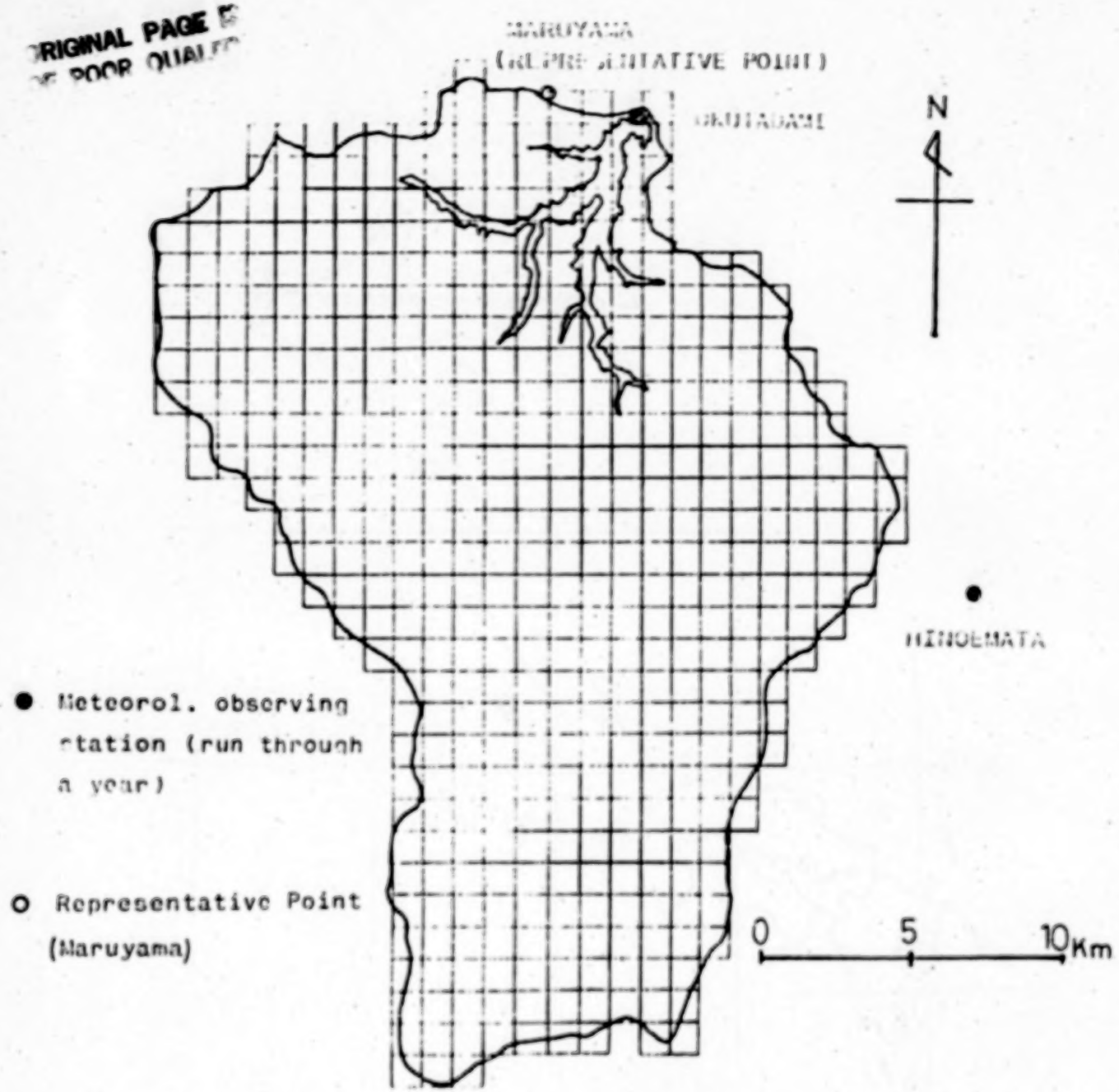

Figure 2. Location of Two Meteorological Observing Stations (Okutadami, Hinoemata) and Representative Point (Maruyama)

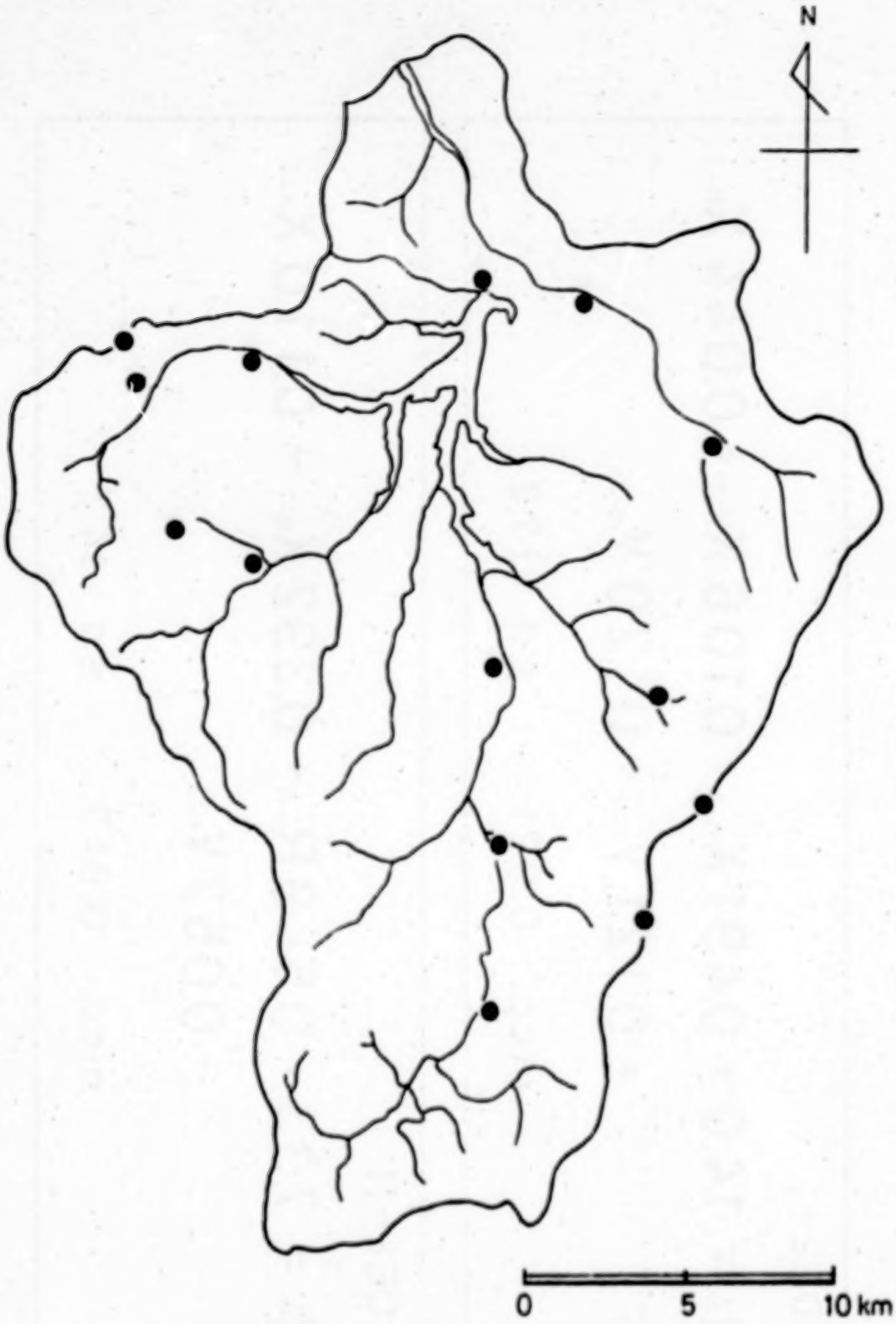

Figure 3. Locations of Points Where Snow Depth and Its Water Equivalent were Measured by Electric Power Development Co.

Table 1
Snowmelt Runoff Model

MODEL-I

$$R_n = 14.0 + 0.491\,X_{n-1} + 0.106\,X_{n-2} + 0.044\,X_{n-3} + 0.121\,Y_{n-1} + 0.120\,Y_{n-2}$$

m.c.c. : 0.921 s.d. : 17.2

MODEL-II

$$R_n = 7.33 + 0.549\,R_{n-1} + 0.392\,X_{n-1} - 0.110\,X_{n-2} - 0.057\,Y_{n-1}$$

m.c.c. : 0.943 s.d. : 14.7

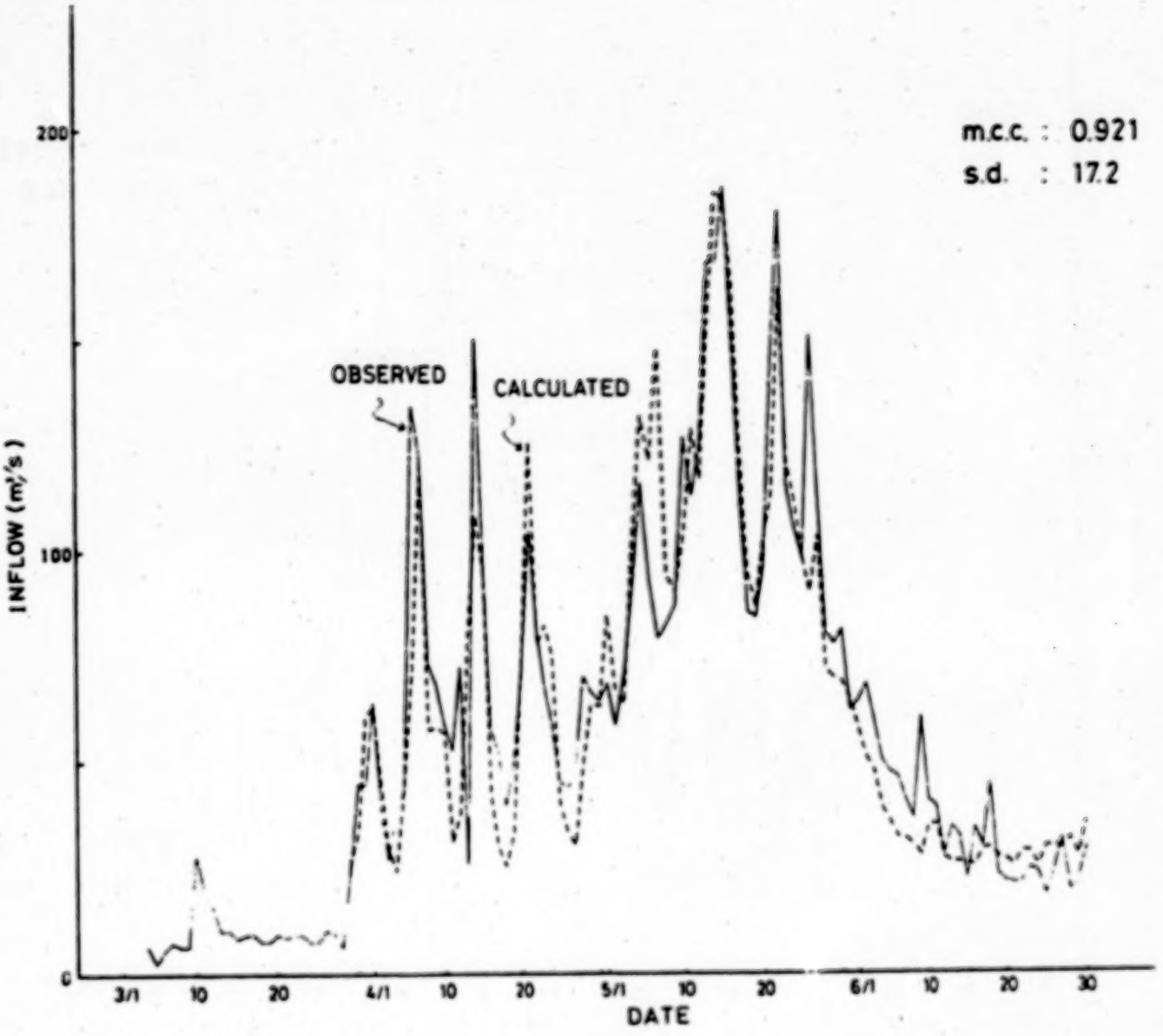

Figure 4. Comparison Between Observed (Solid Line) and Calculated (Broken Line) Inflow in Use of MODEL-I for 1980 Snowmelt Season

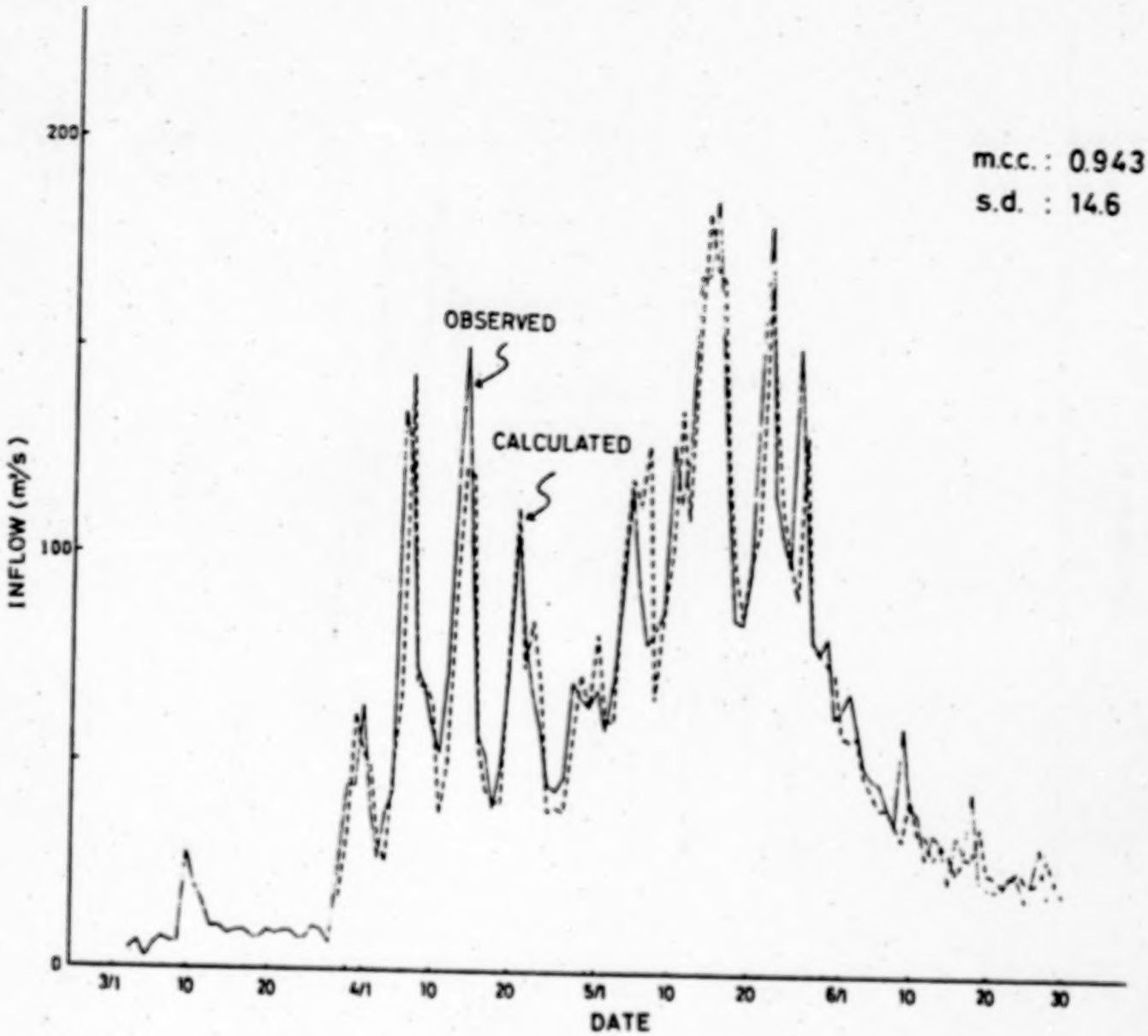

Figure 5. Comparison between observed (Solid Line) and Calculated (Broken Line) Inflow in Use of MODEL-II for 1980 Snowmelt Season

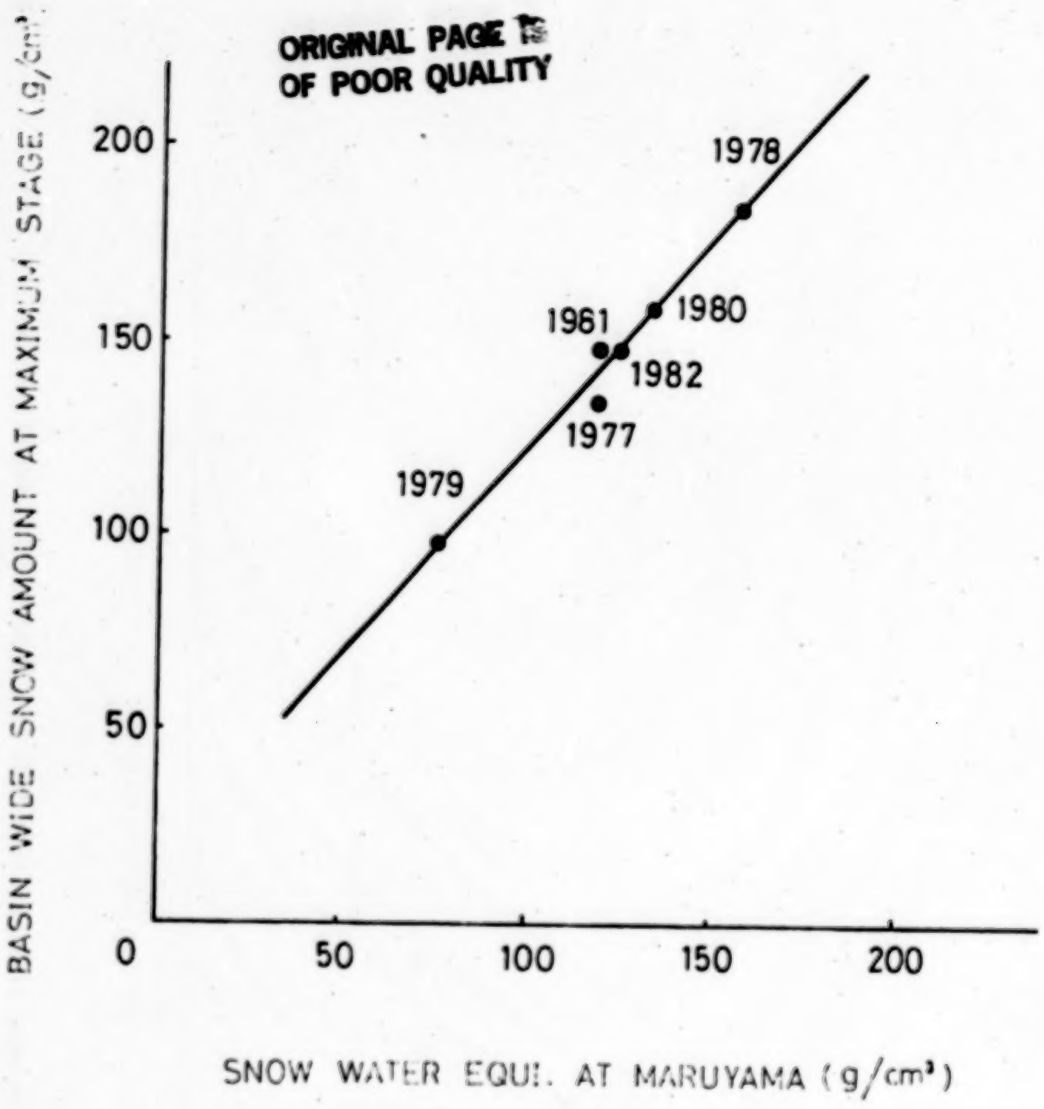

Figure 6. NOMOGRAPH(I) for Basin-Wide Snow Amount at Maximum Stage in Use of Snow Water Equivalent at Maruyama

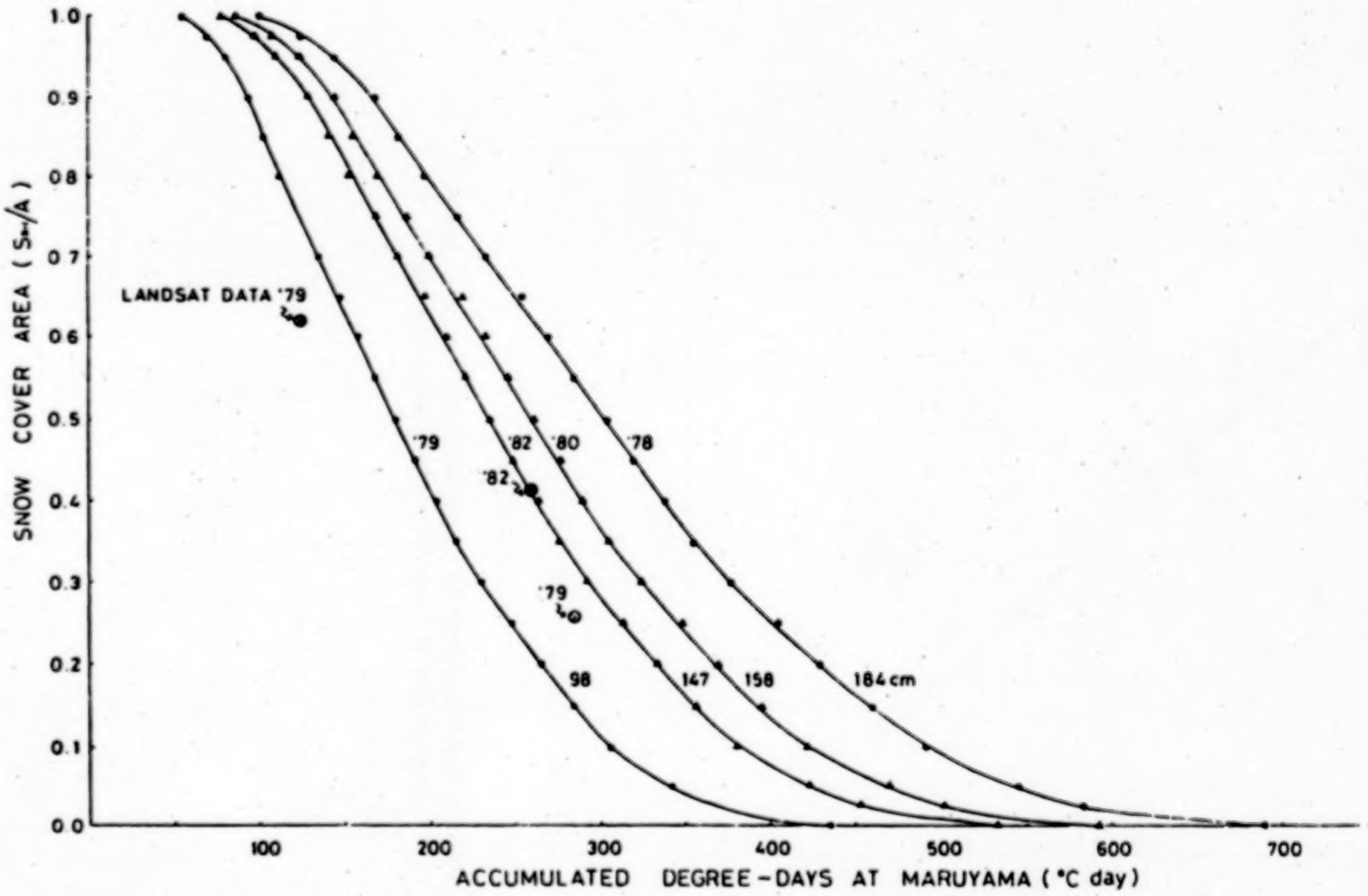

Figure 7. Relationship Between Depletion of Snow Cover Area and Accumulated Degree Days at Maruyama (Parameter: Basin-Wide Snow Amount at Maximum Stage)

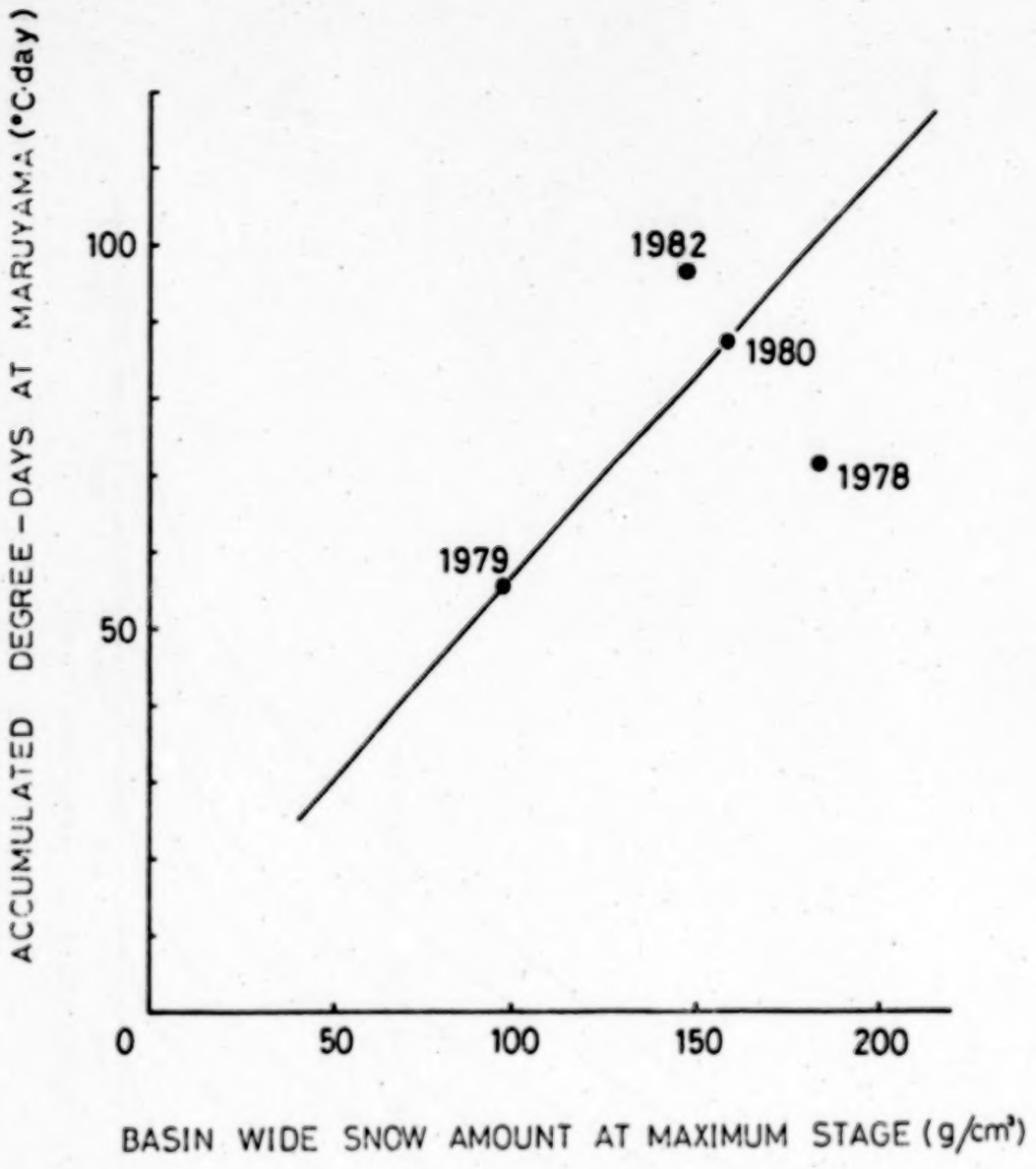

Figure 8. Relationship Between Basin-Wide Snow Amount and Accumulated Degree-Days at Maruyama Before Snow Cover Area Depletion Starts

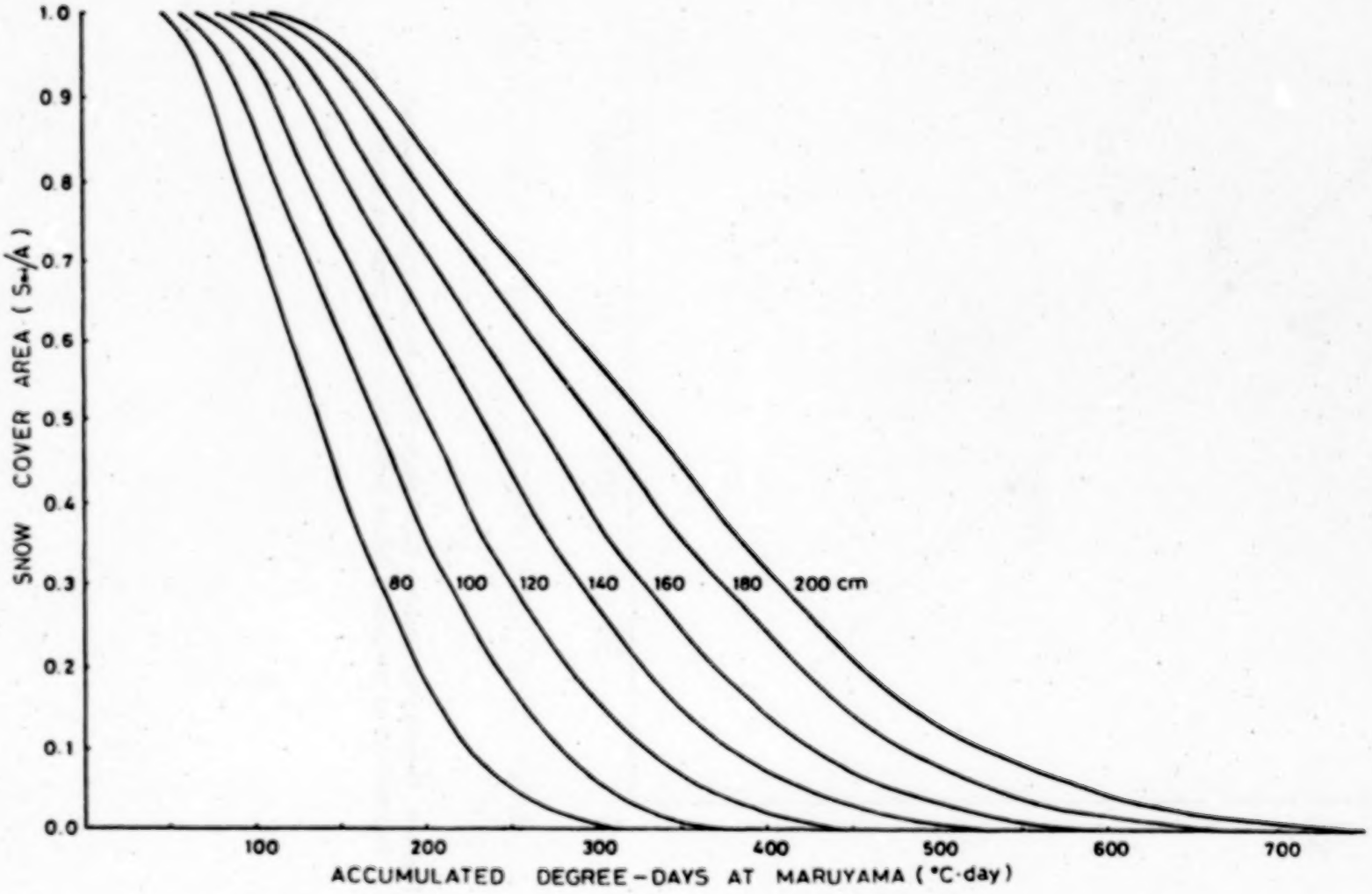

Figure 9. Nomograph(II) for Snow Cover Area. (Parameter: Basin-Wide Snow Amount at Maximum Stage.)

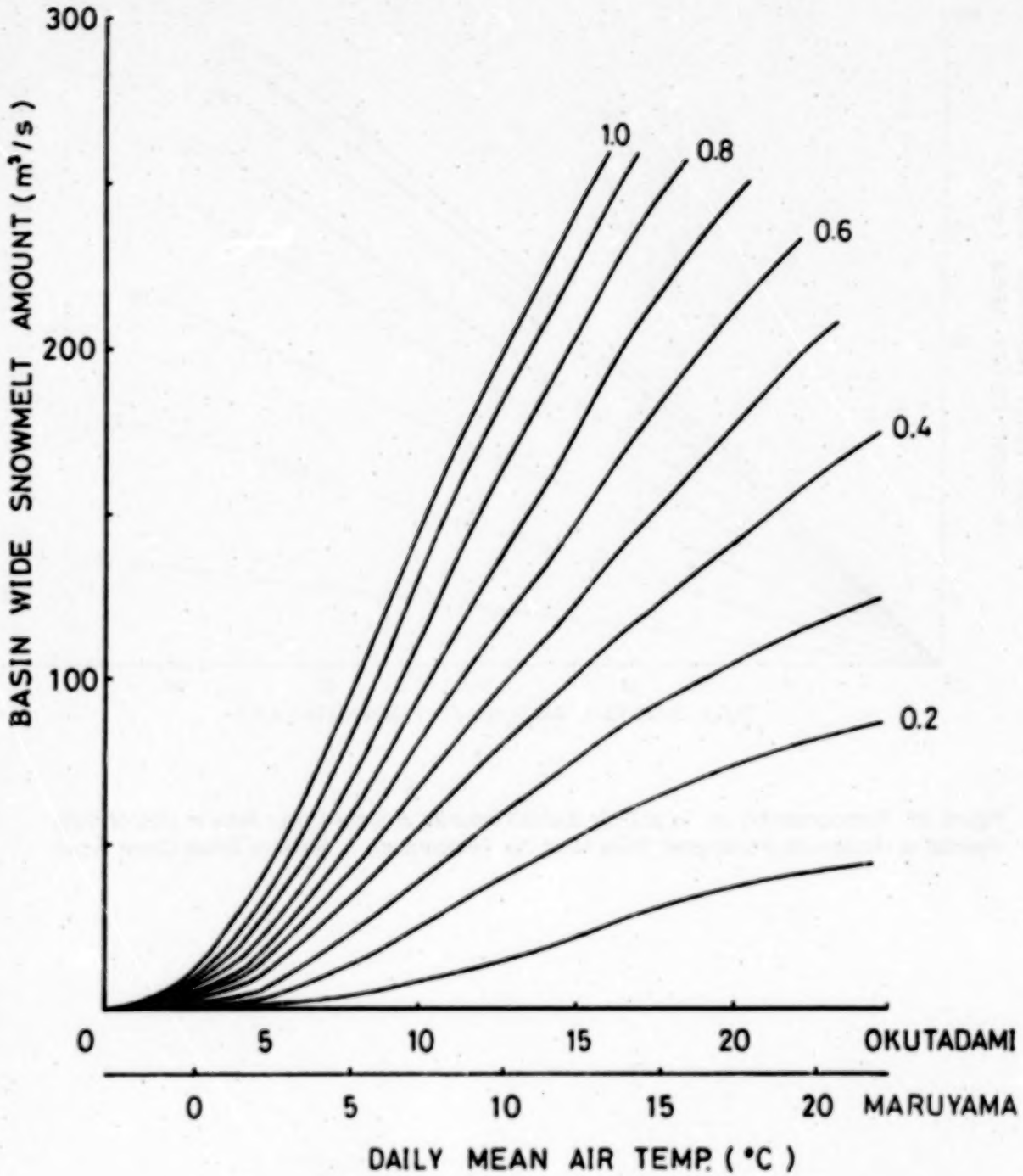

Figure 10. Nomograph(III) for Basin-Wide Snow-Melt in Use of Daily Mean Air Temperature at Maruyama. (Parameter: Relative Snow Cover Area, S_{n-1}/A)

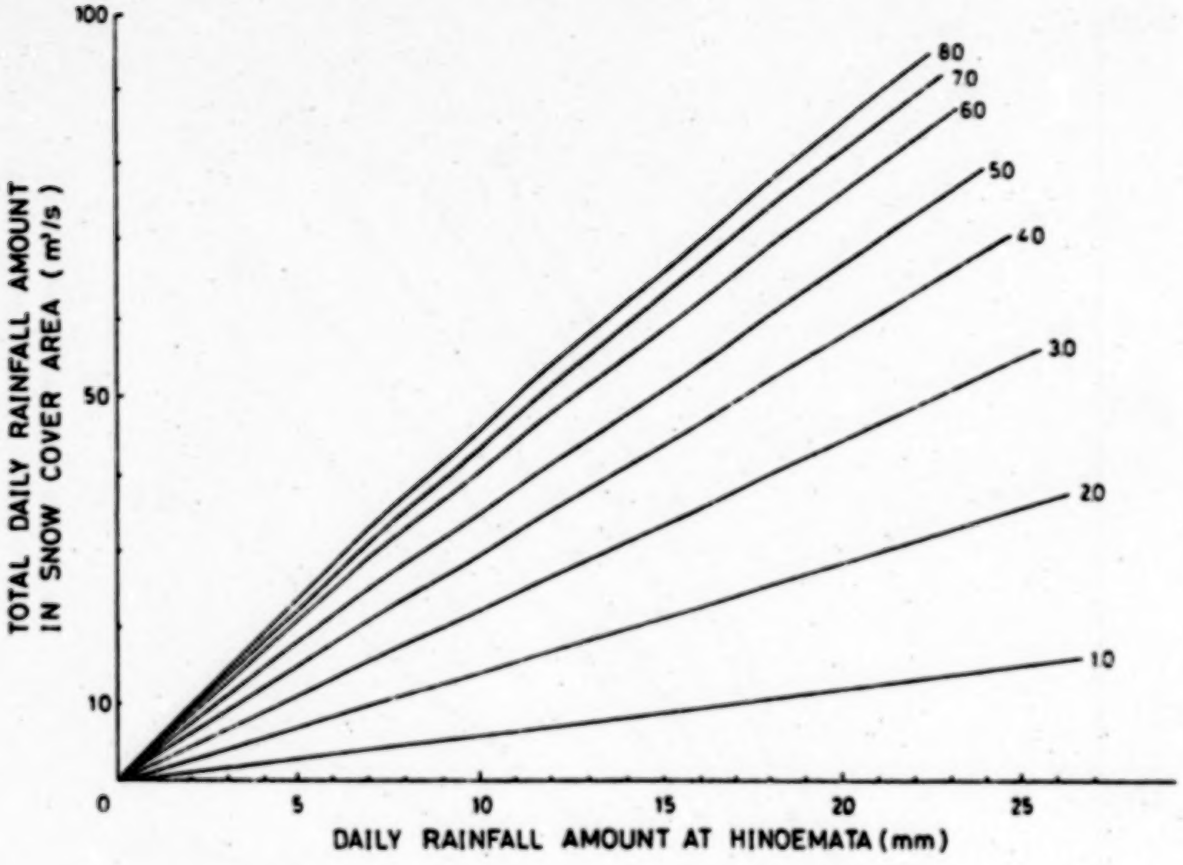

Figure 11. Nomograph(IV) for Total Daily Rainfall Amount in Snow Cover Area in Use of Daily Rainfall at Hinoemata (Parameter: Daily Mean Air Temperature × Relative Snow Cover Area)

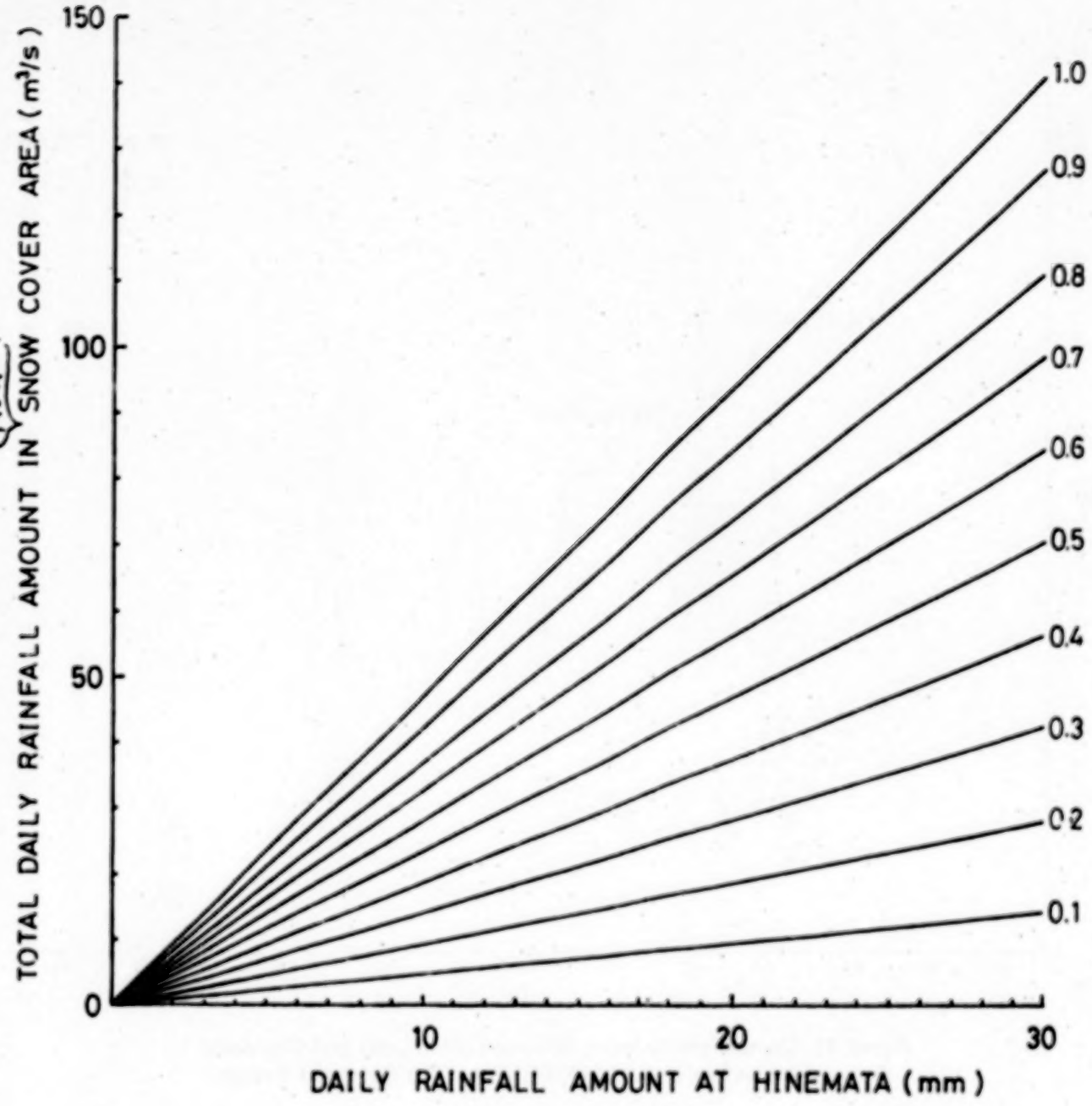

Figure 12. Nomograph(V) for Total Daily Rainfall Amount in Non-Snow Cover Area in Use of Daily Rainfall at Hinoemata Station. (Parameter: Relative Non-Snow Cover Area, $1-S_{n-}/A$)

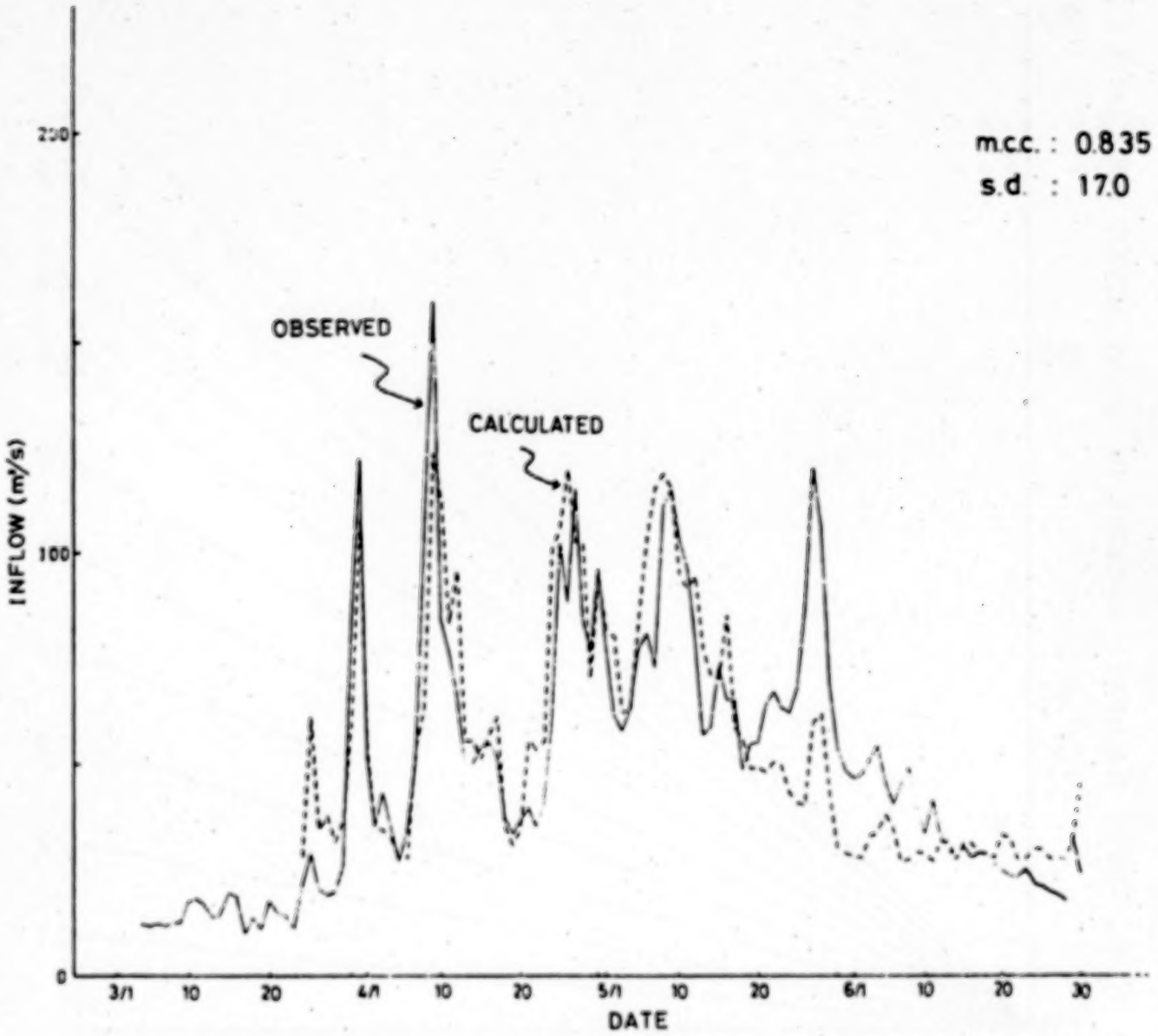

Figure 13. Comparison Between Observed (Solid Line) and Calculated (Broken Line) Inflow in Use of MODEL-I for 1979 Snowmelt Season

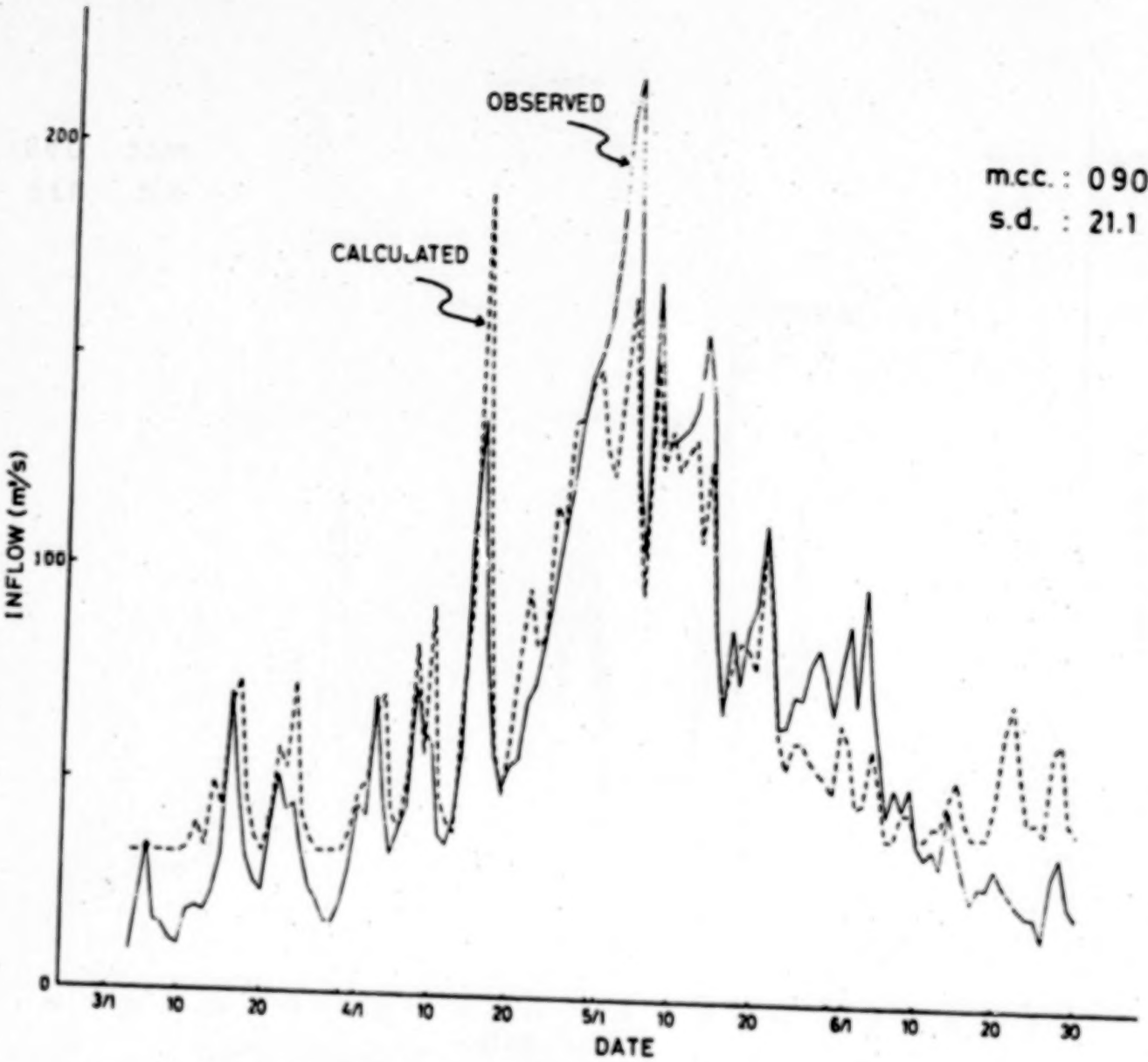

Figure 14. Comparison Between Observed (Solid Line) and Calculated (Broken Line) Inflow in Use of MODEL-I for 1982 Snowmelt Season

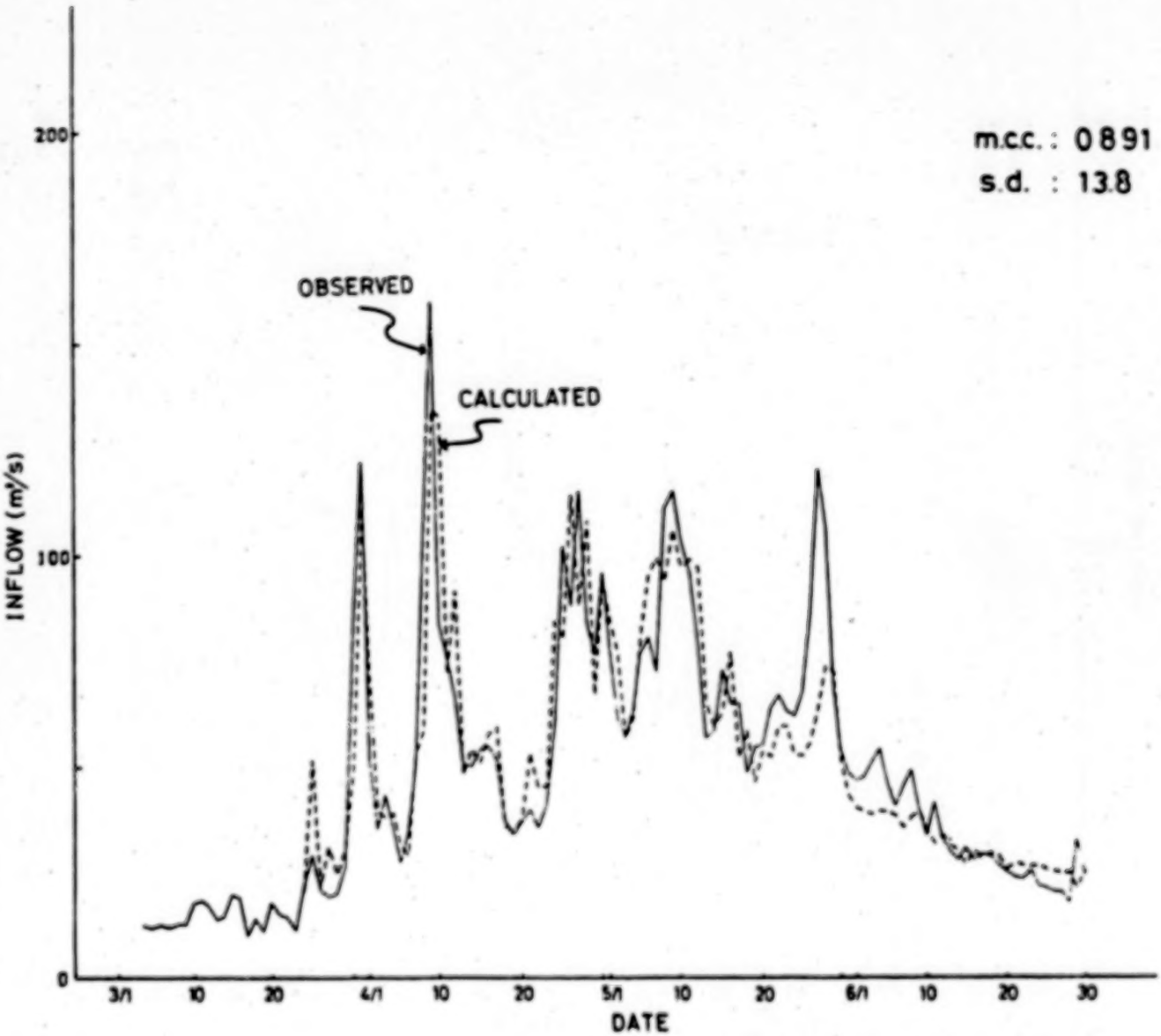

Figure 15. Comparison Between Observed (Solid Line) and Calculated (Broke Line) Inflow in Use of MODEL-II for 1979 Snowmelt Season

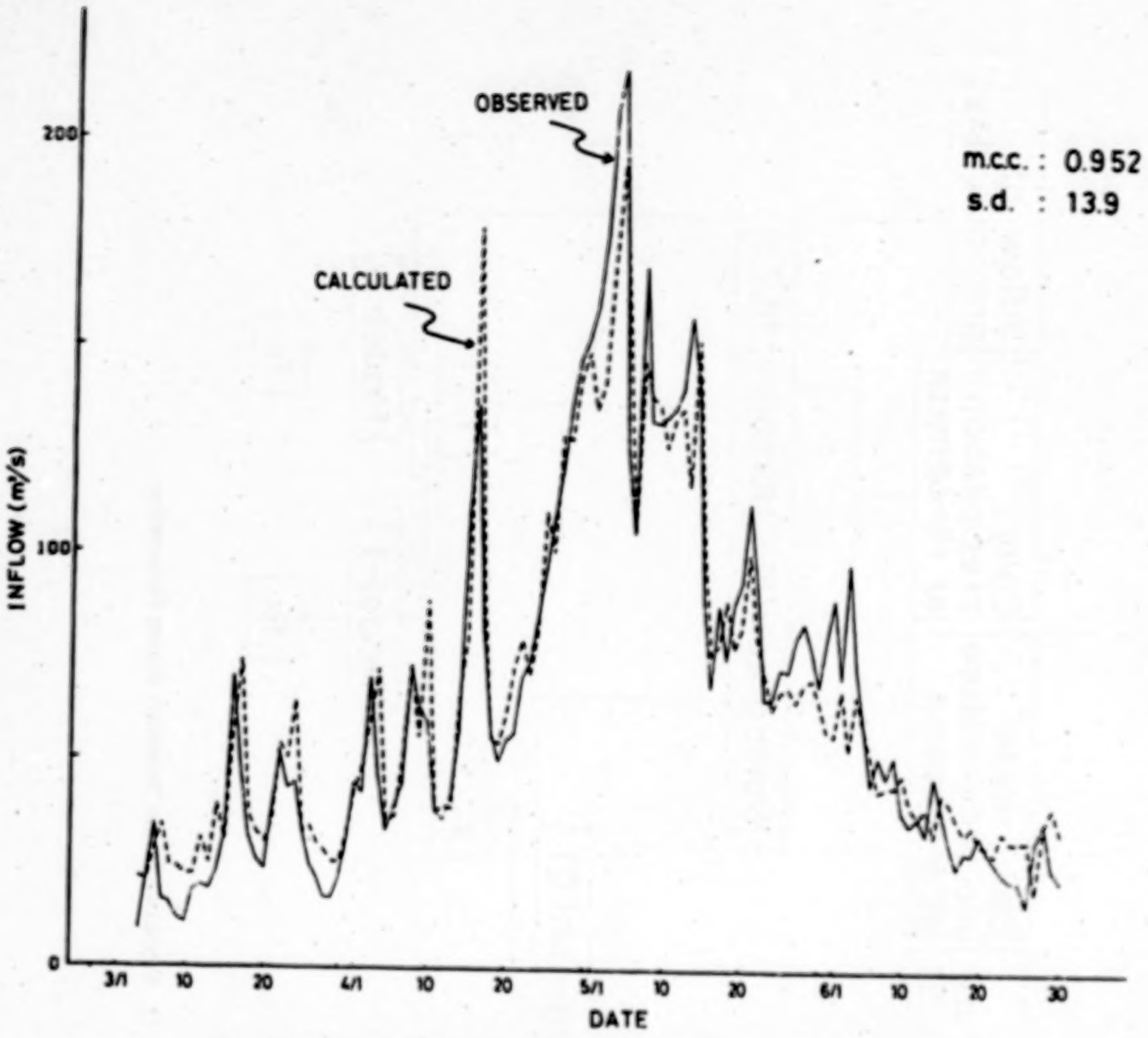

Figure 16. Comparison Between Observed (Solid Line) and Calculated (Broken Line) Inflow in Use of MODEL-II for 1982 Snowmelt Season

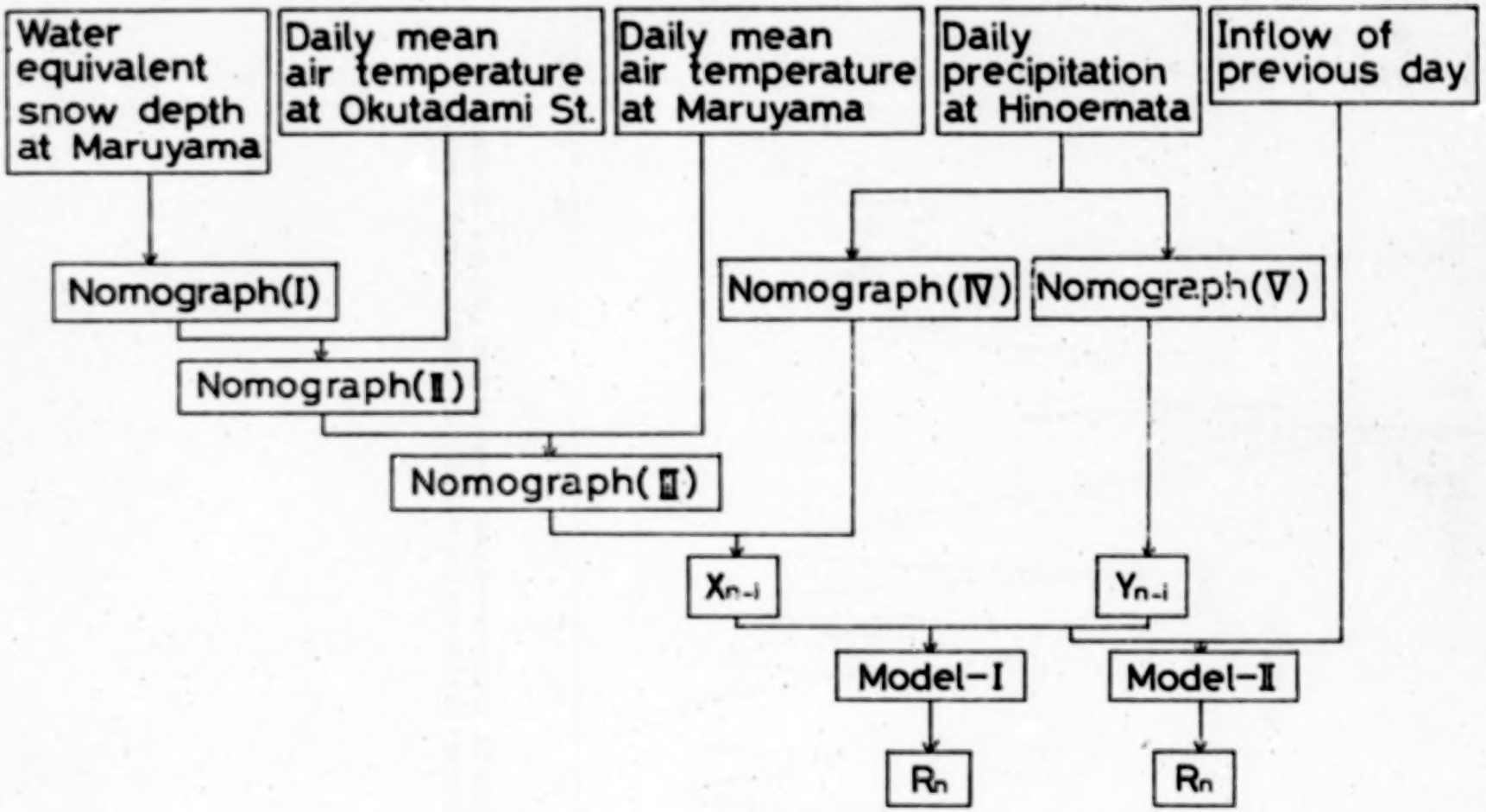

Figure 17. Procedure of the Snowmelt Runoff Forecasting

APPLICATION OF MARTINEC-RANGO MODEL TO RIVER BASIN IN JAPAN

Kenji Tshihara and Masayuki Inoue
Environmental Research & Technology Institute

Kaname Takeda
National Institute of Resource
Science and Technology Agency

INTRODUCTION

The Martinec-Rango model is known as one of the most practical models applicable to various river basins in many countries. The present study deals with the application of the model to Japan's river basins in use of the recently distributed user's manual.

One of the most important input variables of the model is the snow cover area provided by the Landsat imagery. Unfortunately, Japan is covered with much cloud during snowmelt season. Only by chance, one can obtain one or two imageries in the season. Ishihara et al [2] made effective use of a few precious imageries obtained in the past for the standardization of the snow cover depletion curve in connection with the degree-days at a representative point. The model was applied to the Okutadami River Basin, using the same variable data of three snowmelt seasons in 1979, 1980 and 1982 as used in the study by Ishihara et al [2].

APPLICATION OF THE MODEL

The Martinec-Rango Model is expressed by the following equation:

$$Q_{n+1} = C_n [\alpha_n (T_n + \Delta T_n) S_n + P_n] \frac{A \cdot 0.01}{86400} (1 - k_{n+1}) + Q_n k_{n+1} \qquad (1)$$

Variables

$(T_n + \Delta T_n)$ in the equation (1) is given the temperature at Maruyama located roughly at the mean altitude of the basin. The relation between elevation-snow cover area curves is provided by Fig. 1. P_n is assigned by the precipitation at Hinoemata located slightly outside the basin. Q_n is the daily inflow into the reservoir, S_n is given in Ishihara et al [2].

Parameters

Both two coefficients c_n and α_n were evaluated 1.2 and 0.45 [g/°C•day] respectively. The relation of Q_n vs Q_{n+1} shown in Fig. 2 gave the recession equation:

$$k_n = 0.986 Q_{n-1}^{-0.059}$$

This equation is of the intermediate line between the 1:1 line and the lower envelope line.

Results

The thus calculated inflow for three snowmelt seasons is shown in Figures 3, 4 and 5 in conjunction with the observed inflow. When the peak inflow occurs, two values of the calculated and the observed do not coincide with each other. One day lag can be seen between them. However, the most period in the season except such peak stage exhibited a good agreement.

According to the user's manual, it may be good that the test basin is divided into two or three zones.

The altitudes of the highest and lowest points in the basin are 2,346 m and 782 m respectively. The altitude difference is 1,564 m.

REFERENCES

1. Martinec, J., A. Rango and E. Major (1983): The Snowmelt-Runoff Model (SRM) User's Manual. NASA Reference Publication 1100, p. 1-110.

2. Ishihara, K., Y. Nishimura and K. Takeda (1983): Snowmelt runoff model in Japan. Paper Presented at Final Japan/US Snow and Evapotranspiration Workshop, Nov. 1983, Hawaii.

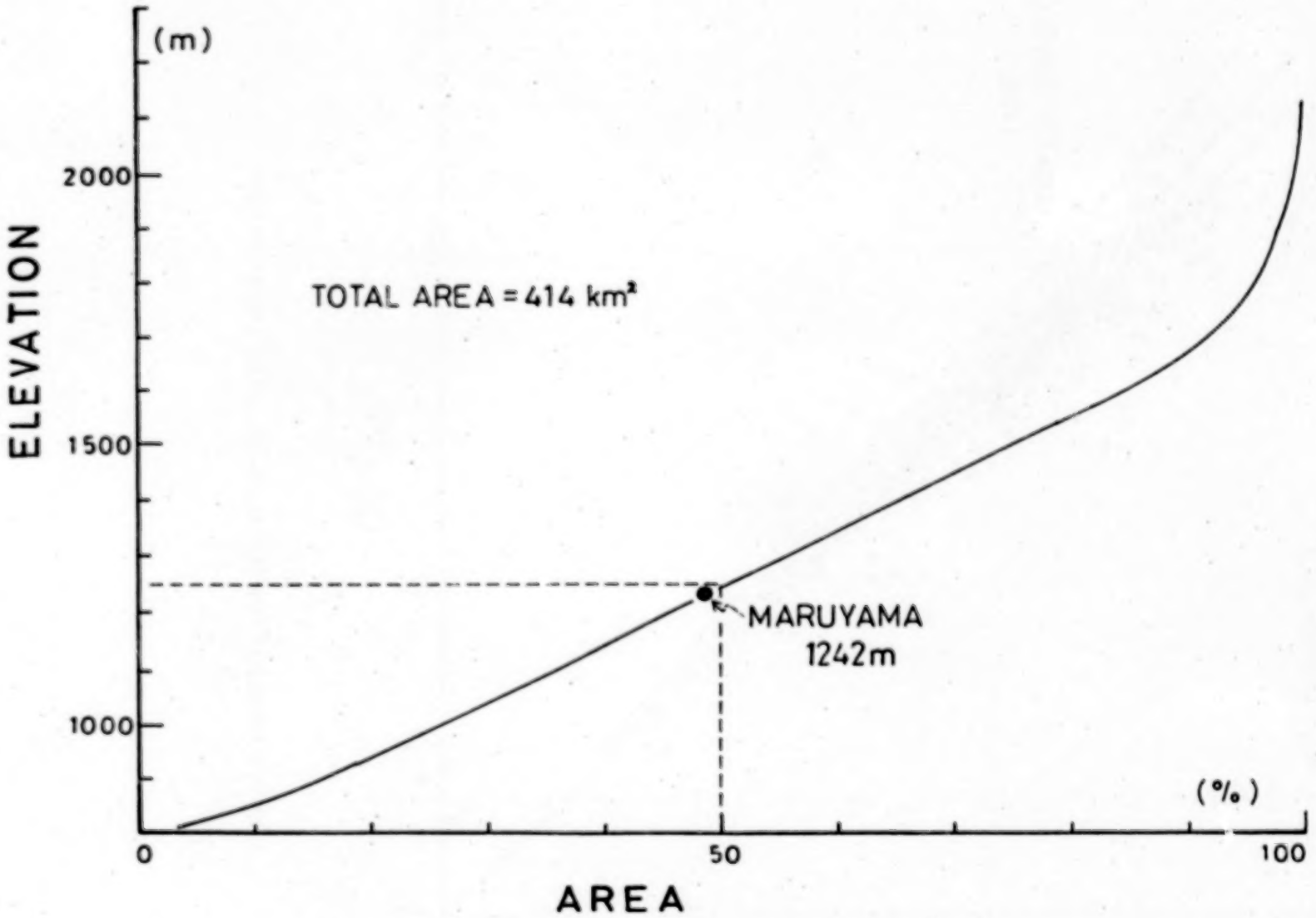

Figure 1. Relation of Elevation vs Area for the Okutadami Basin

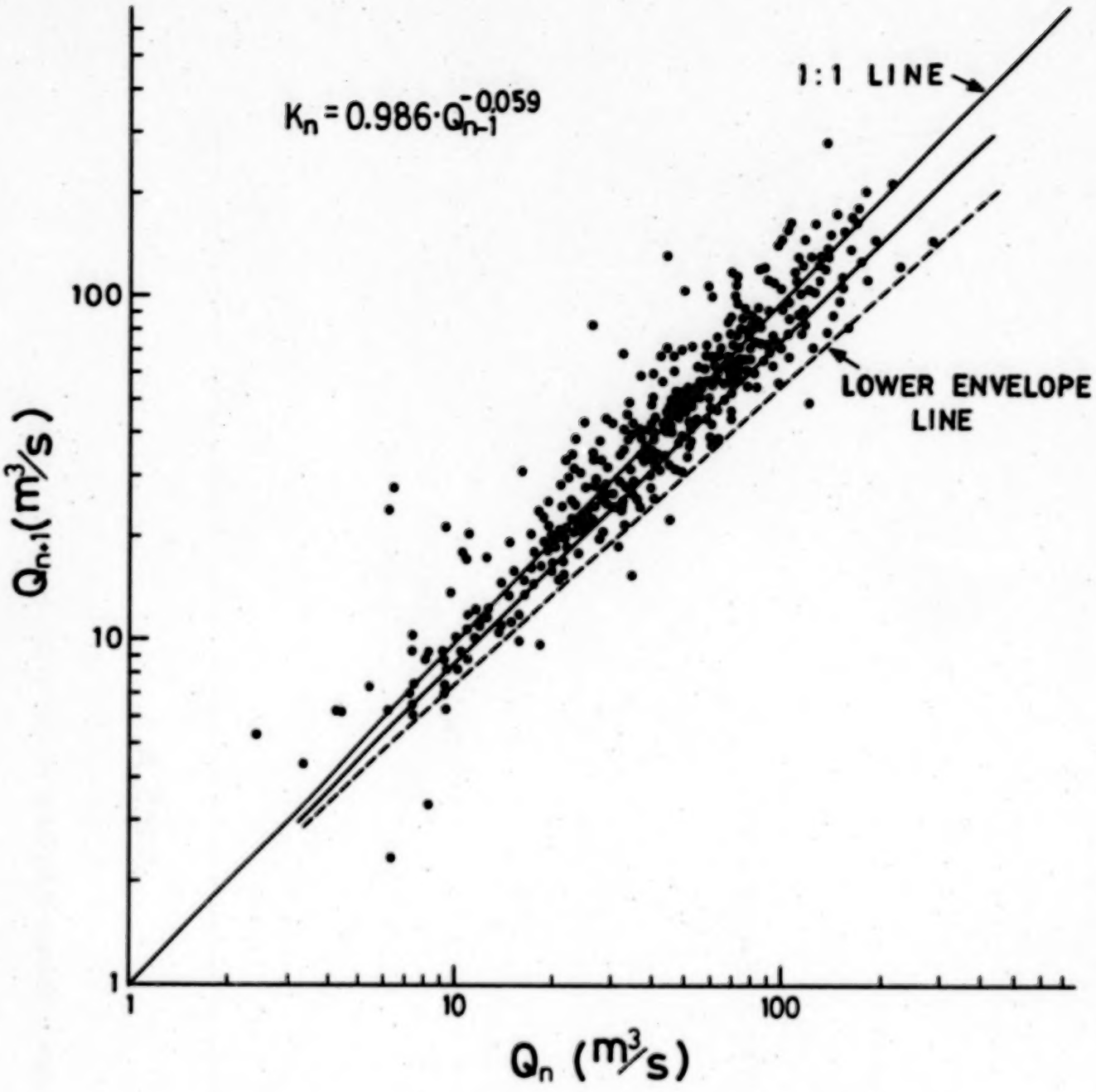

Figure 2. Recession Flow Plot, Q_n vs Q_{n+1} for the Okutadami Basin

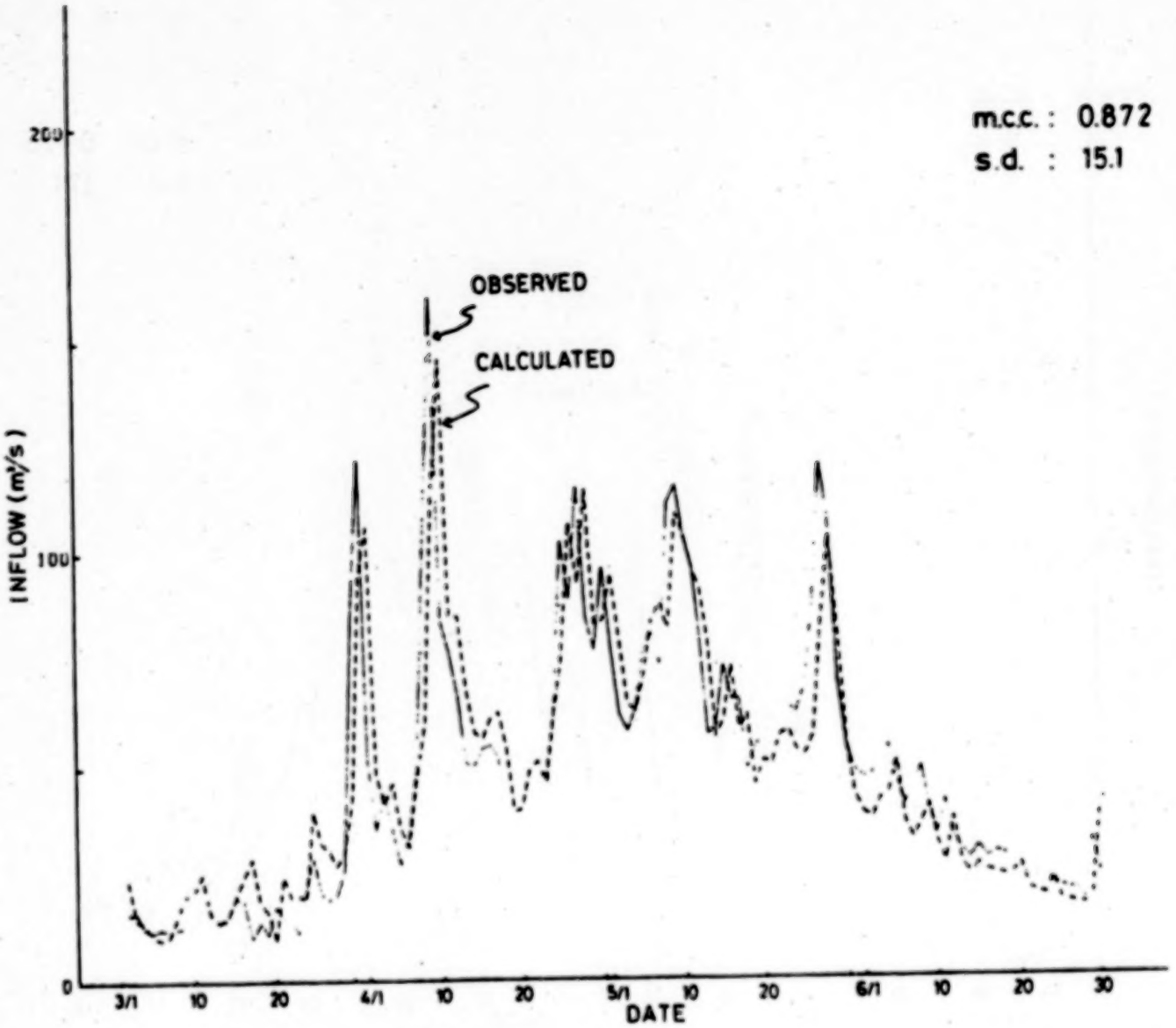

Figure 3. Comparison Between Observed (Solid Line) and Calculated (Broken Line) Inflow in Use of MARTINEC-RANGO MODEL for 1979 Snowmelt Season

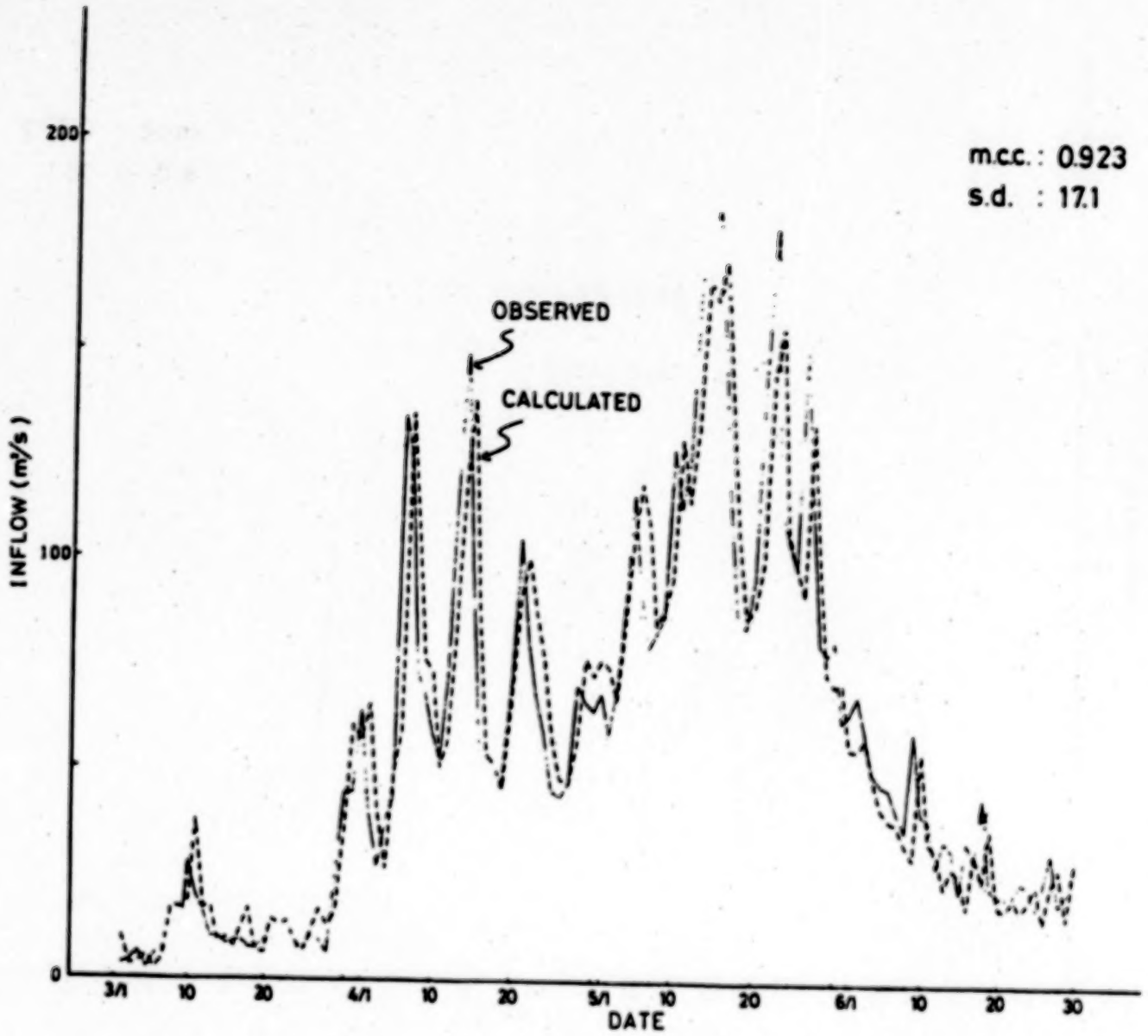

Figure 4. Comparison Between Observed (Solid Line) and Calculated (Broken Line) Inflow in Use of MARTINEC-RANGO MODEL for 1980 Snowmelt Season

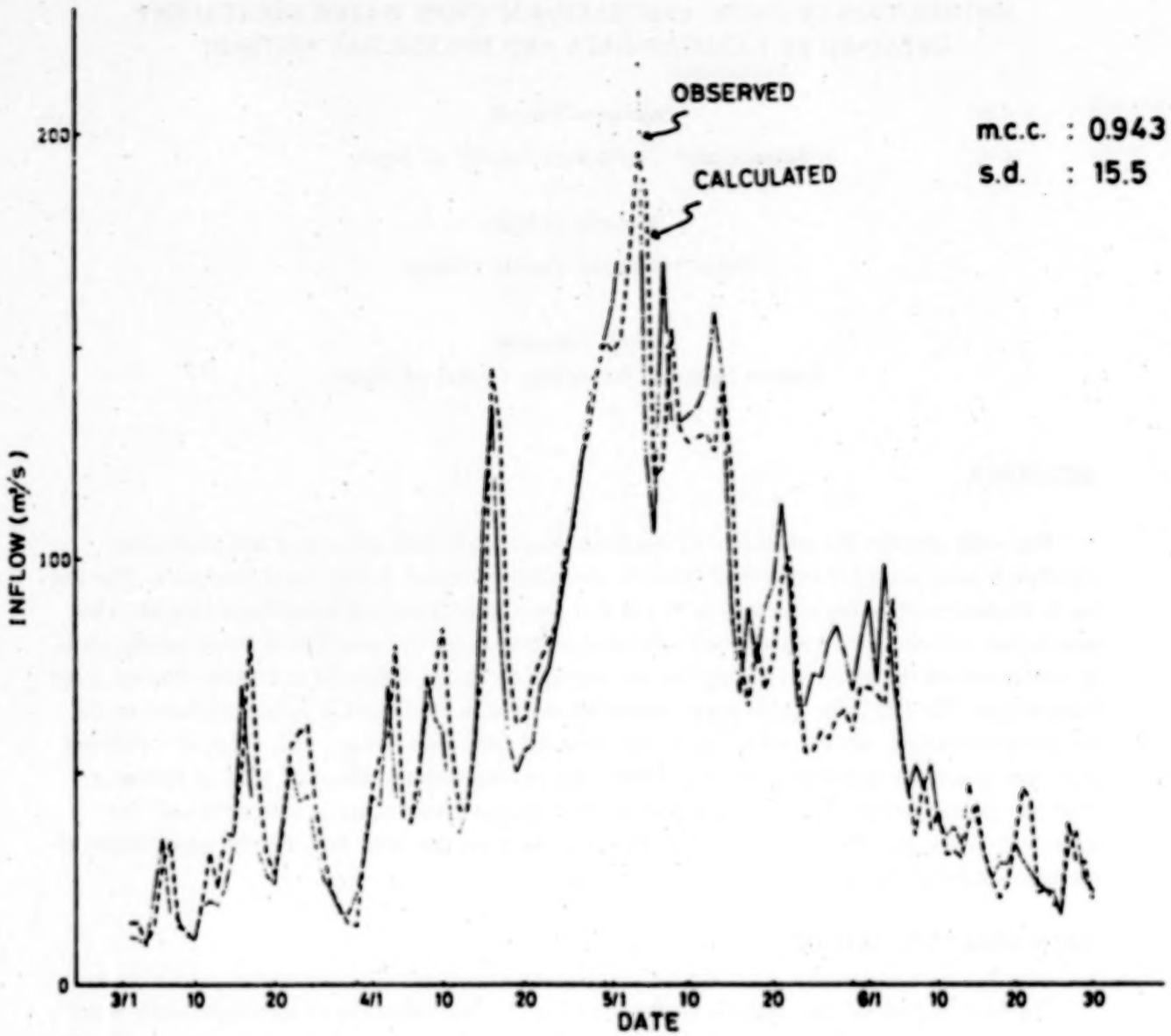

Figure 5. Comparison Between Observed (Solid Line) and Calculated (Broken Line) Inflow in Use of MARTINEC-RANGO MODEL for 1982 Snowmelt Season

D6 N85-23229

DISTRIBUTION OF SNOW AND MAXIMUM SNOW WATER EQUIVALENT OBTAINED BY LANDSAT DATA AND DEGREE DAY METHOD

Kaname Takeda
Science and Technology Agency of Japan

Hiroaki Ochiai
Toba Merchant Marine College

Shoji Takeuchi
Remote Sensing Technology Center of Japan

ABSTRACT

This study attempts the estimation of maximum snow water equivalent map and snowcover distribution using several Landsat data taken in snowmelting season during latest four years. The test site is Okutadami-gawa Basin located in the central position of Tohoku-Kanto-Chubu District. The year-to-year normalization for snowmelt volume computation on the snow line is conducted by year-to-year correction of degree days using the snowcover percentage within the test basin obtained from Landsat data. The maximum snow water equivalent map in the test basin is generated based on the normalized snowmelt volume on the snow line extracted from four Landsat data taken in a different year. The snowcover distribution on an arbitrary day in snowmelting season of 1982 is estimated from the maximum snow water equivalent map. The estimated snowcover is compared with the snowcover area extracted from NOAA-AVHRR data taken on the same day, and the applicability of the snow estimation using Landsat data is discussed.

DATA ANALYSIS METHOD

The flow diagram of data analysis is shown in Fig. 1. The estimation of maximum snow water equivalent map in the test site is based upon the extraction of snow boundary mesh corresponding to the boundary region between snowcover and snow free area, and upon the computation of snowmelt volumes at each snow boundary mesh using accumulative temperature. The snow boundary mesh is extracted as a mesh in which the percent snowcover obtained from a Landsat snowcover extraction image is nearly 50 percent.

The maximum snow water equivalent at each snow boundary mesh is computed as a snowmelt volume obtained by a snowmelt model based on accumulative degree days at the elevation of each snow boundary mesh. The values of maximum snow water equivalent at snow boundary meshes obtained from Landsat data taken in different years are normalized by year-to-year correction of degree-days. The whole map of maximum snow water equivalent in the test site is generated using the above normalized maximum water equivalent values located in various spots in the test site.

The snowcover map on an arbitrary day in snowmelting season can be estimated by the computation of snowmelt volumes on the maximum snow water equivalent map. The snowcover extraction images obtained from NOAA-AVHRR data are used for the assessment of the above estimated snowcover map.

COMPUTATION AND YEAR-TO-YEAR CORRECTION OF SNOWMELT VOLUME USING DEGREE-DAY METHOD

The snowmelt volume on a certain snow line accumulated from the beginning of snowmelt until the appearance of the snow line, which is equivalent to the maximum snow water equivalent on the snow line, can be computed by the following equation based on the degree-day method.

$$M = K\Sigma\overline{Te} \tag{1}$$

where

M : Snowmelt volume (g/cm^2)
$\overline{Te}$: Effective daily average temperature on the snow line (°C)
$\Sigma\overline{Te}$: Degree-days on the snow line (°C•day)
k : Snowmelt coefficient (g/cm^2• °C•day)

$\overline{Te}$ is estimated from the average temperature at the standard weather station in the test basin using the relationship between temperature and elevation as follow,

$$\overline{Te} = \overline{Tb} - 0.6(he - hb)/100 \tag{2}$$

where

$\overline{Tb}$: Effective daily average temperature at the standard weather station
he : Elevation at the snow line
hb : Elevation at the standard weather station

In Eq. (1) a certain year-to-year correction for degree-days makes possible year-to-year normalization of snowmelt volume on the snow line, which makes it possible to use the snow line obtained from the Landsat data taken in a different year. The following two hypotheses are assumed for the year-to-year correction,

(a) snow distribution is equal, that is, the location of snow line is also equal if the snowcover percentage within the basin is equal between two days in a different year.

(b) The snowcover percentage in the basin decreases monotonously and regularly as degree-days increases.

The above hypothesis (a) is considered to be approximately approvable from the fact that the snowcover distribution between two different years Landsat data in which the snowcover percentage is nearly equal agrees very well. Under this hypothesis the correction of degree-days which equalizes the snowcover percentage between two different years' data leads to the year-to-year normalization of snowmelt volume.

Table 1 shows the snowcover percentage obtained from four Landsat data taken in a different year respectively. Photo 1 shows the superimposed image of the snowcover areas extracted from the four Landsat data.

Fig. 2 shows the relationship between snowcover percentage and degree-days in Okutadami-gawa Basin, which is used for year-to-year correction of degree-days. The solid line shows the relationship obtained by applying Eq. (1) to the maximum snow water equivalent map generated based on snow survey, in which the snowmelt coefficient K is assumed 0.45. The mark ⊗ in Fig. 2 shows the location of the snowcover percentage obtained from Landsat data in the snowcover percentage vs. degree-days plane. The dotted lines show the estimated curves for the relationship in 1981 and 1982 using the solid curves of 1978, 1979 and 1980. From Fig. 2, the correction values for degree-days in 1979 and 1981 which equalize the snowcover percentage to that of 1982 are estimated +70 ('79.5.4), +75 ('79.5.22) and −180 ('81.6.16) degree days respectively.

MAXIMUM SNOW WATER EQUIVALENT MAP AND SNOWCOVER DAILY VARIATION MAP

By the year-to-year correction described above, many point estimates of maximum snow water equivalent can be obtained using four Landsat data taken in a different year. Using these point estimates, the maximum snow water equivalent map is generated based on 500 meter mesh. Photo 2 shows the obtained maximum snow water equivalent map of Okutadami-gawa Basin in 1982. The total maximum snow water equivalent within Okutadami-gawa Basin in 1982 is estimated to be about 4.1×10^8 m^3.

The snowcover distribution on an arbitrary day can be estimated by subtracting the snowmelt volume calculated from Eq. (1) at each mesh. Photo 3 shows the estimated snowcover map from April 25 to May 30 in 1982 by seven days. The snowcover areas extracted from NOAA-AVHRR data taken on April 25 and May 23 in 1982 are shown in Photo 4, which can be compared with the estimated snowcover areas in Photo. 3. On April 25, the snowcover extracted from NOAA data is relatively smaller than that of estimated map, however, on May 23, both the snowcover areas are consistent with each other. The primary reason why the snowcover areas are not consistent on April 25 is considered to be unclearness of snow line in NOAA data due to rough resolution and as a result bad precision for snowcover extraction. The consistency of the snowcover areas on May 23, late in the snowmelting season, suggests that the estimation of maximum snow water equivalent and snowcover distribution conducted in this study can be applied practically in this test basin.

CONCLUDING REMARKS

The two hypotheses (a) and (b) assumed for the year-to-year correction of snowmelt volume are not based upon actual snow survey, but for the practical use of Landsat data taken in a different year, which are necessary to be assessed by some experimental snow studies. The satisfactory condition of Landsat data for the application of the estimation method in this study is to be able to compute snowcover percentage within a certain basin, which is rather severe condition for the routinized use of Landsat data considering the weather condition of Japan. It seems necessary to develop the year-to-year correction method using only the local information of snow line.

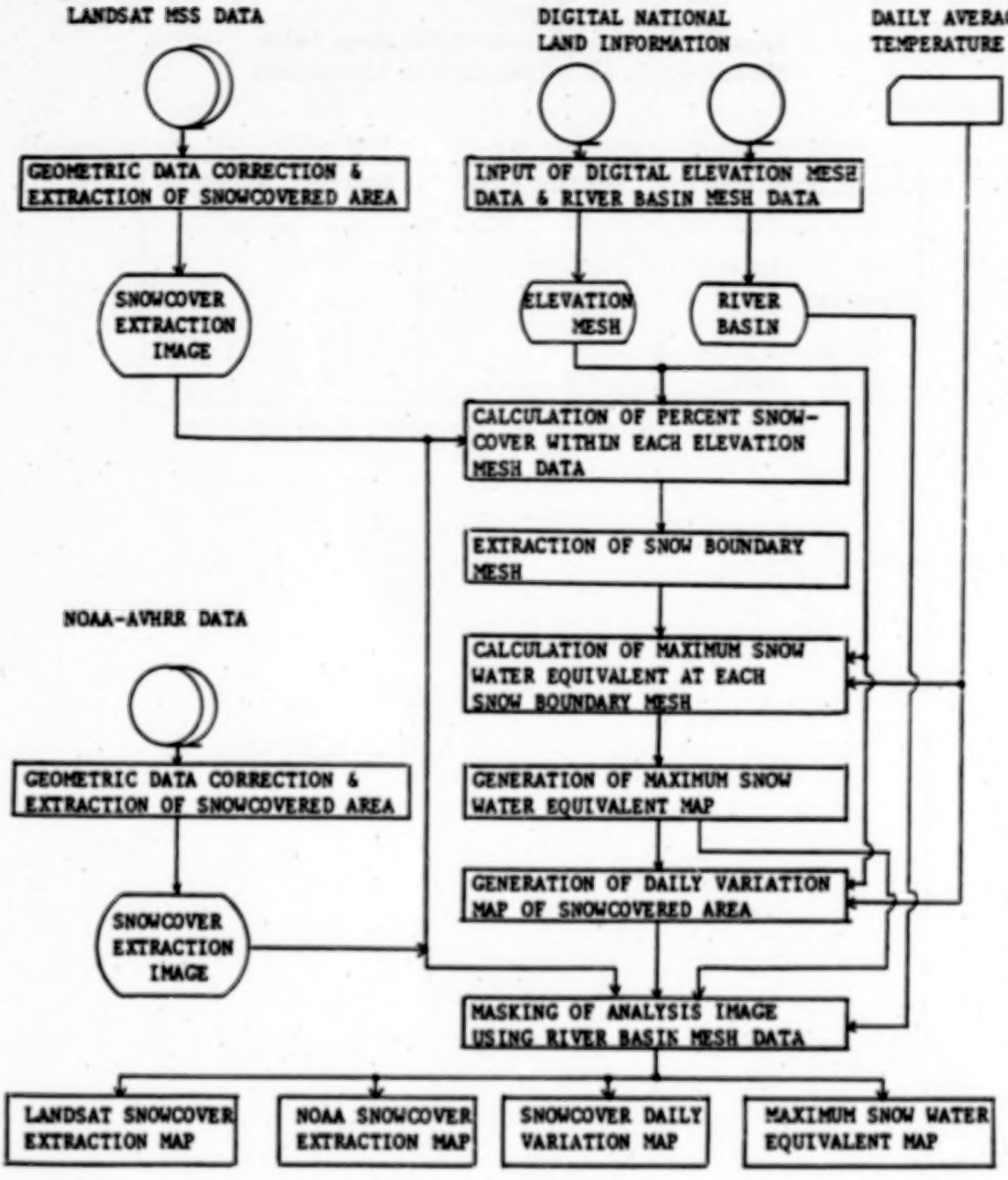

Figure 1. Flow Diagram of Data Analysis

Table 1
Snowcover Area and Snowcover Percentage within
Okutadami-gawa Basin Obtained from Landsat Data

OBSERVATION DATE	SNOWCOVER AREA (Km^2)	SNOWCOVER PERCENTAGE (%)
MAY 4 1979	274.7	63.0
MAY 22 1979	114.7	26.3
JUN 16 1981	70.2	16.1
MAY 15 1982	181.4	41.6

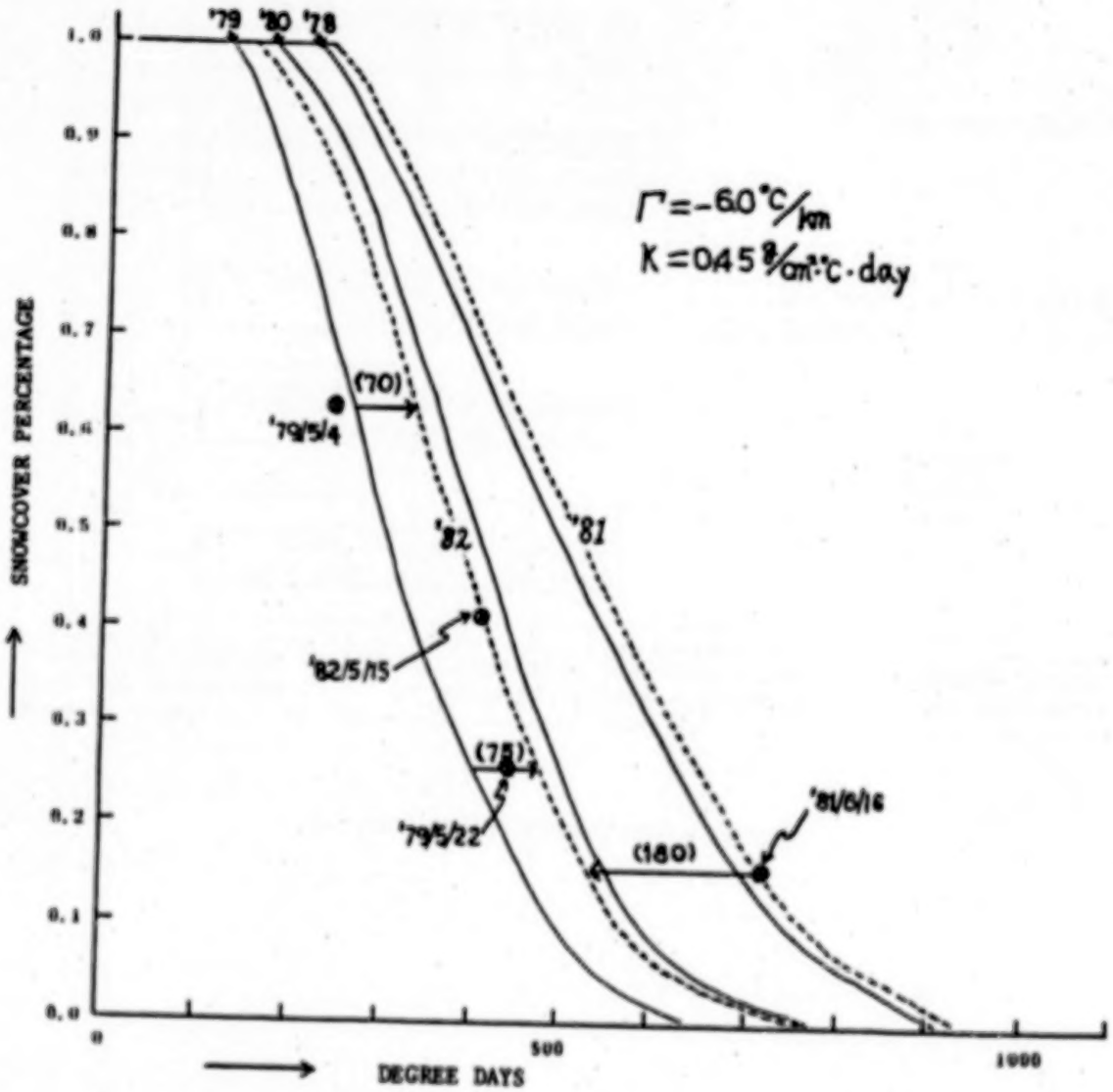

Figure 2. The Relationship Between Snowcover Percentage and Degree Days in Okutadami-gawa Basin

MICROWAVE RADIOMETER OBSERVATIONS OF SNOWPACK PROPERTIES AND COMPARISON OF U.S. JAPANESE RESULTS

A. T. C. Chang

Laboratory for Earth Sciences
NASA/Goddard Space Flight Center
Greenbelt, MD 20771

INTRODUCTION

Recent studies using the Nimbus-5 and Nimbus-6 electrically scanning microwave radiometer (ESMR) have demonstrated the potential of passive microwave sensors in monitoring interested snow properties such as snow covered area, snow depth/water equivalent and wetness. This capability is primarily due to the strong scattering effect of large snow grains and dielectric contrasts between water and ice in the microwave region. The use of dual polarization, multifrequency scanning multichannel microwave radiometer (SMMR) offers an even greater potential to delineate snow properties.

Field experimental data collected in Vermont during the winter of 1981-1982 and data collected in Hokkaido are studied. The Nimbus-7 SMMR data over the U.S. test site (North Dakota) and the Japanese test site (Hokkaido) during February and March for 1979, 1980 and 1981 are studied. Results from these data sets are encouraging for future snowpack study using passive microwave data.

OBSERVATIONS OF MICROWAVE FIELD EXPERIMENT DATA

During the winter of 1981-1982, a field experiment with microwave radiometers was conducted in Vermont. The radiometer system (SMMR Engineering Model) consisted of four frequencies (6.6, 10.7, 18 and 37 GHz) and dual polarization (H and V) and mounted on a steerable hydraulic boom. The antenna was an offset parabola with 80 cm diameter. The normal 3-dB beamwidth were 4.2, 2.6, 1.6 and 0.8 degree for these four frequencies. The radiometers were comparison or Dicke types with square wave modulation and synchronous detection. The noise equivalent brightness temperatures for each channel are 0.6, 0.7, 0.8 and 1.2 K respectively.

Most brightness temperature data were obtained by scanning the instrument unit. In order to remove the potential field inhomogeneity effect, the radiometer antenna was scanned such that it always viewed the same spot on the snowpack while the incidence angle changed. In addition to the scanning measurement, several time sequence measurements and snow removal experiments were made to study the diurnal effect and layering effect on microwave snow signatures.

The general snow conditions for the test sites were dry snow with depth ranged from 0 to 120 cm. Snowpacks typically layered with several ice or crust layers and the grain size was very fine, 0.5 to 1 mm in diameter, throughout the packs except in the ice layers. The air temperatures varied from -3°C to -25°C during the observation period. Physical characterizations of the snowpack were made along with the microwave measurement. The truck unit performed microwave measurements at three separated fields with different snow depth and layering effects.

The data collected during this experiment generally fall into the envelope of brightness temperature with averaged grain radius 0.25 to 0.5 mm (Figure 1). Figure 2 shows the results for a three week study of snow at the Townline test site. The observed brightnesses are following closely with the brightness-snow depth curve for snow grain with 0.25 mm radius. The small grain sizes at the top 50 cm of the snowpack that contributed the major portions of the brightness at 37 GHz dominated the observed brightness.

To study the layering effect, ice layers were removed to measure the changes of microwave responses. Figure 3 shows the variation of the 37 GHz brightness as layers were removed. No significant effect was observed during the experiment. However, in another location (Figure 4) the 6.6 GHz show strong effects due to the ice layers.

The experimental data for Sapporo microwave tower experiment was fitted with 2 layer scattering model and the results are shown in Figure 5. The snow density used for this calculation was based on the averaged ground truth information and the mean radius for each layer was assumed to be 0.2 and 0.35 mm respectively.

OBSERVATIONS OF THE NIMBUS-7 SMMR DATA ON SNOWFIELDS

Two test sites, one in North Dakota and one in Hokkaido, were selected for this study. A total of five time periods of SMMR data were acquired. They were, February and March, 1979, February and March, 1980 and February of 1981. Due to the smooth terrain in the North Dakota site, SMMR data could provide useful information both the snow cover area and snow depth. For the Hokkaido site, the results were different. Since the resolution of SMMR is approximately 25 km for the 0.8 cm radiometer, it is rather difficult to separate out the small geographical features. Mixed pixels are much more difficult to interpret than a uniformed footprint.

Under this condition, the snow cover area could be delineated marginally. Figures 6 and 7 show the 37 GHz brightness as a function of snow depth. They generally fall within the envelope between 0.25 and 0.35 mm radius. However, due to different snow conditions in 1979 and 1980 winter season, different responses were observed. The SMMR data show some potential for studying the snow properties in Hokkaido. If the spatial resolution can be reduced to $\sim$ 5 km, then the snowfield can be delineated much more accurately.

CONCLUSIONS

Microwave data collected by field experiments over Vermont and Hokkaido and Nimbus-7 SMMR over North Dakota and Hokkaido were studied under the Joint U.S.-Japan snowpack property study project. The measured 37 GHz brightness temperatures showed considerable effect of volume scattering by the snow grain. The 37 GHz brightness for a new snowpack with average grain radius of 0.25 mm is generally about 40K higher than the naturally compacted pack with average grain radius of 0.4 mm. The scattering effect is much less distinct for the 6.6 GHz. However, the layering effect is much stronger at the longer wavelength. For 10.7 and 18 GHz, the effect of layering and scattering vary due to different combinations of internal snow grain distribution and layering structures.

Both the microwave observations taken by field experiment and satellite-borne instruments shown that snow properties may be inferred from these observations. In the open area such as North Dakota site, resolutions of 25 km is adequate for snow properties determination. However, over the Hokkaido test site, the SMMR data is too coarse for the snow field. A better spatial resolution is required to study these snow fields.

The challenge in the analysis of the microwave response to snowpack properties lies in the fact that snowpack conditions are complex and their interaction with microwave radiation is not completely understood. The fact that snowpack character can change so rapidly, and, is in fact, constantly changing, adds a complicating factor to data analysis. It is believed that with additional measurements in the coming years, a more quantitative relationship between brightness temperatures and snow depth will be possible for snowpacks of known wetness condition. The near-term goal is to understand the microwave emission from snow so that a system for improved snowpack monitoring from a remote platform can be defined.

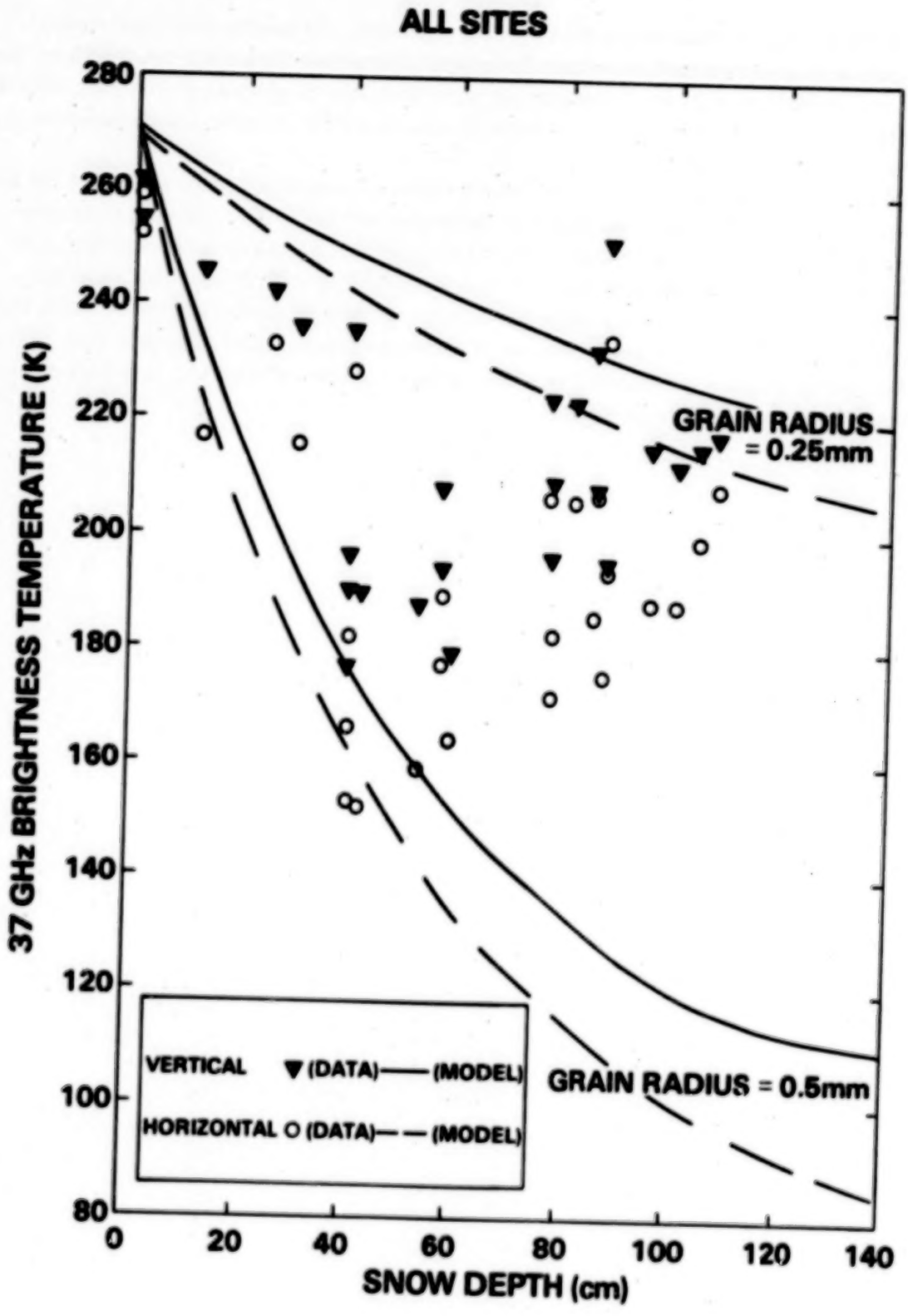

Figure 1. 37 GHz emission vs. snow depth with 50° look angle, Vermont, 1982.

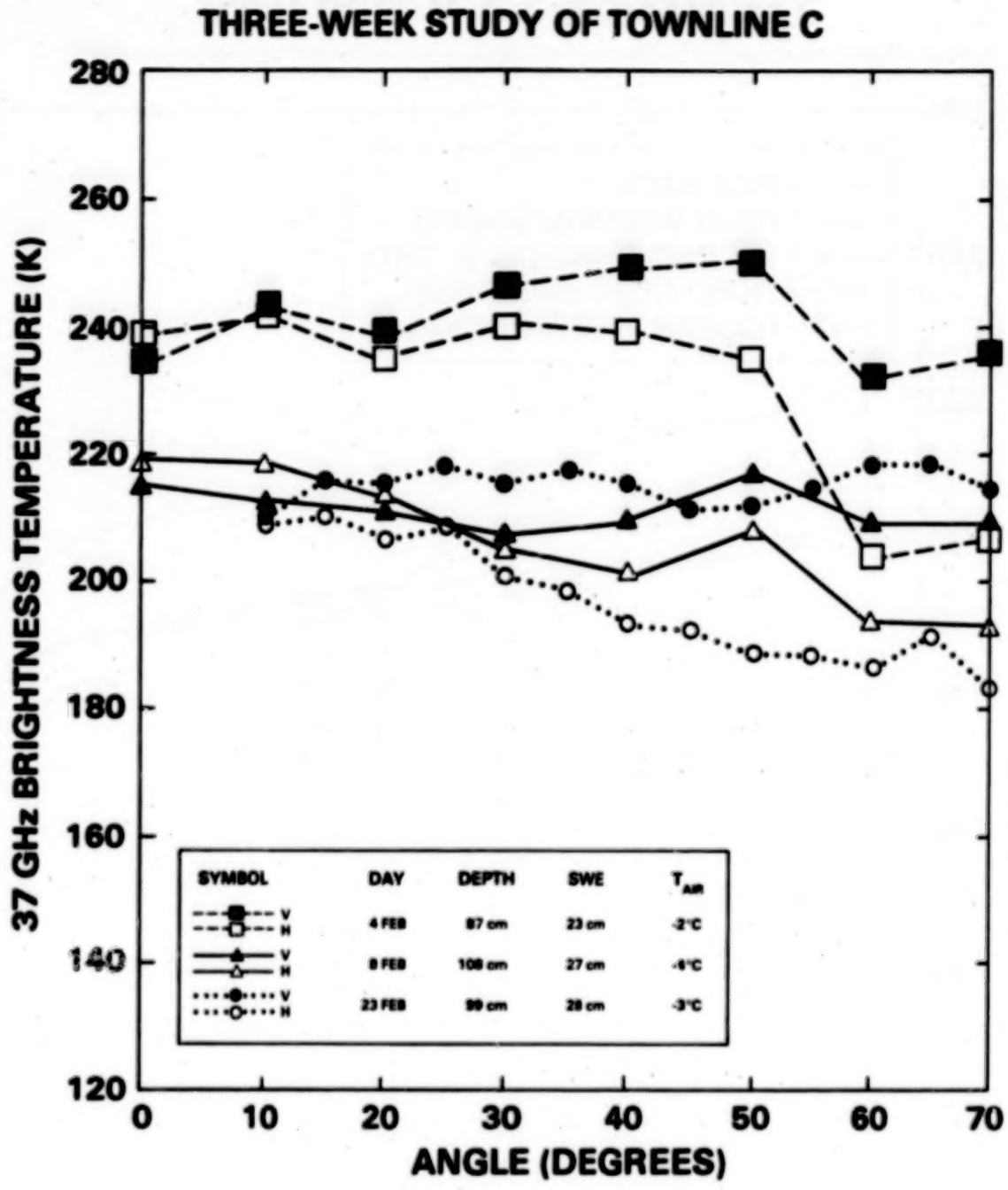

Figure 2. 37 GHz emission from a natural snowpack, Townline, Vermont.

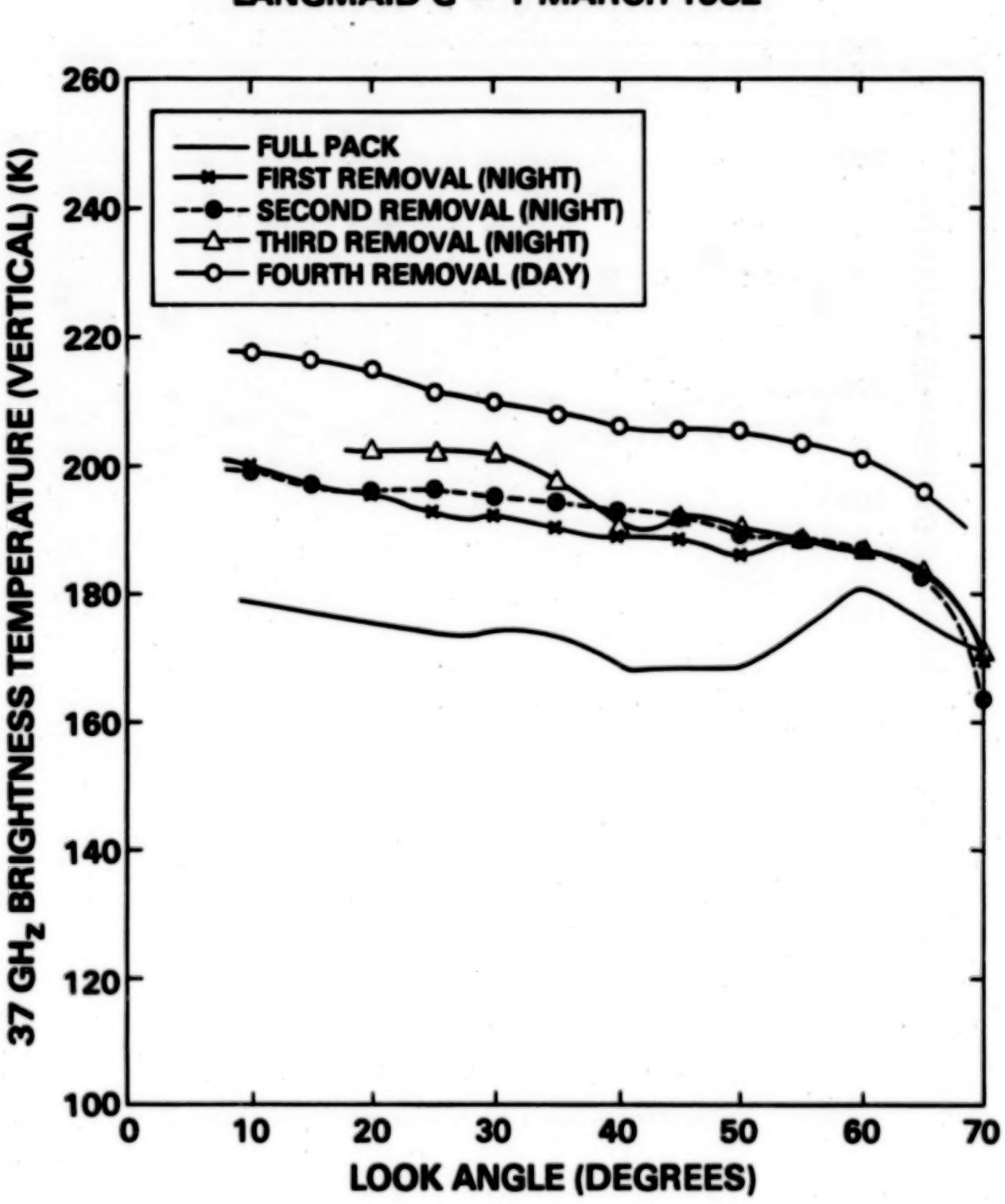

Figure 3. 37 GHz emission from a snow removal experiment, Vermont, 1982.

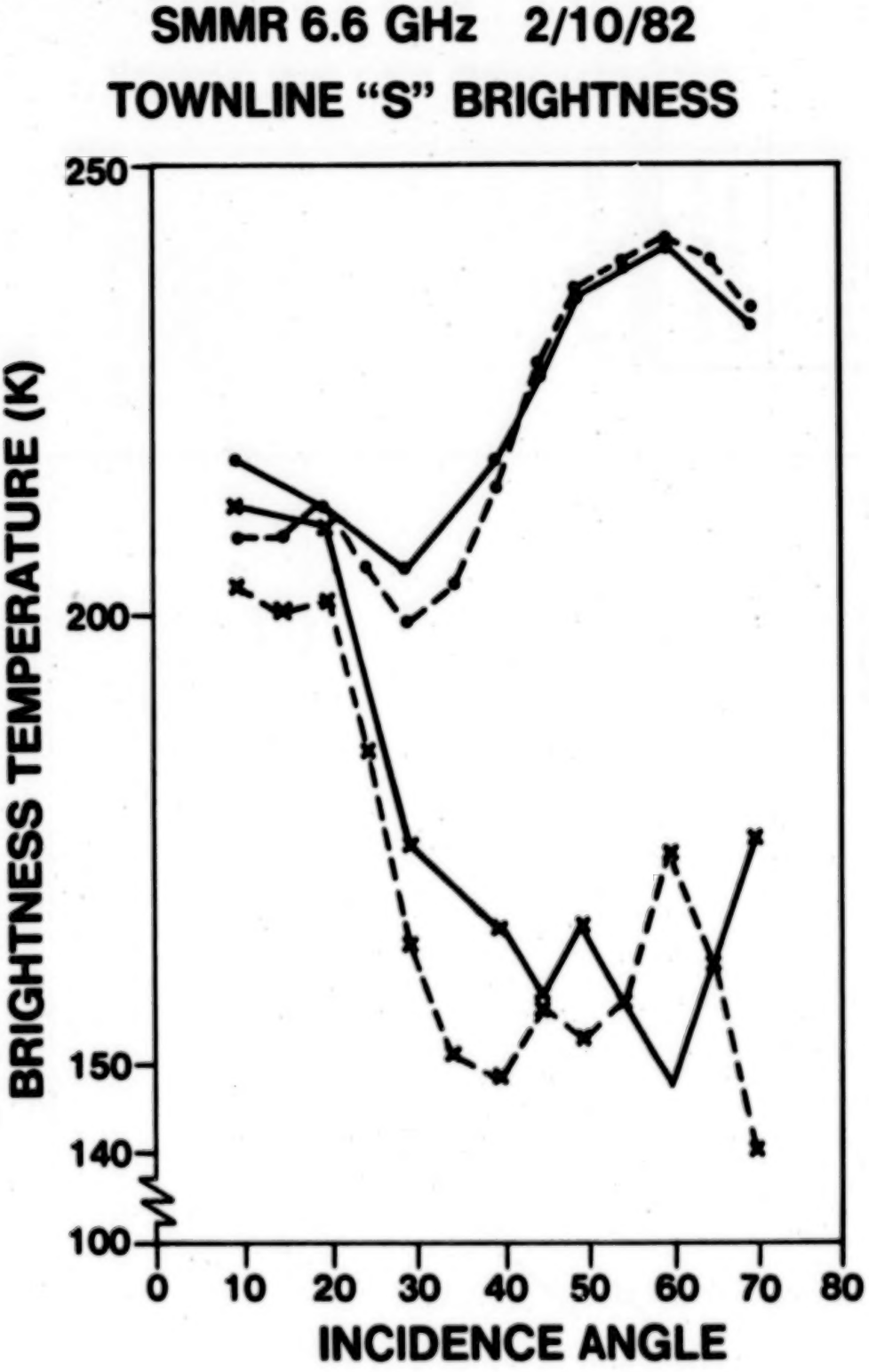

Figure 4. 6.6 GHz emission from a snow removal experiment, Vermont, 1982.

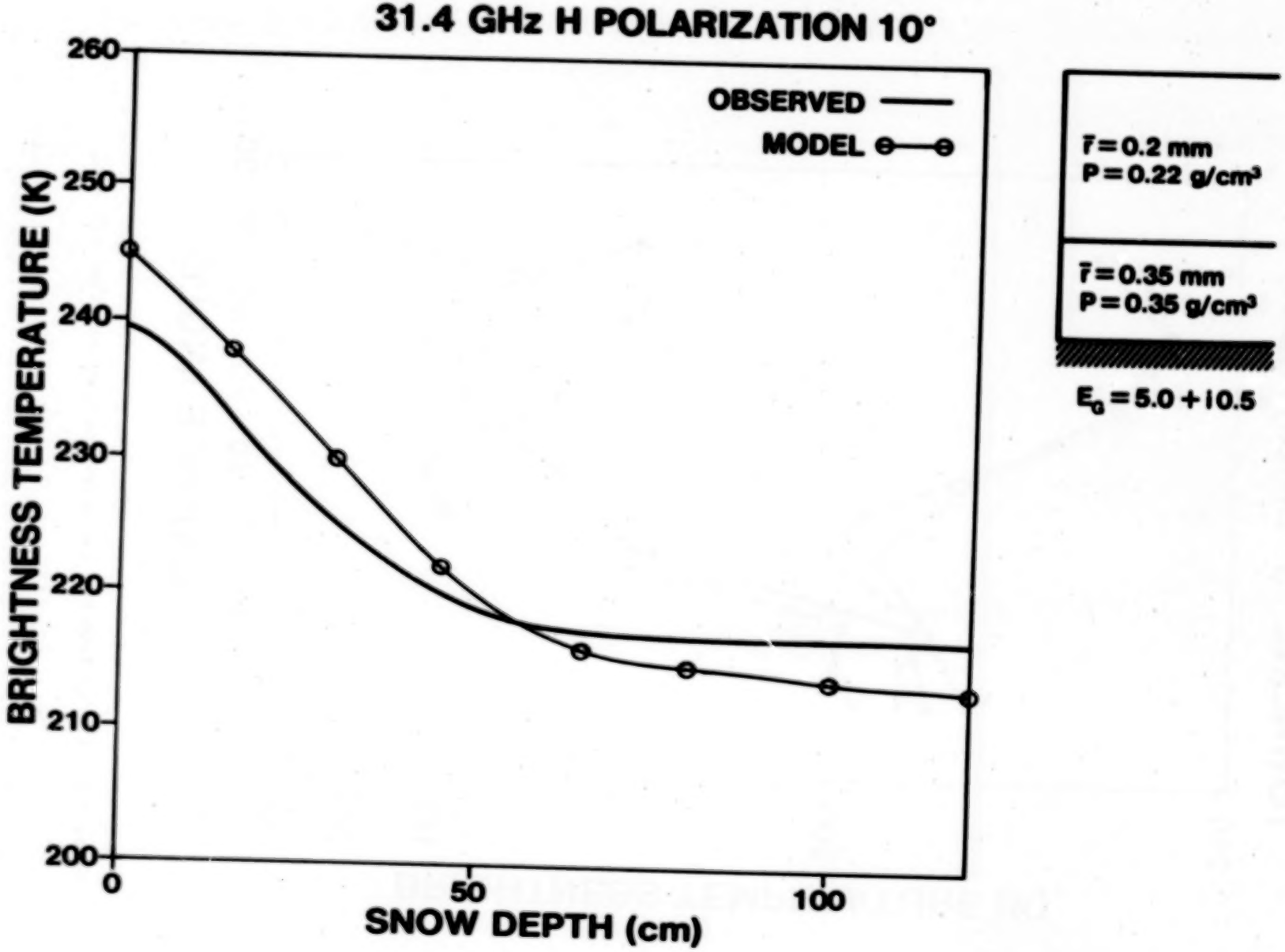

Figure 5. Comparison of calculated and observed 31.4 GHz brightness, Sapporo, 1981.

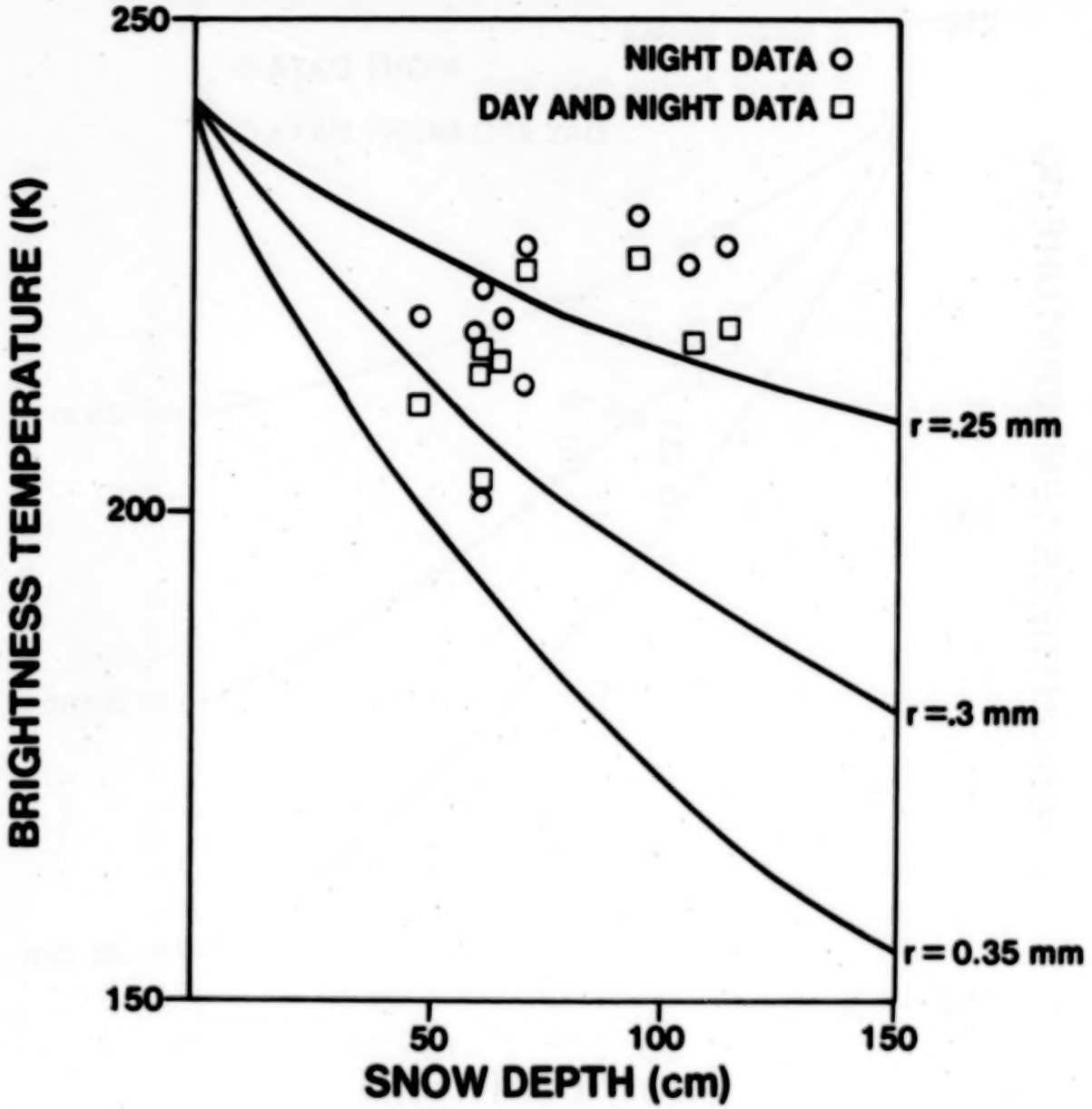

Figure 6. Nimbus-7 SMMR 37 GHz brightness over Hokkaido, Japan, February, 1979.

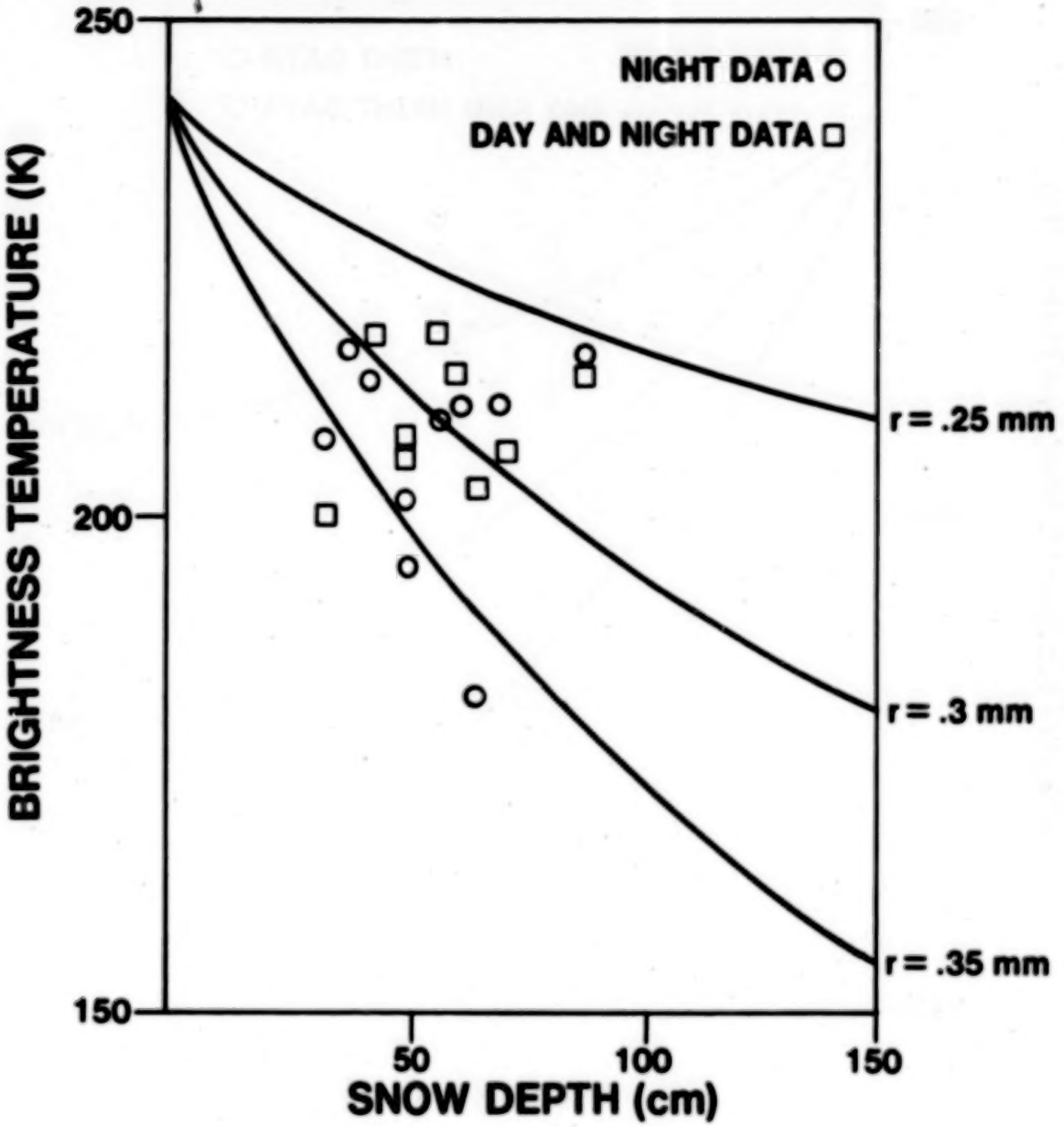

Figure 7. Nimbus-7 SMMR 37 GHz brightness over Hokkaido, Japan, February, 1980.

STUDIES ON PHYSICAL PROPERTIES OF SNOW BASED ON MULTI CHANNEL MICROWAVE RADIOMETER*

Kiyoshi Tsuchiya

Institute of Color & Image Technology, Chiba University
1-33, Yayoi-cho, Chiba-city, Chiba-ken, Japan, 260

Kaname Takeda

National Institute of Resources, Science & Technology Agency
2-2-1, Kasumigaseki, Chiyoda-ku, Tokyo, Japan, 100

ABSTRACT

The analysis of the data observed over a snow field with a breadboard model of MSR (Microwave Scanning Radiometer) to be installed in MOS-1 (Marine Observation Satellite-1) indicates the following features.

(1) The influence of incident angle on brightness temperature is larger in horizontal polarization component than in vertical polarization component. The effect of incident angle depends upon the property of snow with larger value for dry snow. (2) The difference of snow surface configuration consisting of artificially made parallel ditches of 5 cm depth and 5 cm width with spacing of 10 and 30 cm respectively which are oriented normal to electrical axis do not affect brightness temperature significantly. (3) There is high negative correlation between brightness temperature and snow depth up to the depth of 70 cm which suggests that the snow depth can be measured with a two channel microwave radiometer up to this depth.

INTRODUCTION

As a part of Japan/US Cooperative Research Program on Snow Properties/Evapotranspiration, the first field experiments on snow properties using a breadboard model of 2 channel MSR (Microwave Scanning Radiometer) to be installed in Japanese first earth observation satellite, MOS-1 (Marine Observation Satellite-1) were made in January of 1982 the result of which was presented by Tsuchiya (1982) at the first Japan/US Workshop held in March 1982 at Tokyo.

The result of the first experiment indicated that in spite of the fact that the general tendency of the brightness temperature vs snow property relationship was similar to that obtained by other investigators, i.e., England (1975), Hofer and Shanda (1978), Rango and et al (1979), Stiles and Ulaby (1980), Tiuri and Schultz (1980) etc., there was a discrepancy in absolute values.

In an attempt to clarify the discrepancies as well as characteristics of snow for microwave radiation, the second experiements were made in the winter of 1983 in the test site of Hokkaido University. The result of the experiments is reported in the following sections.

---

*Presented at the 2nd US/Japan Snow/Evapotranspiration Workshop, Nov. 15-19, 1983. East-West Center, Honolulu, Hawaii.

CHARACTERISTICS OF MSR USED IN THE EXPERIMENT

The characteristics of MSR (Microwave Scanning Radiometer) used in the experiments are shown in Table 1 and Fig. 1 respectively.

Table 1
Characteristics of MSR (Microwave Scanning Radiometer)
to be Installed MOS-1, the Breadboard Model of Which was Used.

Frequency	23.8 GHz	31.4 GHz
RF Bandwidth	400 MHz	500 MHz
Beam width	1.99 deg.	1.45 deg.
Integration Time	10 & 47 msec	10 & 47 msec
Radiometric Resolution	1.0 K at 300 K	1.0 K at 300 K
Dynamic Range	30 - 330 K	30 - 330 K
Polarization	Horizontal	Vertical

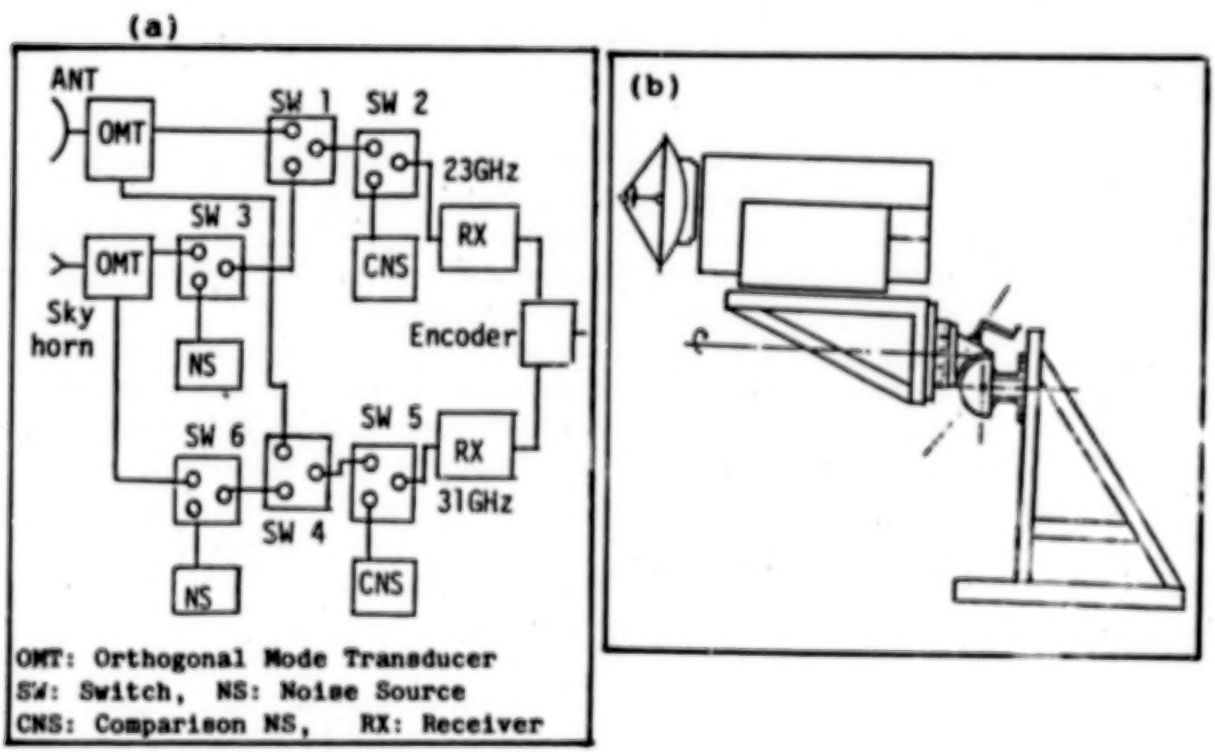

Figure 1. (a) Block Diagram of MSR Used in the Experiment,
(b) A Schematic Representation of MSR Fixed on a Frame.

As is indicated in the table, 23 GHz horizontal component and 31 GHz vertical component are observed simultaneously. Although MSR is kept at incident angle 10 degrees onboard MOS-1 with conical mode of scanning, it was decided to conduct the experiments for various incident angles. The MSR was mounted on a frame extended from the top of 5 meter height tower with capability of adjustable elevation angle with a handle.

Polarization was also adjustable by rotating the radiometer about its electrical axis thus it was possible to measure brightness temperature of snow surface with the incident angle ranging from 0 to 75 degrees in both vertical and horizontal polarization.

In parallel with the brightness temperature observation of snow surface, ground truth data indicated in Table 2 were also acquired.

Table 2
Ground Truth Data Obtained in the Experiments

parameter	Instrument	Parameter	Instrument
Snow Depth	Snow Pole	Solar Radiation	Pyrheliometer
Water Equiv.	Snow Sampler	Radiation Budget	Net Radiometer
Density	Density Gauge	Wind	Anemometer
Snow Surface Temp.	Thermometer	Air Temp.	Thermometer

BRIGHTNESS TEMPERATURE VS INCIDENT ANGLE

Many observations were made for different conditions of snow surface and weather. The analyses of the data indicate a pronounced effect of incident angle on the brightness temperature. A few examples are shown in Fig. 2 (a) through (d). It should be stated that it took about 80 minutes to complete one cycle of observation since rotation of the radiometer about its electrical axis is required to change polarization from horizontal to vertical and vice versa.

When weather condition was unfavorable longer observation time was required, thus the snow surface was not strictly constant during the observation. Consequently careful ground truth observation was made simultaneously.

The figures (a) through (c) are for dry snow while (d) is for wet snow. It can be seen from the figures brightness temperature decreases more sharply in horizontal component than that of vertical. It can also be seen that brightness temperature is higher over wet snow surface than over dry snow surface. This fact indicates the difficulty of interpretation of the data of microwave sensor for measurement of snow.

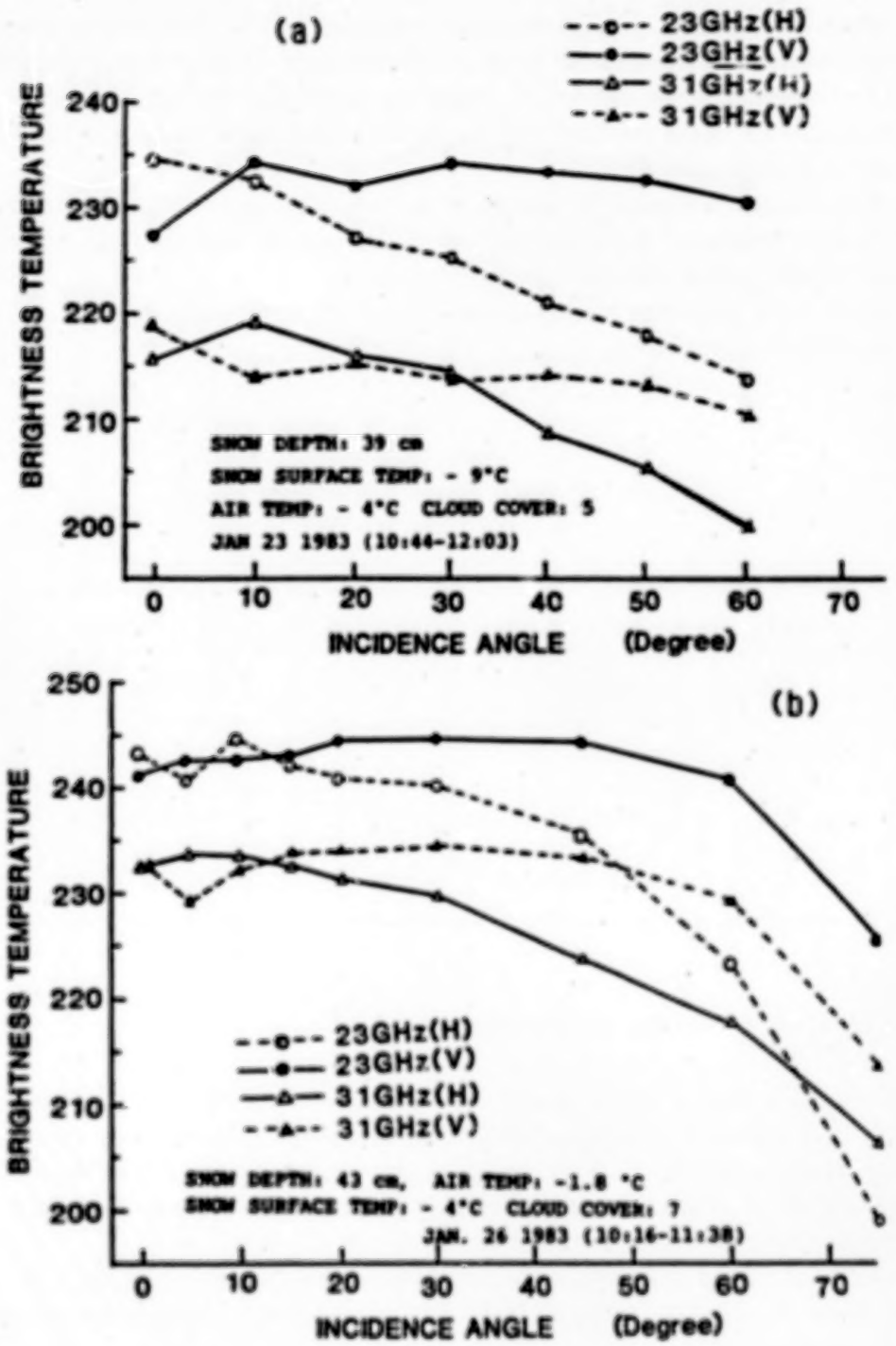

Figure 2. Incident Angle vs Brightness Temperature at 23 & 31 GHz. In the Figure V and H Stand for Vertical and Horizontal Polarization Respectively. The Combination of 23 GHz H + 31 GHz V or 23 GHz V and 31 GHz H is Operated Simultaneously. The Figures (a), (b) and (c) are for Dry Snow While (d) is for Wet Snow.

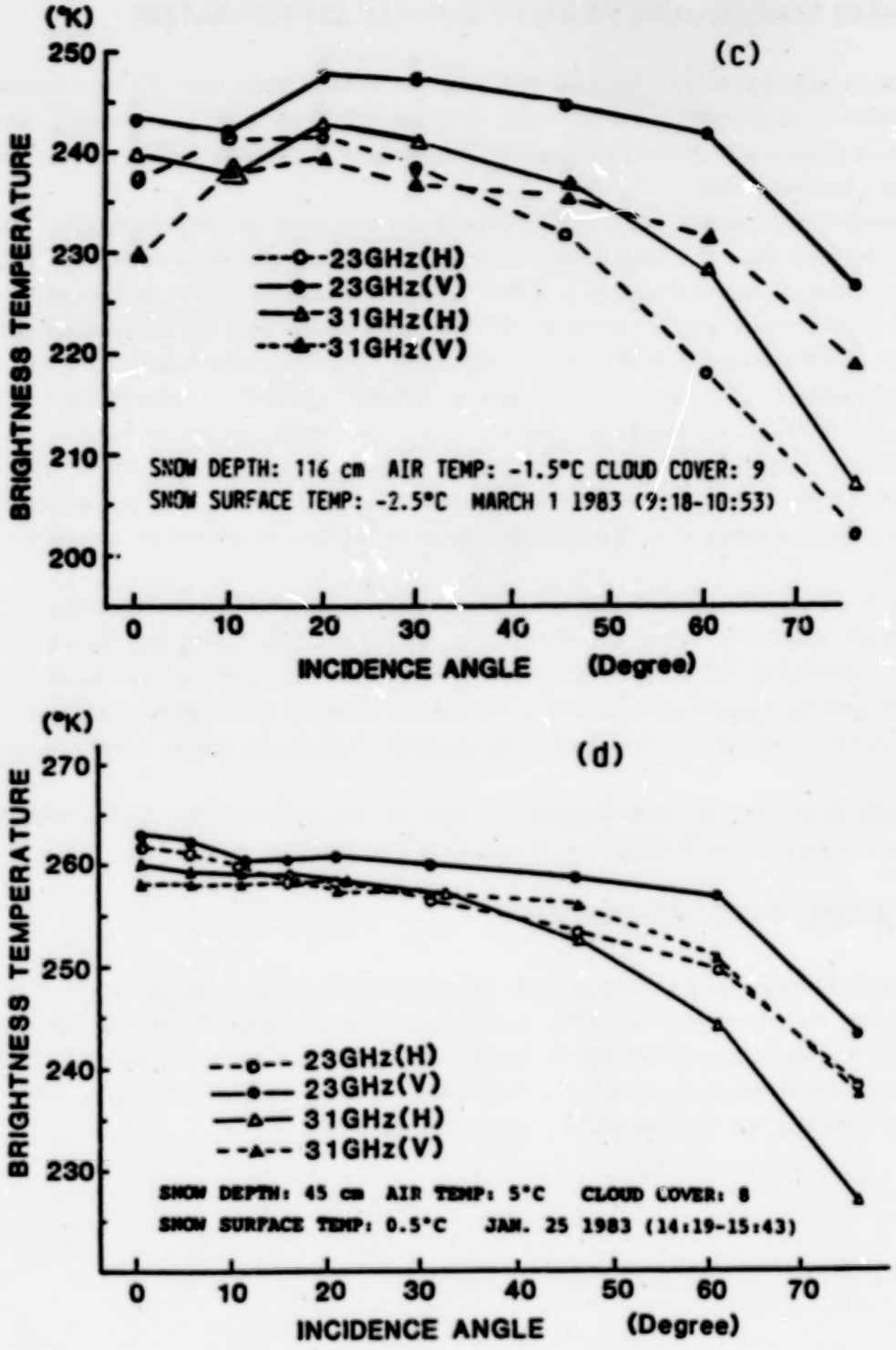

Figure 2. (c) and (d)

C-2

BRIGHTNESS TEMPERATURE VS SNOW SURFACE CONFIGURATION

Brightness temperature was measured with different incident angle over, (1) snow surface with parallel ditches of 5 cm depth and 5 cm width of 30 cm and 10 cm spacing respectively, which are oriented perpendicularly to electrical axis of the radiometer, (2) the snow surface after the ditches were pressed to level surface.

The incident angle dependence over dry snow under cold air temperature indicates a similar feature of dry snow while that made under warm air temperature indicates a feature of wet snow.

The influence of surface condition is shown in Fig. 3 (a) and (b) for dry and wet snow surface conditions respectively. Figure (a) indicates that spacing of ditches does not affect the brightness temperature except the case of 60 degrees incident angle. The figure also indicates that the brightness temperature of the pressed snow surface is higher regardless of incident angle which may lead to a conclusion that a pressed snow surface gives higher brightness temperature.

It should be stated that at the time of brightness temparture measurement, both air and snow surface temperatures rose significantly as is indicated in the figure, therefore it is considered that the rise of the brightness temperature is caused at least partly by the rise of both air and snow surface temperature.

Figure (b), a case of wet snow surface indicates a feature different from that of Fig. (a). It appears that the brightness temperature over 30 cm spacing is a little higher than that over 10 cm spacing. It is extremely interesting to notice that different from the previous case, the brightness temperature over the pressed snow surface is the lowest regardless of the incident angle. It should be again stressed that both air and snow surface temperature continuously fell as is well recognized in the figure.

The analysis of these two cases suggests that both air and surface effects must be taken into account in the interpretation of brightness temperature over the snow surface.

POLARIZATION ANGLE DEPENDENCE

The experiments on the polarization angle dependence were made at incident angle of 10, 30 and 45 degrees. As was pointed out in the previous report by Tsuchiya (1982) there was not a large difference in brightness temperature due to variation of polarization angle. In case of 23 GHz channel data brightness temperature increased corresponding to the increase of polarization angle while the opposite tendency was recognized for 31 GHz channel data.

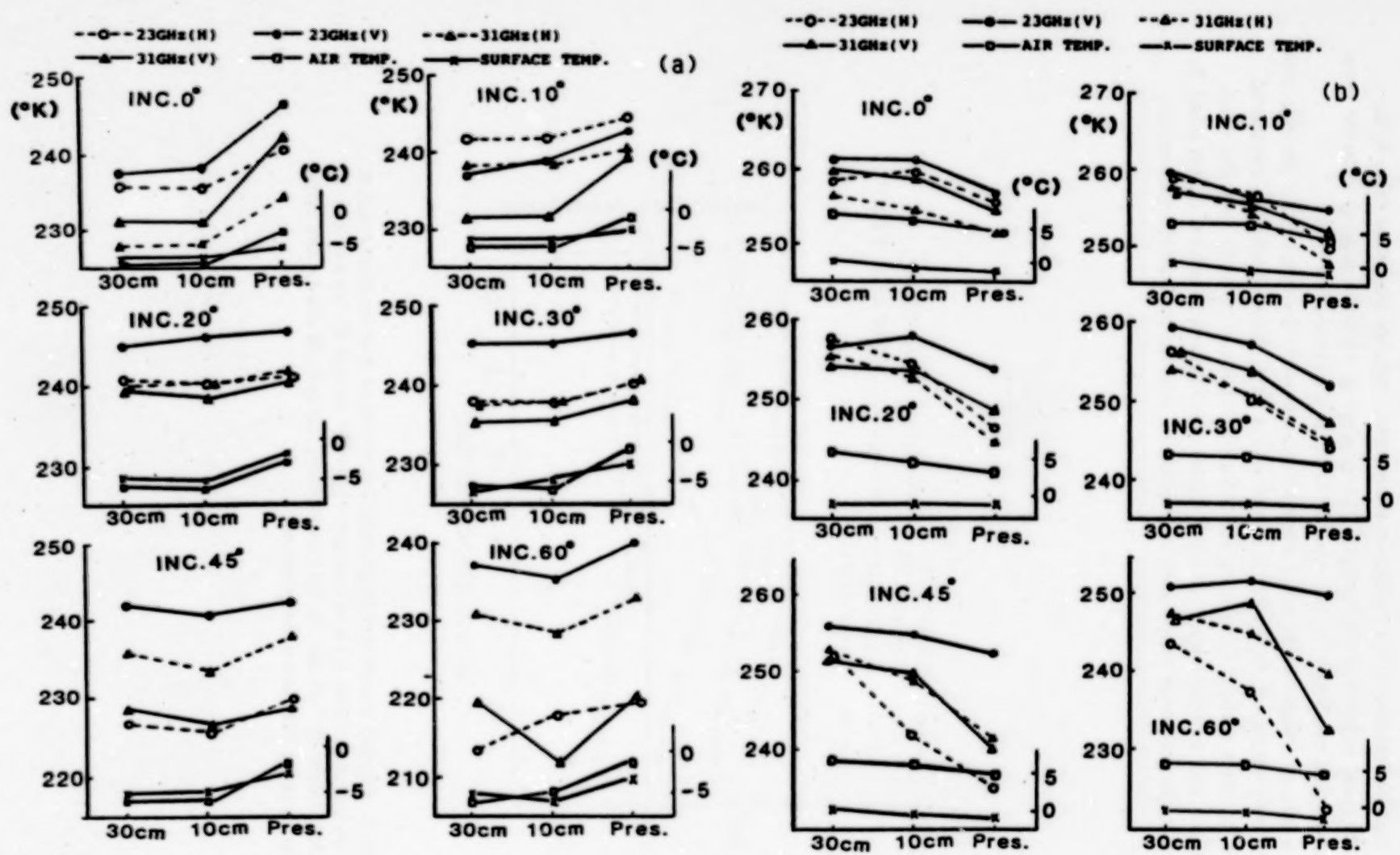

Figure 3. Brightness Temperature vs Incident Angle over Different Snow Surface Condition. 30 and 10 are Spacing of Ditches of 5 cm Depth and 5 cm Width. Pres Means Pressed Snow Surface. (a) is Dry Snow (March 4, 1983) and (b) is Wetsnow (Jan 28 '83).

DIURNAL VARIATION

There was a diurnal variation in the brightness temperature with the maximum value in the daytime with higher value in lower incident angle. The measure of variation depends upon the snow surface and meteorological conditions. A few typical examples are shown in Fig. 4.

Fig. 4 (a) is a case of comparatively small diurnal variation while the figure (b) is the case with a sharp rise in the early afternoon. Figure (c) is a case with a large variation which is considered due to freezing of the snow surface. Comparing the three figures it can be easily seen that when both the snow surface and air temperature are low brightness temperature variation is also small. It can be also seen that the brightness temperature is affected by both air and surface temperature.

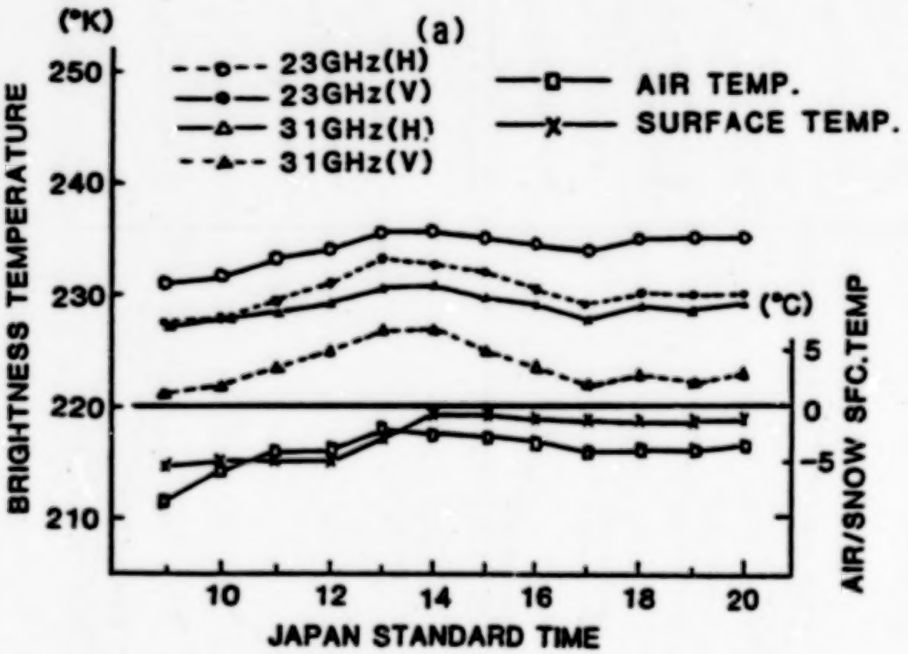

Figure 4. Diurnal Variation of Brightness Temperature is at Incident Angle at 10° on March 2, 1983, (b) is at Incident Angle 45° on Jan 27 '83 and (c) is at Incident Angle 10° on Jan 25 '83 Respectively. (a) and (b) are for Dry Snow While (c) is for Wet Snow Respectively.

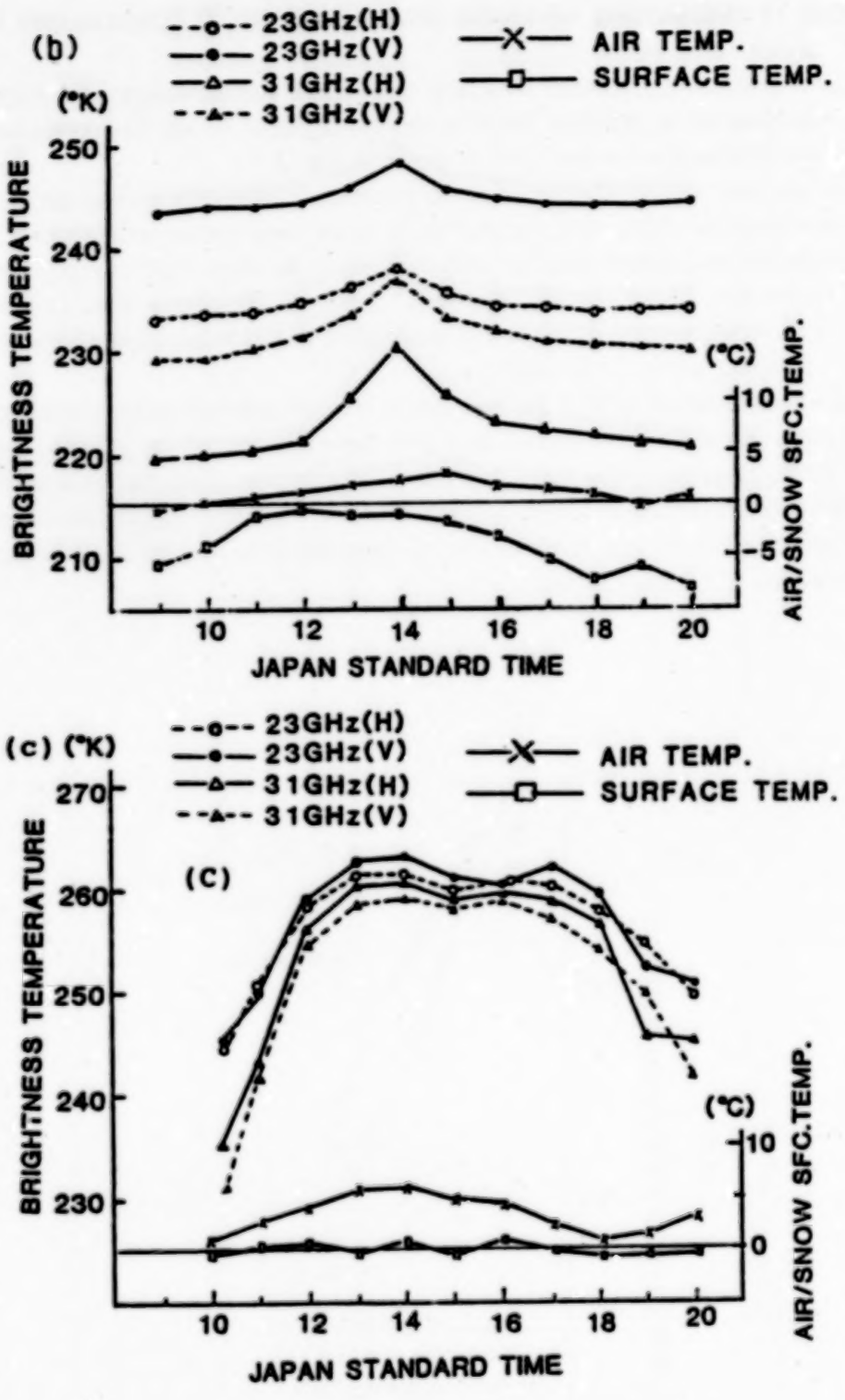

Figure 4. (b) Jan 27 '83. Incident Angle at 45° for Dry Snow. (c) Jan 25 '83 at Incident Angle 10° for Wet Snow.

BRIGHTNESS TEMPERATURE VS SNOW DEPTH AND SNOW EQUIVALENT WATER

To obtain the relationship between brightness temperature and snow depth, the brightness temperature was observed by removing snow at incident angles of 10 and 45 degrees respectively. The result of the observations for two cases is shown in Fig. 5.

It can be seen that the rate of decrease of the brightness temperature corresponding to the increase of snow depth is widely different depending on the snow surface and meteorological conditions. The brightness temperature decrease corresponding to the snow depth is recognized up to the depth of 70 cm for both 23 and 31 GHz horizontal polarization component while in case of vertical polarization component, decrease of brightness temperature ceased at the depth of 60 cm for both channels as is indicated in Fig. 5 (b) and (c).

It should be stated that in spite of the fact that as extreme care was taken to remove the snow, the physical properties of the snow surface must have been affected and the obtained brightness temperature for the respective snow depth might be a little different from that of natural condition. In spite of this defect a qualitative feature of snow depth vs brightness temperature relationship obtained in these experiments will be of an extreme value for understanding snow properties and microwave radiation of the snow surface.

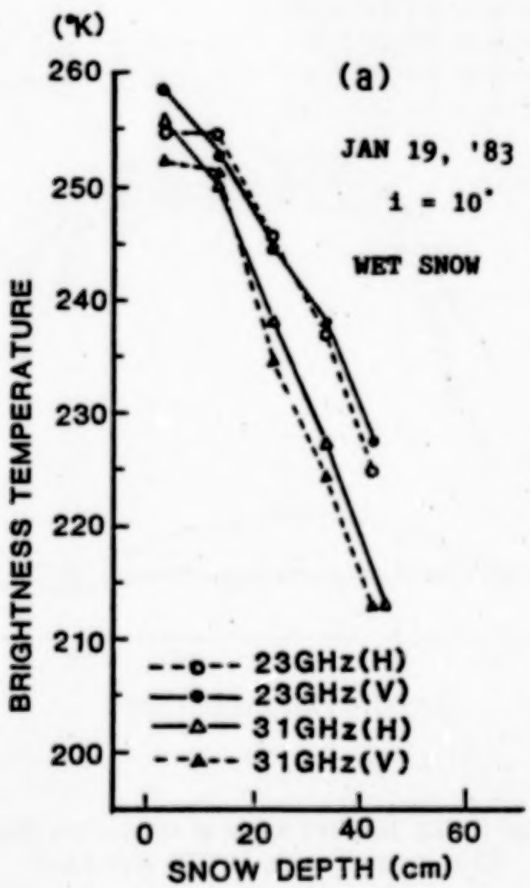

Figure 5. Brightness Temperature vs Snow Depth. (a) Jan 19 '83 at Incident Angle 10° Over Wet Snow Surface. (b) and (c) are Dry Snow.

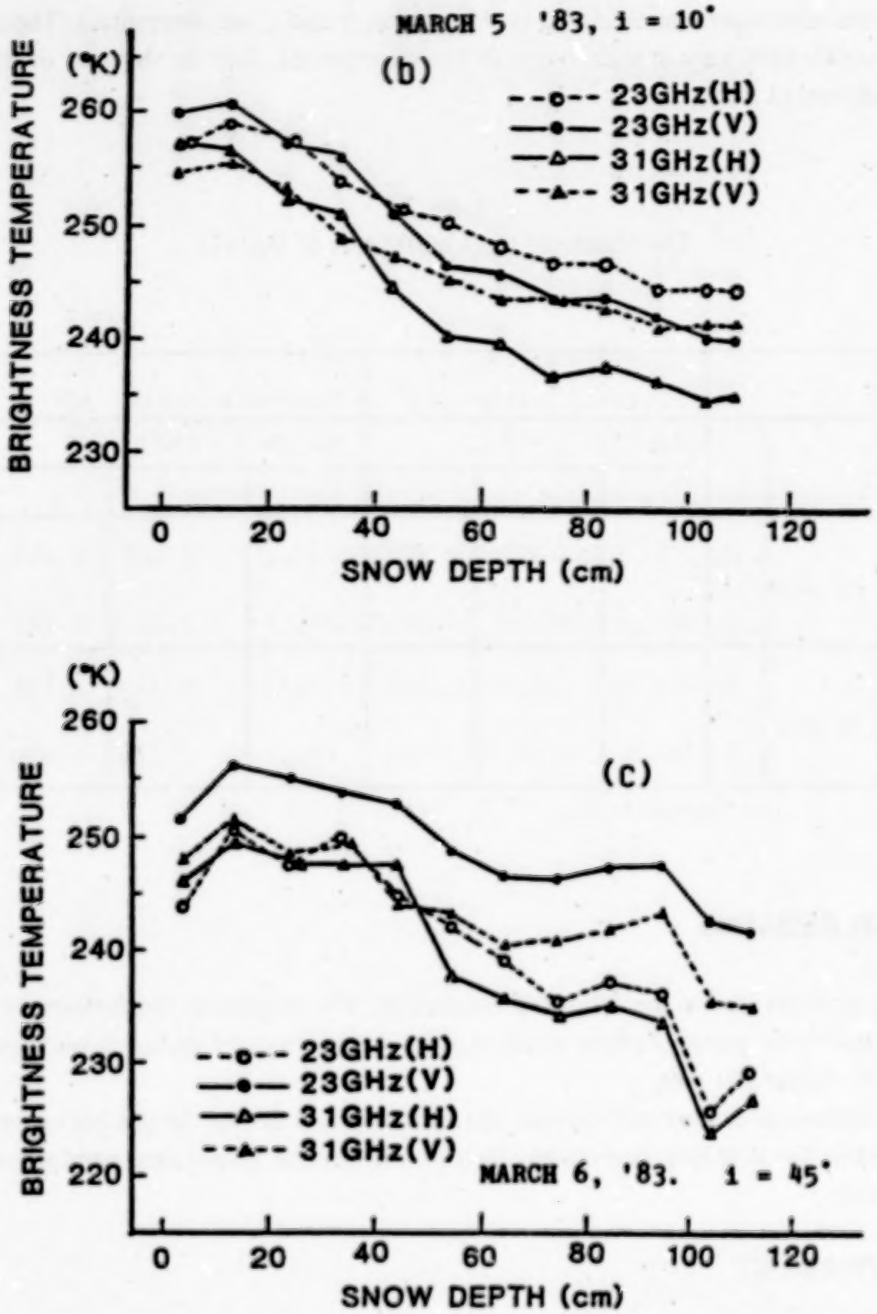

Figure 5. (b) and (c). Dry Snow Surface.

Based on the experimental data, an attempt is made to express the brightness temperature as a function of snow equivalent water for incident angles of 10 and 45 degrees in a form of Eq. (1).

$$T = a + b \exp(-cW) \tag{1}$$

where W is snow equivalent water in the unit of gr/cm^2.

Applying the least square method, the coefficients a, b and c are determined. The obtained values of the coefficients vary in wide range as can be expected. Just for the sake of interest a few examples are shown in Table 3.

Table 3
The Values of the Coefficients of Eq. (1).

		Incident angle: 10°			Incident angle: 45°		
		Jan 29 1983			March 6 1983		
		a	b	c	a	b	c
23 GHz	H	257.7	-2.9	0.244	243.8	- 0.007	0.247
	V	282.2	-28.9	0.073	251.6	- 0.033	0.187
31 GHz	H	276.9	-21.4	0.109	246.2	- 0.367	0.130
	V	271.7	- 20.0	0.107	251.6	- 3.726	0.050

H: Horizontal, V: Vertical

CONCLUDING REMARKS

Foregoing analyses lead to the following conclusion. The brightness temperature of the snow surface is influenced by various factors which suggest complexities of deducing snow properties from microwave radiometer data.

Although limited in number and volume, the data obtained during the present experiments are extremely valuable for obtaining dependable algorithm to deduce geophysical parameters from MOS-1 MSR data.

ACKNOWLEDGEMENT

The present research has been realized under Japan/US Cooperative Research Program, in this respect the authors wish to extend their sincere gratitude to all those who have contributed to realize the program. The authors deep appreciations are due to Messrs Tamotsu Igarashi and Chu Ishida of National Space Development Agency of Japan for their great effort in conducting the experiments. The authors are greatly indebted to Prof. Goro Wakahama of Hokkaido University and staff members of Environmental Research and Technology Institute and Mitsubishi Electric Company in realizing the experiments. The authors are also thankful to Mr. Katsutoshi Kozai of ERTI for his help in data handling.

REFERENCES

England, A. W., 1975: Thermal microwave emission from a scattering layer. J. of Geophys. Res., 80, 4484-4496.

Hofer, R. and E. Shanda, 1978: Signature of snow in the 5-94 GHz range. Radio Science, 13, 365-369.

Rango, A., T. C. Chang and J. L. Foster, 1979: Utilization of spaceborne microwave radiometers for monitoring snowpack properties. Nordic Hydrology, 10, 25-40.

Stiles, W. H. and F. T. Ulaby, 1980: The active and passive microwave response to snow parameters, 1. Wetness. J. of Geophys. Res., 85, 1037-1045.

Tiuri, M. and H. Schultz, 1980: Theoretical and experimental studies of microwave radiation from a natural snow field. Proc. Sensing of Snowpack Properties, 10 pp., fortcollins.

Tsuchiya, K., S. Yamamoto, C. Ishida, K. Takeda, Y. Yajima and S. Morizono, 1982: Two frequency microwave radiometer experiment over snow field. Proc. of the 1st Japan/US Snow/Evapotranspiration Workshop, 127-142 NIR, Science & Technology Agency, Tokyo, Japan.

D8

ANALYSIS OF NIMBUS-7 SMMR DATA*

Kiyoshi Tsuchiya

Institute of Color & Image Technology, Chiba University
1-33, Yayoi-cho, Chiba-city, Chiba-ken, Japan, 260

Kaname Takeda

National Institute of Resources, Science & Technology Agency

Katsutoshi Kozai

Environmental Research and Technology Institute

ABSTRACT

The brightness temperature obtained with SMMR of NIMBUS-7 over snow field of Hokkaido, one of the four major islands of Japan located in the north indicates the following features. (1) The relationship between snow depth and brightness temperature changes when snow depth becomes deeper than 50 cm. (2) Average brightness temperature of the daytime indicates negative correlations with snow depth except 6.6 GHz channel data which indicates weak positive correlation.

INTRODUCTION

It has been reported that NIMBUS-7 SMMR data are applicable to the study of snow [1,2]. As a part of Japan/US cooperative study on snow properties, SMMR data have been analyzed with an objective to find out the applicability to a comparatively small area, such as Hokkaido, one of the 4 major islands of Japan located in the north. The result of the analysis is described in the following sections.

SMMR DATA USED IN THE STUDY

Three types of SMMR data are analyzed, one is the average brightness temperature of day and nighttime passes. The others are the average daytime brightness temperature and the average nighttime brightness temperature. The time of the data are February 1979, March 1979, February 1980, March 1980 and March 1981.

Since the IFOV of SMMR is fairly large, Hokkaido is divided into the subareas consisting of 0.5 degrees of latitude and 0.5 degrees of longitude as is indicated in Fig. 1 (a). As ground truth data, snow and meteorological data are collected from 178 observing stations among them 95 are in the subareas. Based on the snow depth data the average snow depth for each subarea is computed and used in the analyses. For the sake of simplicity the term "average" will be dropped hereafter and referred to simple as "the snow depth". There is at leat 1 station in such subarea except subarea 20 for which average snow depth was extrapolated. An example of the snow depth distribution map on March 4, 1981 is indicated in Fig. 1 (b) in the unit of cm.

---

*Presented at the 2nd US/Japan Snow/Evapotranspiration Workshop. Nov. 15-19, 1983, East-West Center, Honolulu, Hawaii.

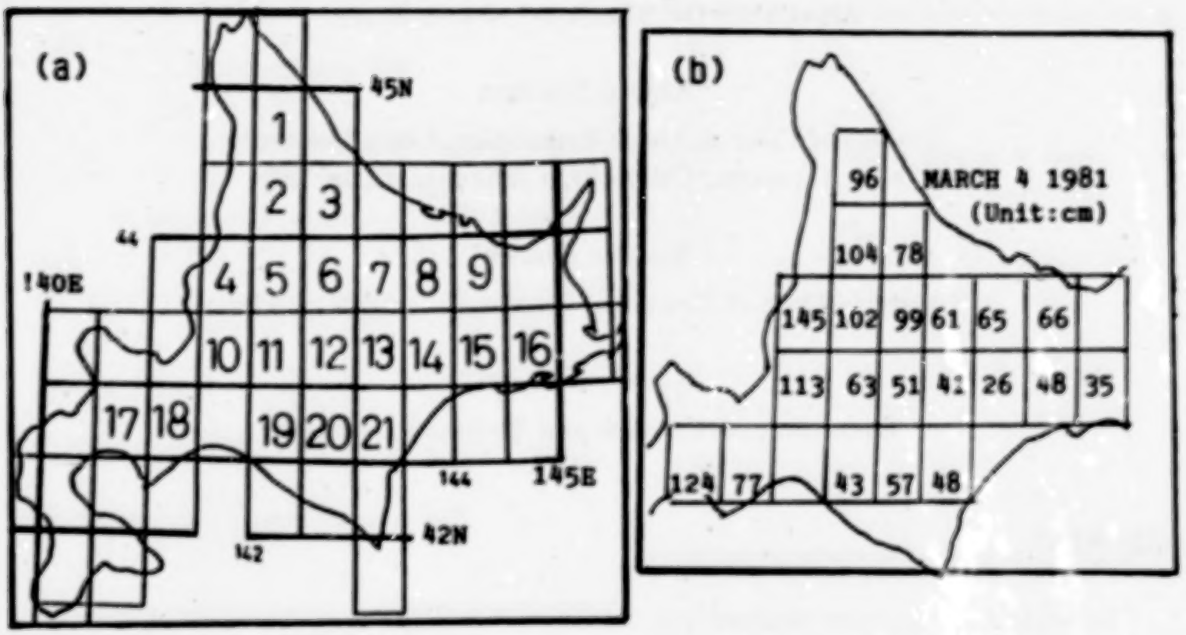

Figure 1. (a) Subareas and Their Number for the Study Area, Hokkaido and (b) Average Snow Depth (cm) on March 4, 1981.

THE RESULT OF THE ANALYSES

Relationship between the snow depth and average brightness temperature of day and nighttime on March 4, 1981 is shown in Fig. 2 for 6.6, 18 and 37 GHz respectively in which due to the limitation of the field of view of SMMR only eastern half of Hokkaido is included.

In the figure it can be seen that there are two clusters, i.e. one is the group with more than 50 cm snow depth while the other is characterized with that less than 50 cm snow depth. The latter indicates a negative correlation between the two. It is found that the latter case is for the subareas located in the plain snow field while the former is for the mountainous subareas.

To differentiate the day and nighttime brightness temperature vs snow depth relationship, Fig. 3 is made. Fig. 3 is the relationship between the brightness temperature and snow depth for the subareas of 14, 15, 16 and 21 which are plain areas. It can be seen that 37 GHz horizontally polarized brightness temperature versus snow depth has a negative correlation, however this feature is not so clear in the rest of the channels. It should be added the average maximum temperature for all the subareas was below freezing point, which indicates the snow was dry condition.

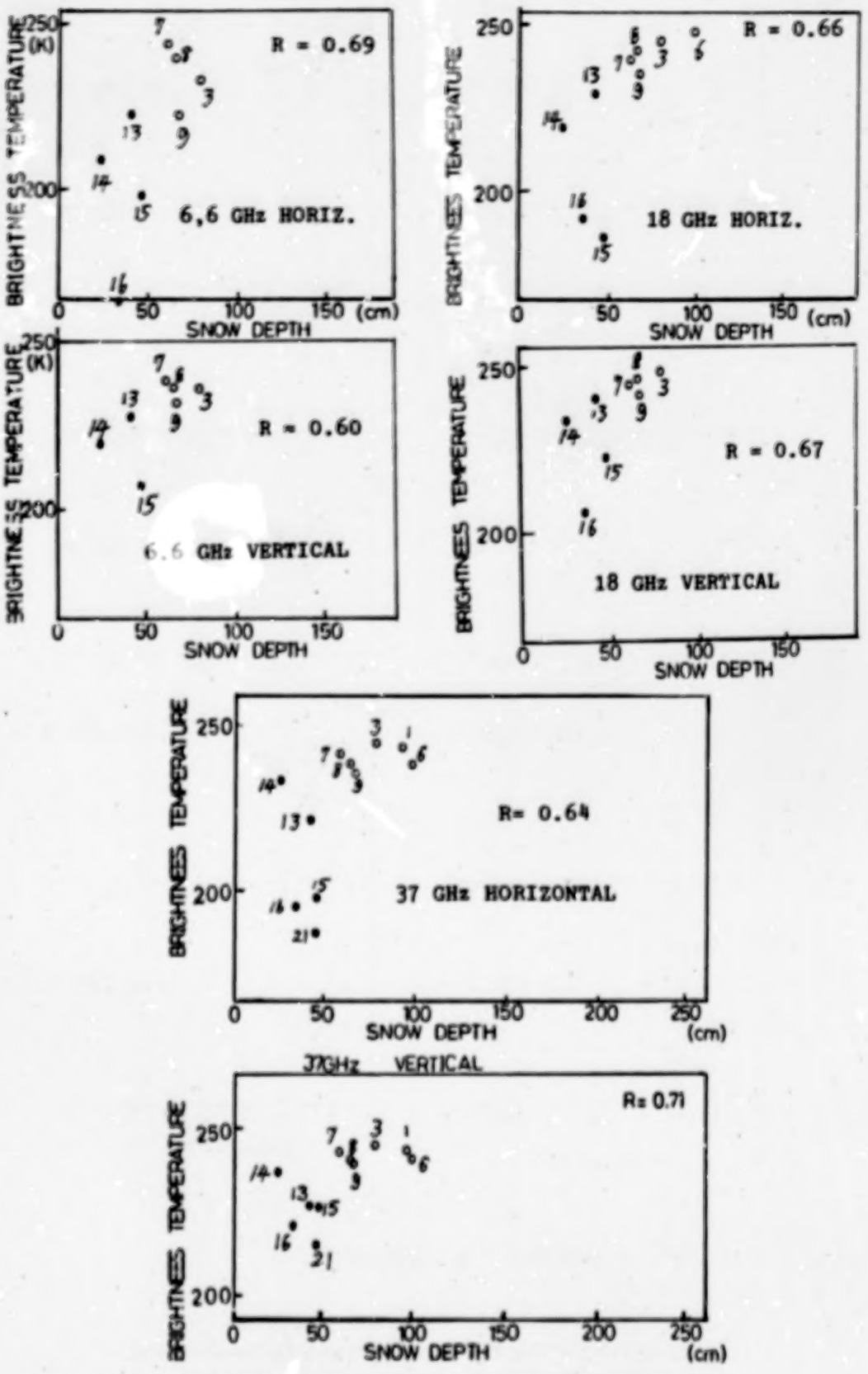

Figure 2. Relationship Between the Snow Depth and Average Brightness Temperature of the Day and Night Passes. March 4, 1981. Numerals are Subarea Number. R is Correlation Coefficient.

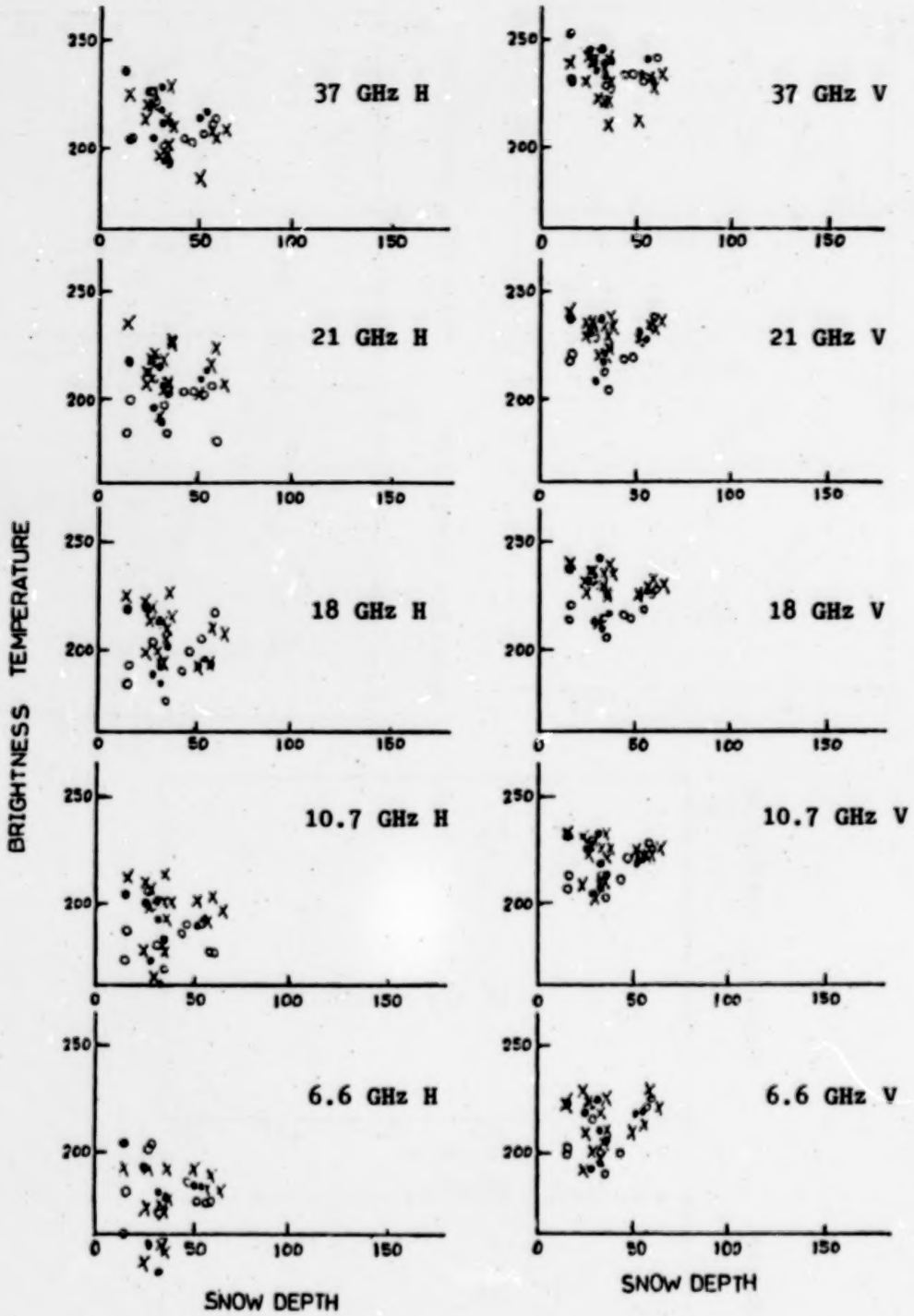

Figure 3. Relationship Between Brightness Temperature and the Snow Depth for the Subareas 14, 15 16 and 21.

The relationship between the snow depth and the daytime average brightness temperature is shown in Fig. 4 for the study period of Feb. 1979. In the figure existence of weak positive correlation is recognized in the lower frequency below 50 cm snow depth which is against a common understanding on the relationship between the two.

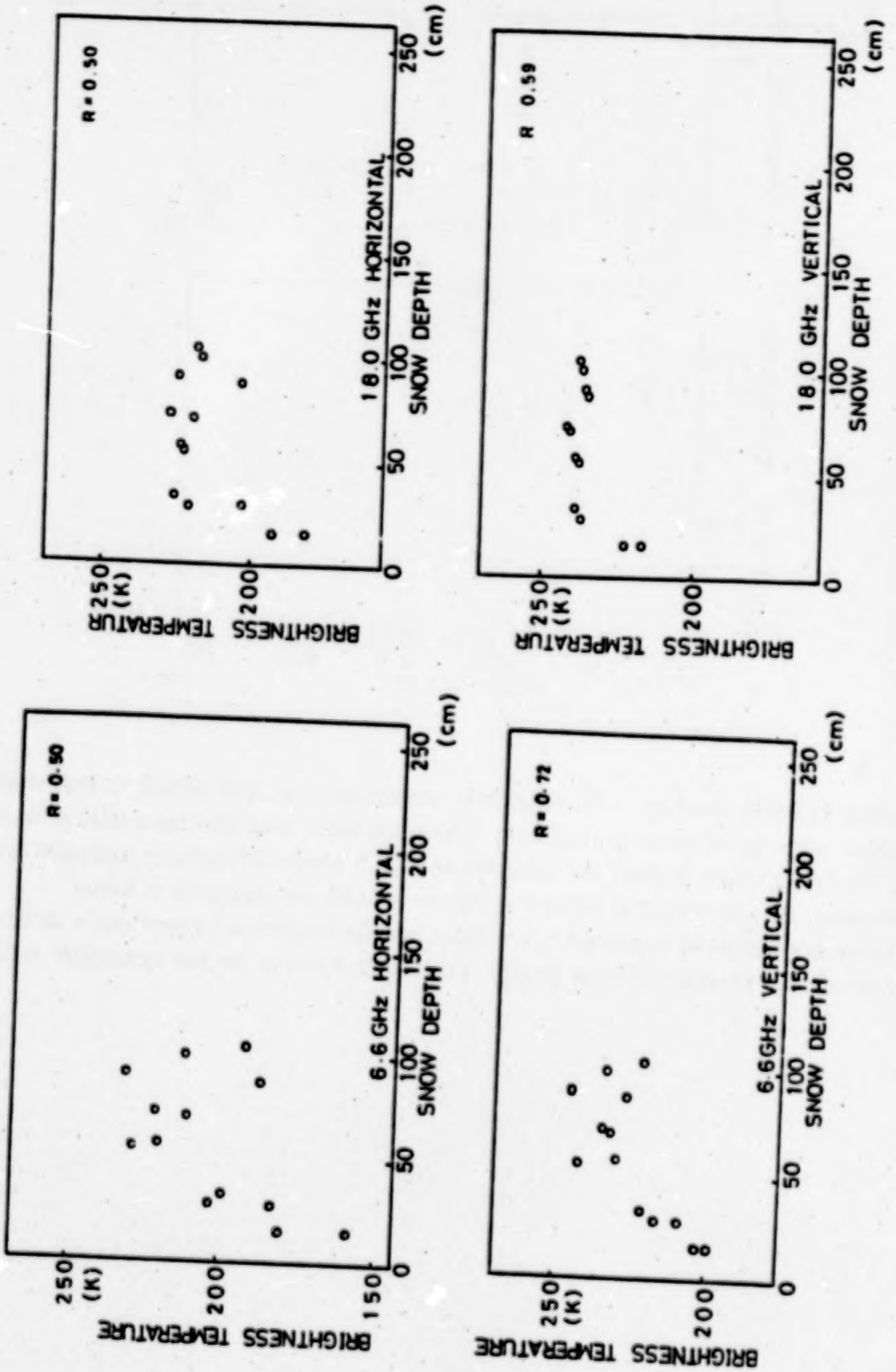

Figure 4. Relationship Between the Snow Depth and the Brightness Temperature of the Daytime in February 1979.

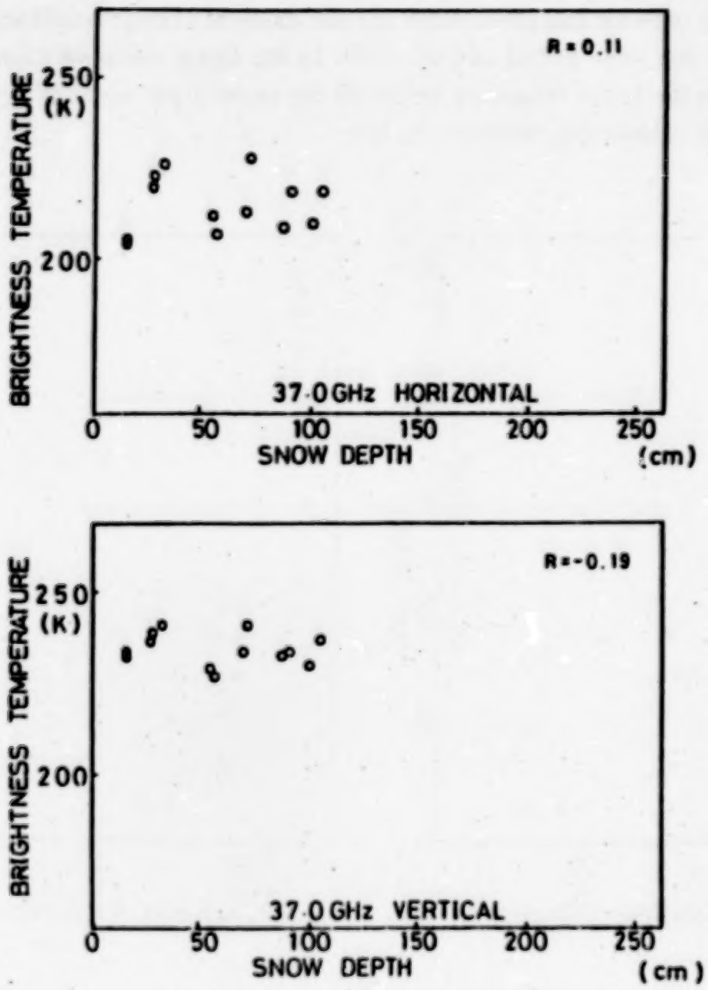

The effect of forest coverage to the brightness temperature was well studied by Hall et al [3]. Here in order to see an influence of vegetation, vegetation index map showing a relative occupation of conifer (evergreen) trees is made and indicated in Fig. 5 which differentiates hardwood area from that of softwood. Here hardwood is defined as the trees which are defoliated in winter.

The relationship between vegetation cover index and the brightness temperature is shown in Fig. 6 which indicates the existence of weak positive correlation between the two parameters in 6.6 GHz.

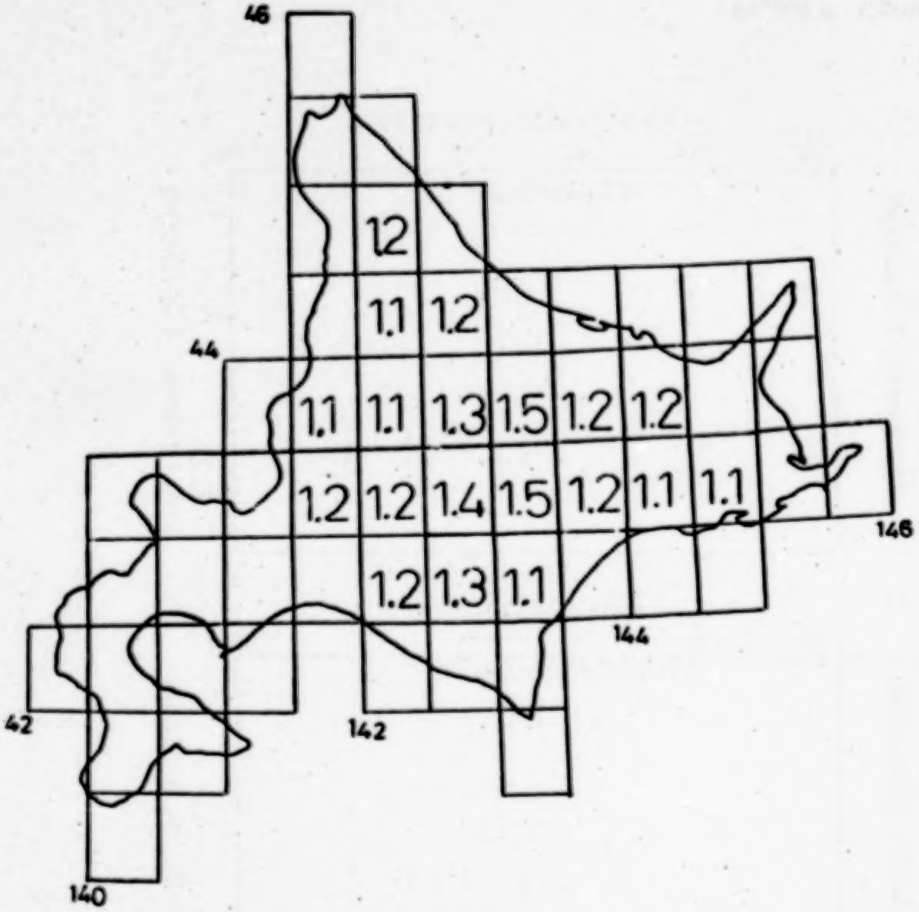

Figure 5. Vegetation Cover Index. 1.0: Sparse (Hardwood), 2.0: Dense (Softwood).

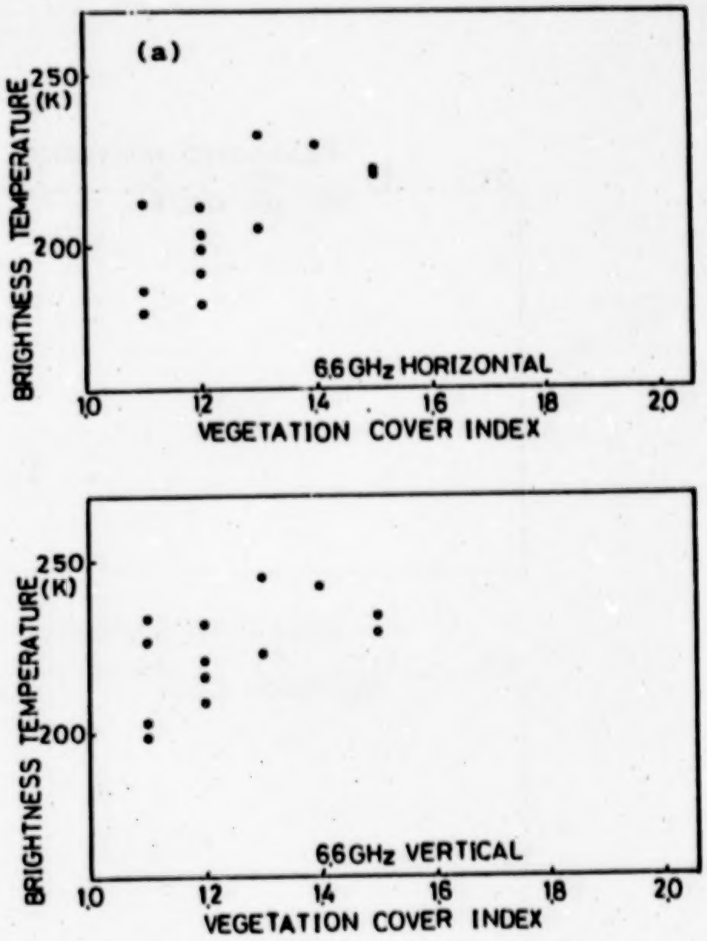

Figure 6. Relationship Between Vegetation Cover Index and Brightness Temperature for the Daytime of February 1979. (a): 6.6 GHZ, (b): 18 GHz, (c): 37 GHz.

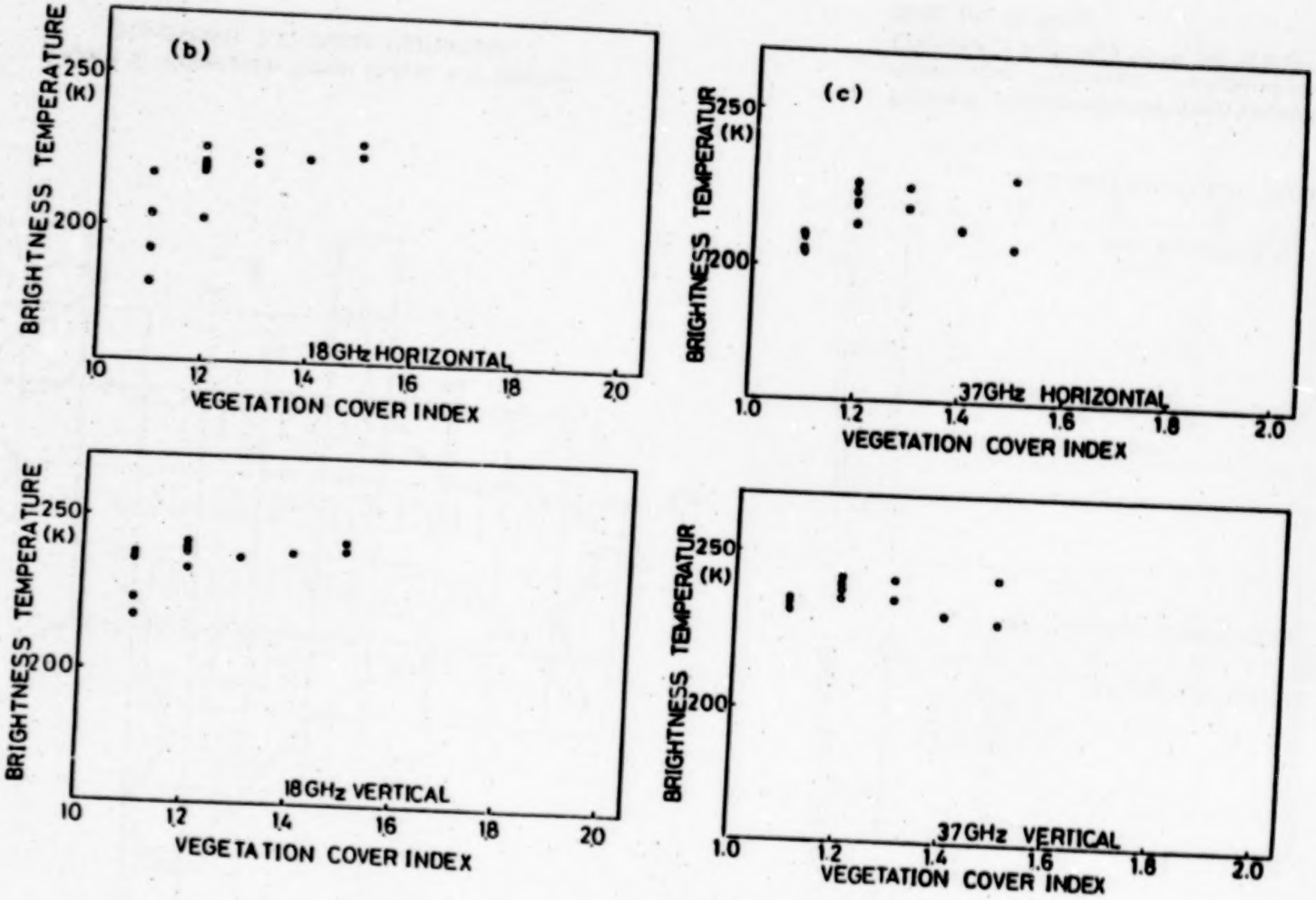

Figure 6. Continued.

Through the analysis of correlation between the snowdepth and the brightness temperature together with the brightness temperature distribution, it is found that there are subareas characterized with lower and higher brightness temperatures which is considered due to surface condition such as lakes and forest type. These subareas are classified as follows (as to the location see Fig. 1).

(i) Subareas characterized with low brightness temperature
(a) extremely low: 15, 16 and 21, (b) comparatively low: 17 and 18.

(ii) Subareas characterized with high brightness temperature
(a) extremely high: 3, 6, 7 and 8, (b) comparatively high; 1, 2, 3, 9, 11, 12 and 13.

If corrections for these effects are made to the brightness temperature, it is found that good negative correlation between the brightness temperature and the snow depth as well as snow equivalent water is obtained.

CONCLUDING REMARK

The foregoing analyses indicate that the interpretation of microwave radiometer data is not so simple since the brightness temperature is affected by various parameters.

ACKNOWLEDGEMENT

Authors' deep appreciation is due to Dr. Chang of GSFC NASA for supplying us the NIMBUS-7 SMMR data.

REFERENCES

1. Madrid, C. R. et al, 1978: The NIMBUS-7 users' guide. NASA GSFC.

2. Rango, A., A. T. C. Chang and J. L. Foster, 1979: The utilization of spaceborne microwave radiometers for monitoring snowpack properties. Nordic Hydrology, 10, 25-40.

3. Hall, D. K., J. L. foster and A. T. C. Chang, 1982: Measurement and modeling of microwave emission from forested snowfield in Michigan. Nordic Hydrology, 13, 129-138.

ESTIMATION OF REGIONAL EVAPOTRANSPIRATION USING REMOTELY SENSED LAND SURFACE TEMPERATURE

K. Kotada, S. Nakagawa, K. Kai, M. M. Yoshino

Environmental Research Center
University of Tsukuba
Sakuramura, Ibaraki, Japan

K. Takeda and K. Seki

National Institute of Resources
Science and Technology Agency
Chiyoda-ku, Tokyo, Japan

ABSTRACT

In order to study the distribution of evapotranspiration in the humid region through the remote sensing technology, first, in the Part I of this paper, the parameter (α) in the Priestley-Taylor model was determined. The daily means of the parameter $\alpha=1.14$ can be available from summer to autumn and $\alpha=1.5\sim2.0$ in winter. Secondly, in Part II of the present paper, the results of the satellite and the airborne sensing done on 21st and 22nd January, 1983, were described. Using the vegetation distribution in the Tsukuba Academic New town, the radiation temperature obtained by the remote sensing and the radiation data observed at the ground surface, the evapotranspiration was calculated for each vegetation type by the Priestley-Taylor method. The daily mean evapotranspiration on 22nd January, 1983, was approximately 0.4 mm/day. The differences of evapotranspiration between the vegetation types were not detectable, because the magnitude of evapotranspiration is very little in winter.

PART I
Measurement of Evapotranspiration at the Environmental Research Center, University of Tsukuba

and

Determination of Priestley-Taylor Parameter

K. Kotoda, S. Nakagawa, K. Kai and M. M. Yoshino

Environmental Research Center
University of Tsukuba
Sakuramura, Ibaraki, Japan

INTRODUCTION

Evaporation is the physical process by which a substance is converted from a liquid or solid state into a vapor state. In natural environment, evaporation of water is one of the main components

of the hydrological cycle. Water, entering into an evaporation phase in the hydrological cycle, becomes unavailable for further use by plants and human activities. Therefore, accurate knowledge of evaporation is indispensable for the planning and management of water resources.

Direct measurement of evapotranspiration over long time period is difficult because of the lack of routinely usable instruments. Moreover, evaluation of regional evapotranspiration is very difficult owing to the complex land properties. Therefore, many estimation methods for evapotranspiration have been developed and several concepts of evapotranspiration have been proposed.

The "potential evaporation", proposed by Priestley and Taylor (1972), is one of these concepts. They took the "equilibrium evaporation", presented by Slatyer and McIlroy (1961), as the basis for the estimation of potential evaporation. Potential evaporation, which is represented by Eq. (1), is defined as the evapotranspiration from a horizontally uniform saturated surface with a minimal advection

$$\lambda Ep = \alpha \frac{\Delta}{\Delta + \gamma} (Rn - G) = \alpha \lambda Eeq \qquad (1)$$

where λ is the latent heat for vaporization, Ep the potential evaporation, α the parameter, Rn the net radiation, G the soil heat flux, Δ the slope of the saturation vapor pressure curve, γ the psychrometric constant, Eeq the equilibrium evaporation. As the method proposed by Priestley and Taylor was very simple and physically sound, many applications have been made over a variety of surfaces.

The equation presented by Priestley and Taylor only needs climatological parameters so that it seems a promising tool for the estimation of evapotranspiration by a remote sensing approach. The value of α in Eq. (1), however, have been found to vary widely from crop to crop even under wet soil conditions. In this paper, the proposed values of α are reviewed first. After that, the representative value of α for pasture under wet soil conditions and the factors affecting the seasonal variations of α are discussed.

PARAMETER OF THE PRIESTLEY-TAYLOR MODEL

The applicability of the Priestley and Taylor model (hereafter referred to as P-T model), which is represented by Eq. (1), for the estimation of evapotranspiration from various surfaces has been examined in many places.

(1) Open water

For open water, the value of $\alpha = 1.26$ is supported by Stewart and Rouse (1976, 1977) for shallow lakes and ponds, de Bruin and Keijman (1979) for Lake Flevo over the summer and early autumn.

(2) Bare soil surface

Priestley and Taylor (1972) found that $\alpha = 1.08$ for bare soil surface on a day after a heavy rainfall by analysing the data obtained by Dyer and Hicks (1970). Barton (1979) obtained $\alpha = 1.05$ for a bare soil in a burnt area under potential conditions. However, Jackson et al. (1976) studied evaporation from clay loam soil to obtain $\alpha = 1.37$ under wet soil conditions by using daytime Rn and assuming G to be negligible.

(3) Land surface with short vegetation

In cases of land surfaces covered with fairly short vegetation, the data obtained by Stewart and Rouse (1977) for sedge meadow, Williams et al. (1978) for wheat, Nakayma and Nakamura (1982) for radish supported the value of $\alpha=1.26$. Davies and Allen (1973) obtained the value of $\alpha=1.27$ for well watered perennial ryegrass, Jury and Tanner (1975) $\alpha=1.28$ for potatoes and Mukammal et al. (1977) $\alpha=1.29$ for grass. However, Jury and Tanner (1975) obtained $\alpha=1.42$ for alfalfa, Kanemasu et al. (1976) $\alpha=1.43$ for soybean and Heilman et al. (1976) $\alpha=1.35$ for winter wheat. These values of α are greater than 1.26. The fact that the values of α are greater than 1.26 may suggest the existence of remarkable advection.

(4) Land surface with tall vegatation

For tall vegetation, like forests, McNaughton and Black (1973) found $\alpha=1.18$ for young Douglas fir forest (8 m high) on a day after rain had fallen and $\alpha=1.05$ from the data of well supplied with water but not wet condition. Spittlehouse and Black (1981) obtained $\alpha=1.1$ for Douglas fir and Stewart and Thom (1973) $\alpha=0.6\sim0.7$ for pine trees. Shuttleworth and Calder (1979) compared equilibrium evaporation (Eeq) with long-term evaporation (Ea) for a spruce forest in Plylimon, Wales, and with a Scot Pine forest in Thetford, Norfolk, and proposed the relationship of

$$Ea = (0.72\pm0.07)\Delta(Rn-G)/[\lambda(\Delta+\gamma)] + (0.27\pm0.08)P \qquad (2)$$

They suggested that the possibility of significant variability in evapotranspiration from forest vegetation in response to precipitation input P.

EXPERIMENTAL METHOD

Experimental site

The study was conducted at the heat and water balance experimental field of the Environmental Research Center (ERC), University of Tsukuba, Ibaraki Pref., Japan (36°05'N, 140°06'E). University of Tsukuba is located in the core of the Tsukuba Academic New Town about 60 km northeast of Tokyo (Fig. 3-1).

The experimental field is a circular plot with a radius of 80 m and has a 30-m meteorological tower at its center. The vegetation of the field consists of mixed pasture. The pasture approaches maturity in summer and mowing is done in early winter. The surroundings of the field are not completely homogeneous due to some buildings and pine trees. To the north of the field, there exists a large and long building which contains a large experimental flume, 188-m long and 9.5-m high. Pine trees with a height of about 10 m exist to the northwest and the southeast of the field.

Instrumentation

Research on the evapotranspiration is facilitated by a grass covered experimental field 80 m in radius (over 20,000 m²) and the 30-m meteorological tower. In the field and on the tower are a number of instruments including: sonic anemometer-thermometers (at 30.5, 29.5, 12.3 and 1.6 m),

resistance thermometers (at 29.5, 12.3 and 1.6 m), dew-point hygrometers (at 29.5, 12.3 and 1.6 m), resistance thermometers (at −2, −10, −50 and −100 cm), heat flux plates (at −2 and −10 cm), ground water level gauges (at −2, −10 and −20 m), a pryheliometer, a total hemispherical radiometer, a net radiometer, a weighing lysimeter, an evaporation pan, a rainfall intensity recorder, a rainfall gauge, and a discharge meter (for measuring runoff from the experimental field). Table 3-1 shows the observations items and instruments, and Fig. 3-2 shows the locations of the instruments in the field.

In addition to the 30-m tower there is also an 8-m observation pole. Psychrometers and 3-cup anemometers at heights of 0.5, 1.0, 2.0, 4.0 and 8.0 m provide data on wind speeds and wet and dry air temperatures. Periodic measurements are made of area and height of the grass growing in the experimental field.

Data collection

All of the instruments on the tower and in the field are tied into a terminal box that leads to a computer-controlled data acquisition system (Oriental Electronics Inc., Model A2270) and eventually to a printout form. The system consists of an analog-to-digital converter, a multiplexor for multichannel analysis, a microcomputer for system control, a cassette magnetic tape unit and a dot printer. The system records and prints out hourly and daily mean values of the observation items automatically.

DEVELOPMENT OF EQUILIBRIUM EVAPORATION MODEL

Determination of actual evapotranspiration

To obtain detailed information on evapotranspiration (E), intensive field observations were carried out from July 20 to August 31, 1980 at ERC experimental field. At the time of observation, the experimental field was covered with 40-cm tall pasture. During this period, 2-m high poles for the determinations of the profiles for air temperature, vapor pressure and wind speed were installed. Air temperatures and vapor pressures were observed at heights of 0.1, 0.2, 0.4, 0.8 and 1.6 m by ventilated psychrometers with C-C thermocouples. Wind speeds were observed at heights of 0.4, 0.8, 1.2, 1.6 and 2 m by three-cup anemometers.

For a short time period such as 1-hr, the use of a weighing lysimeter for the determination of actual evapotranspiration is very difficult, because of measurement errors caused mainly by wind. Therefore, an energy budget-Bowen ratio (EBBR) method was used for the determination of hourly evapotranspiration. As mentioned, temperature and vapor pressure were measured at three levels above the crop surface, namely 0.8, 1.2 and 1.6 m. The combinations of 1.2 with 1.6 m or 0.8 with 1.6 m were used for the calculation of Bowen ratio. The EBBR method, however, could not be used occasionally at either sunrise or sunset. Also on occasions there might be a drying of a wet-bulb. The energy budget with wind and scalar profile (EBWSP) method (Brutsaert, 1982) was used, when the EBBR method could not be applied. Temperatures and wind speeds measured at heights of 0.8 and 1.6 m were used in the EBWSP method.

Daily evapotranspiration was obtained by a weighing lysimeter.

Relationship between actual evapotranspiration and equilibrium evaporation

The method proposed by Priestley and Taylor (1972) has been applied to a variety of surfaces owing to its simple and reasonable form. The value of $\alpha=1.26$ was universally obtained for evaporation from open water surfaces. It has been reported, however, that the value of α is not necessarily equal to 1.26 over bare soil or vegetated surfaces even under wet soil conditions and that it varies depending on surface properties.

Analyses were made to determine the representative value of α for pasture. The pF values of soil water matric potential were below the critical value when soil water limits the evapotranspiration.

Figure 4-1 shows the hourly variations of α obtained from hourly values of actual evapotranspiration and equilibrium evaporation. Although the hourly variations of α differ from day to day, it can be seen as a general pattern that α takes maxima early in the morning and late in the afternoon, and that a minimum occurs near midday with few exceptions (e.g., August 12, 13 and 29). Except for these days, α values are between 0.95 to 1.4. The diurnal variations of α obtained here differ from the previous results for a grass by Yap and Oke (1974) and for a lake by de Bruin and Keijman (1979). They observed the diurnal variations of α with a midday minimum followed by a rise to mid-to-late afternoon. It is worth noting that the diurnal patterns of α obtained in this analysis differ from the previous observational results described above. That is, large values of α occur not only in the afternoon but also early in the morning. In addition, the value of α early in the morning tends to be larger than that in the late afternoon.

To consider the reason of the large values of α in the early morning, the amount of nighttime dewfall and the duration of dew evaporation were calculated. The amount of nighttime dewfall was calculated by summing up negative E values obtained by the EBWSP method. The duration of dew evaporation was obtained as follows: firstly, dew evaporation was considered to start when positive E occurred. Secondly, dew evaporation was considered to stop when the accumulated positive E became larger than the amount of dewfall. By comparing the durations of dew evaporation with the value of α, the large value of α in the early morning proved to be caused by the fact that an evaporating surface acts as a completely saturated surface due to the evaporation of dew. The gradual drops of α observed late in the afternoon on August 12 and 13 may be attributed to an increase in the aridity of air.

Figure 4-2 shows the relationship between actual evapotranspiration (E) and equilibrium evaporation (Eeq). It can be seen in Fig. 4-2 that, on the whole, actual evapotranspiration falls in the range between the equilibrium evaporation ($\alpha=1$) and the potential evaporation ($\alpha=1.26$). From Figs. 4-1 and 4-2, it is obtained that the value of α early in the morning is usually near 1.26 but for the rest of the day α tends to be smaller than 1.26. The average value of α during the evaporation of dew proves to be 1.25 ± 0.02, which is very close to the value of $\alpha=1.26$ for saturated surfaces. The $\pm$ notation is used to denote the standard error of the mean. On the other hand, actual evapotranspiration is nearly equal to the equilibrium evaporation only very humid days (i.e., August 29 and 30). The overall mean of α is taken as 1.16 ± 0.01, which is smaller than the value of α for completely wetted surface.

From the above discussion, it becomes clear that the upper limit of evapotranspiration is represented by the potential evaporation and the lower limit by the equilibrium evaporation for actively growing pasture with no shortage of water. Actual evapotranspiration, however, is usually

smaller than the potential evaporation even if there is no shortage of soil water for evapotranspiration. Actual evapotranspiration becomes equal to the potential evaporation when the evaporating surface acts as a completely saturated surface during the evaporation of dew.

Figure 4-3 shows the relationship between the daily actual evapotranspiration (Ely) and the daily equilibrium evaporation (Eeq). As shown in Fig. 4-2 α ranges from 1.0 to 1.26. However, the scatters of data are smaller than those in Fig. 4-2. The average value of α is found to be 1.14 ± 0.03, which is almost the same average value of α obtained from the analysis of hourly data but it is smaller than 1.26 for completely wetted surfaces.

Validity of the equilibrium evaporation model

As stated above, daily evapotranspiration from actively growing pasture under a non-limiting soil water condition can be expressed as

$$E = \alpha Eeq \tag{3}$$

where α is a constant equal to 1.14. Hereafter, the estimation method of evapotranspiration with equilibrium evaporation as a basis is referred to as "equilibrium evaporation model" (E-E model), which is expressed by Eq. (3).

The test of $\alpha=1.14$ in the E-E model is made for the whole observation period in the summer of 1980 (from July 20 to August 31). Figure 4-4 shows the daily variations of actual evapotranspiration (Ely) measured by a weighing lysimeter and estimated evapotranspiration (Ees) from the E-E model with $\alpha=1.14$. The plot for August 5 is missing because of lack of data. Evapotranspiration was zero on August 3 due to an all-day rain. As can be seen in Fig. 4-4, the daily variations of Ees and Ely are closely related.

The summer of 1980 was a season of unusual weather because of low rainfall, low sunshine and low temperature (Murakami, 1981). Hence, it is questionable whether the value of α obtained in 1980 is valid for other years. To investigate this question, the E-E model was tested again using summer data of 1978. The summer of 1978 was hot, in contrast to the summer of 1980. In 1978, net radiation and soil heat flux measurements were only available from August 4 to 24. Figure 4-5 shows the daily patterns of Ely and Ees for 1978. Similar to the results for 1980, there exist close relationships between Ely and Ees, which confirms the validity of $\alpha=1.14$ in the E-E model.

Table 4-1 shows the totals of Ely, Eeq and Ees for both observation periods. It can be seen in Table 4-1 that evapotranspiration from actively growing pasture with no soil water shortage can be estimated with an accuracy of about 5% by the E-E model with $\alpha=1.14$

APPLICATION OF EQUILIBRIUM EVAPORATION MODEL TO SEASONAL EVAPOTRANSPIRATION

Seasonal Variations of α

Net radiation, soil heat flux, air temperature and evapotranspiration had been measured continuously until April 17, 1981 after intensive observations during the summer in 1980. The applicabilities of the equilibrium evaporation model (E-E model), especially the variations of the proportional constant α in Eq. (3) were investigated using the data obtained from September to April.

The day-to-day variations of daily values of α in the E-E model shows very complex features (Fig. 5-1). Moreover, the values of α become very large especially in winter months and in some cases they exceed the value of $\alpha=1.26$ for completely saturated surface.

Factors affecting the seasonal variations of α

Seasonal variations of α have been reported by Jackson et al. (1976), McNaughton et al. (1979), de Bruin and Keijman (1979) and Nakayama and Nakamura (1982) for bare soil, pasture, shallow lake and radish, respectively. All of them found an increase in α in cool season but seasonal variations of α from winter to spring have not been reported yet. It has been pointed out that large value of α is obtained when daily energy balance terms are used rather than daytime ones (Yap and Oke, 1974; Kanemasu et al., 1976; Tanner and Jury, 1976).

To evaluate the factors affecting the seasonal variation of α, an analysis based on daytime data was conducted.

In this analysis, the daytime period was considered as the period during which available energy $(Rn\text{-}G) \geq \mu 0$. The day-to-day variations of α, obtained from daytime data, show small fluctations and the value of α do not exceed 1.14, which was obtained from the summer data (Fig. 5-2). Furthermore, the march of α shows a distinctive seasonal trend.

Figure 5-3 shows seasonal variations of monthly mean values of α. Daily α and daytime α are almost equal in August but daily α is consistently greater than daytime after September. Month-to-month variations of daily α show a complicated pattern. On the contrary, daytime α shows a distinctive month-to-month variation pattern which may reflect the physiological nature of pasture.

To examine the effect of nighttime radiative cooling on the differences in α with different averaging time, the degree of nighttime decrease rate of available energy (R') was calculated from

$$R' = \frac{\overline{(Rn - G)} - (Rn - G)_d}{(Rn - G)_d} \tag{4}$$

where the bar and the subscript d represent daily values and daytime values, respectively. Figure 5-4 shows the seasonal trend of R'. By comparing Fig. 5-4 with Fig. 5-3, it may be found that the variations in R' and those in the difference between daytime α and daily α have similar seasonal patterns. To investigate the relationship between them, the rate of increase in $\alpha(\alpha')$ was calculated by

$$\alpha' = \frac{\bar{\alpha} - \alpha_d}{\alpha_d} \tag{5}$$

where the meanings of bar and subscript d are the same as those in Eq. (4). Figure 5-5 shows the relationship between α' and R' calculated from monthly means values. As can be seen in Fig. 5-5, there exists an almost linear relationship between α' and R', which implies that the differences between daily α and daytime α are caused by the nighttime decrease in available energy.

As described above, α in the E-E model proves to be an effective parameters showing distinctive seasonal variations which may reflect the activity of pasture. Special attention, however, should be paid to the application of the E-E model to periods with strong nighttime radiative cooling.

Monthly evapotranspiration estimate with equilibrium evaporation model

To apply the E-E model to the annual evapotranspiration estimate, the values of α for May and June must be included. The daily integrated radiation data by the routine measuring system became

available from August 1981. Therefore, the values of α for May and June were calculated from the routine data in 1982. Since data of soil heat flux (G) were not available in May and June in 1982, G was estimated from the regression equation between Rn and G observed from September, 1980 to April, 1981. As a result, α=1.15 for May and α=1.12 for June were obtained. The monthly mean values of daily α are summarized in Table 5-1. It is noticeable in Table 5-1 that α takes nearly the same value from May to August, during which pasture grows actively and the effects of nighttime radiative cooling on daily available energy are considered slight.

The estimation of monthly evapotranspiration by the E-E model with α listed in Table 5-1 was carried out for the periods from 1980 to 1982. The results are shown in Fig. 5-6. It is clear from Fig. 5-6 that there exists close agreement between estimated and measured monthly evapotranspiration. In addition, annual evapotranspiration can be estimated within 10% accuracy by the E-E model.

PROBLEMS OF ADVECTION

Advection due to incomplete adjustment of atmospheric variables to a surface may affect the components of heat balance and then estimated values of evapotranspiration.

To evaluate the magnitude of the advection effect, the following calculation was done. The heat balance equation for a vegetated surface may be given by

$$Rn = \lambda E + H + G + \Delta M \tag{6}$$

$$\Delta M = Av + \mu Fp + B \tag{7}$$

where Av is the advective energy, μ the thermal conversion factor for fixation of carbon dioxide, Fp the specific flux of CO_2, B the rate of energy stored per unit area in the layer. The exact nature of each term depends on the type of layer. However, for many practical purposes, some of the terms can be negligible. If Fp and B are negligibly small compared with other terms, such as G, the substance of ΔM may be representative of advection.

In this study, Rn, λE, H and G were measured independently. Therefore, ΔM can be estimated from day to day and from season to season. The result is shown in Fig. 6-1. As shown in the figure, the values of ΔM are remarkable in winter (from December to February) and April. However, from summer to autumn except August, ΔM are negligibly small compared with Rn. It means that, if we consider the daily amount of evapotranspiration, α in the E-E model can be fixed as a constant during summer and autumn seasons. However, in winter and early spring it may be necessary to consider the effect of advection on α.

Table 6-1 shows the result of the measured monthly evapotranspiration rate and the relevant components of heat balance for a grass land.

CONCLUSION

The hydrologic cycle of evaporation is one of an integral part of water balance and heat balance of the earth's surface. Recently, the development of remote-sensing techniques by using satellites can enable to take a huge amount of data from the earth's surface and numerous attempts have been made to overcome the difficulties of estimating the regional evaporation.

The parameterization of equilibrium evaporation model proposed by Priestley and Taylor is one of them. However, studies in humid region are scarce and suitable parameterization for the humid regions has yet to be developed.

The applicabilities of the equilibrium evaporation model to estimate the regional evapotranspiration were studied by using the remotely sensed measurements.

The results are summarized as follows:

(1) The potential evapotranspiration, defined by a vapor-saturated surface condition, tends to overestimate the evapotranspiration from actively growing pasture grass with ample soil water.

(2) Hourly variations of α for a pasture grass land falls into the range of 0.95 to 1.4 during summer season.

(3) The daily actual evapotranspiration from pasture, without a serious soil water shortage in summer, falls in the range between Eeq (α = 1) and the potential evaporation Epe (α = 1.26).

(4) The average value of $\alpha = 1.14 \pm 0.03$ was induced by using the data of Ely and Eeq for pasture grass. It was found that evapotranspiration from actively growing pasture with no soil water shortage can be estimated with an accuracy of about 5% by the equilibrium evaporation model.

(5) The applicabilities of the equilibrium evaporation model (E-E model), especially the vibrations of the proportional constant α in $E = \alpha Eeq$, were investigated. The day-to-day variations of daily values of α and daytime values of α are shown in the figures accompanied, respectively. As the result of investigation, it was found that the differences of α between daily α and daytime α are caused by the nighttime decrease in available energy.

(6) The monthly mean values of daily α are nearly the same value from May to August, during which the pasture grows actively and the effects of nighttime radiative cooling on daily available energy are considered slight. It was found that the estimation of monthly evapotranspiration by the E-E model can be estimated within 10% accuracy.

(7) Seasonal variation of advective effects on heat balance terms was evaluated. The results showed that the value of α can be fixed as a constant during the season of summer and autumn. However, it was found that the more suitable value of the α-parameter is necessary to estimate the evapotranspiration in winter and early spring.

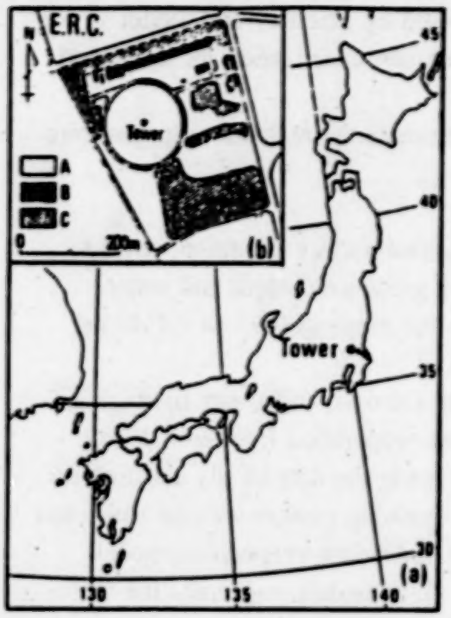

Figure 3-1. Location of the experimental site.
A = Grass field, B-Buildings, C-Pine trees

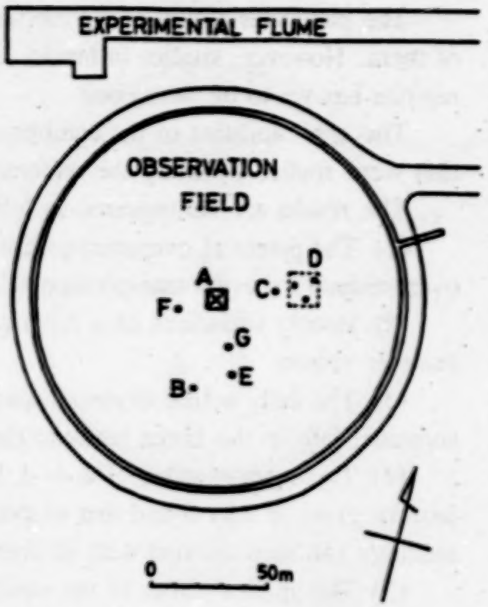

Figure 3-2. Location of instruments in the experimental field. A-G show observation points.

Table 3-1
Observation items and instruments.

番号 No.	観測項目 Item	記号 Symbol	高さ Height	観測場所 Site	機器名 Instrument	製作会社名 Maker	形式 Model
1	wind direction	D	30.5m	ERC Tower, A	sonic anemometer	Kaijo Denki	SA-200
2	wind speed 1	U-1	1.6	〃	sonic anemometer-thermometer	〃	PAT-311
3	〃 2	U-2	12.3	〃	〃	〃	〃
4	〃 3	U-3	29.5	〃	〃	〃	〃
5	momentum flux 1	UW-1	1.6	〃	〃	〃	〃
6	〃 2	UW-2	12.3	〃	〃	〃	〃
7	〃 3	UW-3	29.5	〃	〃	〃	〃
8	sensible heat flux 1	WT-1	1.6	〃	〃	〃	〃
9	〃 2	WT-2	12.3	〃	〃	〃	〃
10	〃 3	WT-3	29.5	〃	〃	〃	〃
11	short-wave radiation	I	1.5	ERC Field, B	pyranometer (Gorcynski type)	Eiko Seiki	MS-43F
12	net radiation	RN	1.5	〃	net radiometer (Middlton type)	〃	CN-11
13	soil heat flux	G 1	-0.02	ERC Field, C	soil heat flux meter	〃	CN-81
14	air temperature 1	T-1	1.6	ERC Tower, A	Pt resistance thermometer (with ventilater)	Nakaasa	E-731
15	〃 2	T-2	12.3	〃	〃	〃	〃
16	〃 3	T-3	29.5	〃	〃	〃	〃
17	soil temperature 1	ST-1	-0.02	ERC Field, C	Pt resistance thermometer	〃	E-751
18	〃 2	ST-2	-0.10	〃	〃	〃	〃
19	〃 3	ST-3	-0.50	〃	〃	〃	〃
20	〃 4	ST-4	-1.00	〃	〃	〃	〃
21	groundwater level 1	GW-1	depth	ERC Field, D	water level gauge (float type)	〃	W-131
22	〃 2	GW-2	from the	〃	〃	〃	〃
23	〃 3	GW-3	S. Level	〃	〃	〃	〃
24	dewpoint temperature 1	TD-1	1.6	ERC Tower, A	dew-point hygrometer(LiCl dew cell)	〃	E-771
25	〃 2	TD-2	12.3	〃	〃	〃	〃
26	〃 3	TD-3	29.5	〃	〃	〃	〃
27	evaporation	E	+0.20	ERC Field, G	evaporation pan	〃	Class A(D-211)
28	precipitation	P	+0.30	ERC Field, E	rain gauge (tipping bucket type)	〃	B-011-00
29	evapotranspiration	ET	0.00	ERC Field, F	weighing lysimeter(2mø, 2m depth)	Shimasu	RL-15TFA
30	atmospheric pressure	AP	+5.00	ERC Building		Nakaasa	F-601

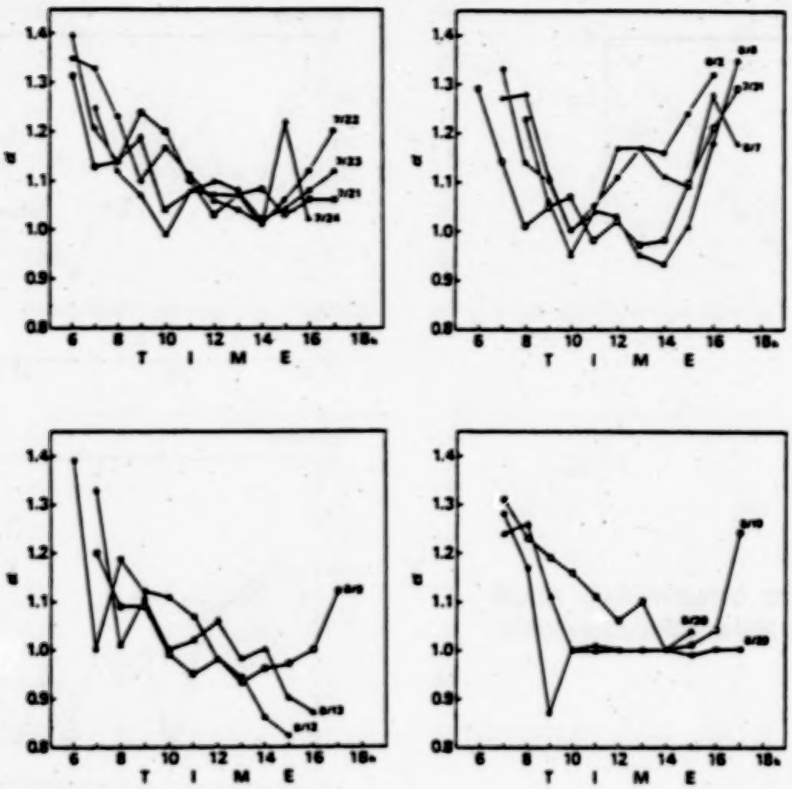

Figure 4-1. Hourly variations of α.

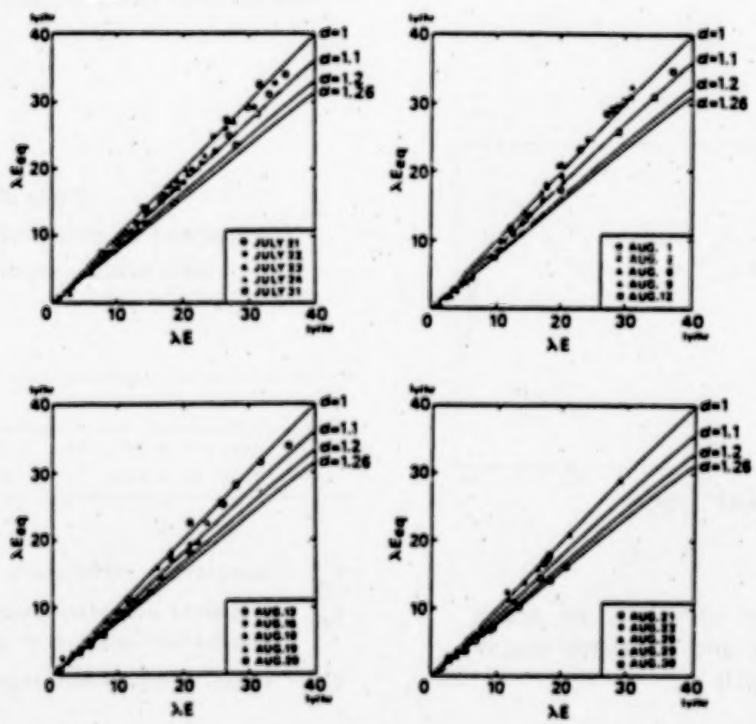

Figure 4-2. Relationship between hourly actual latent heat flux (λE) and hourly equilibrium latent heat flux (λEeq).

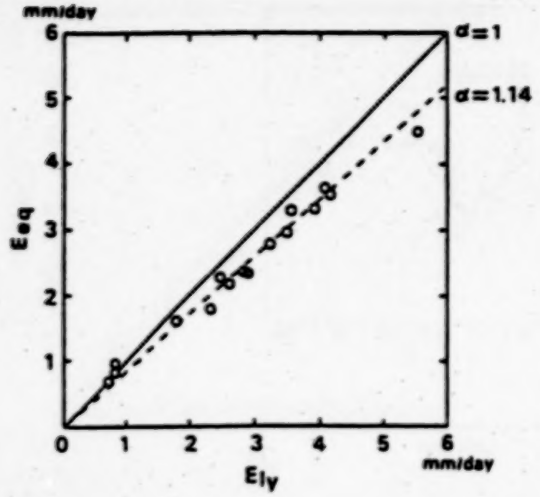

Figure 4-3. Relationship between daily actual evapotranspiration (Ely) and equilibrium evaporation (Eeq).

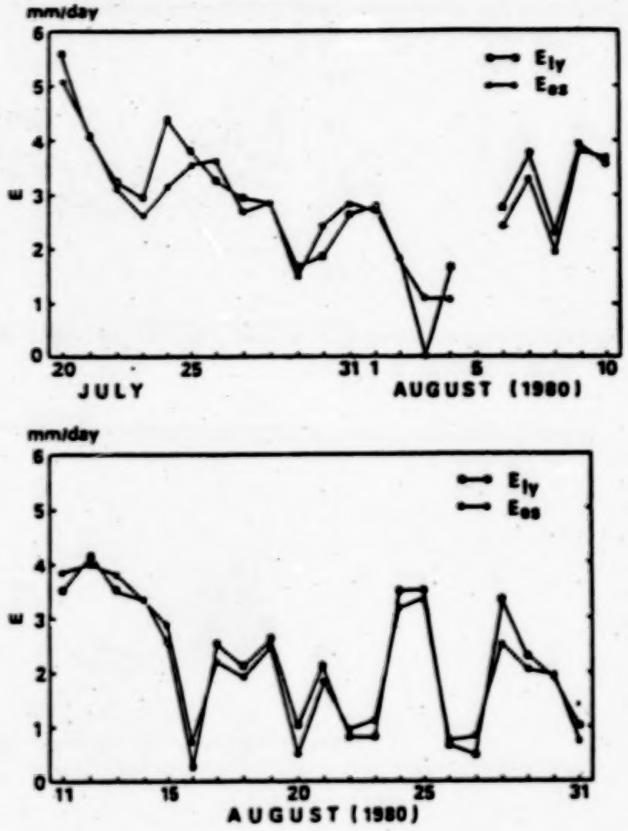

Figure 4-4. Day-to-day variations of actual evapotranspiration (Ely) and estimated evapotranspiration (Ees) in 1980.

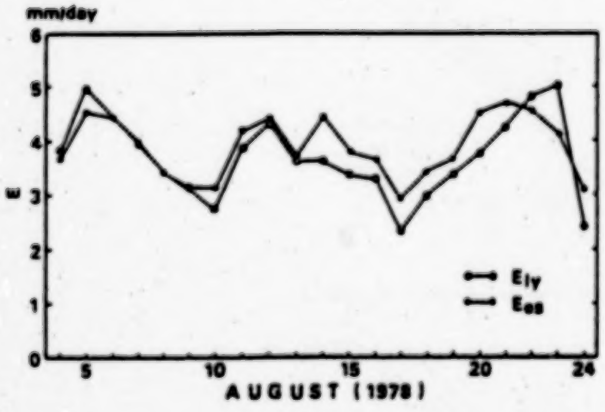

Figure 4-5. Day-to-day variations of actual evapotranspiration (Ely) and estimated evapotranspiration (Ees) in 1978.

Table 4-1
Comparison of estimated evapotranspiration with actual evapotranspiration.

		E_{eq}	E_{es}	E_{ly}
1978	Aug. 4 ∿ Aug. 24	71.4	81.4	77.0
1980	July 20 ∿ Aug. 31	91.5	104.3	108.1

(unit : mm)

E_{eq} : equilibrium evaporation

E_{es} : estimated evapotranspiration by the equilibrium evaporation model with α = 1.14

E_{ly} : actual evapotranspiration by a weighing lysimeter

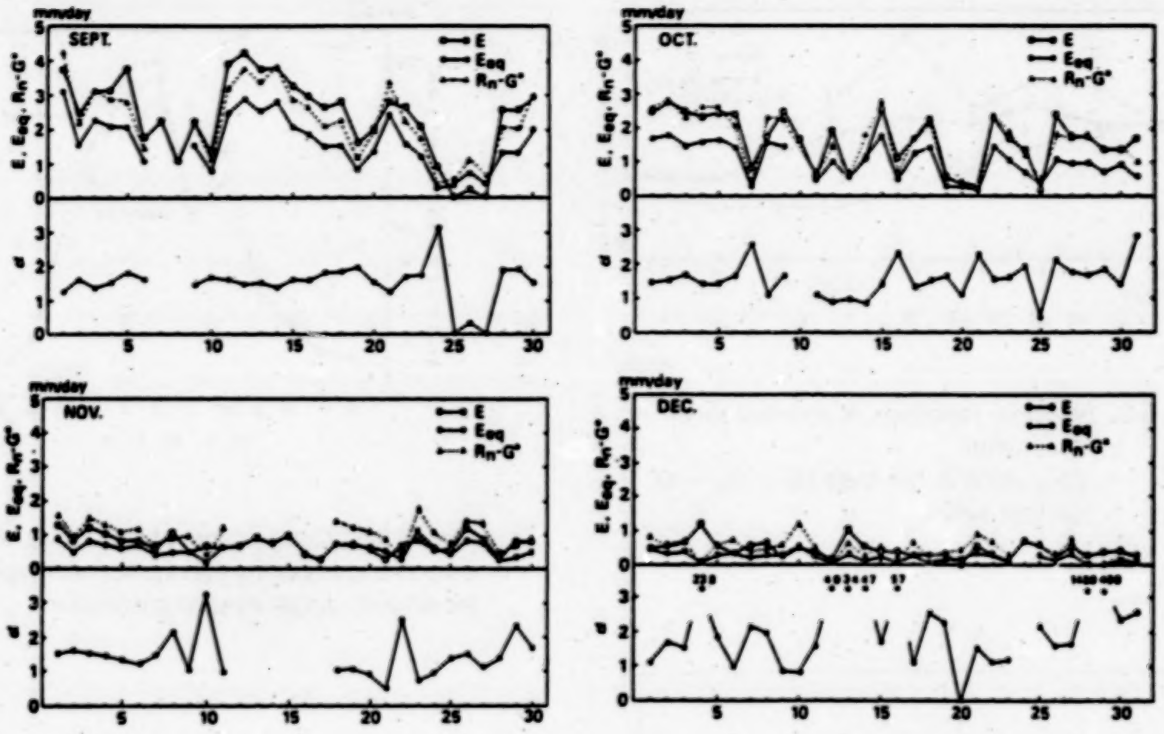

Figure 5-1. Day-to-day variations of daily evapotranspiration (E), equilibrium evaporation (Eeq), available energy in evaporation equivalence (Rn – G°), and the parameter α in the equilibrium evaporation model. Figures in α represent the value of α.

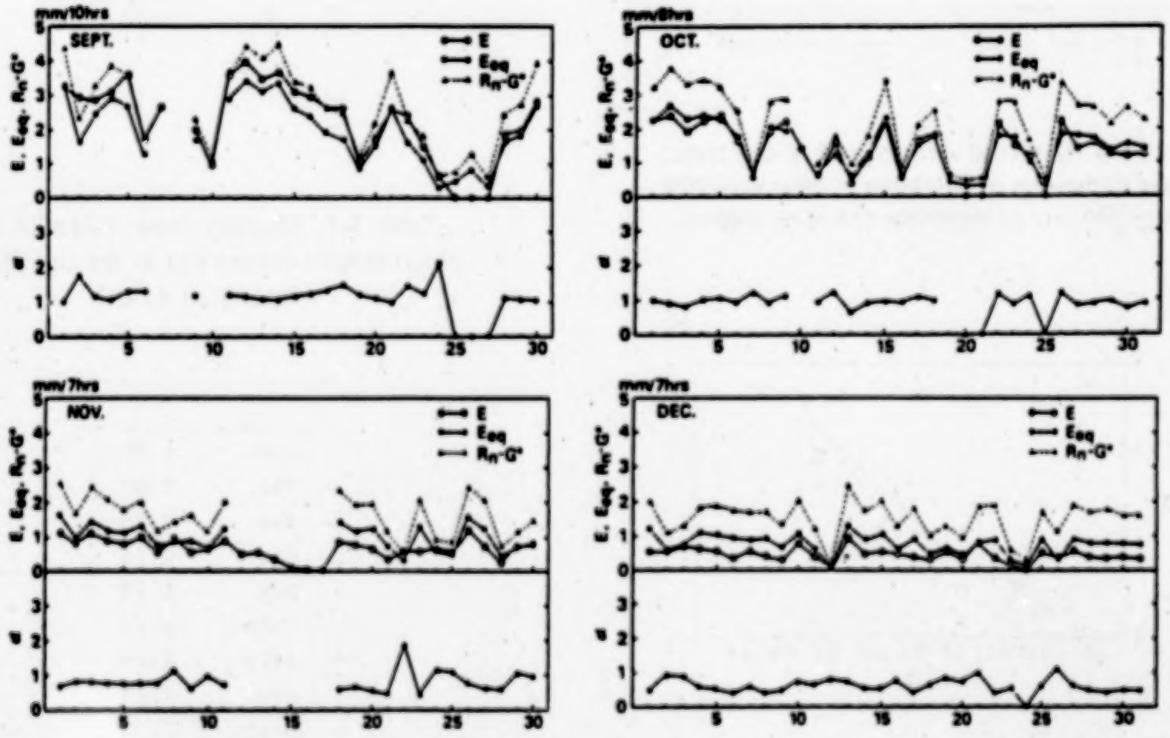

Figure 5-2. Day-to-day variations of daytime evapotranspiration (E), equilibrium evaporation (Eeq), available energy in evaporation equibalance (Rn – G°), and the parameter α in the equilibrium evaporation model.

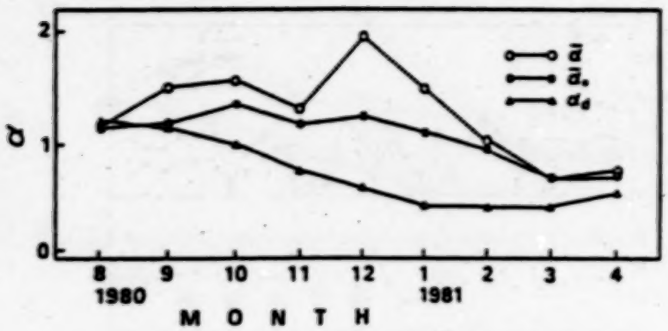

Figure 5-3. Seasonal variations of monthly mean α.
$\overline{\alpha}$: daily value
$\overline{\alpha^e}$: daily value in the case $\lambda E < R_n - G$
α_d : daytime value

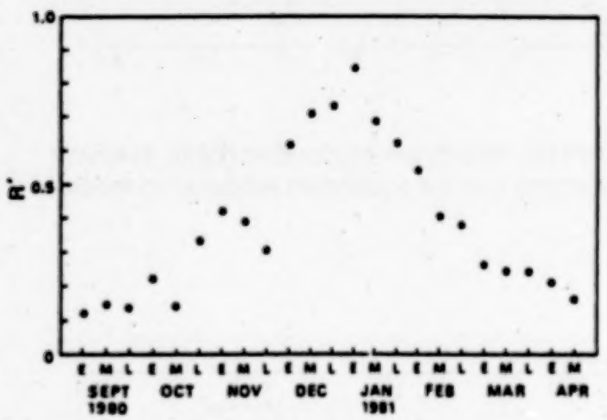

Figure 5-4. Seasonal variations of 10-day mean values of the rate of decrease in daily available energy (R′) due to nighttime radiative cooling.

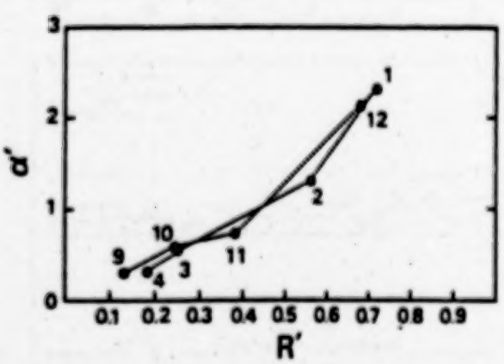

Figure 5-5. Relationship between the rate of increase in α (α') and the rate of decrease in available energy (R′). Figures represent month.

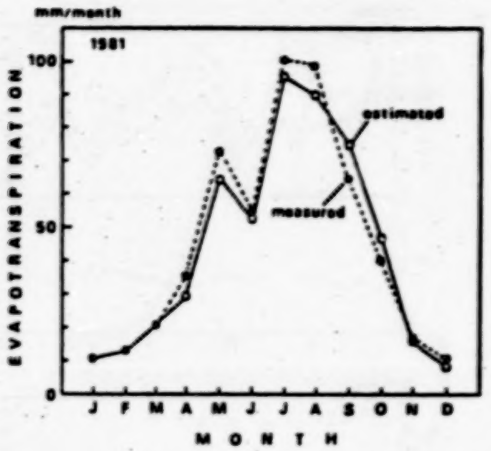

Figure 5-6. Comparison of estimated monthly evapotranspiration by the equilibrium evaporation model with actual evapotranspiration.

Table 5-1. Monthly mean values of the proportional constant (α) in the equilibrium evaporation model.

	α
Jan.	1.50
Feb.	1.03
Mar.	0.70
Apr.	0.75
May	1.15
June	1.12
July	1.14
Aug.	1.14
Sept.	1.50
Oct.	1.56
Nov.	1.31
Dec.	1.95

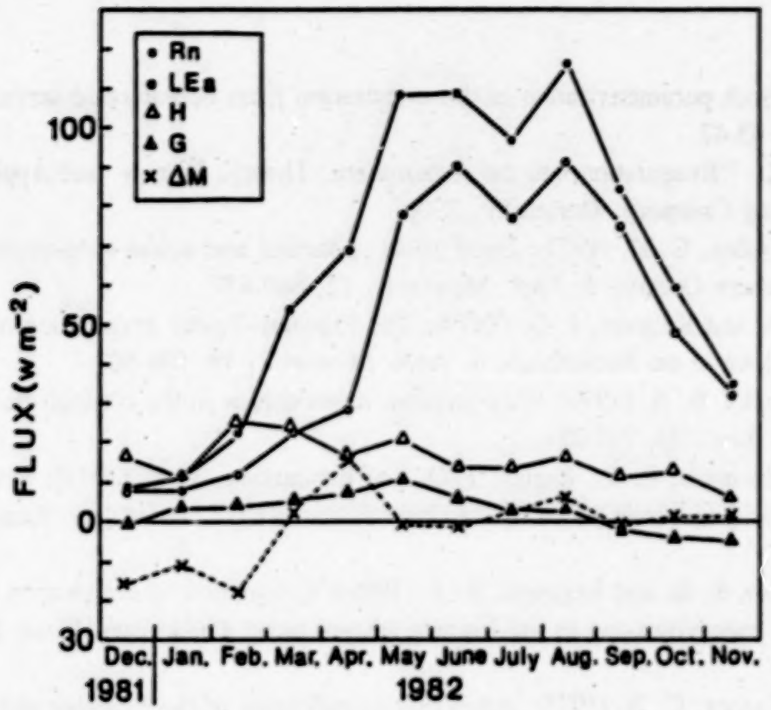

Figure 6-1. Monthly variations of heat balance and its residual term (ΔM) for a grass land.

Table 6-1. Monthly variations of heat balance and its residual term (ΔM) for a grass land.
r = [ΔM / (Rn − G)] X 100 (%)

	NO.	Rn	G	Rn-G	LEa	Ea	H	ΔM	r
	days		W / M²			mm/day	W / M²		%
Dec. 1981	14	8.19	-0.88	9.07	8.44	0.29	17.42	-16.80	-185.3
Jan. 1982	12	11.51	3.50	8.00	7.86	0.27	11.87	-11.72	-146.4
Feb.	12	22.76	3.64	19.12	11.66	0.40	25.55	-18.09	-94.6
Mar.	12	54.35	5.02	49.32	22.58	0.79	23.80	2.94	6.0
Apr.	14	69.65	7.21	62.44	28.41	0.99	17.40	16.64	26.6
May	23	108.11	10.65	97.46	77.76	2.74	20.94	-1.24	-1.3
June	13	109.02	5.93	103.09	90.40	3.19	14.60	-1.92	-1.9
July	13	97.70	2.87	94.82	77.77	2.74	14.06	3.00	3.2
Aug.	19	116.11	2.70	113.41	91.13	3.23	15.96	6.32	5.6
Sep.	13	84.96	-2.37	87.33	75.37	2.66	12.84	-0.88	-1.0
Oct.	12	59.07	-4.15	63.22	48.47	1.70	13.52	1.23	2.0
Nov.	7	34.99	-4.76	39.74	32.45	1.13	5.84	1.45	3.7
MEAN		64.70	2.45	62.25	47.69	1.68	16.15	-1.59	-32.0

REFERENCES

Barton, I. J. (1979): A parameterization of the evaporation from nonsaturated surfaces. J. Appl. Meteorol., 18, 43-47.

Brutsaert, W.(1982): "Evaporation into the Atmosphere. Theory, History, and Applications". D. Reidel Publishing Company, Doretrecht, 299p.

Davies, J. A. and Allen, C. D. (1973): Equilibrium, potential and actual evaporation from cropped surfaces in southern Ontario. J. Appl. Meteorol., 12, 649-657.

De Briun, H. A. R. and Keijman, J. Q. (1979): The Priestley-Taylor evaporation model applied to a large, shallow lake in the Netherlands. J. Appl. Meteorol., 18, 898-903.

Dyer, A. J. and Hicks, B. B. (1979): Flux-gradient relationships in the constant flux layer. Quart. J. Roy. Meteorol. Soc., 96, 715-721.

Heilman, J. L., Kanemasu, E. T., Bagley, J. O. and Rasmussen, V. P. (1977): Evaluating soil moisture and yield of winter wheat in the Great Plains using Landsat data. Remote Sens. Env., 6, 315-326.

Jackson, R. D., Idso, S. B. and Reginato, R. J. (1976): Calculation of evaporation rates during the transition from energy-limiting to soil-limiting phases using albedo data. Water Resour. Res., 12, 23-26.

Jury, W. A. and Tanner, C. B. (1975): Advection modification of the Priestley and Taylor evapotranspiration formula. Agron. J., 67, 840-842.

Kanemasu, E. T., Stone, L. R. and Powers, W. L. (1976): Evapotranspiration model tested for soybean and sorghum. Agron. J., 68, 569-572.

McNaughton, K. G. and Black, T. A. (1973): A study of evapotranspiration from a Douglas fir forest using the energy balance approach. Water Resour. Res., 9, 1579-1590.

Mukammal, E. I. and Neumann, H. H. (1977): Application of the Priestley-Taylor evaporation model to assess the influence of soil moisture on the evaporation from a large weighing lysimeter and Class A pan. Boundary-Layer Meterorol., 12, 243-256.

Murakami, R. (1981): Distinctive feature and cause of the 1980 cool summer weather in Japan. J. Agric. Meteorol. Japan, 37, 249-253. (in Japanese)

Nakayama, K. and Nakamura, A. (1982): Estimating potential evapotranspiration by the Priestley-Taylor model. J. Agric. Meteorol. Japan, 37, 297-302. (in Japanese with English summary)

Priestley, C. H. B. and Taylor, R. J. (1972): On the assessment of surface heat flux and evaporation using large-scale parameters. Monthly Weath. Rev., 100, 81-92.

Shuttleworth, W. J. and Calder, I. R. (1979): Has the Priestley-Taylor equation any relevance to forest evaporation? J. Appl. Meteorol., 18, 639-646.

Slatyer, R. O. and McIlroy, I. C. (1961): "Practical Micrometeorology", CSIRO, Melbourne, Australia, 310 p.

Stewart, J. B. and Thom, A. S. (1973): Energy budgets in pine forest. Quart. J. Roy. Meteorol. Soc., 99, 154-170.

Stewart, R. B. and Rouse, W. R. (1976): A simple method for determining the evaporation from shallow lakes and ponds. Water Resour. Res., 12, 623-628.

Stewart, R. B. and Rouse, W. R. (1977): Substantiation of the Priestley and Taylor parameter $\alpha=1.26$ for potential evaporation in high latitudes. J. Appl. Meteorol., 16, 649-650.

Tanner, C. B. and Jury, W. A. (1976): Estimating evaporation and transpiration from a row crop during incomplete cover. Agron. J., 68, 239-243.

Williams, R. J., Broersma, K. and van Ryswyk, A. L. (1978): Equilibrium and actual evapotranspiration from a very dry vegetated surface. J. Appl. Meteorol., 17, 1827-1832.

Yap, D. and Oke, T. R. (1974): Eddy-correlation measurements of sensible heat fluxes over a grass surface. Boundary-Layer Meteorol., 7, 151-163.

D16

PART II
Application of Equilibrium Evaporation Model to Estimate Evapotranspiration by Remote Sensing Technique

K. Kotoda, S. Nakagawa, K. Kai and M. M. Yoshino

Environmental Research Center
University of Tsukuba
Sakuramura, Ibaraki, Japan

K. Takeda and K. Seki

National Institute of Resources
Science and Technology Agency
Chiyoda-ku, Tokyo, Japan

INTRODUCTION

In the process of evapotranspiration, there are three things required to occur: (1) energy for the change of phase of the water; (2) a source of the water; (3) a sink for the water. Remote sensing can contribute information to the first two of these conditions by providing estimates of solar insolution, surface albedo, surface temperature, vegetation cover, and soil moisture content (Schmugge and Gurney, 1982). Many methods for estimating of evapotranspiration have been studied (Rosema et al., 1978; Soer, 1980; Carlson et al., 1981; Elkington and Hogg, 1981; Gurney and Camillo, 1982), which are reviewed by Schmugge and Gurney (1982).

In a humid region like Japan, it seems that radiation term in energy balance equation plays an important role for evapotranspiration rather than vapor pressure difference between the surface and lower atmospheric boundary layer. For this reason, the present study adopted a Priestley-Taylor type of equation which is called in this paper an "Equilibrium Evaporation Model" to estimate evapotranspiration. This method acquires the data of net radiation, soil heat flux and surface temperature, but not necessary to get the data of vapor pressure and wind speed. Carlson et al. (1981), Thomas and Kanemasu (1981) and Kanemasu (1982) used the GOES data to estimate daily solar radiation. However, in the present study, such data were not available, and we used only temperature data obtained by remotely sensed techniques.

LAND USE AND VEGETATION

Compared with continental countries, the land use of Japan is very minute and tremendously complicated. Topography around the test area can be divided into two parts, one is diluvial upland (altitude 25-30 m) and the other is alluvial lowland (altitude 10-15 m). The most part of the alluvial lowland is occupied mostly by rice field. Therefore, the vegetation of lowland is fairly monotonous and landscape is relatively simple. On the contrary, diluvial upland is a complex of farms, residential quarters, forest, orchards and others. Most parts of the upland are occupied by farms (mainly vegetable fields), residential quarters and towns, red pine forests and grass land.

A test study was carried out at the Tsukuba Academic New Town on 21st and 22nd Jan., 1983 during which field survey provided ground truth data for comparison with satellite (LANDSAT) imagery and airborne sensing information. In the present study, however, the satellite image from LANDSAT was inadequate for identifying the land use and vegetation categories required. This is due to the facts that one is cloud cover when LANDSAT flew over the test area on 21st Jan. and the other is due to the spectral resolution which could not provide inadequate intervegetation differentiation.

Fig. 2-1 shows an example of the actual vegetation map of Tsukuba Academic New Town and its surrounding districts (Nakamura et al., 1980) obtained by field survey.

RADIATION REGIME AND SURFACE TEMPERATURE

Surface temperature was measured every two minutes by a Barnes Infrared Thermometer (model PRT-5) from 0800h to 1600h for the purpose of ground truth of surface temperature.

As shown in Fig. 3-1, it was fine on January 22nd, when the flight was done. However, there existed fluctuations in incoming short-wave radiation (Rs↓) and net radiation (Rn) from 1150h to 1430h (Fig. 3-2). The fluctuations were caused by scattered cloud which shaded sunshine for a short time interval.

Surface temperature (Ts) showed fluctuations in response to those of Rs (Fig. 3-3). Before 1100h, Ts showed a smooth increase and the fluctuations of Ts were within 2°C. After that, it became partly cloudy by the traveling of scattered cloud. As a result, Ts changed rapidly and greatly. The maximum change of Ts was about 9°C in two minutes. These large and rapid fluctuations were true in the case of 10-min average Ts (Fig. 3-3).

In contrast to this, fluctuations in air temperature (Ta) were very small and responded slowly to the changes in Rs↓.

SURFACE TEMPERATURE MEASUREMENTS BY REMOTE SENSING

Remotely sensed measurements of surface temperature were made from two types of platforms: One was a satellite, i.e. LANDSAT, the other was an aircraft. The LANDSAT offers large coverage but suffers from reduced spatial resolution compared to aircraft. The aircraft platform was primarily used for experimental studies because of the greater control and resolution possible.

Airborne remote sensing was conducted over the Tsukuba Academic New Town at 8:52, 12:02 and 15:09 JST on 22nd Jan., 1983. Fig. 4-1 shows a flight course and coverage area. The flight height was about 2000 m, and the ground resolution (one pixel) was an area of 15 m x 15 m. Fig. 4-2 shows synoptic conditions on 22nd. The day was clear, and the wind was northwesterly at 1 to 4 m/s at the height of 1.6 m from the ground surface. The clearing sky provided moderately favorable conditions for the remote sensing.

Airborne MSS information was used to estimate the surface temperatures and to give maps of them. The surface temperatures were estimated from measurements at thermal infrared wavelengths, i.e. the 8.0 to 14.0 micron meters, of the emitted radiant flux, and were calibrated by the ground truth. Fig. 4-3 shows distributions of the surface temperatures at 8:52, 12:02 and 15:09 JST on the 22nd.

METHOD OF ANALYSIS

As described in Part I of this paper, evaporation equation can be expressed as

$$E = \frac{\alpha}{\lambda}\left(\frac{\Delta}{\Delta+\gamma}\right)(Rn\text{-}G) \tag{1}$$

where Δ is the slope of the saturation water vapor pressure curve, and γ is the psychrometric constant. Using the data of temperature, the values of Δ and γ can be estimated as follows:

$$\Delta = 0.4476 + (0.030669 + 0.000493T + 0.000023T^2)T \quad (mb \cdot {}^\circ C^{-1}) \tag{2}$$

$$\gamma = \frac{Cp\ P}{0.622\lambda} \quad (mb \cdot {}^\circ C^{-1}) \tag{3}$$

$$\lambda = (2501 - 2.37T) \times 10^3 \quad (JKg^{-1}) \tag{4}$$

where T (°C) is the surface temperature obtained by remote sensing, c_p is the specific heat of air ($=1005\ Jkg^{-1}{}^\circ C^{-1}$), P is the atmospheric pressure ($=1013$ mb), and λ is the latent heat of vaporization.

The net radiation flux, the result of incoming and outgoing radiation fluxes, is given as

$$Rn + (1-a_s)R_s + \epsilon(L\downarrow - \sigma T^4) \tag{5}$$

where Rs is the incoming total short-wave radiation flux, a_s is the albedo, L↓ is the downward long-wave radiation flux, T is the surface temperature, ϵ is the emission coefficient of the surface ($=0.98$) and σ is the Stefan-Boltzmann constant [$(5.67 \times 10^{-8})\ Wm^{-2}K^{-4}$].

The heat flux into the soil is proportional to the temperature gradient and the heat conductivity in the soil depending on the soil moisture content. In this study, the following relationship was used.

$$G = a_r Rn \tag{6}$$

where a_r is the proportional constant depend on the soil conditions. The values of a_s and a_r vary with surface condition and time of day. In this study daily mean values are used to estimate the evapotranspiration. So, it is necessary to convert the momentary evapotranspiration data into 24-hr estimates of evapotranspiration. For the practical purpose, if we know the relationships momentary data and daily mean data, it may be estimated from the daily mean evapotranspiration.

In order to avoid the complexity of calculation, land use / land cover are classified in 8 categories. Using the data of Rs = 180 Wm^{-2}, L↓ = 403 Wm^{-2} which are the typical summer climatological conditions at Tsukuba, and assuming T = 20 °C, α = 1.0, evapotranspiration from various surface covers can be calculated (Table 5-1). It seems that the results are reasonable compared with the lysimeter data obtained in August, 1979 (Kotoda, 1980) and the data of lake evaporation obtained at Lake Kasumigaura in August and September 1981 (Takeda et al., 1982).

CONCLUDING REMARKS

Using the surface temperature obtained by airborne remote sensing and other necessary data measured at experimental field at ERC, University of Tsukuba (Kotoda et al., 1983), evapotranspiration from various surfaces were calculated. The result (point A) is shown in Fig. 6-1 with other data of evapotranspiration from grass land which were measured by lysimeter at ERC. Calculated daily mean evapotranspiration on 22nd Jan., 1983 is approximately 0.4 mm/day, however the differences of evapotranspiration with the vegetation types were not detectable, because the magnitude of evapotranspiration is very little in winter.

The future subject of remote sensing techniques to the estimate of evapotranspiration will depend on establishing correlations between land surface reflectance and hydrometeorological parameters related to heat balance terms, such as Rn, H or G. As a satellite monitoring, more frequent operational satellite, like a geostationary satellite is desired, because the present LANDSAT can operate nothing but one or two days measurement per month.

The future use of remote sensing techniques to the estimate of evapotranspiration will depend on establishing correlations between land surface reflectance and hydrometerological parameters related to heat balance terms, such as Rn, St or G. As for satellite monitoring, more frequent operational satellite coverage, like geostationary, is desired, because the present LANDSAT can operate nothing but one or two days of measurements per month.

Figure 2-1. An example of the actual vegetation map of Tsukuba academic New town and its surrounding districts. E : ERC

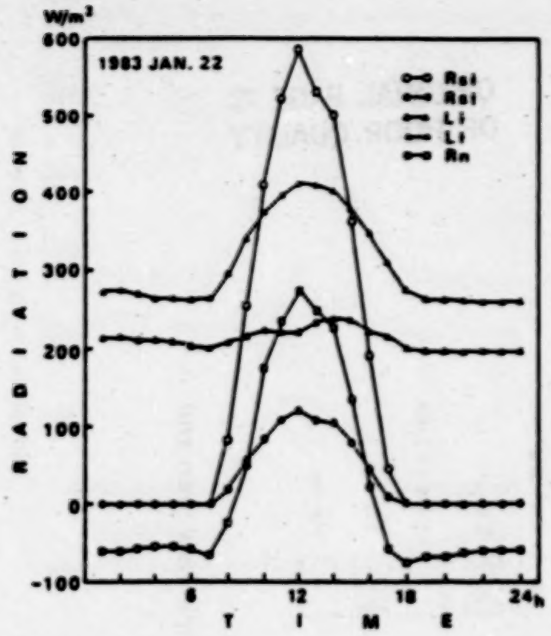

Figure 3-1. Diurnal variations of radiation balance components observed at the Aerological Observatory, Tateno.

Rsi : incoming short-wave radiation
Rsi : reflected short-wave radiation
Li : downward long-wave radiation
Li : upward long-wave radiation
Rn : net radiation

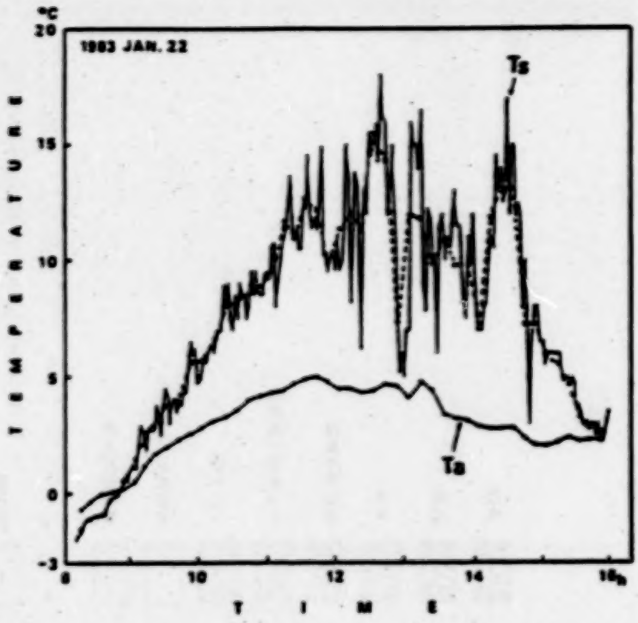

Figure 3-2. Hourly variations of surface temperature (Ts) and air temperature (Ta) at ERC. Broken line in Ts and Ta are 10-min averaged values. Ta was observed at a height of 1.6 m.

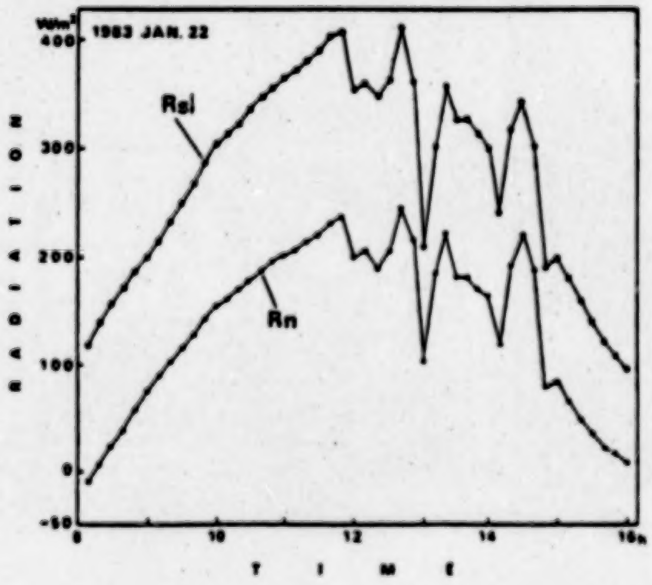

Figure 3-3. Hourly variations of incoming short-wave radiation (Rsi) and net radiation (Rn) at ERC. Rsi and Rn are 10-min averaged values.

Figure 4-1. Flight course and coverage area.

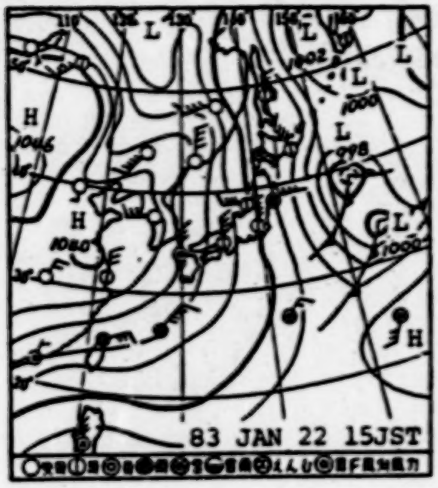

(a)

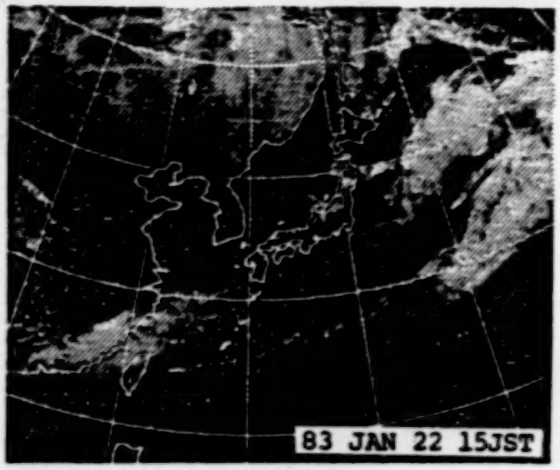

(b)

Figure 4-2. Synoptic conditions on 22nd January, 1983.
(a) Surface weather map at 15 JST 22 January, 1983
(b) GMS VIS imagery at 15 JST 22 January, 1983

ORIGINAL PAGE
COLOR PHOTOGRAPH

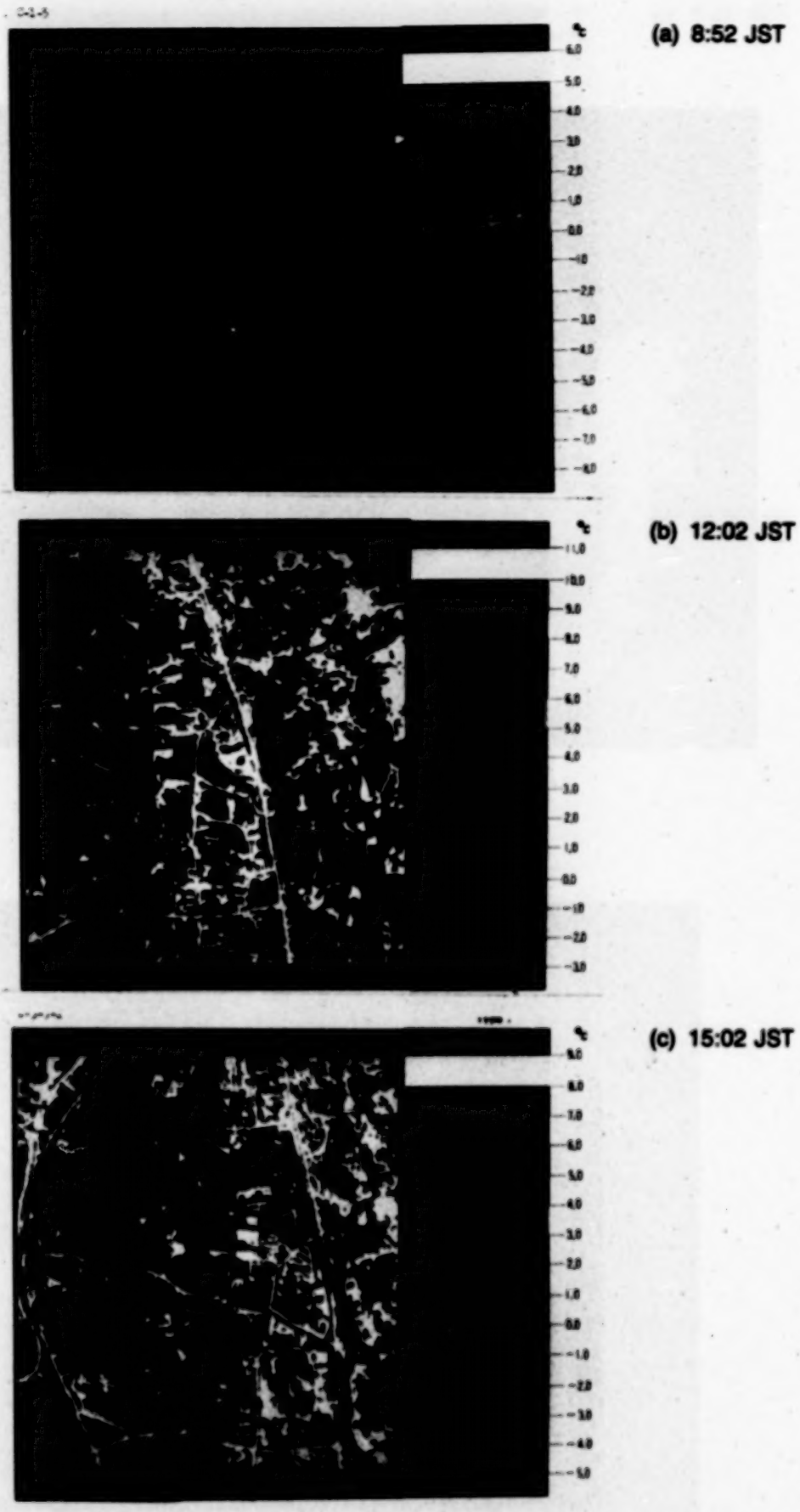

Figure 4-3. Surface temperature distributions at 8:52, 12:02 and 15:09 on 22nd, January, 1983

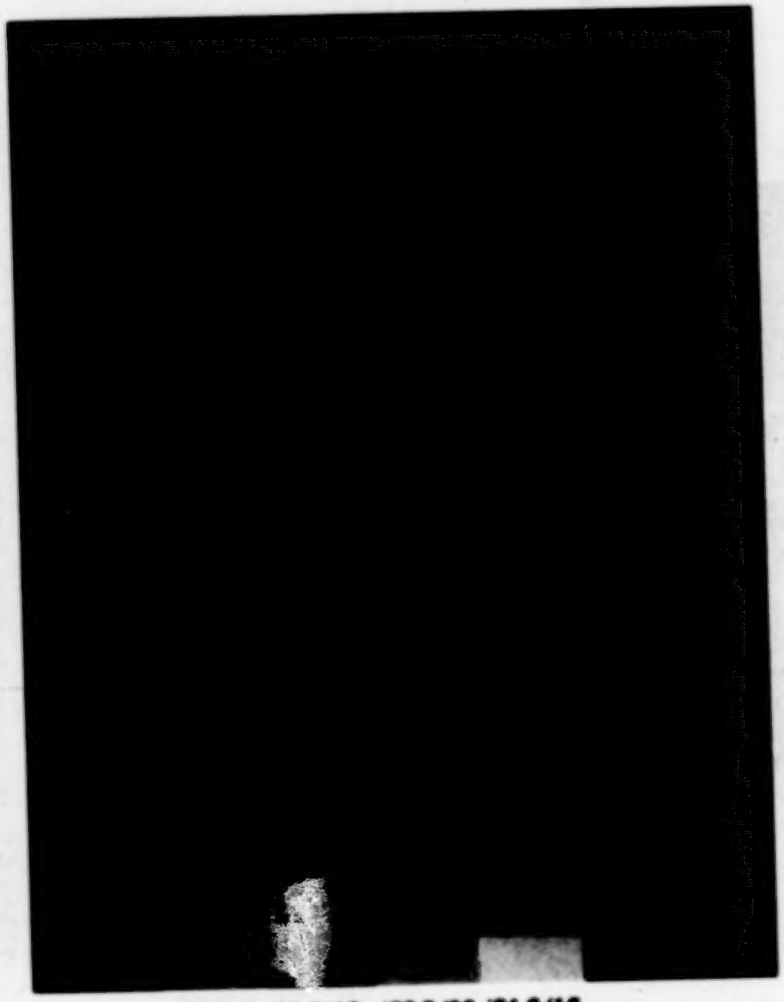

Photo 1. Superimposed Image of Snowcover Areas Extracted from Landsat Data

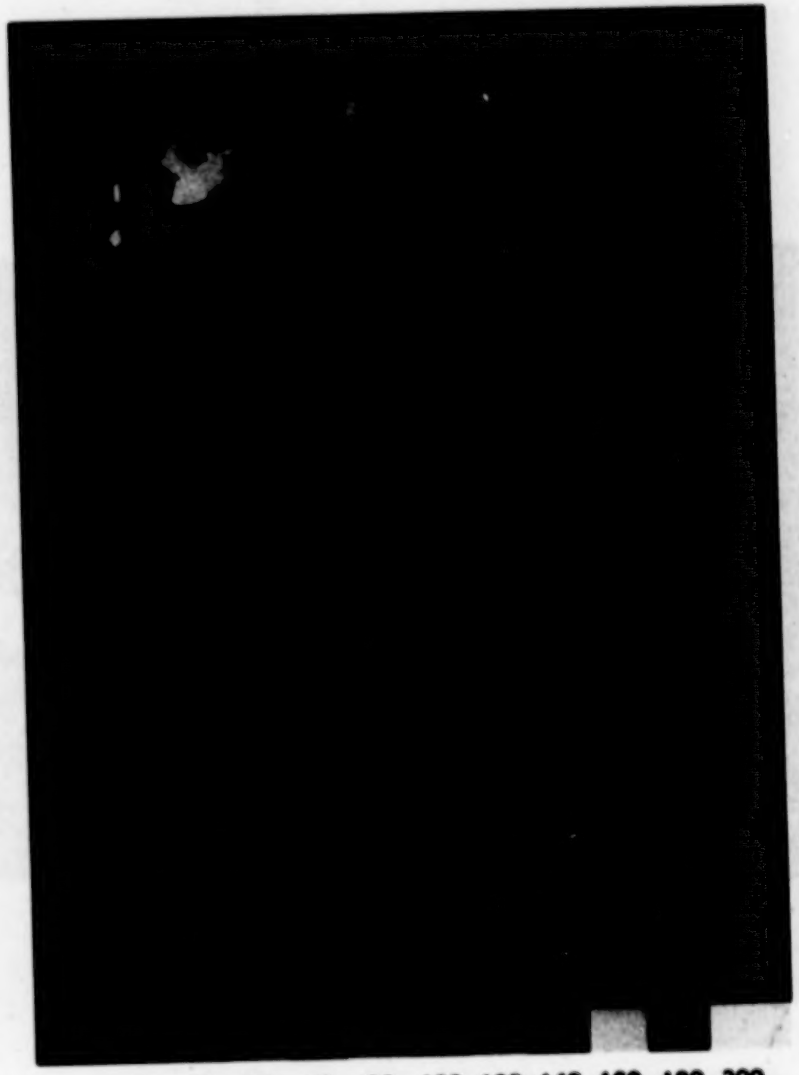

Photo 2. Maximum Snow Water Equivalent Map of Okutadami-gawa Bain in 1982

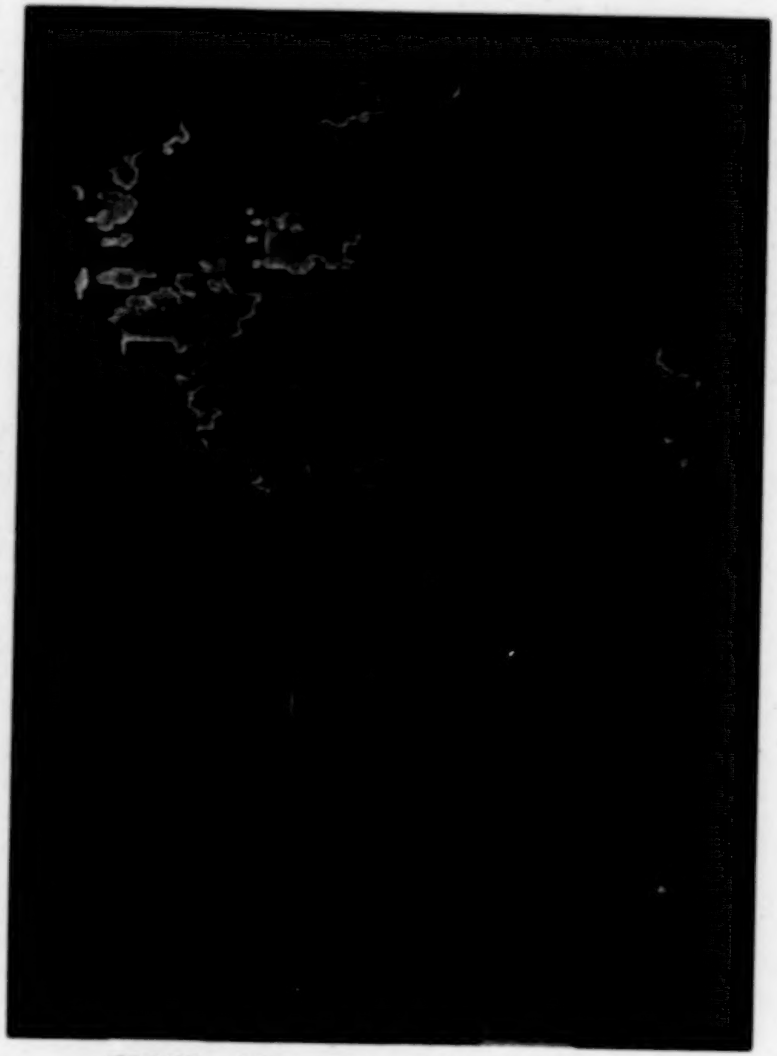

Photo 3. Snowcover Daily Variation Map Estimated From the Maximum Snow Water Equivalent Map Shown in Photo 2

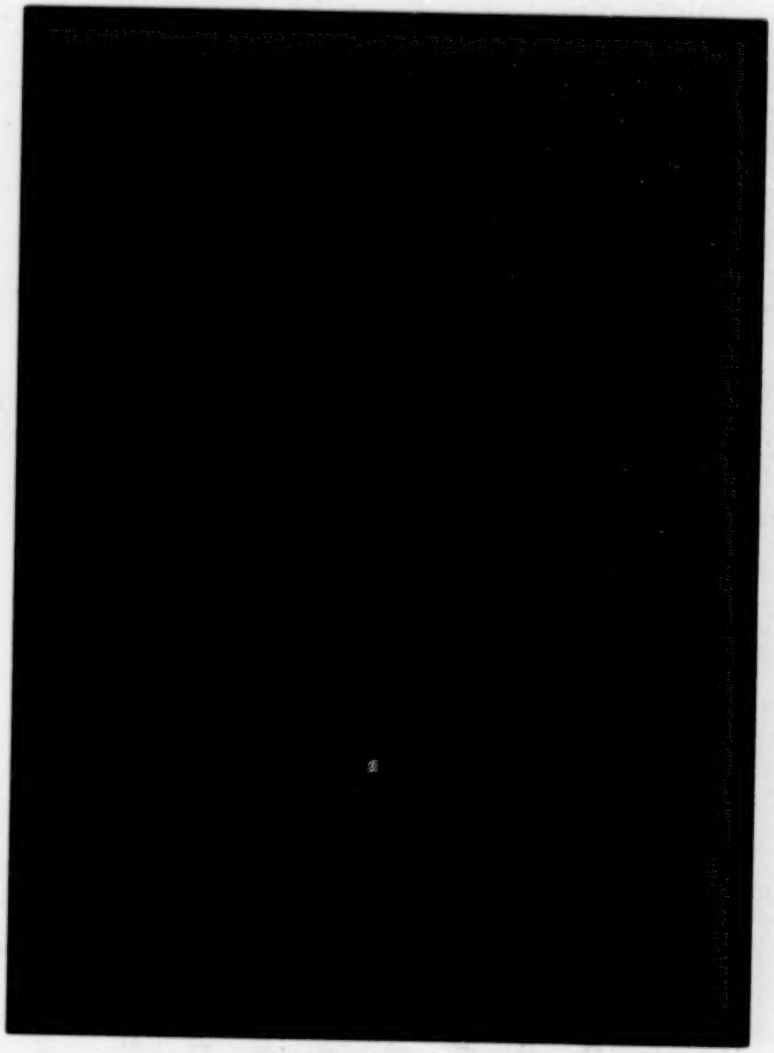

Photo 4. Snowcover Areas Extracted From NOAA-AVHRR Data

Table 5-1
Evaportranspiration from various surfaces

NO.	categories	a_s	a_r	Rn	G	λE	E
				Wm^{-2}			mmd^{-1}
1	open water	0.06	0.20	153.8	30.8	84.1	2.96
2	urbanized area	0.30	0.30	110.6	33.2	52.9	0.47
3	tall vegetation (ever green)	0.15	0.08	137.6	11.0	86.5	3.05
4	tall vegetation (deciduous)	0.15	0.08	137.6	11.0	86.5	3.05
5	short vegetation (sparse)	0.18	0.10	132.2	13.2	81.3	2.86
6	short vegetation (dense)	0.15	0.05	137.6	6.9	89.4	3.15
7	bare soil(dry)	0.25	0.30	119.6	35.9	57.2	2.02
8	bare soil(wet)	0.20	0.30	128.6	38.6	61.5	2.17

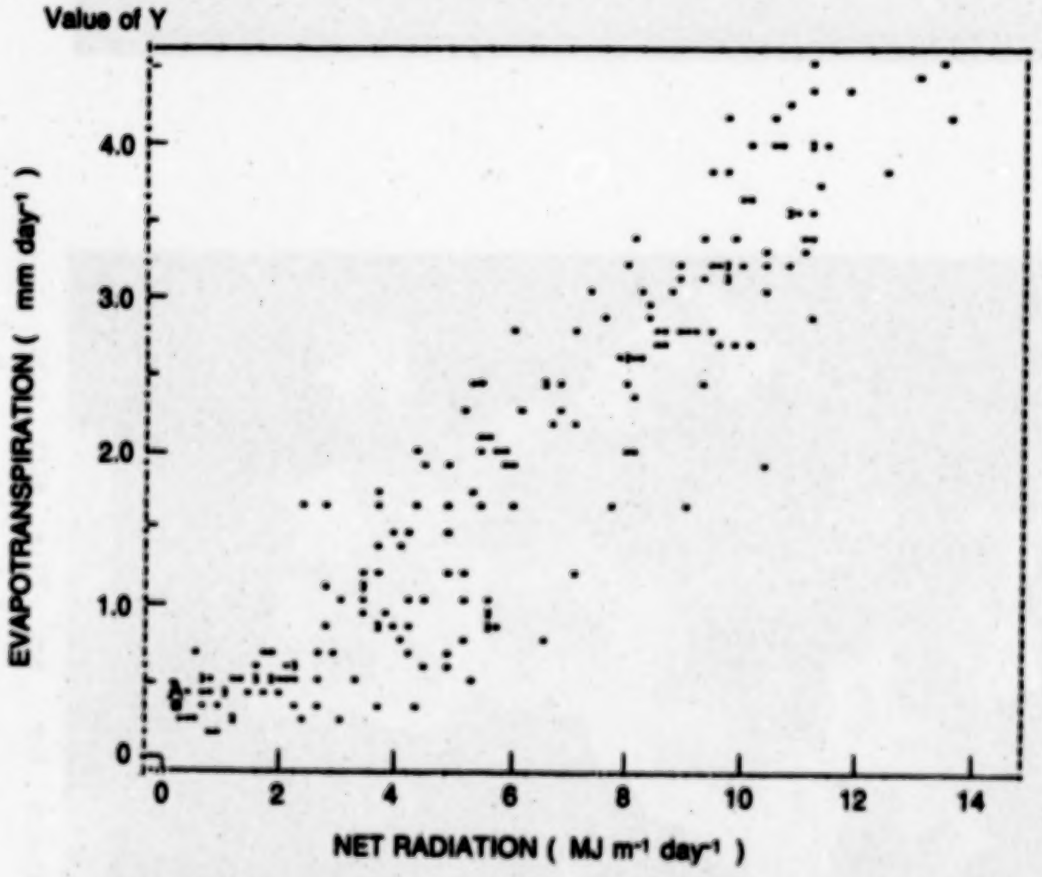

Figure 6-1. Relationship between evapotranspiration and net radiation. The value of point A is estimated evapotranspiration observed on 22nd, Jan., 1983 and the others are actual evapotranspiration obtained by lysimeter at ERC, Univ. of Tsukuba through the year of 1982 except rain day.

REFERENCES

Carlson, J. N., Dodd, J. K., Benjamin, S. G. and Cooper, J. N. (1981): Satellite estimate of the surface energy balance, moisture availability and thermal inertia. J. Appl. Meteorol., 20, 67-87.

Elkington, M. D. and Hogg, J. (1981): The characteristics of soil moisture content and actual evapotranspiration from crop canopies using thermal infrared remote sensing. Proc. Remote Sensing Soc., Reading.

Gurney, R. J. and Camillo, P. J. (1982): The effects of soil and atmospheric boundary layer variables on evapotranspiration and soil moisture studies. The First U.S.-Japan Evapotranspiration and Snowpack Properties Project Meeting, 43 p.

Kanemasu, E. T. (1982): Use of satellite information to estimate evapotranspiration. The First U.S.-Japan Evapotranspiration and Snowpack Properties Research Project Meeting, 10 p.

Kotoda, K. (1980): Comparison of evapotranspiration measurement using weighing lysimeter and energy balance method. Bull. Environmental Research Center, Univ. of Tsukuba, 4, 1-9. (in Japanese)

Kotoda, K., Kai, K. and Nakagawa, S. (1983): On the real time data processor for meteorological and hydrological measurements. Bull. Environmental Research Center, Univ. of Tsukuba, 7, 75-85. (in Japanese)

Nakamura, T., Namekawa, H. and Chow, K. (1980): The actual vegetation map of Tsukuba Academic New Town and its surrounding districts. Environmental Studies of Tsukuba, 5, A, 111-113. (in Japanese)

Rosema, A., Bijleveld, J. H., Reiniger, P., Tassone, G., Blyth, K. and Gurney, R. J. (1978): TELL-US, a combined surface temperature, soil moisture and evaporation mapping approach. Proc. 12th ERIM Symp. on Remote Sensing of Environm. Manila, 2267-2276.

Schumugge, T. and Gurney, R (1982): Evapotranspiration and remote sensing. The First U.S.-Japan Evapotranspiration and Snowpack Properties Research Project Meeting, 15 p.

Soer, G. J. R. (1980): Estimation of regional evapotranspiration and soil moisture conditions using remotely sensed crop surface temperatures. Remote Sens. Env., 9, 27-45.

Takeda, K., Yajima, Y. and Morizono, S. (1982): Experimental studies on evaporation of the Lake Okutadami and Lake Dasumigaura using LANDSAT data. National Institute of Resources Paper, 97, 184-232. (in Japanese)

Thomas, W. B. and Kanemasu, E. T. (1981): Insolation estimation from satellite measurements of reflected radiation. Remote Sens. Env., 11, 157-167.

MICROWAVE REMOTE SENSING OF SOIL MOISTURE

Thomas J. Schmugge

Hydrological Sciences Branch, Code 924
NASA/Goddard Space Flight Center
Greenbelt, Maryland 20771

ABSTRACT

Because of the large contrast between the dielectric constant of liquid water and that of dry soil at microwave wavelength, there is a strong dependence of the thermal emission and radar backscatter from the soil on its moisture content. This dependence provides a means for the remote sensing of the moisture content in a surface layer approximately 5 cm thick. The feasibility of these techniques has been demonstrated from field, aircraft and spacecraft platforms. The soil texture, surface roughness, and vegetative cover affect the sensitivity of the microwave response to moisture variations with vegetation being the most important. It serves as an attenuating layer which can totally obscure the surface. Research has indicated that it is possible to obtain 5 or more levels of moisture discrimination and that a mature corn crop is the limiting vegetation situation.

INTRODUCTION

Since the early sixties, the meteorological and Landsat series of satellites have provided much data useful for water resources management. The sensors, on board these satellites, operated in the visible and infrared portions of the spectrum and were able to observe such parameters as snow cover and surface water areas, land use, and surface temperature. Unfortunately, these sensors are restricted by cloud cover and are limited in the hydrological parameters which they can observe. Variables such as soil moisture, snow water equivalent, snow wetness, precipitation distribution and timely observations of floods are not amenable to measurements by these shorter wavelength sensors.

The microwave portion of the electromagnetic spectrum offers potential for monitoring several of these parameters, and in particular, the one which is the subject of this paper, soil moisture. For purposes of this paper, the wavelength range from 0.3 cm to 50 cm will be considered the microwave portion of the spectrum and for soil moisture sensing, only those wavelengths longer than about 5 cm are particularly effective. An advantage of the microwave wavelengths for remote sensing is that there is very little atmospheric absorption of radiation at these wavelengths; thus, observations of the earth's surface can be made from aircraft or satellite altitudes with little or no atmospheric obscuration.

Electromagnetic radiation at these wavelengths is particularly effective for soil moisture sensing because of the large contrast between the dielectric properties of liquid water and those of dry soil. The large dielectric constant of water results from the alignment of the permanent electric dipole moment of the water molecule. The dielectric constant of water at the lower microwave frequencies is approximately 80 compared with 3 to 5 for dry soils; as a result, the dielectric constant of wet soils can reach values of 20 or more. This produces a range of soil emissivity from about 0.95 for dry soils to 0.6 or less for wet soils with changes of a corresponding magnitude in the soil's reflectivity.

In this paper we will present results indicating the current status of the use of microwave approaches for the remote sensing of soil moisture. Both active and passive microwave approaches will be discussed. The passive microwave approach (radiometry) involves the measurement of the thermal emission from the surface at microwave wavelengths. This emission depends on the temperature and emissivity of the surface medium. This is to be contrasted with the active microwave approach (radar) in which a pulse of microwave energy is transmitted by the sensor and the return or reflected signal is measured. The strength of the return depends on the surface roughness and dielectric properties of the terrain being studied, but not directly on the temperature of the medium. The Second Edition Manual of Remote Sensing, published by the American Society of Photogrammetry, gives very complete descriptions of both these approaches[1]. Another excellent reference is the series of books on Microwave Remote Sensing by Ulaby, Moore and Fung[2]. The methods of soil moisture determination are summarized in the review paper by Schmugge et al.[3].

DIELECTRIC PROPERTIES OF SOILS

As noted in the introduction, it is the large dielectric constant (ε) for water as compared to those for the soil minerals which makes the microwave approaches useful for soil moisture sensing. The frequency dependence of the dielectric properties of water are described by a Debye relaxation spectrum given by

$$\varepsilon(\omega) = \varepsilon_\infty + \frac{\varepsilon_s - \varepsilon_\infty}{1 + i\omega\tau} \qquad (1)$$

where $i = \sqrt{-1}$, ω = angular frequency, ε_s is the low frequency ($\omega\tau < 1$) value of ε, ε_∞ is the high frequency ($\omega\tau > 1$) of ε, and τ, the relaxation time, is a measure of the time required for the molecule to align itself with an applied field. For water $\varepsilon_s \approx 80$ while $\varepsilon_\infty \approx 3.5$. For liquid water $1/\tau \approx 10^{10}$ Hz while for ice $1/\tau \approx 10^{3}$. Thus, if the frequency of the electric field oscillation is too high, the dipole moment of the H_2O molecule will not become aligned and its dielectric contribution will be reduced to the high frequency value, ε_∞.

When water is first added to a soil, it will be tightly bound to the particle surface and will not be able to rotate freely. As more water is added, the molecules are further away from the particle surface and are more free to rotate. After about 8 or 9 layers, the molecules behave as free water and contribute significantly to the dielectric properties of the soil. In measurements of the dielectric properties of soils, Hoekstra and Delaney[4] observed a frequency dependence similar to that expected by Equation (1) with the exception that the soil water has a range of relaxation times longer than that of liquid H_2O.

Laboratory measurements of the dielectric constant for three soils ranging from a sandy loam to a heavy clay at a wavelength of 21 cm are presented in Figure 1. For all three soils there is a region at low moisture levels where there is a slow increase in ε and above this region there is much steeper increase in ε with moisture content. It can be seen that the region of slowly increasing ε is greater for the clay soils than for the sandy loam. Due to the greater surface area present in the clay soils, more water is tightly bound to soil particles at a given moisture level in sandy soils, and is less able to contribute to the soils dielectric properties.

The curves in Figure 1 are the results from an empirical model which estimates ε of soils as a function of moisture content developed by Wang and Schmugge[5]. As Hoekstra and Delaney[4] point out in their paper, the dielectric behavior of water in soils is different from that in the bulk liquid phase, i.e., the tightly bound water has dielectric properties similar to those of ice while the loosely bound water has dielectric properties similar to those of the liquid state and the crossover occurs at the transition moisture

W_t. This is the point where the slope of the dielectric constant curve changes. Therefore, to obtain the dielectric properties of the moist soil a simple mixing formula is used in which the components are the dielectric constants of the soil mineral (or rock), air and water (ϵ_x), with ϵ_x being a function of the water content, W_c, in the soil. At zero water content $\epsilon_x = \epsilon_{ice}$ and it increases linearly until the transition moisture W_t is reached, at which point ϵ_x has a value approaching that for liquid water. In Wang and Schmugge[5], the values of W_t were determined for 18 soils by a least squares fit to the data. These values of W_t are compared with values of the soils' wilting points (WP) calculated from the known soil textures. The correlation coefficient for W_t = 0.9 indicating that there is a strong dependence of W_t on WP and that texture data can be used to estimate the value of W_t for a soil. Thus, it appears that reasonable estimates of the dielectric constant for soils can be made both as a function of moisture content and microwave frequency if the knowledge of the soil texture or moisture characteristics is available. The frequency dependence is contained in the dielectric constant for water. At the present time, it is assumed that there is no frequency dependence of W_t within the microwave spectral region but this needs to be studied further.

Recall that the dielectric constants of the medium describe propagation characteristics for an electromagnetic wave in the medium. Therefore, they determine the emissive and reflective properties for a smooth surface and it is the observation of these properties which makes possible the remote sensing of soil moisture.

MICROWAVE SENSORS

These changes in surface emissivity and reflectivity can be observed by passive and active microwave sensors. The former are radiometers which measure the thermal emission from the ground at microwave wavelengths. The latter are radars which transmit a pulse of electromagnetic energy and then measure the backscattered return.

Microwave Radiometry

A microwave radiometer measures the thermal emission from the surface and, at these wavelengths, the intensity of the observed emission is proportional to the product of the temperature and emissivity of the surface (Rayleigh-Jeans approximation). This product is commonly called the brightness temperature (T_B). The value of T_B measured by a radiometer at a height, h, above the surface is:

$$T_B = \tau(rT_{sky} + (1 - r)T_{soil}) + T_{atm} \qquad (2)$$

where r is the surface reflectivity and τ the atmospheric transmission. The first term is the reflected sky brightness temperature which depends on wavelength and atmospheric conditions; the second term in the emission from the soil ($1 - r = e$, the emissivity); and the third term is the contribution from the atmosphere between the surface and the receiver. As mentioned in the introduction, the normal range of condition atmospheric effects are

small at the longer wavelengths, e.g. T_{sky} = 5 to 6K at 1.42 GHz with 3K of it being the constant cosmic background radiation and τ is typically 0.98 - 0.99. Therefore, Equation (2) reduces to $T_B = e\ T_{soil}$ where T_{soil} is the effective radiating temperature of the soil and can be estimated from the soil temperature[6].

Measurement of this thermal emission requires very sensitive radiometers of the type used for radio astronomy. These consist of a large antenna, typically about one meter in size depending on the platform, and a very sensitive radio receiver. The size of the antenna determines the angular resolution of the radiometer which is approximately λ/D, where D is the size of the antenna. Thus, a one meter antenna at the 21 cm wavelength yield an angular resolution of about 1/5 of a radian or 12°. This dependence of the spatial resolution on the antenna size is a major factor in the potential use or radiometric systems from space. For example, a 1.4 GHz radiometer with a 10 meter antenna operating on a satellite in a 500 km orbit would have a spatial resolution of 10 km. With this type of resolution, it would be possible to resolve the soil moisture variations resulting from large rain systems.

The range of dielectric constants shown in Figure 1 will produce a change in emissivity from about 0.95 or dry soils to 0.60 or so for wet soils. This approximate range has been observed in field experiments where a radiometer is mounted on a tower and the observed brightness temperature can be compared with actual soil moisture measurements. An example of the results is given in Figure 2. Here normalized brightness temperatures at a wavelength of 21 cm (frequency = 1.42 GHz), i.e. measured brightness temperatures are divided by the physical temperature of the soil and are compared with soil moisture values for the 0 to 2 or 0 to 2.5 cm layer of the soil. The data were obtained for fields with sandy loam soils, one in California and the other in Maryland. The data illustrate the basic sensitivity of the microwave emissivity to soil moisture variations and one of the major limitations, i.e. the microwave sensors respond to surface layer (~ 2 to 5 cm thick) moisture variations. This is true for both active and passive sensors.

A further example of the radiometer sensitivity is shown in Figure 3 where aircraft observations of the normalized brightness temperatures at 21 and 6 cm wavelengths are compared with surface measurement of soil moisture for native grass pastures in Oklahoma[7]. The non-linear behavior for the λ = 6 cm data imply that it is responding to the moisture in thinner layers at the surface. The high altitude data taken at 1500 or 3000 m agree very well with that obtained at the 300 m altitude.

On the basis of extensive field and aircraft experiments such as these, we have concluded that radiometers operating the 21 cm wavelength are the most effective for the passive remote sensing of soil moisture. They can operate at incidence angles within ± 30° off nadir with little change in sensitivity and thus can be scanned. For the off nadir observations, the horizontal polarization, i.e. where the electric fields of the wave has a component parallel to the surface is preferred. The particular wavelength of 21 cm was chosen because it is a radio astronomy quiet band, where there are no

man-made sources of radiation being broadcast. Shorter wavelengths have less ability to penetrate vegetation and have a shallower sampling depth. While longer wavelengths would have greater penetration capability, they would have poorer spatial resolution and would be more subject to man-made interference.

Radar

An active microwave sensor or radar sends out a pulse of microwave radiation and then measures the return that is reflected back to it as represented in Figure 4. The intensity of this reflected signal is described by what is called the backscattering coefficient. An advantage of the radar is that the energy in the received pulses can be angularly separated into the return from different locations on ground. Thus, if the radar is on board an aircraft, it is possible to produce radar backscatter image of the ground.

Analogous to the optical reflectivity of terrain, the backscattering coefficient σ° (sigma zero) describes the scattering properties of terrain in the direction of the illuminating source. The scattering behavior of terrain is governed by the geometrical and dielectric properties of the surface (or volume) relative to the wave properties (wavelength, polarization, and angle of incidence) of the incidence illumination. Recall from Figure 1 that the dielectric constant of a soil-water mixture is strongly dependent on its water content. Thus, in general σ° of terrain is dependent on the soil moisture content of an effective surface layer whose thickness is governed by the properties of the terrain at the wavelength used; this thickness will be approximately the same for active and passive microwave approaches. In addition to this dependence on soil moisture content, however, σ° is also, in general, a function of the surface roughness and vegetation or snow cover (if not bare). The variations of σ° with soil moisture, surface roughness, incidence angle, vegetation cover and observation frequency have been studied extensively in ground based experiments conducted by scientists at the University of Kansas[8,9,10] using a truck mounted 1-18 GHz active microwave system. Some of their conclusions based on these investigations will be presented here.

Look angle and roughness effects. The dependence of backscatter intensity on surface roughness is represented schematically in Figure 4. Smooth surfaces behave as specular reflectors and therefore only have strong backscatter when the incidence angle is near zero. Rough surfaces, on the other hand, behave as isotropic scatterers and thus there is minimal angular variation. Depending on the wavelength, soil surfaces can display this range of behavior as is demonstrated in the plots of σ° versus angle presented in Figure 5 for five fields with essentially the same moisture content but with considerably different surface roughness. At the longest wavelength (1.1 GHz, Figure 5a), σ° for the smoother fields is very sensitive to incidence angle near nadir, i.e. specular behavior, while for the rough field σ° is almost independent of angle. At an angle of about 7°, the curves intersect and the effects of roughness are minimized. As the wavelength decreases, Figure 5b and 5c, all the fields appear rougher, especially the smooth field, and as a result, the intersection point of the five curves moves out to

larger angles. At 4.25 GHz, the intersection occurs at 10°, and it was this combination of angle and frequency that yielded the best sensitivity to soil moisture independent of the soil's surface roughness. Based on these results, the following set of optimum parameters was determined: frequency = 4-5 GHz, θ = 7° - 17° from nadir, and horizontal transmit horizontal receive polarization[8].

SOIL TEXTURE

In the earlier discussion of the soil dielectric properties, the dependence on soil type or texture was pointed out and attributed to the differing soil particle surface areas. In the radiometric response to soil moisture this dependence is manifested by differing slopes of the emissivity versus soil moisture curves. Similarly, for the active microwave response there will be a dependence of the slope of the σ° versus soil moisture curve on soil type. This is demonstrated in Figure 6a where the regression lines of σ° versus soil moisture data are plotted for three different soils[10]. In this figure, the soil moisture values are expressed in volumetric units (g/cm^3) and the three soils have different shapes. When the soil moisture values are normalized by dividing by the 1/3 bar moisture content (field capacity), the slopes for the three soils are brought into relatively close agreement. This behavior was also observed in radiometric observations from aircraft[11] and field[12] platforms. This result implies that the microwave sensors are responding to the state of the water in the soil or perhaps to the amount of water above some critical level, e.g. the wilting point[13]. The use of the 1/3 bar moisture level as the normalizing factor is the first approach for explaining the soil texture effects and was developed on the basis of our understanding of the nature of the behavior of water in soils. We expect that there will be further refinements.

SOIL-MOISTURE SAMPLING DEPTH

The relationship between both the active and passive microwave responses and soil moisture content depends on the dielectric contrast across the air-soil interface. The question arises as to how thick a soil layer needs to be considered for determining the dielectric properties of the soil. Wilheit[14] determined theoretically that this transition layer is on the order of a few tenths of a wavelength thick. Experimentally this result is difficult to verify, but Newton et al.[15] have attempted to measure this thickness by comparing the dry-down curves for various soil layers with soil moistures predicted by radiometer observations at 1.4, 4.9, and 10.7 GHz (wavelengths: 21, 6.0, and 2.8 cm). They measured the moisture content for three layers (0-2 cm, 0-5 cm, and 0-9 cm) at the surface as functions of time and found that the soil moistures predicted by the two higher frequencies dried at about the same rate which was faster than that observed for the 0 to 2 cm layer, implying that these radiometers were responding to an even thinner layer at the surface. At 1.4 GHz, the drying rate was somewhere between that observed for the 0 to 2 cm and the 0 to 5 cm layer, indicating that at this frequency the sampling depth is in the 2 to 5 cm range of about two tenths of a wavelength. This is the reason for the different behaviors at 6 and 21 cm wavelengths seen in Figure 3.

VEGETATION EFFECTS

A vegetation layer covering the soil will absorb and scatter some of the microwave radiation incident on it. The absorption will be primarily due to the water content in the vegetation. The precise sources for the scattering are not understood at the present time and are the subject of much current research both experimental and theoretical.

The effect of vegetation on radar backscatter expressed in natural units (m**2/m**2) is schematically represented in Figure 7 in terms of the backscatter coefficient σ_v° of the vegetation and the loss factor L for the vegetation.

From the analysis of extensive field data, the group at the University of Kansas has determined values for the σ_v° and the loss factor L of a number of different types of vegetation[16,17]. These results are presented in Figure 8 where curves representing the data for several types of vegetation are shown along with values of σ_v° and L. It is clear that corn has the largest backscatter. They found that σ_v° is dominant at low soil-moisture values, below about 50 percent of field capacity, but that in the range between 50 and 150 percent of field capacity, the measured σ° is dominated by the soil contribution with the absorption by the vegetation being cmpensated for by its backscatter.

In addition to scattering and absorption, for passive sensors the emission from the vegetation will be significant also. A model for the effects of vegetation on the microwave emission from soils is given in Figure 9. The radiation measured by a passive sensor can be expressed as the sum of three terms: the first is the emission from the soil reduced by the vegetation absorption, the second and third are the emissions from the vegetation, both direct and that reflected from the soil surface. Note that the last term will increase with increasing soil moisture thus partially counteracting the decrease from the first term. The factor ω is a single scattering albedo parameter for the vegetation and τ is the optical depth for the canopy. The canopy absorption is given by exp (τ). The values of ω and τ were found by a statistical fit to data obtained in field experiments[18]. The resultant values of τ for several observations over soybean, corn, and grass fields are given in Figure 10. These data show a linear dependence of τ on W, the plant water content. Mo et al. in the analysis of field radiometer data found that $\omega \leq 0.1$ and $\tau \leq 0.5$ for mature corn, soybeans, and grass fields. In a separate analysis of the same data, Jackson et al.[19] found that τ is a linear function of the plant water content with a proportionality factor = 0.11 for the water content expressed in kg/m**2. Aircraft data at the 21 cm wavelength over 2 meter corn fields in Kansas showed a 30 Kelvin range of brightness temperature between wet and dry conditions[20]. Analyses of these data showed similar values of ω and τ. Based on these observations, I estimate that a mature corn canopy will be the limiting vegetation condition for the remote sensing of soil moisture.

SPACECRAFT RESULTS

The flights of microwave sensors on recent satellites, e.g. Skylab, Seasat, and Nimbus 5, 6, and 7, have provided opportunities to do case studies on the remote sensing of soil moisture. The S-194 instrument on Skylab was a non-scanning 1.42 GHz radiometer with a 110 km field of view. With such coarse spatial resolution, it is difficult to compare directly the sensor response with in situ moisture measurements. However, there have been several indirect comparisons. Figure 11 shows a comparison of the Skylab brightness temperatures observed for several passes over the central plains of the United States with the Antecedent Precipitation Index (API). The error bars represent the standard deviation of the API values obtained for the 6 to 10 stations within each resolution element. Additional analyses of the Skylab data have been reported by McFarland[21], Wang[22], and Eagleman and Lin[23]. The The higher resolution of SAR on Seasat afforded the opportunity to compare the satellite observations directly with ground measurements. Blanchard et al.[24] did this for data over a site in the Oklahoma panhandle. They compared the digitally processed Seasat backscatter data with soil moisture for bare, alfalfa, and milo fields. They found a linear relation between σ° and soil moisture with a $r^2 = 0.7$. However, they found that the backscatter from corn fields, either cut or standing, was much stronger than that observed from the other fields and showed no sensitivity to soil moisture. This good correlation between satellite observations and soil moisture is very encouraging; however, the strong backscatter from corn and the inherent sensitivity to surface slope and roughness indicate the need for knowledge of the surface conditions before quantitative estimates of soil moisture can be inferred.

DISCUSSION AND CONCLUSIONS

The results presented here are examples of the progress that has been made in improving our fundamental understanding on the use of microwave remote sensors for the remote sensing of soil moisture. The next step in the process should be a demonstration of the capabilities of the sensors for determining surface soil moisture. An example of this type of result is given in Figure 12. Here 21 cm emissivities as measured by an airborne radiometer were used to estimate the 0 to 2.5 cm soil moisture and compared with the ground measurements for this layer. The data are from a series of nine flights over an agricultural area in Hand County, South Dakota[25]. The algorithm used to extract the soil moisture values was developed using calculated emissivities for actual soil-moisture profiles measured at the U.S. Water Conservation Laboratory in Phoenix, Arizona. The resulting emissivities versus soil moisture relationship was adjusted for estimated surface roughness and vegetation effects and then applied to the observed 21 cm emissivities to calculate soil moisture. The rms difference between the observed and calculated values was 4-5 percent. In an analysis of the ground data form these flights, Owe et al.[25] found that the average value of the coefficient of variation (CV is the standard deviation/mean) for the 0 - 2.5 cm layer was 0.25 with it being greater at the lower moisture levels. Thus, the rms difference observed in Figure 13 is comparable to the standard

deviation observed in the ground measurements of soil moisture, particularly for the wetter cases.

As described here, remote sensing techniques can provide estimates of the soil moisture content for a surface layer about 5 cm thick. This depth is shallow compared to the 1 to 2 m rooting depth of many crops. Estimating the root-zone soil moisture from surface measurements has been studied using correlation techniques[26] and modeling studies[27] which assumed a moisture profile in hydraulic equilibrium. The conclusion from both approaches was that, if the water content of the surface 10 cm is known, the moisture content in the top meter could be calculated within acceptable limits, and that the lowest errors were obtained when the surface water contents were measured just before dawn. Using a similar technique, combined with airborne radiometric measurements of surface layer moistures, Kondratyev et al.[28] in the U.S.S.R. obtained large area estimates of the pre-planting moisture stored in the top one meter of the soil. This is an example of Soviet efforts to use the surface water content measurements to obtain information concerning the water status of the root-zone[29]. Efforts are continuing to improve our understanding of the relationship between surface and root zone moisture conditions for a wider range of climatic and crop conditions so that the potential of the remote sensing methods described in this paper can be fully exploited.

Alternatively, knowledge of the surface-layer moisture can be used to estimate moisture fluxes at the soil surface. These could then be used in water balance models to estimate the moisture in the profile. Barton[30] in Australia used soil moistures as determined with an airborne 2.8 cm radiometer in a model for determining evapotranspiration (ET) from grasslands. Bernard et al.[31] did the same sort of thing using simulated radar backscatter data. In the follow-up paper they verified the technique using field measurements with a radar system[32]. Both groups reported considerable success in estimating ET rates and the approach is being studied further.

The microwave remote sensing of soil moisture is at a threshold at the present time. Theoretical and experimental research over the past 10 to 15 years have pretty much defined the capabilities of the active and passive microwave approaches. Briefly summarized they are: the ability to measure the moisture content of a surface layer about 5 cm thick to a relative accuracy of between 10 and 20 percent; the measurement can be made under all weather conditions and through a light to moderate vegetative canopies, i.e. the limiting case appears to be a mature corn crop; and the factors of soil texture and surface roughness will introduce uncertainties into the soil moisture determinations. Before these systems are flown on spacecraft or even before ground studies are enlarged, it will be necessary to convince the management of the utility of such a remotely sensed soil moisture measurement. In closing, I think it is important to realize that remote sensing measurements will not provide as accurate or as deep a measurement of soil moisture as can be obtained by conventional in-situ measurements, but they do provide a means for getting repetitive measurements over large areas of the surface layer soil moisture condition, and thus these microwave

approaches provide an unique opportunity to obtain previously unattainable information about the land surface.

REFERENCES

1. Colwell, R. N., Editor, Manual of Remote Sensing, Second Edition, American Society of Photogrammetry, Falls Church, Virginia, 1983.

2. Ulaby, F. T., R. K. Moore, and A. K. Fung, Microwave Remote Sensing: Volumes I and II, Addison Wesley, Reading, Massachusetts, 1982.

3. Schmugge, T. J., T. J. Jackson, and H. L. McKim, "Survey of Methods for Soil Moisture Determination," Water Resources Res., Vol. 16, pp. 961-979, 1980.

4. Hoekstra, P. and A. Delaney, "Dielectric Properties of Soils at UHF and Microwave Frequencies," J. Geophys. Res., Vol. 79, pp. 1699-1708, 1974.

5. Wang, J. R. and T. J. Schmugge, "An Empirical Model for the Complex Dielectric Permittivity of Soils as a Function of Water Content," IEEE Trans. Geosci. Remote Sensing, Vol. GE-18, pp. 288-295, 1980.

6. Choudhury, B. J. and T. J. Schmugge, "A Parameterization of Effective Soil Temperature for Microwave Emission," J. of Geophys. Res., Vol. 87, pp. 1301-1304, 1982.

7. Jackson, T. J., T. J. Schmugge, and P. O'Neill, "Passive Microwave Remote Sensing of Soil Moisture from an Aircraft Platform," Remote Sens. Environ., Vol. 14, pp. 135-151, 1984.

8. Ulaby, F. T., P. P. Batlivala, and M. C. Dobson, "Microwave Backscatter Dependence on Surface Roughness, Soil Moisture, and Soil Texture: Part I --Bare Soil," IEEE Trans. Geosci. Electron., Vol. GE-16, pp. 286-295, 1978.

9. Ulaby, F. T., G. A. Bradley, and M. C. Dobson, "Microwave Backscatter Dependence on Surface Roughness, Soil Moisture, and Soil Texture: Part II--Vegetation-Covered Soil," IEEE Trans. Geosci. Electron., Vol. GE-17, pp. 33-40, 1979.

10. Dobson, M. C. and F. T. Ulaby, "Microwave Backscatter Dependence on Surface Roughness, Soil Moisture, and Soil Texture: Part III-Soil Tension," IEEE Trans. Geosci. Remote Sensing, Vol. GE-19, pp. 51-61, 1981.

11. Schmugge, T. J., "Effect of Soil Texture on the Microwave Emission from Soils," IEEE Trans. Geosci. Remote Sensing, Vol. GE-18, pp. 353-361, 1980.

12. Wang, J. R., P. E. O'Neill, T. J. Jackson, and E. T. Engman, "A Multifrequency Measurement of Thermal Microwave Emission from Soils: the Effects of Soil Texture and Surface Roughness," IEEE Trans. on Geosci. and Remote Sensing, Vol. GE-21(1), pp. 44-51, 1983.

13. Schmugge, T., "Reply to Comments on the Effects of Texture on Microwave Emissions from Soils," IEEE Trans. Geosci. Remote Sensing, Vol. GE-21, pp. 510-511, 1983.

14. Wilheit, T. T., "Radiative Transfer in a Plane Stratified Dielectric," IEEE Trans. on Geosci. Electron., Vol. GE-16, pp. 138-143, 1978.

15. Newton, R. W., Q. R. Black, S. Makanvand, A. J. Blanchard, and B. R. Jean, "Soil Moisture Information and Thermal Microwave Emission," IEEE Trans. Geosci. Remote Sensing, Vol. GE-20, pp. 275-281, 1982.

16. Ulaby, F. T., M. C. Dobson, and D. C. Brunfeldt, "Improvement of Moisture Estimation Accuracy of Vegetation-Covered Soil by Combined Active/Passive Microwave Sensing," IEEE Trans. Geosci. Remote Sensing, Vol. GE-21, pp. 300-307, 1983.

17. Ulaby, F. T., A. Aslam, and M. C. Dobson, "Effects of Vegetation Cover on the Radar Sensitivity to Soil Moisture," IEEE Trans. Geosci. Remote Sensing, Vol. GE-20, pp. 476-481, 1982.

18. Mo, T., B. J. Choudhury, T. J. Schmugge, J. R. Wang, and T. J. Jackson, "A Model for Microwave Emission from Vegetation Covered Fields," J. Geophys. Res., Vol. 87, pp. 11,229-11,237, 1982.

19. Jackson, T. J., T. J. Schmugge, and J. R. Wang, "Passive Microwave Sensing of Soil Moisture under Vegetation Canopies," Water Resources Res., Vol. 18, pp. 1137-1142, 1982.

20. Ulaby, F. T., M. Razani, and M. C. Dobson, "Effects of Vegetation Cover in the Microwave Sensitivity to Soil Moisture," IEEE Trans. Geosci. Remote Sensing, Vol. GE-21, pp. 51-61, 1983.

21. McFarland, M. J., "The Correlation of Skylab L-band Brightness Temperatures with Antecedent Precipitation," in Conf. Hydrometeorology, Pre-Preprints, Forth Worth, TX, 1976.

22. Wang, J., "Passive Microwave Sensing of Soil Moisture with Satellite Sensors," submitted for publication in Remote Sens. Environ, 1984.

23. Eagleman, J. R. and W. C. Lin, "Remote Sensing of Soil Moisture by a 21 cm Passive Radiometer," J. Geophys. Res., Vol. 81, pp. 3660-3666, 1976.

24. Blanchard, B. J. and A. T. C. Chang, "Estimation of Soil Moisture from Seasat SAR Data," Water Resources Bull., Vol. 19, pp. 803-810, 1983.

25. Owe, M., E. B. Jones, and T. J. Schmugge, "Soil Moisture Patterns Observed in Hand County, South Dakota," Water Resources Bull., Vol. 18, pp. 949-954, 1982.

26. Blanchard, B. J., M. J. McFarland, T. J. Schmugge, and E. Rhoades, "Estimation of Soil Moisture with API Algorithms and Microwave Emission," Water Resources Bull., Vol. 17, pp. 767-774, 1981.

27. Jackson, T. J., "Profile Soil Moisture from Surface Measurements," J. Irrigation Drainage Div., Vol. IR-2, ASCE, pp. 81-92, 1980.

28. Kondratyev, K. Y., V. V. Malentyev, Y. Rabinovich, and E. M. Shulgina, "Passive Microwave Remote Sensing of Soil Moisture," in Proc. 11th Int. Symp. Remote Sensing Environ., Vol. 2, pp. 1641-1661, 1977.

29. Jackson, T. J., "Survey of Applications of Passive Microwave Remote Sensing for Soil Moisture in the USSR," EOS, Trans. Amer. Geophys. Union, Vol. 63, pp. 497-498, 1982.

30. Barton, I. J., "A Case Study Comparison of Microwave Radiometer Measurements Over Bare and Vegetated Surfaces," J. Geophys. Res., Vol. 83, pp. 3513-3517, 1978.

31. Bernard, R., M. Vauclin, M., and D. Vidal-Madjar, "Possible use of Active Microwave Remote Sensing Data for Prediction of Regional Evaporation by Numerical Simulation of Soil Water Movement in the Unsaturated Zone," Water Resources Res., Vol. 17, pp. 1603-1610, 1981.

32. Prevot, L., R. Bernard, O. Taconet, and D. Vidal-Madjar, "Evaporation from a Bare Soil Evaluated from a Soil Water Transfer Model, Using Remotely Sensed Surface Soil Moisture Data," to be published in Water Resources Res., 1984.

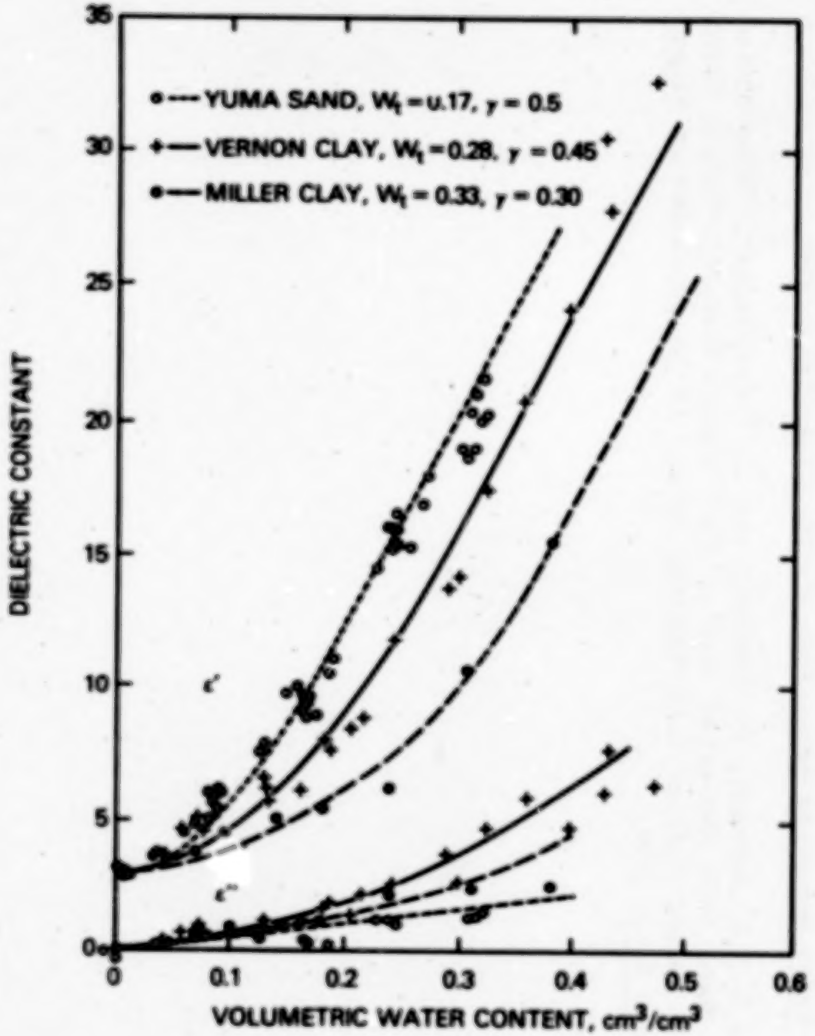

Figure 1. Laboratory measurements of the real and imaginary parts of the dielectric constant for 3 soils at a wavelength of 21 cm.

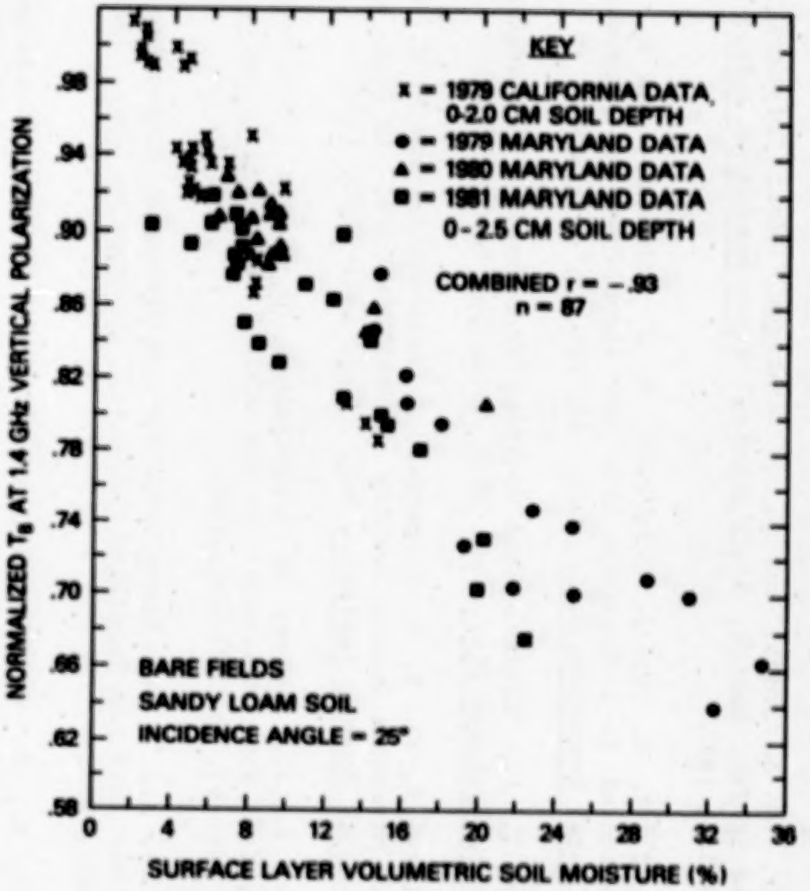

Figure 2. Observations of microwave emissivity from a tower.

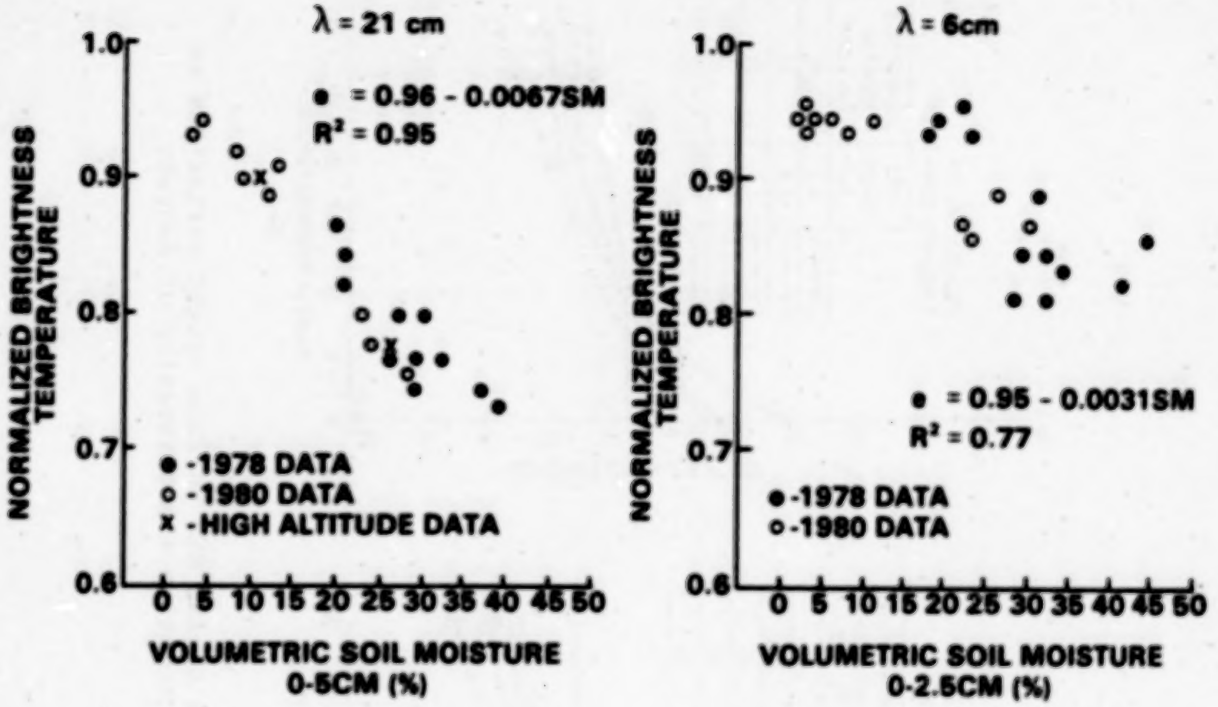

Figure 3. Obeervations of microwave emissivity at nadir from an aircraft at an altitude of 300 m.

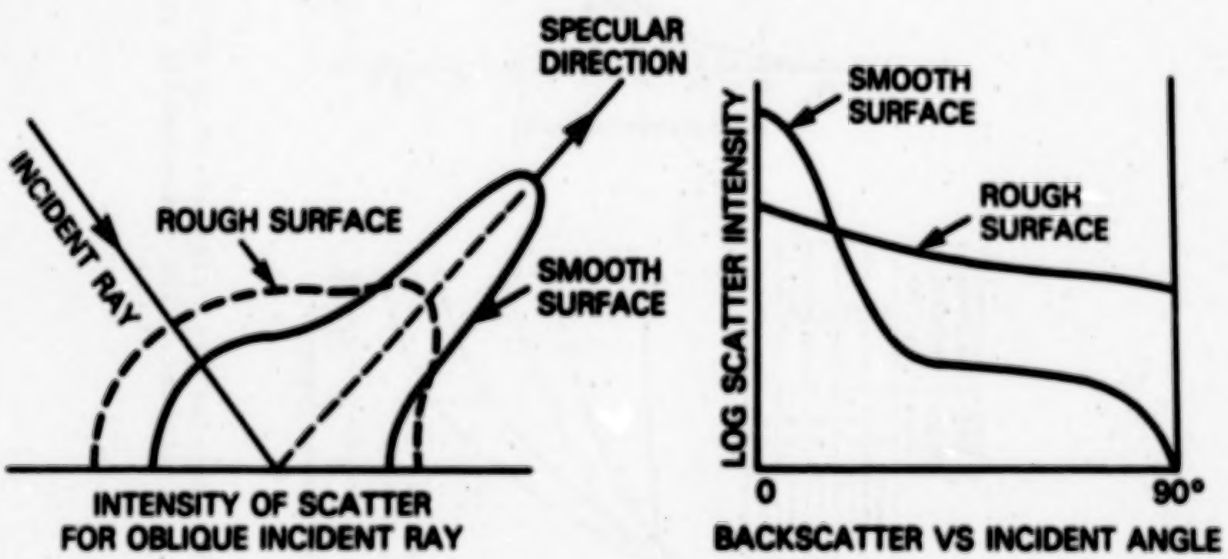

Figure 4. Schematic of radar intensity patterns showing the different behaviors of smooth and rough surfaces. The backscatter (σ°) is the intensity in the direction of incidence.

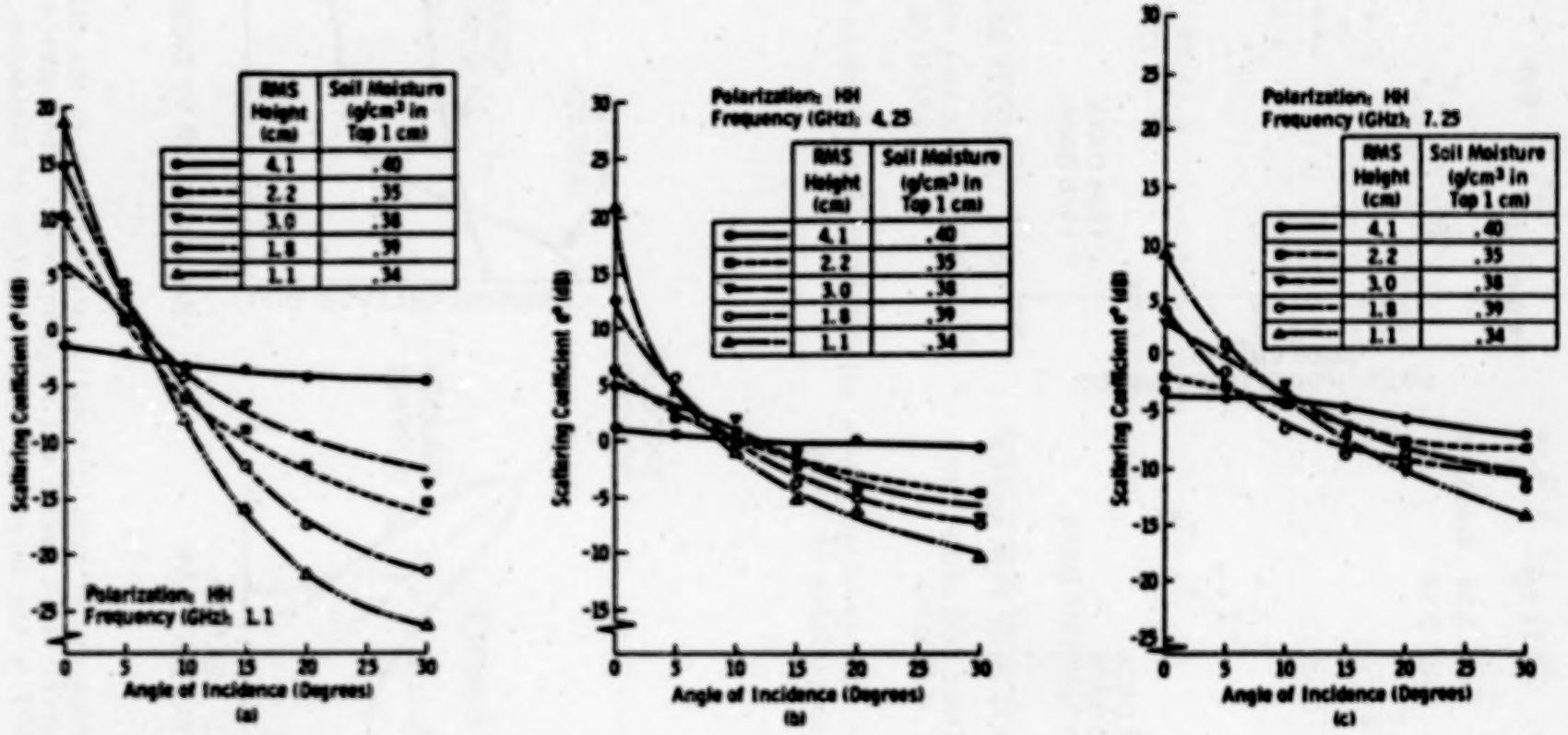

Figure 5. Angular variation of σ° in dB for 5 wet fields having RMS surface height variations as indicated. The measurements were made from a tower at the Univerasity of Kansas.

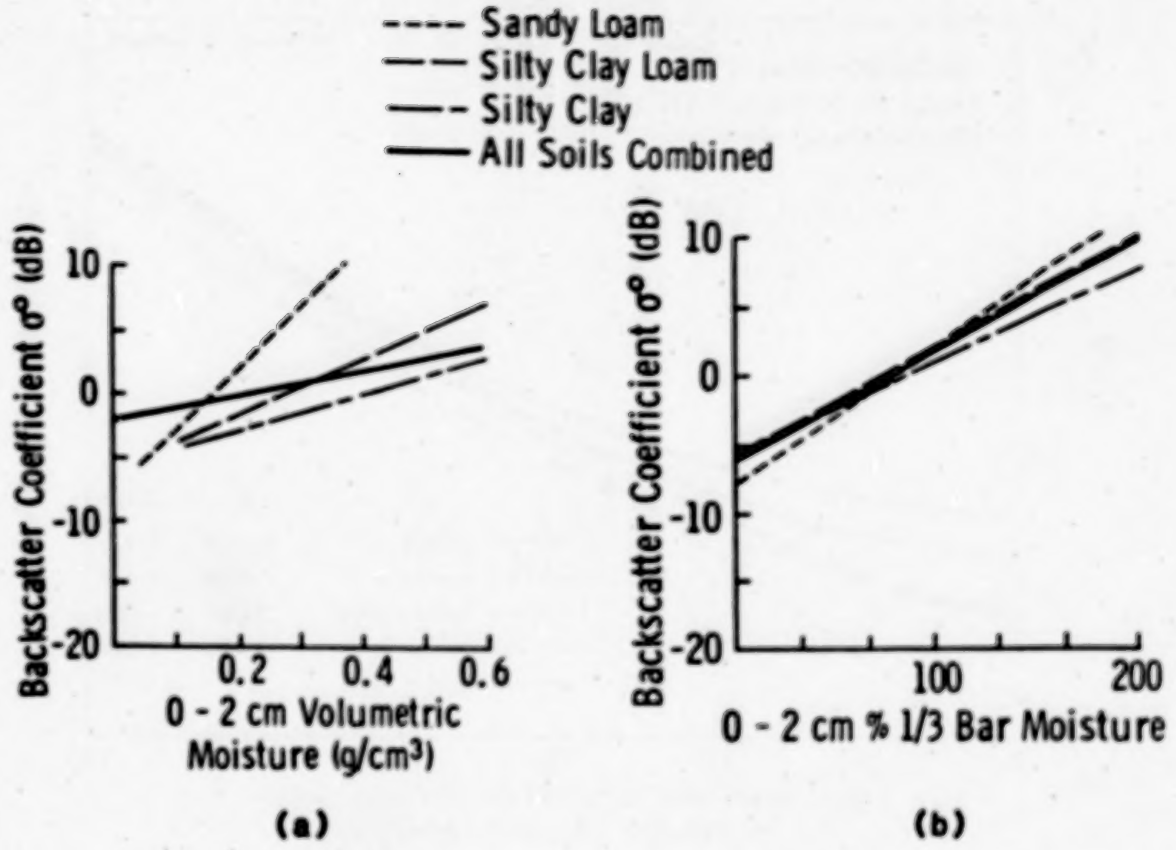

Figure 6. Regression results of tower measurements of σ° vs. soil moisture.

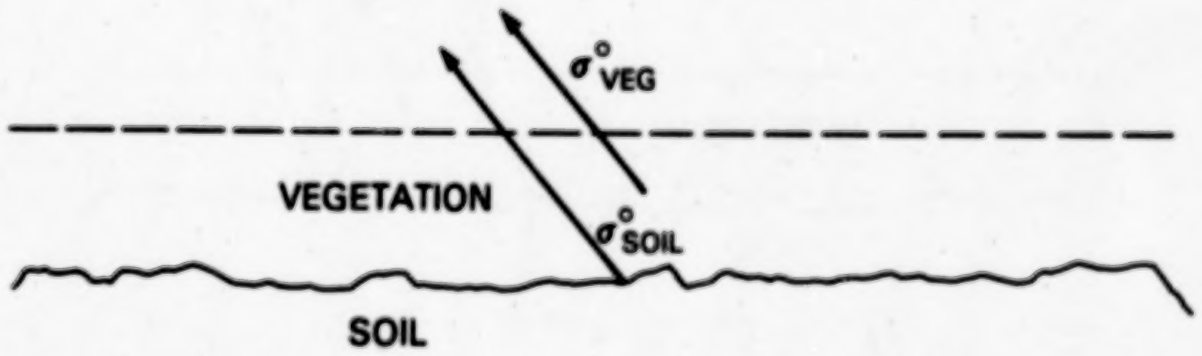

$$\sigma^\circ_{CANOPY} = \sigma^\circ_{VEG} + \sigma^\circ_{SOIL}/L^2$$

Figure 7. Schematic representation of the sources of radar backscatter from vegetated soils, where L is the canopy loss factor.

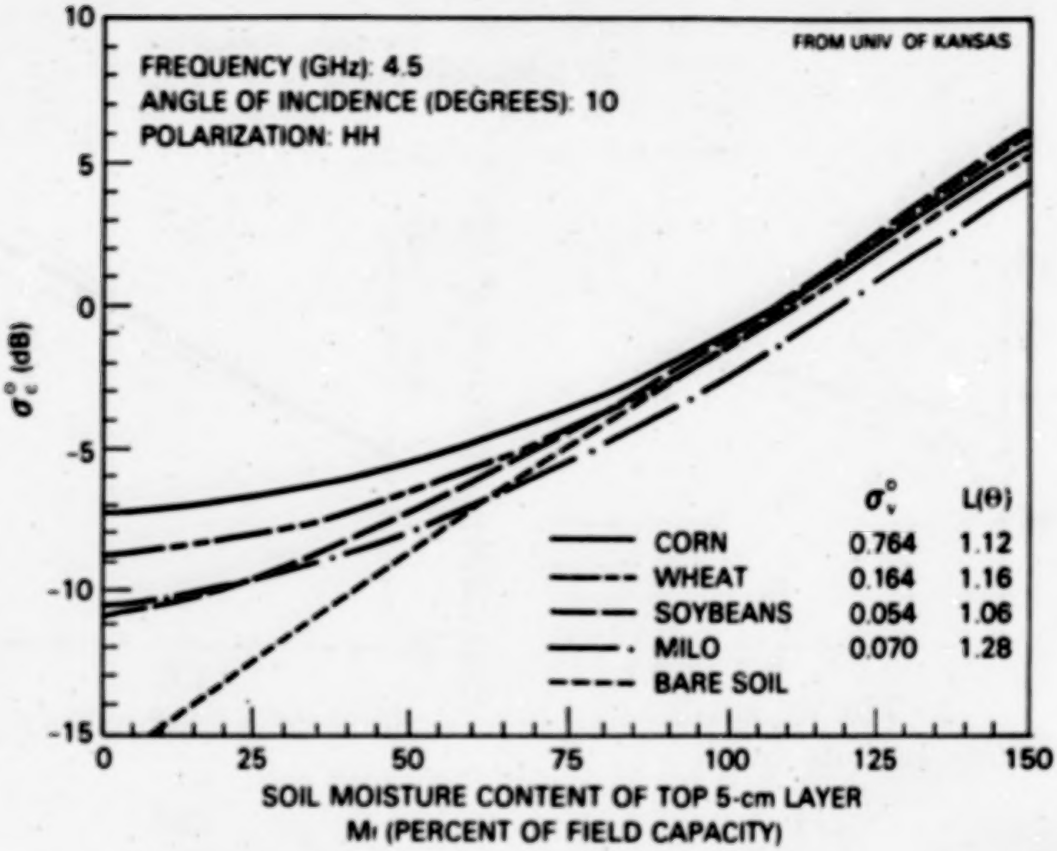

Figure 8. Variation of tower measurements of σ° for 4 crops.

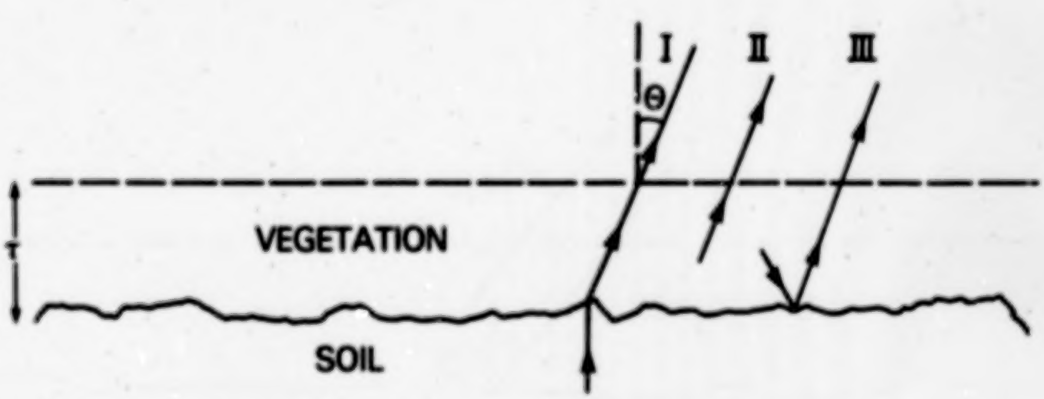

$$T_B^{H,V} = \varepsilon_S^{H,V}\ T_{eff}\ e^{-\tau/\cos\theta} \qquad \text{I}$$

$$+ (1-\omega)\ T_V\ [1 - e^{-\tau/\cos\theta}] \qquad \text{II}$$

$$+ (1-\omega)\ T_V\ [1 - e^{-\tau/\cos\theta}]\ R_S\ e^{-\tau/\cos\theta} \qquad \text{III}$$

Figure 9. Schematic representation of the sources of microwave emission for a vegetated soil. For comparison L = $exp\ (+\tau)$.

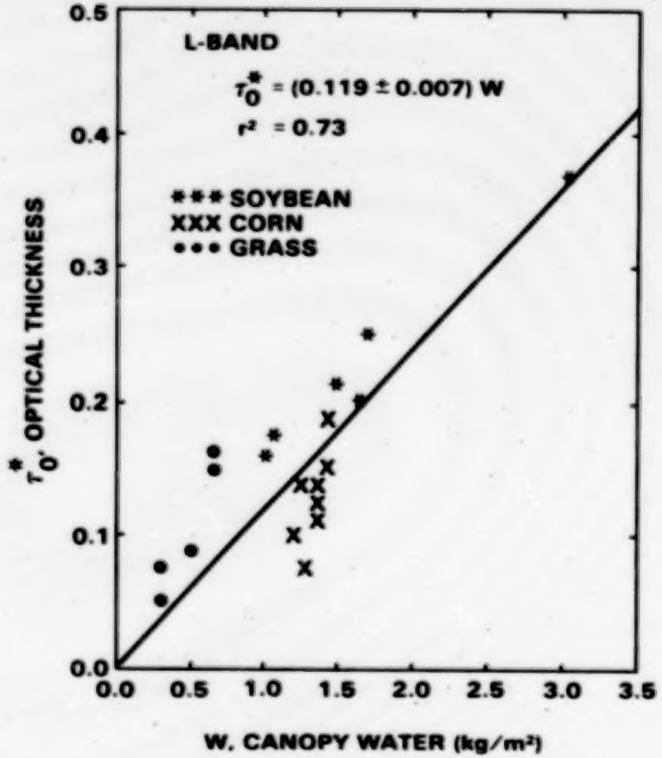

Figure 10. Variation of optical depth (τ) with canopy water content for 3 crops. Results from tower measurements at 2 km.

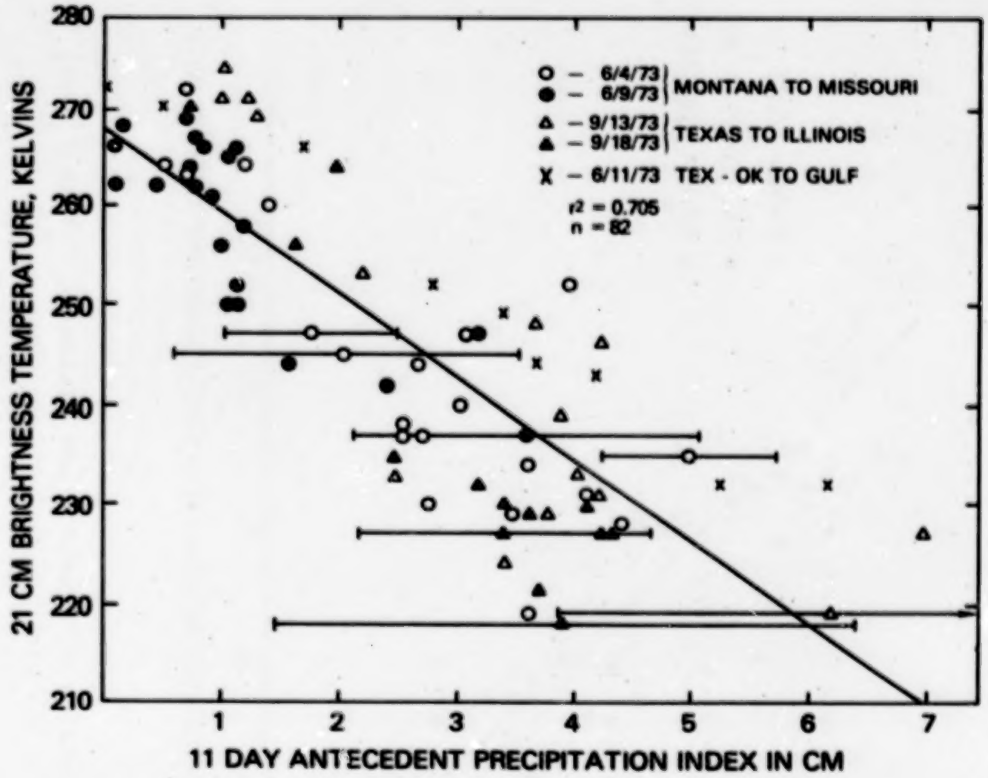

Figure 11. Satellite observations of T_B versus API.

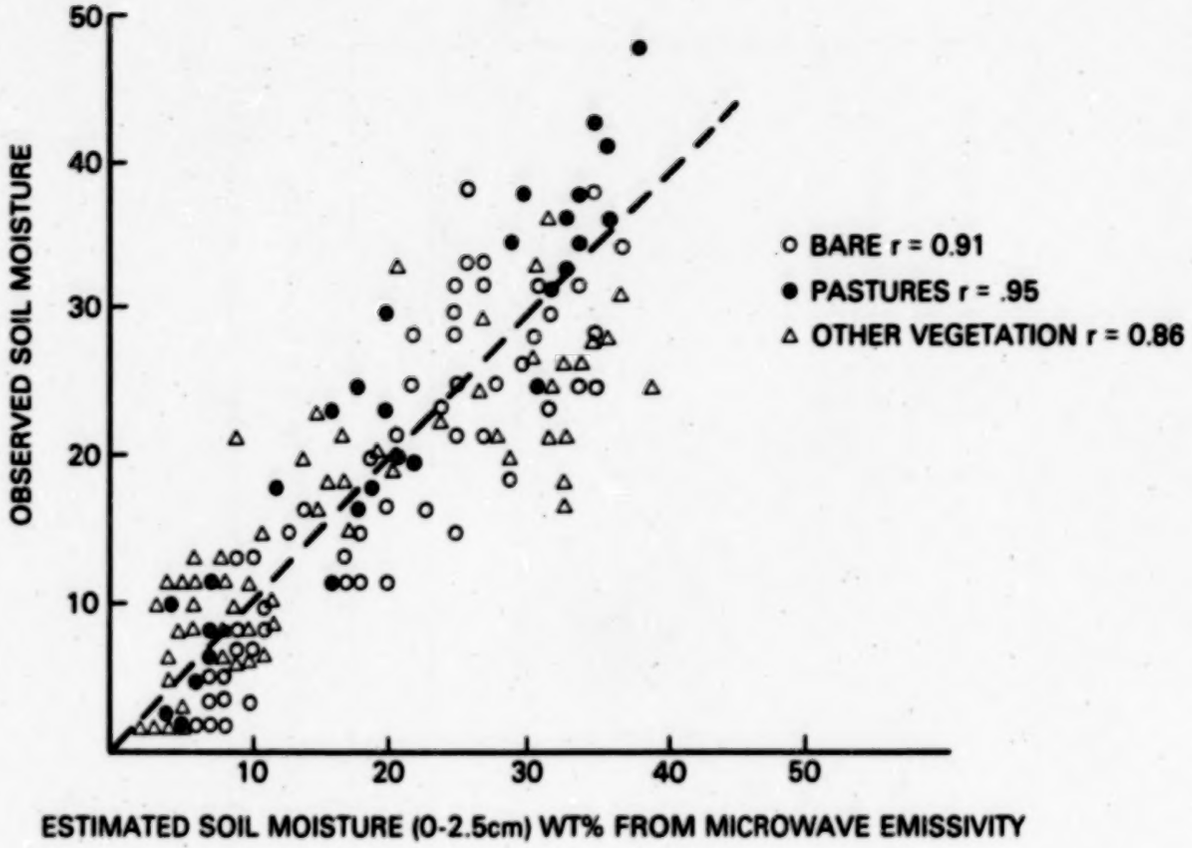

Figure 12. Comparison of measured and estimated values of soil moisture.

D13

TESTING AN ENERGY BALANCE MODEL FOR ESTIMATING ACTUAL EVAPOTRANSPIRATION USING REMOTELY SENSED DATA

R. J. Gurney
Department of Civil Engineering
University of Maryland
College Park, MD 20740

P. J. Camillo
SAR
6811 Kenilworth Avenue
Riverdale, MD 20737

ABSTRACT

An energy-balance model is used to estimate daily evapotranspiration for 3 days for a barley field and a wheat field near Hannover, Federal Republic of Germany. The model was calibrated using once-daily estimates of surface temperatures, which may be remotely sensed. The evaporation estimates were within the 95% error bounds of independent eddy correlation estimates for the daytime periods for all 3 days for both sites, but the energy-balance estimates are generally higher; it is unclear which estimate is biassed. Soil moisture in the top 2 cm of soil, which may be remotely sensed, may be used to improve these evaporation estimates under partial ground cover. Sensitivity studies indicate the amount of ground data required is not excessive.

INTRODUCTION

Evaporation and soil-moisture status are important hydrological parameters which are difficult to estimate conventionally over large areas. There are some indications that remotely-sensed measurements may be able to assist in their estimation for these large areas (e.g., Rosema et al., 1978; Schmugge et al., 1980; Soer, 1980). One remotely-sensed measurement, of the surface temperature, may be used in numerical energy-balance models of the atmospheric boundary layer and upper soil to make inferences of several hydrological parameters of interest, including soil-moisture status and evapotranspiration. The principle of these models is to solve the equation:

$$S = R_N + L \cdot E + H \qquad (1)$$

where R_N is the net radiation; $L \cdot E$ and H the latent and sensible heat flux across the atmospheric boundary layer, respectively; and S is the soil heat flux. L is the latent heat of vaporization and E is the evapotranspiration flux. Each of these terms depends partly on the surface temperature, and on a set of boundary conditions such as the air temperature, the vapour pressure and the wind speed at some level above the surface, the incoming radiation and the temperature at some level in the soil. Given measurements of the boundary conditions, the surface temperature may be estimated, compared with remotely-sensed measurements of the surface temperature, and the two made to agree by parameter fitting. As remotely-sensed measurements are likely to be available only a few times daily in an operational scheme because of orbital constraints, and yet daily means or totals are of most use, the parameters are usually fitted at the times when remotely-sensed data are available and used for all simulation times during a day.

An extension of this type of model was described by Camillo et al. (1983), where both the energy and moisture balances were modelled for a bare soil surface. The equations are solved using a predictor--corrector optimization scheme. This model has advantages over previous models of greater computational efficiency and stability and of greater physical realism for bare soil. In a test using data from an experiment in the Federal Republic of Germany, the agreement between estimated and measured temperatures was better than 1 K and was most sensitive to two parameters, the surface roughness and the thermal conductivity of the soil solids. However, most of the earth's land surface is vegetated, and so extensions to the original model must be made in order to handle vegetated surfaces satisfactorily.

There are several problems with dealing with vegetated surfaces, including energy exchanges within a vegetated canopy and partitioning the energy and moisture exchanges between the plants and the soil surface. The classical way to estimate transfer across the boundary is to find relationships between measurable variables which may be explained by introducing combinations of resistances to movement, analogous to Ohm's law (Shuttleworth, 1976). For vegetation canopies this approach easily introduces large numbers of additional parameters. For a practical application using remotely-sensed data, it is better to have a few parameters which may be updated regularly (daily or even more frequently with spacecraft-borne sensors) rather than to try to

estimate many parameter values from a close succession of intensive ground measurements and then use them for long periods of time. A method such as described here may give reliable evapotranspiration estimates and error bars over large areas with minimal ground data.

The additions to the bare soil model required to model vegetated surfaces and a discussion of the simplifications required from the complex resistance models is described next.

MODEL DESCRIPTION

As in Camillo et al. (1983), the net radiation was measured, and the other components of the surface energy balance were modelled, as follows:

$$L \cdot E = - C_1 U_a (e_s - e_a) \tag{2}$$

$$H = - \gamma \, C_1 U_a (T_s - T_a) \tag{3}$$

$$S = - \lambda_1 (T_1 - T_s)/Z_1 \tag{4}$$

where T_s is the surface temperature; T_a the air temperature; e_s the surface vapour pressure; e_a the atmospheric vapour pressure; U_a the wind speed; and γ the psychrometric constant. λ_1, T_1 and Z_1 are the thermal conductivity, temperature at the center and depth to the center of the first layer, respectively.

The constant C_1 in Eqs. (2) and (3) is the bulk diffusion coefficient for neutrally stable atmospheric conditions which was used in the bare-soil simulations. A more complete evapotranspiration model which includes a plant resistance would be formulated as follows:

$$L \cdot E = - (\rho C_p/\gamma)[e_s - e_a)/(r_a + r_s)] \tag{5}$$

where ρ and C_p are the density and heat capacity of air; respectively, and r_a and r_s are aerodynamic and stomatal resistances, respectively. Under neutrally stable conditions, the aerodynamic resistance may be modelled (Brutsaert, 1982) as:

$$r_a = \frac{\ln^2(z/z_o)}{k^2 U_a} \tag{6}$$

where z is the height at which the meteorological data are measured; z_o is the roughness length; and k is von Karman's constant. Putting this resistance into Eq. (5), rearranging, and comparing to Eq. (2) gives:

$$C_1 = \frac{\rho C_p k^2}{\gamma \ln^2(z/z_o)(1 + r_s/r_a)} \tag{7}$$

The easiest application of this type of model using remotely-sensed data requires the bulk diffusion parameter C_1 to be constant between calibration times. This paper provides the presentation of the model, assuming a constant C_1 but allowing evaporation to be less than potential through constraints on the water balance through the soil-moisture flux. The model is tested by comparing the estimates of evaporation produced by the model against those produced by a more conventional eddy correlation and energy-balance approach for one set of ground conditions in the F.R.G. Further testing of the model under different conditions is clearly desirable.

For C_1 to be considered a constant, Eq. (7) shows either that the stomatal resistance must always be small when compared to the aerodynamic resistance, or that the ratio of the two must always be constant. Neither of these conditions is likely to be met, especially for stressed vegetation. However, there are mathematically- and physically-based reasons for taking this position, in addition to the simplicitly required for remote-sensing applications: (1) there must be some constant value of C_1 which, when used in Eqs. (2) and (3), will give the correct value for evapotranspiration integrated over some time period; and (2) an increase in stomatal resistance is accompanied by an increase in the surface temperature, due to the reduction in the latent heat flux. Thus, we can bypass fitting on the stomatal resistance, since the feedback mechanisms (the heat balance at the soil surface, Eqs. (1-4)) couple its behavior to that of the surface temperature, to which we are fitting. Eq. (7) shows that increasing, r_s should cause a smaller C_1, precisely the behaviour found in this study.

The soil heat flux term (Eq. (4)) may be rewritten to solve for T_s:

$$T_s = (z_1/\lambda_1)S + T_1 \tag{8}$$

Substituting the heat-balance equation (Eq. (1)) into this equation gives:

$$T_s = T_1 + (z_1/\lambda_1)[R_N(T_s) + L \cdot E(T_s) + H(T_s)] \tag{9}$$

Solving for T_s also gives the heat and moisture upper-boundary fluxes of the soil, S and E, respectively. These are used with the soil-moisture (q_θ) and heat (q_h) fluxes in the soil profile, computed from soil physical properties and temperature and moisture profiles, to solve the equations for temperature and moisture within the soil:

$$dT/dt = - C^{-1}(\partial q_h/\partial z) \tag{10a}$$

$$d\theta/dt = - \partial q/\partial z_\theta \tag{10b}$$

where θ is the volumetric moisture content; and C the volumetric heat capacity of the soil. The general layout of the soil model is described by Camillo et al. (1983).

In Eq. (2), E is the total evapotranspiration demand (cm s^{-1}), which for vegetated surfaces must be divided into an evaporation flux E_s from the soil surface and a transpiration flux E_p from the plants. The iterative structure of this model is used to facilitate this. A constant fraction of this demand function E is allocated to the soil evaporation E_s. If the soil-moisture supply cannot support this potential, E_s is reduced to the flux supplied to the first layer from below (Hillel, 1980). Then the transpiration, E_p, is set equal to the difference between E and E_s. If the plant is stressed so that this demand cannot be met, E_p is set to zero. Finally, E is reset to the sum of E_s and E_p. Thus, non-potential evapotranspiration is modelled by allowing the demand to match the supply, as defined by the soil-moisture extraction terms of the model, rather than as is conventionally done by reducing the atmospheric demand function directly, using a resistance formulation and then assuming that this demand can be met.

The model of the transpiration E_p is provided by an estimate of the crown potential, estimated using a root-water extraction model described in detail by Camillo and Schmugge (1983), and comparing this estimate of the crown potential to the atmospheric demand. The root model provides an additional term W in the soil-moisture flux Eq. (10b), so that:

$$d\theta/dt = - \partial q/\partial z_\theta - W \tag{11}$$

The model for the sink term W is:

$$W(z,t) = [\phi_s(z) - \phi_p(t)]/[\Omega_s(z) + \Omega_p(z)] \tag{12}$$

where $\phi_s(\theta,z)$ is the total potential energy of the soil water (the sum of the gravitational and matrix potential); $\phi_p(t)$ is the plant potential, or crown potential, which is allowed to vary with time but which is assumed constant with depth; Ω_s is the soil resistance; and Ω_p is the plant resistance. The soil resistance Ω_s may be modelled as:

$$\Omega_s = 1/[K(\theta)R(z)] \tag{13}$$

where $K(\theta)$ is the hydraulic conductivity (cm s^{-1}); and R(z) is the relative root density (cm^{-2}), and the resistance to flow in the roots may be modelled as:

$$\Omega_p(z) = r/R(z) \tag{14}$$

where r is the specific resistance, the inverse of the hydraulic conductivity in the roots (Hillel, 1980). Rearranging and substituting in Eq. (12) gives the sink term for each layer:

$$W_i = [K_i R_i(\psi_i - z_i - \phi_p)]/(1 + rK_i) \tag{15}$$

where ψ_i is the matrix potential; and $- z_i$ is the gravitational potential of moisture in the ith layer. R_i is often considered as the length of active roots per volume of soil, although there is no conclusive experimental evidence

about this. However, the relative root density appears more important than the absolute values at any depth, because the model only requires that R(z) represent the relative ability of the roots to absorb water at each depth.

The crown potential ϕ_p is modelled as a response to the atmospheric evapotranspiration demand function, and is computed by requiring that the integral of the sink terms over the soil profile be equal to this demand function E_p. Thus, for a profile divided into N layers, of thickness dz_j:

$$E_p = -\sum_{j=1}^{N} W_j dz_j \tag{16}$$

Inserting W_j from Eq. (15) into Eq. (16) and solving for the crown potential gives:

$$\phi p(t) = \frac{E_p(t) + \sum_{j=1}^{N} [K_j R_j (\psi_j - z_j) dz_j / (1 + rK_j)]}{\sum_{j=1}^{N} [K_j R_j dz_j / (1 + rK_j)]} \tag{17}$$

Once the crown potential is evaluated, the sink term may be evaluated for each layer using Eq. (15). To allow for the evidence that water flux from plants to the soil is negligible (Molz and Peterson, 1976), any negative sink terms W_j are set to zero and the remaining positive terms are reduced by the scale factor to satisfy Eq. (16).

Even though the transpiration model does not include stomatal resistance, a rudimentary mechanism does exist to model extreme plant stress. For periods of large demand or dry-soil conditions, the magnitudes of E_p and ψ_j (or possibly both) in Eq. (17) will be large, giving a large magnitude for the crown potential. There is a limit below which this negative potential cannot go, and if ϕ_p from Eq. (17) exceeds this limit, it is reset to equal the limit. As the soil dries further ϕ_s will become more negative, with no compensating change in ϕ_p possible; eventually the sink terms (Eq. (15)) will become negative and are, therefore, set to zero. In this way, the large stress modelled by a lower limit for ϕ_p may eventually cause transpiration to cease.

MODEL VALIDATION

The model has a somewhat different structure and philosophy from existing models of evapotranspiration, and so extensive validation of the approach is required for many different vegetation types under many different conditions. The validation described here is somewhat limited, being for wheat and barley crops under near-potential conditions for a site in the F.R.G., the data being taken in June 1979. The model must work well under these conditions if it is to have any general application. Although the surface temperature

data were collected for small areas only in this intensive measurement campaign, the data were exactly analagous to the soil surface temperatures that may be collected over large areas by remotely-sensed methods.

The data used to validate the model were taken during the experiment performed in Ruthe, F.R.G., in the summer of 1979. The Joint Measuring Campaign 1979 in Ruthe was organized to study the water budget of an agricultural area, and to explore the potential of remote sensing in regional water-balance studies (van der Ploeg et al., 1980). The experiment was undertaken as part of the Tellus Project, under the auspices of the Joint Research Centre, Ispra, Italy, of the European Economic Community. The Tellus Project was also one of the investigations of the NASA Heat Capacity Mapping Mission. An area of ~ 4 x 4 km, 15 km south of Hannover, F.R.G., was used for this experiment. The area, near Ruthe, has little relief in an open landscape with few trees, bushes, buildings or other windbreaks. The soils, developed in a Pleistocene loess ~ 2 m thick, are very homogeneous over large areas. The individual fields are large, with an average size of ~ 7.5 ha.

The data used in this study came from wheat and barley fields. Soil surface temperatures and soil temperature profiles were collected, together with gravimetric soil-moisture data and information about soil thermal conductivity and heat capacity, and net radiation, and wind speed, air temperature and vapour pressure profiles. These data were collected largely by the Institute of Hydrology and the University of Reading, Great Britain.

The root mean square error between measured and estimated surface temperatures for each day for both wheat and barley are given in Table 1 for a variety of bulk diffusion coefficients C_1 and an evaporation fraction f_s of zero. Taking the wheat field as an example for which data for two measurement sites, D and G, are available, it may be seen that there is a minimum root mean square error against site D temperature measurements for a value of C_1 of ~ 10^{-5} on each day, while for site G the root mean square error function is rather flat because the measured temperatures are usually below the estimated values, while the meteorological measurements used are more representative of those at site D. Similar conclusions may be inferred for the barley field. It should be noted that the root mean square error values given refer to all 24 hour values. The worst fit occurs at night, when least evapotranspiration occurs. Root mean square error values for daytime only would therefore be much below the values in the tables.

A test of the accuracy of the results is shown in Table 2, which compares the estimates of hourly evapotranspiration from the model with estimates produced using an eddy correlation technique (B. A. Callander, pers. commun., 1980). Eddy correlation methods have several possible sources of inaccuracy, because of instrument errors and atmospheric stability problems; B. A. Callander (pers. commun., 1980) associated root mean square errors with his estimates which are reproduced in Table 2. The eddy correlation techniques produce large errors at night under low-wind-speed stable conditions, and so only daytime estimates are made. It may be seen that the model estimates are within the allowable errors on the eddy correlation estimates, assuming 95% confidence intervals, but that the model estimates are consistently higher

than the eddy correlation estimates. This is probably due to the very simple way in which the eddy correlation method used partitioned the estimated fluxes. The net radiation was measured, and the sensible heat flux was estimated using wind and temperature data. The soil heat flux was estimated using wind and temperature data. The soil heat flux was estimated as a fixed proportion of the net radiation, the the latent heat flux was estimated as a remainder term using Eq. (1). Consistent biasses of the latent-heat flux term are thus difficult to detect, and it should be noted that the day-to-day variations in hourly evapotranspiration rates are similar for the two estimation methods. The data for the wheat site on June 21 are modelled using a resistance formulation (Monteith, 1973) using crop resistance data from June 20, and so there are additional errors on this "eddy correlation" estimate, as reflected in Table 2.

These results show that the good agreement which can be found between measured and estimated surface temperatures leads to reasonable evapotranspiration estimates. There is also the suggestion that remote sensing of the surface soil moisture could reduce the errors of estimating the cumulative daily evapotranspiration. However, there are many assumptions inherent in this analysis, and these should be examined.

First, the area examined was evaporating and transpiring under relatively unstressed conditions, reducing the effects of stomatal resistance. A constant C_1 does reasonably well for fitting the wheat data for 3 days. However, it is necessary to use further data sets taken under stressed conditions to see how frequently the bulk diffusion coefficient C_1 needs to be re-estimated in order to give reasonable estimates of the daily cumulative evapotranspiration, and to see the assistance that surface soil-moisture data may give to reduce the errors of the estimates.

SAMPLING INTERVAL REQUIRED ON METEOROLOGICAL DATA

One of the characteristics of the remotely sensed data is that it is available repetitively for large areas. It thus provides a good way of getting estimates of hydrological variables over large areas that are very difficult or expensive to get by other methods. However, it is important that the requirements for ground data not be excessive, or the use of the remotely sensed data becomes rather superfluous. The requirement for ground meteorological data to accompany the satellite data is examined here. The meteorological data (air temperature, vapour pressure, and wind speed in the boundary layer, and optionally the components of the net radiation at the soil surface) are used to evaluate the surface heat balance equation fluxes. It is the strong dependence of these fluxes on the surface temperature which allows that measurement to be used for model calibration.

Camillo and Gurney (1984) studied the sensitivity of evaporation estimates produced by the numerical model of the atmospheric boundary layer and upper soil to random errors and constant biasses in the meteorological inputs, using the same data from West Germany described above. It was found that for the bare soil the errors in the net radiation had the most significant effect on the evaporation estimates while for the wheat field the effects of errors

in the vapor pressure and the air temperature were as important as the effect of errors in the net radiation. Bias errors were found to produce larger errors than random errors of the same magnitude for both fields.

Plots and tables of evapotranspiration errors as a function of the meteorological data random and bias errors were computed. The next stage in this sensitivity analysis is to relate these maximum allowable errors on the meteorological inputs, as determined from the maximum evaporation errors which may be tolerated for the application in mind, to the temporal and spatial sampling frequencies of the meteorological input data. This may be done using the spatial and temporal auto-correlation structure of the meteorological variables, which allows cross-correlations between variables and spacetime trade-offs to be considered (Jones et al., 1979). However, it is also of interest to examine the temporal sampling problem separately from the spatial sampling problem. This was done here by running the model with various sampling intervals on the meteorological data and then comparing the resultant errors on the evaporation.

SENSITIVITY STUDY METHODOLOGY

The baseline run used data integrated over five-minute intervals from an automatic weather station. This had been shown by Gurney and Camillo (1984) do agree well with eddy correlation estimates of evaporation. The results from all other simulations are compared to this baseline run.

Two different methods were used for acquiring meteorological data to be used in the simulations. First, the actual data were reduced to one value representing a fixed time interval. Two reduction methods were used; sampling the five-minute data at the middle of the interval, and averaging the five-minute data throughout the interval, as follows:

a) Samples: Single values to represent one, three and six hour intervals were taken from the data set. Thus, one five-minute value was taken to represent net radiation, air temperature and vapor pressure. The five-minute data from the middle of each period was used for the sample data. Where the mid-point fell at the end of a five minute sample period, the five minute period immediately preceding the mid-point was used. Anemometers are usually coupled to integrating recording instruments, so the average wind speed throughout the period was used.

b) Averages: One, three and six-hour averages were taken from the data set. This is in many ways a method more analagous to those becoming operational, where integrating recorders are used to get more representative values of all the meteorological variables, not just the wind speed. The hourly averaged data are shown in Figure 1 to illustrate the way the meteorological data vary.

Second, we tested some commonly used algorithms either to model unmeasured data or to interpolate between infrequently measured values. These models are described below.

SENSITIVITY STUDY RESULTS

Sampling and Averaging

Table 3 shows cumulative daily evaporation for the three days for the baseline, sampling, and averaging runs. It is immediately apparent from Table 3 from a comparison of the baseline and hourly average runs that, for all the three days, using hourly averaged data gives virtually identical results to the baseline. The three and six hourly averages are less good but still adequate, with the respective maximum daily variations from the baseline values being .10 mm and .15 mm respectively.

The hourly sampled data also gave adequate results, the largest error in evaporation being .14 mm. However, sampling at three and six hour intervals gave unacceptably large evaporation errors with minimum daily errors of 0.80 mm and 0.57 mm respectively.

For each of the three time intervals averaging gives more accurate evaporation estimates than does sampling. This is to be expected, as the sampling technique could easily miss fluctuations such as passing clouds which affect evaporation rates, whereas the averaging technique includes these effects to some extent.

Interpolation and Modeling

Closely related to sampling and averaging is the idea of using sparse measurements in the model. We have examined commonly used methods for using sparse measurements of air temperature, vapor pressure and wind speed, and for using net radiation models when no net radiation data are available. The data used are those reported in standard meteorological reports from secondary meteorological stations. We discuss each data type in turn. Results are shown in Table 4.

Air Temperature

Linear interpolation between the daily minimum and maximum values is commonly used to provide estimates of the air temperature at other times of the day. We have modified this algorithm to include the 9 a.m. temperature, as this value is also usually available. We therefore linearly interpolate between the daily minimum and 9 a.m., 9 a.m. and the daily maximum, and then to the next daily minimum. The evaporation estimates derived from using this 16 scheme for the air temperature are in the second column of Table 4. The third column shows the results when, instead of the true times of the extrema, the minimum and maximum are assumed to occur at 5 a.m. and 1 p.m. respectively.

A comparison of the two shows that there are no significant differences between the daily evaporation from the two schemes. If one is to use this method, the simpler case of assuming a fixed time for the daily extrema could be adopted, particularly as most synoptic reports of temperature maxima and minima do not include the time of these extrema.

The evaporation errors, which do not exceed .4 mm in any one day, should be acceptable for most applications.

Wind Speed

For an unattended weather station only the daily wind run may be available, so we have examined the use of one daily average wind speed. The results are shown in the fourth column of Table 2. Comparison to the baseline run shows good agreement for the first simulation day and progressively worse results for the next two days, for which evaporation was underestimated by .8 and 1.2 mm respectively. The reason is that for the first day the daily average, 129 cm sec^{-1}, happened to represent the wind speed for all daylight hours when evaporation is greatest (Figure 1). However, the second and third day averages were 70 cm sec^{-1} and 90 cm sec^{-1} respectively, and a comparison of these numbers to the hourly averaged data in Figure 1 shows that they grossly underestimate the wind during the periods of greatest evaporation.

These results are not surprising, as the correlation between wind speed and high evaporation is well known. The lesson applicable to data sampling is that the deviations from the mean must be small over the averaging interval. If only the daily wind run is available, it may be possible to use other meteorological data (such as the times of the passage of fronts) to reconstruct some of the variations in wind speed within the day and thereby improve evaporation estimates.

Net Radiation

It is possible to use a numerical model for the net radiation if measurements are not available. As models of this sort are commonly used, it is important to assess the effect of their use on evaporation estimates. The model used here may be summarized as follows (Eagleson, 1970):

$$R_{net} = (1-a)\, I_o \sin\alpha \exp(-.128\, n/\sin\alpha) + \sigma\epsilon_s\, E_a\, T_a^4 - \sigma\epsilon_s\, T_s^4 \qquad (18)$$

where a is the albedo, I_o is the solar energy flux at the top of the atmosphere (120 cal cm^{-2} hr^{-1}), α is the angle between the sun and the local tangent plane, n is a factor relating to atmospheric scattering of visible and near infrared radiation, σ is the Stefan-Boltzmann constant, ϵ_s is the surface emissivity, and E_a is the emissivity of the air, which may be modelled as a function of the atmospheric vapor pressure and/or air temperature. The surface dependent parameters, the albedo and emissivity, were measured with values of .18 and .96 respectively. The attenuation factor, n, was treated as a fitting parameter, the only one used in the radiation model. Figure 1 shows the hourly averaged data (solid line) and the best fit (dashed line) for n = 3, as determined by eye.

The irregularities in the data not reproduced by the model are due to cloudy conditions, which were not modelled but could be easily included as an extra factor in Eq. (18). On a daily averaged basis, June 19 was considered completely cloud covered, June 20 about 40% cloud covered, and June 21 about

15% cloud covered. The distribution over time on June 21 (the only day for which such data are available) was 25% at 11 a.m., 60% from 1 p.m. to 4 p.m., and 10% after 6 p.m. This cloud distribution is reflected in the differences between the measured and modelled net radiation in Figure 1.

The effect of these inaccuracies is tabulated in column 5 of Table 4. The deviations of the estimated evaporation from the baseline for the three days are 1 mm, -.54 mm and -.75 mm respectively.

Vapor Pressure

The 9 a.m. vapor pressure is widely available, so we have examined the errors in evaporation from using this value throughout the day. The hourly averaged values are plotted in Figure 1. The 9 a.m. values for the three days were 14.7 mb, 17.8 mb, and 22.4 mb, and column 6 of Table 4 shows the evaporation estimates. The deviations from the baseline values for the three days are .3 mm, -.4 mm, and -1.0 mm. Thus, we conclude that using the 9 a.m. measurement throughout the day when the daily variations are large (i.e. 10 mb on June 21) gives evaporation estimates with unacceptably large errors.

This sensitivity to the vapor pressure is a direct result of the important role it plays in the diffusion model, Eq. (2). Previous work (Camillo and Gurney, 1984) has shown that in a diffusion model of this type, vapor pressure errors can be as important as net radiation errors.

Vapor Pressure and Temperature

In the absence of advection, vapor pressure changes very closely with the air temperature. It is thus of interest to see the errors where the vapor pressure is calculated with the psychrometric equation, using the 9 a.m. wet bulb temperature throughout the day and the interpolated air temperature. This should give more acceptable errors than using one value for the vapor pressure throughout the day. It may be seen from Table 4 that the errors on evaporation are .5 mm, .0 mm and 0.4 mm, which should be just acceptable for many applications.

All Variables Modelled or Interpolated

It is also of interest to see how well the model performs when the net radiation is modelled and when the other meteorological data are all interpolated from sparse measurements. The air temperature was interpolated using assumed times for the maxima and minima, and the vapor pressure was calculated with the aid of the interpolated air temperature and 9 a.m. wet bulb temperature. It may be seen that the resultant errors in daily evaporation for the three days are 1.1 mm, .0 mm and .9 mm, respectively. The errors on two of the days are thus unacceptably high.

SENSITIVITY ANALYSIS DISCUSSION

We have examined the sensitivity of evaporation estimates from an energy and moisture balance model to various ways of obtaining the meteorological data

which drive the model. First, we have examined the use of averaged and sampled data, with varying time intervals represented by each data point. Hourly averages gave virtually identical results to the baseline run, in which 5 minute averages were used. Hourly sampled data gave less good but adequate results. For all intervals averaging the data gave smaller errors than did sampling so that errors from averaging over three and six hour intervals also gave acceptable results.

We also considered various other commonly used methods for providing the meteorological data. Using one average wind speed throughout the day was acceptable only when the fluctuations from this mean value were small. A linear interpolation scheme to calculate the air temperature from the daily minimum, 9 a.m., and maximum values provided acceptable results. Use of standard net radiation models could be adequate for clear sky conditions, or if they included a factor for reducing the solar radiation during cloudy conditions; this would require cloud distribution data throughout the day. We found that using the 9 a.m. vapor pressure throughout the day gave unacceptably large evaporation errors, but using the 9 a.m. wet bulb temperature and the hourly temperature interpolated from maxima, minima and 9 a.m. values gave much improved results and yielded acceptable errors. Using these interpolation and modelling algorithms together gave unacceptable results on two of the three days. However, it should be noted that these algorithms were very simplified, and somewhat more realistic algorithms, as discussed above, using ancillary data from meteorological satellites for cloud cover, or numerical weather analysis for other variables, could yield much more acceptable results. It is interesting that the results are as good as they are for such sparse data, and gives hope that the approach is reasonable for operational purposes using remotely sensed data.

ACKNOWLEDGEMENTS

Dr. R. J. Gurney is funded by NASA Goddard Space Flight Center under Grant NAG 5-9. Dr. P. J. Camillo is funded by NASA Goddard Space Flight Center under Contract NAS5-23450.

REFERENCES

1. Camillo, P. J. and R. J. Gurney, "A Sensitivity Analysis of a Numerical Model for Estimating Evapotranspiration," Water Resources Research, V. 20, 1984.

2. Camillo, P. J. and T. J. Schmugge, "Estimation of Soil Moisture Storage in the Root Zone from Surface Measurements," Soil Science, V. 135, pp. 245-264, 1983.

3. Camillo, P. J., R. J. Gurney, and T. J. Schmugge, "A Soil and Atmospheric Boundary Layer Model for Evapotranspiration and Soil Moisture Studies," Water Resources Research, V. 19, pp. 371-380, 1983.

4. Eagleson, P. S.,"Dynamic Hydrology," McGraw-Hill, New York, 1970.

5. Hillel, D.,"Fundamentals of Soil Physics," Academic Press, New York, 1980.

6. Jones, D. A., R. J. Gurney, and P. E. O'Connell, "Network Design Using Optimal Estimation Procedures, Water Resources Research," V. 15, pp. 1801 -1812, 1979.

7. Molz, F. J. and C. M. Peterson, "Water Transport from Roots to Soil," Agronomic Journal, V. 68, pp. 901-904, 1976.

8. Monteith, J. L., "Principles of Environmental Physics," American Elsevier, New York, 1973.

9. Rosema, A., J. H. B'jleveld, P. Reiniger, G. Tassone, R. J. Gurney, and K. Blyth, "Tellus, a Combined Surface Temperature, Soil Moisture and Evaporation Mapping Approach," Proceedings of the Environmental Research Institute of Michigan Symposium on Remote Sensing, Ann Arbor, Michigan, 12th, pp. 2267-2276, 1978.

10. Schmugge, T. J., T. J. Jackson, and H. L. McKim, "Survey of Methods for Soil Moisture Determination," Water Resources Research, V. 16, pp. 961-979, 1980.

11. Shuttleworth, W. J., "A One-Dimensional Theoretical Description of the Vegetation-Atmospheric Interaction," Boundary Layer Meteorology, V. 10, pp. 273-302, 1976.

12. Soer, G. J. R., "Estimation of Regional Evapotranspiration and Soil Moisture Conditions Using Remotely Sensed Crop Surface Temperature," Remote Sensing of the Environment, V. 9, pp. 27-45, 1980.

13. van der Ploeg, R. R., G. Tassone, and J. von Hoyningen-Huene, "The Joint Measuring Campaign 1979 in Ruthe (West Germany), Description and Preliminary Data, European Economic Community, Joint Research Centre, Ispra, 1980.

Table 1 - Root mean square errors between measured and estimated surface temperatures (K) for both wheat and barley fields.

	C_1					
	0.5	1.0	1.5	2.0	2.5	3.0
WHEAT						
Site D:						
June 19, 1979	1.4	1.1	1.1	1.1	1.2	1.2
June 20, 1979	2.2	1.8	2.2	2.3	2.6	2.6
June 21, 1979	2.2	1.5	2.1	2.5	2.6	2.5
Site G:						
June 19, 1979	2.0	1.4	1.2	1.1	1.1	1.1
June 20, 1979	3.9	2.3	1.7	1.6	1.5	1.4
June 21, 1979	4.2	2.2	1.6	1.2	1.0	0.9
BARLEY						
Site K:						
June 19, 1979	1.6	1.1	1.1	1.1	1.1	1.2
June 20, 1979	2.6	1.4	1.4	1.6	1.6	1.7
June 21, 1979	3.3	3.6	3.9	4.1	4.2	4.3
Site I:						
June 19, 1979	2.3	1.6	1.4	1.3	1.2	1.3
June 20, 1979	3.6	2.0	1.6	1.4	1.3	1.3
June 21, 1979	3.5	1.8	1.2	1.1	1.0	1.1

Table 2 - Comparison of eddy correlation and energy balance model estimates of hourly evaporation rates (mm $hr.^{-1}$).

	Eddy Correlation	Root Mean Square Error	Energy Balance
Wheat:			
June 19, 1979	0.239	0.061	0.233
June 20, 1979	0.280	0.104	0.438
June 21, 1979	0.411	0.146	0.531
Barley:			
June 19, 1979	0.149	0.086	0.267
June 20, 1979	0.325	0.110	0.481
June 21, 1979	0.354	0.112	0.470

Table 3 - Cumulative daily evaporation (mm) for three days, for the baseline run and runs using various averaging and sampling intervals.

Date	Baseline	Hourly Average	3-Hourly Average	6-Hourly Average	Hourly Sample	3-Hourly Sample	6-Hourly Sample
June 19	3.24	3.26	3.25	3.17	3.19	3.47	3.78
June 20	5.31	5.32	5.24	5.16	5.21	6.11	5.88
June 21	6.94	6.93	6.84	6.79	7.08	6.17	7.46
3 Day Total	15.49	15.51	15.33	15.12	15.48	15.75	17.12

Table 4 - Cumulative daily evaporation (mm) for three days, for the baseline run and for runs using various methods to use sparse data (air temperature, vapor pressure, wind speed) or model non-existent data (net radiation).

A: Baseline run.

B: Air Temperature linearly interpolated between daily minimum, 9 a.m. temperature and daily maximum, with true times of minima and maxima.

C: Air temperature linearly interpolated between daily minimum, 9 a.m. temperature and daily maximum, with times of minima and maxima assumed at 5 a.m. and 1 p.m. respectively.

D: Daily wind run.

E: Net radiation model.

F: 9 a.m. vapor pressure used throughout day.

G: 9 a.m. vapor pressure interpolated using interpolated air temperature.

H: All variables interpolated or modelled.

Date	A	B	C	D	E	F	G	H
June 19	3.24	3.49	3.55	3.29	4.22	3.58	2.76	4.32
June 20	5.31	5.47	5.43	4.55	4.77	4.96	5.34	5.34
June 21	6.94	6.78	7.18	5.74	6.19	5.95	7.32	7.87
3 Day Total	15.49	15.74	16.16	13.58	15.18	14.49	14.41	17.53

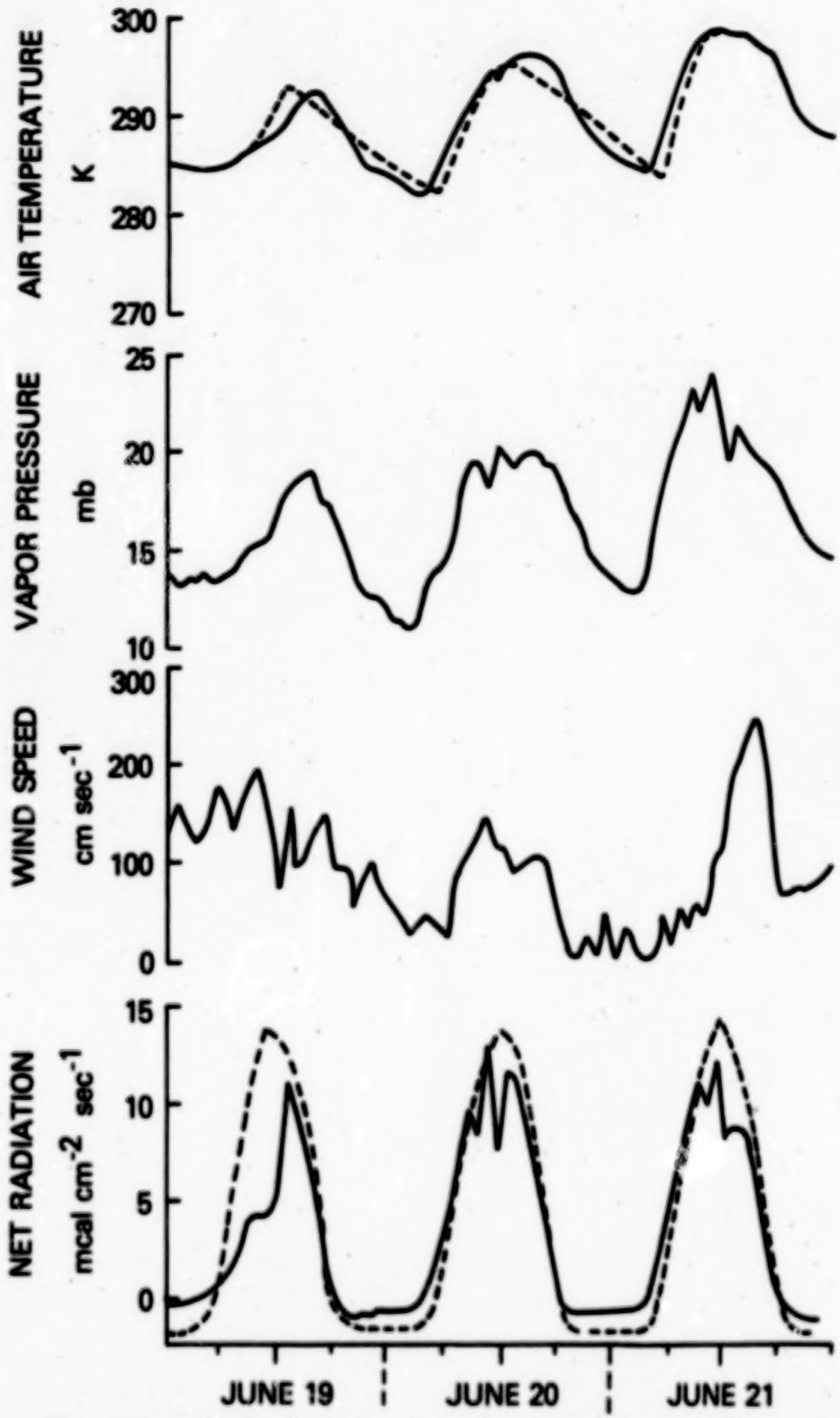

Figure 1. The meteorological input data input to the baseline run, showing air temperature, wind speed, net radiation and vapor pressure respectively. The modelled radiation data and interpolated air temperature also shown as dashed lines.

END

DATE

FILMED

JUN 11 1985